

2.1 Studies with Bibenzyl Trisulfide

2.1.1 The reaction of $[\text{CpCr}(\text{CO})_3]_2$ (**1**) with Bibenzyl Trisulfide

A deep green solution of $[\text{CpCr}(\text{CO})_3]_2$ (**1**) underwent complete reaction with one mole equivalent of Bz_2S_3 under rigorous stirring at ambient temperature for 2 h. Column chromatography of the resultant yellowish brown solution led to the isolation of $[\text{CpCr}(\text{CO})_2]_2\text{S}$ (**5**) [46a-b] (57.4% yield) as brownish green crystalline solids, $[\text{CpCr}(\text{CO})_2(\text{SBz})]_2$ (**6**) (33.3% yield) as dark brown crystalline solids and $[\text{CpCr}(\text{SBz})]_2\text{S}$ (**7**) (4.3% yield) as dark purple platelets. A similar reaction at an elevated temperature of 60 °C for 5 h, produced **5** and **7** in 80.8% and 13.7% yield, respectively, apparently at the expense of **6**. The product composition is inevitably altered by the temperature of the reaction.

From NMR tube reaction studies, it was shown that the reaction of **6** with Bz_2S_3 at ambient temperature for a prolonged period of 26 h gave a substantial yield of **5** (27.5% yield). However, the cothermolysis of **5** with Bz_2S_3 at 60 °C after 24 h gave unreacted **5** (74.4% recovery), **7** (1.1% yield) and $\text{Cp}_4\text{Cr}_4\text{S}_4$ (**8**) [46b] (2.5% yield).

Thermolysis of **6** at 80 °C for 1 h, afforded the following products of **5** (36.0% yield) and **7** (27.4% yield). Similarly, thermolysis of **7** at 100 °C for a prolonged 20 h gave **8** (22%) with unreacted **7** (35%) and a greenish blue layer which remains uneluted. From these observations, it was deduced that both **5** and **6** are the primary products. The total decarbonylated products of **7** and **8** are the secondary products from the thermal degradation of **5** and **6**.

2.1.2 The reaction of $[\text{CpCr}(\text{CO})_2]_2$ (**2**) with Bibenzyl Trisulfide

A deep green solution of $[\text{CpCr}(\text{CO})_2]_2$ (**2**) was reacted with one mole equivalent of Bz_2S_3 at ambient temperature with stirring for 72 h. The resultant dirty brown reaction mixture was chromatographed onto a silica gel column to afford **5** and **7** in 5.1% and 15.8% yields, respectively.

2.1.3 Thermolysis Studies

(a) Thermolysis of $[\text{CpCr}(\text{CO})_2(\text{SBz})]_2$

Thermolysis of $[\text{CpCr}(\text{CO})_2(\text{SBz})]_2$ (**6**) in toluene for 1 h at 80 °C led to the complete degradation to $[\text{CpCr}(\text{CO})_2]_2\text{S}$ (**5**) and $[\text{CpCr}(\text{SBz})]_2\text{S}$ (**7**) in 36% and 27.4% yields, respectively. The finding indicates that **6** is not stable under thermolytic condition which easily degrades to $[\text{CpCr}(\text{CO})_2]_2\text{S}$ (**5**) and finally undergoes total decarbonylation to afford $[\text{CpCr}(\text{SBz})]_2\text{S}$ (**7**).

(b) Thermolysis of $[\text{CpCr}(\text{SBz})]_2\text{S}$

Thermolysis of $[\text{CpCr}(\text{SBz})]_2\text{S}$ (**7**) in toluene at 100 °C for prolonged 20 h, led to the isolation of the final thermolyzed product of $\text{Cp}_4\text{Cr}_4\text{S}_4$ (22.0% yield) and the unreacted **7** (35% recovery). The deduction from these thermolytic studies suggests that the primary product of **6** degrades to **7** which subsequently gave $\text{Cp}_4\text{Cr}_4\text{S}_4$ as the final thermolyzed product in the reaction of $[\text{CpCr}(\text{CO})_3]_2$ (**1**) with Bz_2S_3 .

2.1.4 NMR spectral studies

(a) Reaction of $[\text{CpCr}(\text{CO})_2]_2\text{S}$ (**5**) with Bz_2S_3 at 60 °C

The reaction of **5** with one mole equivalent of Bz_2S_3 at 60 °C has been monitored *via* ^1H NMR at intervals for which the product compositions are given in Table 1. After 2 h, the spectrum showed the presence of $[\text{CpCr}(\text{SBz})]_2\text{S}$ (**7**) and $\text{Cp}_4\text{Cr}_4\text{S}_4$ (**8**) in 1.7% and 0.7% yields, respectively, together with unreacted **5** (80.5% recovery). Subsequently, after 16 h, the relative yield of **7** and **8** increased slightly to 2.1% and 1.2%, respectively. However, the yield of **7** decreased to 1.1%, while there are increases in **8** (2.5%), together with unreacted **5** (74.4% recovery) after 24 h, which might indicate that **7** may have decomposed to **8** under thermolytic condition. This observation also highlights the alternative pathway to **7** apart from the thermolysis of $[\text{CpCr}(\text{CO})_2(\text{SBz})]_2$ (**6**).

(b) Reaction of $[\text{CpCr}(\text{CO})_2(\text{SBz})]_2$ (**6**) with Bz_2S_3 at ambient temperature

The reaction of **6** with one mole equivalent of Bz_2S_3 at ambient temperature has been monitored *via* ^1H NMR at regular intervals. From the spectra, $[\text{CpCr}(\text{CO})_2]_2\text{S}$ (**5**) (27.5%) and **6** (33.4%) were found after 26 h of reaction. This shows that excess amount of Bz_2S_3 in the reaction mixture will increase the yield of $[\text{CpCr}(\text{CO})_2]_2\text{S}$.

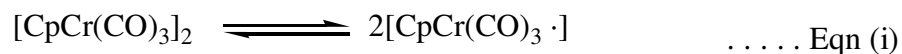
Table 1. Variation of product composition^a from the reaction of $[\text{CpCr}(\text{CO})_2]_2\text{S}$ (**5**) with Bz_2S_3 at 60 °C

Time (h)	Complexes (%)	$[\text{CpCr}(\text{CO})_2]_2\text{S}$ (5)	$[\text{CpCr}(\text{SBz})]_2\text{S}$ (7)	$\text{Cp}_4\text{Cr}_4\text{S}_4$ (8)
2		80.5	1.7	0.7
4		78.2	0.8	0.7
16		77.1	2.1	1.2
24		74.4	1.1	2.5

^a - Product yields by integration of Cp resonances in ^1H NMR spectrum of product mixture

2.1.5 Mechanistic pathways: Formation of $[\text{CpCr}(\text{CO})_2(\text{SBz})]_2$ (**6**) and $[\text{CpCr}(\text{SBz})]_2\text{S}$ (**7**)

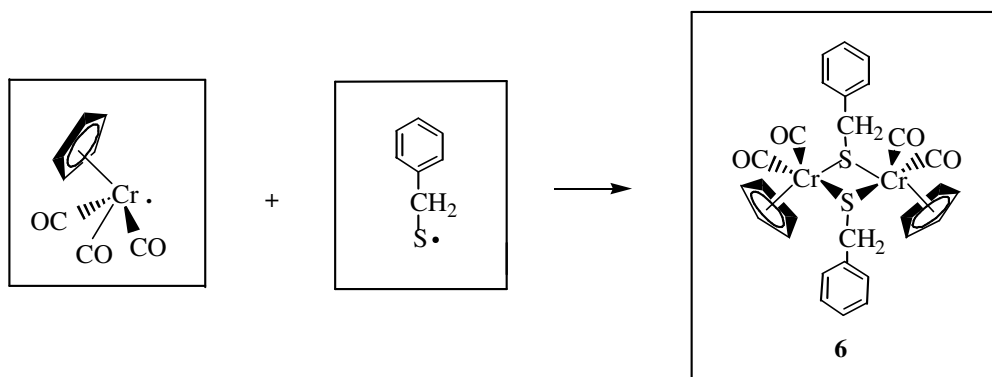
From the observed facile reactivity of **1** with Bz_2S_3 , it is conceivable that the ease of reaction in this case derives from the high propensity of **1** to dissociate into its monomer radicals (Eqn (i)) [4a-f].



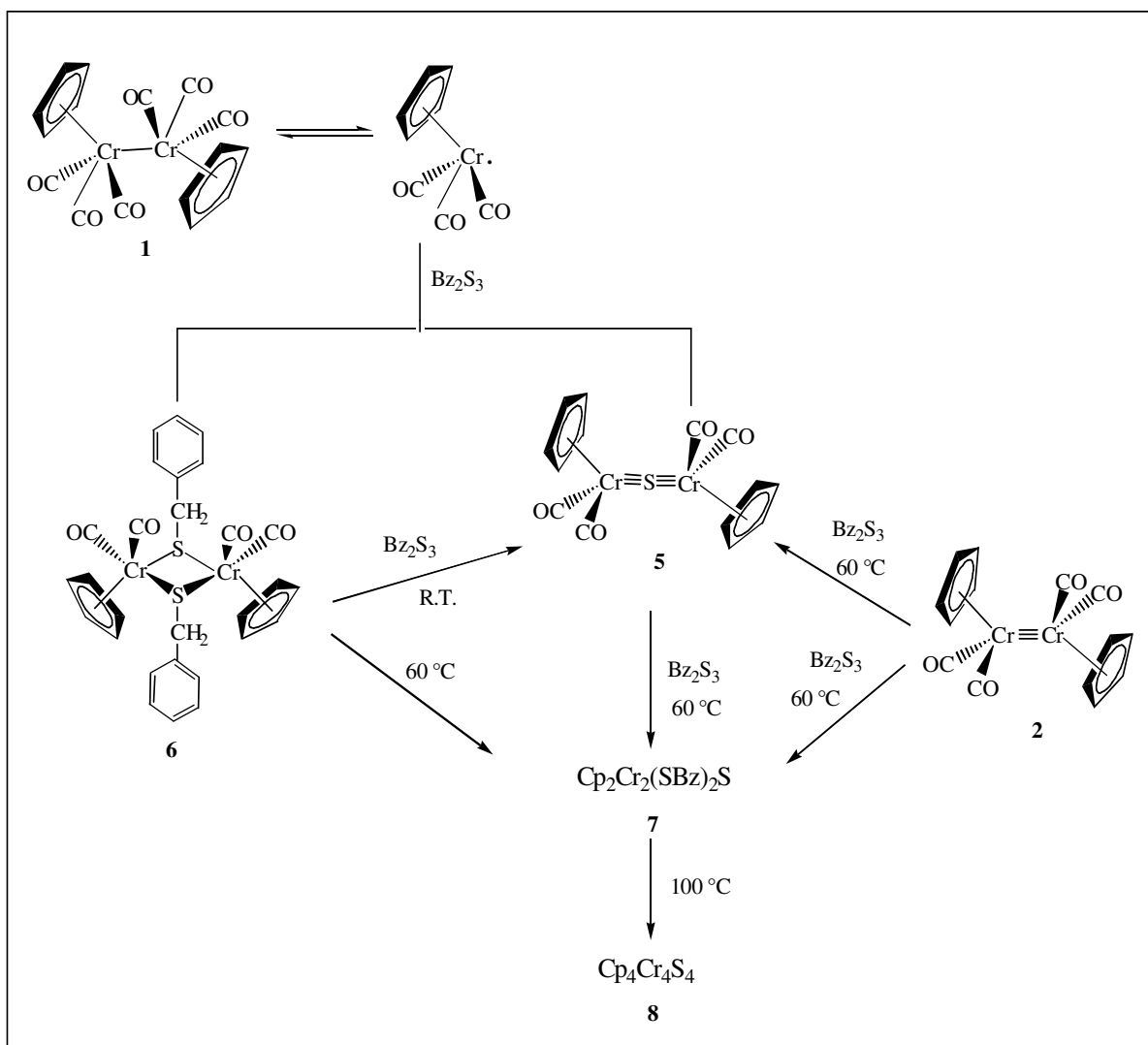
Such a reaction that proceeds *via* the 17-electron radical pathway was also postulated in a previous work carried out by Goh *et al* with systems such as Ph_2S_2 [47], P_4E_3 (E = S, Se) [54a-b, 55a] and elemental P_4 [78] and As_4 [53a].

The vulnerability of the S-S linkage to cleavage processes in organic disulfides by various species is well documented [50, 79a-b]. Likewise, closely related organic trisulfides such as Bz_2S_3 showed similar susceptibility toward cleavages by nucleophiles, electrophiles and radical attack. In this case, the desulfurization process is targeted towards the central sulfur of the –S-S-S- linkage [80]. It is conceivable that initial radical attack on the Bz_2S_3 leads to the primary formation of **5** by sulfur insertion between two $\text{CpCr}(\text{CO})_2$ fragments. Formation of **6** which is a thiolate-bridged dimer is likely to have resulted from further radical attack on the benzyl moiety obtained after desulfurization of Bz_2S_3 as shown in Scheme 18. At elevated temperatures, thermal degradation of **6** leads to total decarbonylation which converts to yield **7**. Further prolonged thermolysis ultimately resulted in the isolation of the cubane-like cluster $\text{Cp}_4\text{Cr}_4\text{S}_4$. The synthetic pathways proposed for the observed reactions as described above are illustrated in Scheme 19.

Scheme 18. Mechanistic pathways for the formation of $[\text{CpCr}(\text{CO})_2(\text{SBz})]_2$ (**6**)



Scheme 19. Proposed synthetic pathways for the reactions of $[\text{CpCr}(\text{CO})_n]_2$ ($n=2, 3$) with dibenzyl trisulfide



2.1.6 Physical properties

[CpCr(CO)₂(SBz)₂]₂ (6)

The complex exists as dark red block crystals, air-stable for extended periods at ambient temperature. It is soluble in toluene giving a dark brown solution which is fairly stable at room temperature under an inert atmosphere.

[CpCr(SBz)]₂S (7)

The complex exists as dark purple fine crystalline platelets which are air-stable for extended periods at ambient temperature. It is soluble in both ether and THF, giving a purple solution which is fairly stable at room temperature under inert atmosphere for a couple of hours.

2.1.7 Spectral characteristics

2.1.7.1 IR spectra

[CpCr(CO)₂(SBz)]₂ (6)

The IR spectrum in nujol shows $\nu(\text{CO})$ stretching frequencies at 1986s, 1954m, 1901vs cm^{-1} (refer to Appendix I).

[CpCr(SBz)]₂S (7)

The IR spectrum in nujol shows stretching frequencies at 1063vw, 1015vw, 840w, 732w cm^{-1} (refer to Appendix I).

2.1.7.2 NMR spectra

[CpCr(CO)₂(SBz)]₂ (**6**)

The complex is diamagnetic, and is highly symmetrical. The Cp rings, CO and the bibenzyl (–CH₂-S) ligands appeared as singlet in both the ¹H and ¹³C NMR spectra in benzene-*d*₆. The ¹H chemical shifts for Cp and –CH₂-S are δ 4.16 and δ 3.63, respectively. For ¹³C NMR the chemical shift for Cp was recorded at δ 94.62, –CH₂-S at δ 35.92, C₆H₅- at δ 141.07, 130.43, 128.83, 127.82 and CO at δ 264.25.

[CpCr(SBz)]₂S (**7**)

Complex **7** is a paramagnetic species which shows a broad peak at δ 13.89 (br, Cp, $\nu_{1/2} = 57$ Hz) and a –CH₂-S signal at δ 3.34 in its ¹H NMR spectrum in benzene-*d*₆. In the ¹³C NMR spectrum in benzene-*d*₆, the chemical shift for Cp was recorded at δ 101.03, –CH₂-S at δ 21.76, 15.93 and C₆H₅- at δ 138.21, 135.62, 133.14, 129.67, 129.59, 129.18, 128.90, 126.02. The ¹³C NMR resonances indicate that both the benzylthio ligands in **7** is unsymmetrical and with two symmetrical Cp rings lying at a parallel position to each other.

2.1.7.3 Mass Spectrum

[CpCr(CO)₂(SBz)]₂ (**6**)

The ESI mass spectrum shows the parent ion $m/z = 592$ [CpCr(CO)₂(SBz)]₂ as well as [CpCr(CO)₂]₂S and Cp₄Cr₄S₄, which are consistent with its facile degradation to **5** and **8** observed under thermolytic conditions (Table 2).

Table 2. Electrospray ionization mass spectrum of [CpCr(CO)₂(SBz)]₂ (**6**)

m/z	Assignments
592	[Cp ₂ Cr ₂ (CO) ₄ Bz ₂ S ₂]
560	[Cp ₂ Cr ₂ (CO) ₄ Bz ₂ S]
468	[Cp ₄ Cr ₄]
401	[CpCr ₄ S ₄]
378	[CpCr(CO) ₂] ₂ S
346	[CpCr(CO) ₄ Bz ₂ S]
261	CpCr(CO) ₄ S
237	[CpCr(CO) ₂ S ₂]
205	[CpCr(CO) ₂ S]
149	[CpCrS]

[CpCr(SBz)]₂S (7**)**

The mass spectrum of **7** shows the parent ion $m/z = 512$ [CpCr(SBz)]₂S and its fragmentation ions as listed in Table 3.

Table 3. Electrospray ionization mass spectrum of [CpCr(SBz)]₂S (**7**)

m/z	Assignments
500	[Cp ₂ Cr ₂ Bz ₂ S ₃]
468	[Cp ₂ Cr ₂ Bz ₂ S ₂]
401	[CpCr ₄ S ₄]
371	[Cp ₂ Cr ₂ Bz ₂ S]

360

[Cp₂Cr₂S]

295

[CpCr₂S]

149

[CpCrS]

2.1.8 Molecular structure

[CpCr(CO)₂(SBz)]₂ (**6**)

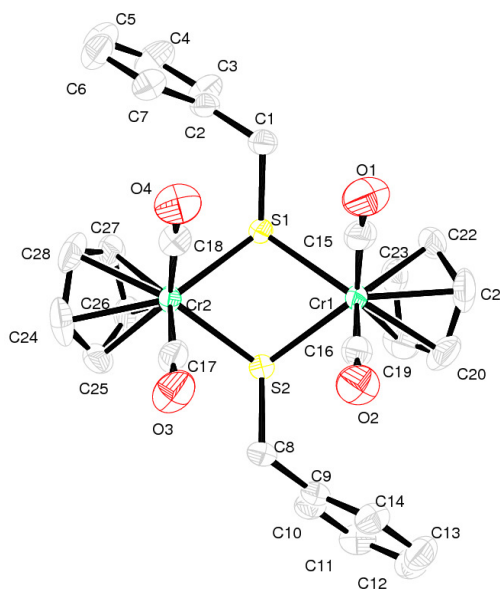


Figure 10. Molecular structure of [CpCr(CO)₂(SBz)]₂ (**6**)

The perspective view of **6** is shown in Figure 10 and its bonding parameters given in Table 4. **6** was found as an isomer of *cis* arrangement of the carbonyl ligands which is different from those of [CpM(CO)₂(SPh)]₂ [M = Cr[47], Mo[81]]. As with other related complexes mentioned earlier, **6** also maintained the same type of non-planar Cr₂S₂ fragment. The dihedral angle between Cr(1)-S(1)-Cr(2) and Cr(1)-S(2)-Cr(2) is 35.4(2)° as compared to [CpCr(CO)₂(SPh)]₂ [47] (44.9(2)°). Each chromium atom is in a tetragonal-pyramidal coordination environment with the cyclopentadienyl group occupying the axial position. The two tetragonal pyramids share a basal edge [S(1) . . . S(2)] in an anti-

relationship, the dihedral angle between the two basal planes are being 75.86(7)°. The Cr(1)...Cr(2) separation with 3.702(7) Å is very close to [CpCr(CO)₂(SPh)]₂ (3.808(2) Å) and is much longer than the normal Cr-Cr single bonded complexes, for example, 2.950(2) Å for [CpCr(μ-SPh)(NO)]₂ [82] and 2.906(3) Å for Cp₂Cr₂(NO)₂(μ-SCMe₃)-(μ-S-SCMe₃) [83]. This indicates that the Cr(1)...Cr(2) in **6** is not bonded together.

Table 4. Bond lengths [Å] and angles [°] for [CpCr(CO)₂(SBz)]₂ (**6**)

Bond lengths			
Cr(1)-C(15)	1.827 (2)	Cr(1)...Cr(2)	3.702 (7)
Cr(1)-C(16)	1.829 (3)	S(2)-C(8)	1.843 (2)
Cr(1)-S(1)	2.416 (8)	S(2)...S(1)	2.725 (8)
Cr(1)-S(2)	2.423 (7)	S(1)-C(1)	1.848 (2)
Cr(2)-S(1)	2.405 (7)	O(1)-C(15)	1.152 (3)
Cr(2)-S(2)	2.419 (8)	O(2)-C(16)	1.148 (3)
Cr(2)-C(17)	1.826 (2)	O(3)-C(17)	1.151 (3)
Cr(2)-C(18)	1.828 (2)	O(4)-C(18)	1.152 (3)
Bond angles			
C(15)-Cr(1)-C(16)	74.62 (11)	S(1)-Cr(1)-S(2)	68.54 (2)
C(15)-Cr(1)-S(1)	82.22 (7)	C(15)-Cr(1)...Cr(2)	85.70 (8)
C(16)-Cr(1)-S(1)	124.98 (8)	C(16)-Cr(1)...Cr(2)	88.69 (8)
C(15)-Cr(1)-S(2)	121.41 (8)	S(1)-Cr(1)...Cr(2)	39.72 (16)
C(16)-Cr(1)-S(2)	82.31 (7)	S(1)-Cr(1)...Cr(2)	39.72 (16)
C(17)-Cr(2)-C(18)	74.10 (11)	S(1)-Cr(2)-S(2)	68.79 (18)
C(17)-Cr(2)-S(1)	82.62 (7)	C(17)-Cr(2)...Cr(1)	88.33 (7)
C(18)-Cr(2)-S(1)	122.34 (8)	C(18)-Cr(2)...Cr(1)	86.68 (7)
C(17)-Cr(2)-S(2)	124.77 (8)	S(1)-Cr(2)...Cr(1)	39.95 (14)
C(18)-Cr(2)-S(2)	82.70 (7)	S(2)-Cr(2)...Cr(1)	40.17 (17)
Cr(2)-S(1)-Cr(1)	100.33 (2)	Cr(2)-S(2)-Cr(1)	99.73 (2)
Cr(1)-S(1)-S(2)	55.84 (2)	Cr(1)-S(2)-S(1)	55.61 (2)
Cr(2)-S(1)-S(2)	55.86 (2)	Cr(2)-S(2)...S(1)	55.35 (19)
C(1)-S(1)...S(2)	157.45 (8)	C(8)-S(2)-Cr(2)	115.14 (8)
		C(8)-S(2)-Cr(1)	114.04 (7)
		C(8)-S(2)...S(1)	158.67 (8)
O(1)-C(15)-Cr(1)	177.30 (2)	O(3)-C(17)-Cr(2)	176.10 (2)
O(2)-C(16)-Cr(1)	175.80 (2)	O(4)-C(18)-Cr(2)	176.60 (2)

Symmetry transformations used to generate equivalent atoms: # x, y, z; -x, -y, -z

2.2 Studies of [CpMo(CO)₃]₂ (**3**) with Bibenzyl Trisulfide

2.2.1 The reaction of [CpMo(CO)₃]₂ (**3**) with equimolar Bibenzyl Trisulfide

A reddish purple solution of [CpMo(CO)₃]₂ (**3**) in toluene reacted with Bz₂S₃ rigorously at 60 °C with stirring for 3.5 h. The resultant reddish brown solution had led to the isolation of [CpMo(CO)₂(SBz)]₂ (**9**), [CpMo(SBz)S]₂ (**10a** & **b**), and [CpMo(CO)(SBz)]₂S (**11**) in 16.3%, 61.3% and 2.9% yield, respectively. Thermolysis of [CpMo(CO)₂(SBz)]₂ (**9**) at 60 °C for 14.5 h has resulted in the isolation of **10** and **11** in 16.3 and 25.9% yields, respectively. Prolonged thermolysis of **9** at an elevated temperature of 100 °C for 18 h resulted in the isolation of [CpMo(SBz)(S)]₂ (**10**) in 25.0% yield. NMR tube reaction study of **9** under similar thermolytic condition, but in the presence of Bz₂S₃, gave higher yields of **10** (49%) and **11** (31%). Likewise, thermolysis of **11** in the presence of Bz₂S₃ also resulted in a higher yield of **10** (47%). The product [CpMo(CO)(SBz)]₂ (**12**) was not isolated but its presence was observed in the NMR tube reaction.

2.2.2 NMR spectral studies

(a) Reaction of [CpMo(CO)₂(SBz)]₂ with Bz₂S₃ at 60 °C

A time dependent variation of the product composition from the reaction of [CpMo(CO)₂(SBz)]₂ (**9**) with one mole equivalent of Bz₂S₃ in benzene-*d*₆ at 60 °C has been studied *via* ¹H NMR scans. After 1 h, the major product formed is [CpMo(CO)(SBz)]₂S (**11**) (28% yield) together with smaller amounts of [CpMo(CO)(SBz)]₂ (**12**) (9% yield), [CpMo(SBz)(S)]₂ (**10**) (27% yield), and the unreacted [CpMo(CO)₂(SBz)]₂ (**9**) (33% recovery). A gradual increase in the products **10**, **11** and **12** with time was observed. Finally, all of **9** has converted to other secondary products after 9.5 h. The result obtained from this reaction is tabulated in Table 5.

Table 5. Variation of product composition^a from the reaction of [CpMo(CO)₂(SBz)]₂ (**9**) with Bz₂S₃ at 60 °C

Complexes (%) Time (h)	[CpMo(CO) ₂ (SBz)] ₂ (9)	[CpMo(SBz)(S)] ₂ (10)	[CpMo(CO)(SBz)] ₂ S (11)	[CpMo(CO)(SBz)] ₂ (12)
1	33	27	28	9
5.5	3	40.8	33	12
7.5	0.8	45.6	36.8	9.6
9.5	0	49	31	5.3

^a - Product yields by integration of Cp resonances in ¹H NMR spectrum of products mixture

(b) Reaction of [CpMo(CO)(SBz)]₂S (11**) with Bz₂S₃ at 110 °C**

A pinkish brown solution of [CpMo(CO)(SBz)]₂S (20 mg, 0.030 mmol) in *d*₈-toluene (0.6 mL) in a 5 mm NMR tube was heated with an equivalent of Bz₂S₃ (8 mg, 0.030 mmol) at 110 °C for 15 h. The ¹H NMR spectrum showed that the final resultant solution consists of [CpMo(SBz)(S)]₂ (**10**) (47% yield) together with some uncharacterized dark brown precipitates.

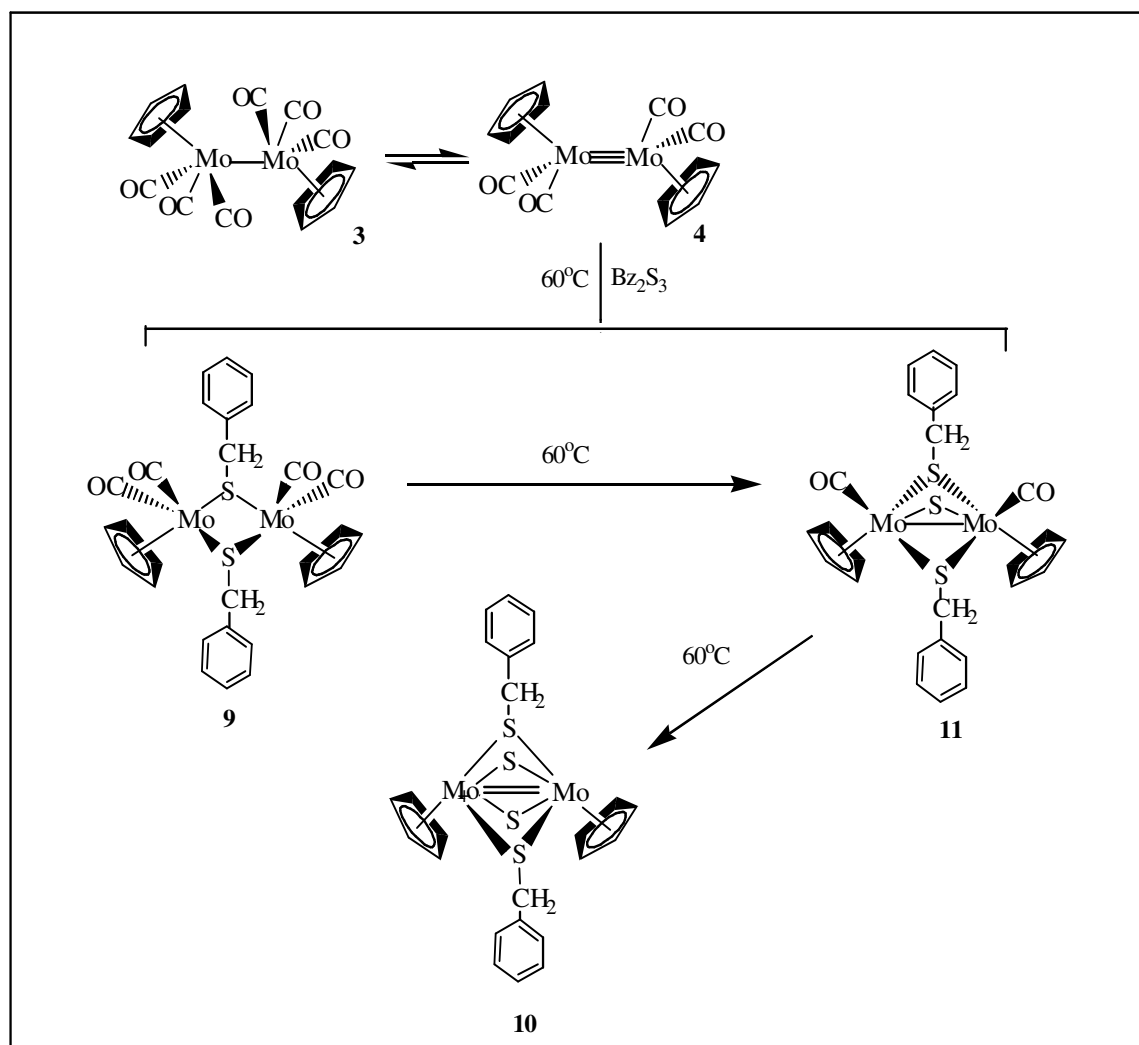
2.2.3 Thermolysis studies of [CpMo(CO)₂(SBz)]₂ (9**) and [CpMo(CO)(SBz)]₂S (**11**)**

A reddish brown solution of [CpMo(CO)₂(SBz)]₂ (**9**) in toluene was thermolyzed at 60 °C for 14.5 h which led to the isolation of [CpMo(SBz)(S)]₂ (**10**) and [CpMo(CO)(SBz)]₂S (**11**) in 16.3% and 25.9% yields, respectively. A pinkish brown solution of [CpMo(CO)(SBz)]₂S (**11**) heated at 110 °C for 18 h only gave [CpMo(SBz)(S)]₂ in 25% yield as the only isolated product. This observation indicates that **9** is the primary product which subsequently undergoes further degradation to give [CpMo(CO)(SBz)]₂S (**11**) as a secondary product and finally to the ultimate total decarbonylated product **10**.

2.2.4 Mechanistic pathways: Formation of $[\text{CpMo}(\text{CO})_2(\text{SBz})]_2$ (**9**), $[\text{CpMo}(\text{SBz})\text{S}]_2$ (**10a & b**), and $[\text{CpMo}(\text{CO})(\text{SBz})]_2\text{S}$ (**11**)

A major consequence of reactions involving organic disulfides (RSSR) is the susceptibility of their S-S linkage to be cleaved by nucleophilic, electrophilic or radical processes [50, 79a, 84]. The closely related organic trisulfides (RSSSR) having two adjacent sulfur-sulfur bonds as in Bz_2S_3 is expected to undergo similar desulfurization process as well. In this case, the desulfurization process is targeted towards the central sulfur of the -S-S-S- linkage which is rationalized by the hard-soft acid-base (HSAB) theory developed by Pearson [85]. According to this hypothesis, considered independently by Harpp [80] and Ho [86], the central sulfur atom being bonded to two soft sulfur atoms, would be a softer acceptor than a terminal sulfur atom that is bonded to a carbon atom. For this reaction, it is postulated that the coordination of the thiobenzyl moiety from the desulfurized Bz_2S_3 has led to the formation of the thiolate-bridged dimer $[\text{CpMo}(\text{CO})_2(\text{SBz})]_2$ (**9**) which was observed previously in a similar reaction with the Cr analogue [87]. Initial isolation of **9** which undergoes stepwise decarbonylation to yield $[\text{CpMo}(\text{CO})(\text{SBz})]_2\text{S}$ (**11**) and finally to the completely decarbonylated $[\text{CpMo}(\text{SBz})(\text{S})]_2$ (**10**) after prolonged thermolysis indicates that **9** is a primary product (Scheme 20). The partial decarbonylation of **9** results in the loss of two carbonyl ligands but proceeds with a formal insertion of an S(0) atom across the singly-bonded Mo center to form the Mo-(μ_2 -S)-Mo bridged complex **11**. Finally, **11** succumbed to complete decarbonylation, coupled with concomitant sulfur insertions which ultimately give rise to the mixed quadruply thiolato-bridged complex **10**. A different synthetic route reported by Franz *et al.* [88] involves a two-step exchange of both the μ_2 -SH groups from $[\text{CpMo}(\mu\text{-S})(\mu\text{-SH})]_2$ with benzylthiol to give the final dibenzyl substituted cluster similar to **10** which was characterized by NMR spectroscopy. As with the Cr analogue, $[\text{CpMo}(\text{CO})_3]_2$ (**3**) also

demonstrates the ability to desulfurize trisulfides to disulfides and monosulfides in an effective manner.



Scheme 20. Proposed synthetic pathway for the reaction of $[\text{CpMo}(\text{CO})_3]_2$ (**3**) with Bz_2S_3

2.2.5 Physical properties

[CpMo(CO)₂(SBz)]₂ (**9**)

The complex exists as dark brown crystalline solids, stable at ambient temperature under an inert atmosphere and air-stable for extended periods at ambient temperature. It is soluble in *n*-hexane/toluene mixture giving a dark brown solution which is fairly stable at room temperature under an inert atmosphere.

[CpMo(SBz)S]₂ (**10a & b**)

10a exists as a pink crystalline precipitate whereas **10b** exists as a dark pink crystalline precipitate. Both isomers are stable at ambient temperature under an inert atmosphere and are air-stable for extended periods at ambient temperature. Both of the complexes are slightly soluble in toluene but are easily soluble in ether giving a pink and brownish pink solution, respectively.

[CpMo(CO)(SBz)]₂S (**11**)

Complex **11** exists as pinkish brown crystalline solids. It is stable at ambient temperature under an inert atmosphere and as well as being air-stable for extended periods at ambient temperature. **11** is soluble in ether to give a pinkish brown solution.

2.2.6 Spectral properties

2.2.6.1 IR spectra

[CpMo(CO)₂(SBz)]₂ (**9**)

The IR spectrum in nujol shows $\nu(\text{CO})$ stretching frequencies at 1944vs, 1918s, 1849vs, 1831sh, other bands, 1067vw, 1029vw, 1009w, 842w, 808m, 768w, 700m cm⁻¹ (refer to Appendix I).

[CpMo(SBz)S]₂ (10a & 10b)

The IR spectra for both **10a** and **10b** in nujol showed the same stretching frequencies at 1667m, 1599w, 1317w, 1277m, 1008w, 808m, 698s cm⁻¹ (refer to Appendix I). A comparison of the I.R. spectra for both **10a** and **10b** are shown in Appendix I.

[CpMo(CO)(SBz)]₂S (11)

The IR spectrum in nujol shows $\nu(\text{CO})$ stretching frequencies at 1925vs, 1869s, 1846sh cm⁻¹; with other bands at 1061vw, 1031vw, 1011vw, 813m, 760m, 700m cm⁻¹ (refer to Appendix I).

2.2.6.2 NMR spectra

[CpMo(CO)₂(SBz)]₂ (9)

The complex is highly symmetrical and is similar to its Cr analogue which only contains a singlet for both Cp signal at δ 4.61 and -CH₂-S signal at δ 3.69 in the ¹H NMR spectrum in benzene-*d*₆. In the ¹³C NMR spectrum, the Cp signal was recorded at δ 96.72, -CH₂-S signal at δ 38.85, C₆H₅- signals at δ 144.15, 130.32, 128.73, 127.72 and a singlet for CO at δ 256.67 in benzene-*d*₆.

[CpMo(SBz)S]₂ (10a & b)

Even though both complexes **10a** and **10b** are polymorphic, they possess different chemical shifts in their ¹H and ¹³C NMR spectra. In the ¹H NMR (benzene-*d*₆) for **10a**, Cp signal is at δ 5.89 and -CH₂-S signal is at δ 2.72; for **10b**, Cp signal is at δ 5.84 and -CH₂-S signal is at δ 2.78. In the ¹³C NMR (benzene-*d*₆) for **10a**, the Cp signal is at δ 98.19, -CH₂-S signal is at δ 38.8 and C₆H₅- signals are at δ 142.26, 129.79, 129.62; for **10b**, the Cp

signal is at δ 97.95, the $-\text{CH}_2\text{-S}$ signal is at δ 41.57 and the $\text{C}_6\text{H}_5\text{-}$ signals are at δ 142.05, 130.32, 129.37.

[CpMo(CO)(SBz)]₂S (11)

Complex **11** is a symmetrical molybdenum dimer and the Cp rings show a signal as a singlet in the ^1H NMR (benzene-*d*₆) at δ 4.83 and the $-\text{CH}_2\text{-S}$ signal is at δ 4.02. In the ^{13}C NMR (benzene-*d*₆), the Cp rings signal was recorded at δ 91.03, while the $-\text{CH}_2\text{-S}$ signal is at δ 49.37, $\text{C}_6\text{H}_5\text{-}$ signals are at δ 143.10, 128.74 and the CO signal at δ 244.10. All the Cp, $-\text{CH}_2\text{-S}$ and CO moieties only showed one signal in either the ^1H or ^{13}C NMR spectra which agreed with the molecular structure as analyzed by the single crystal X-ray diffraction analyses.

2.2.7 Molecular Structures

[CpMo(CO)₂(SBz)]₂ (9)

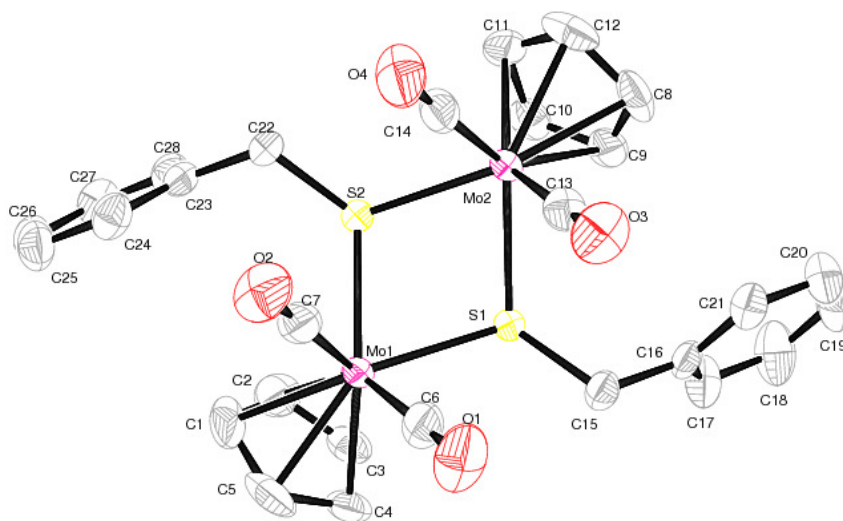


Figure 11. Molecular structure of [CpMo(CO)₂(SBz)]₂ (**9**)

The molecular structure of compound **9** as illustrated in Figure 11 is isostructural to that of the above mentioned chromium analogue but is not isostructural with the similar

molybdenum compound of $[\text{CpMo}(\text{CO})_2(\text{SPh})]_2$ which was synthesized by Benson *et al*[39]. The bond lengths and angles for $[\text{CpMo}(\text{CO})_2(\text{SBz})]_2$ (**9**) are shown in Table 6. The two pairs of carbonyl ligands in **9** are in the *cis*-configuration which is different from $[\text{CpMo}(\text{CO})_2(\text{SPh})]_2$. The similarity between **9** and $[\text{CpMo}(\text{CO})_2(\text{SPh})]_2$ indicates that their Cp rings both adopt a mutually *trans*-configuration and the benzyl moiety are *anti* with respect to the S1---S2 vector. The Mo---Mo distance of 3.836 Å is slightly shorter than the Mo---Mo distance found in $[\text{CpMo}(\text{CO})_2(\text{SPh})]_2$ (3.940(2) Å) but is much longer than that in $[\text{CpMo}(\text{CO})_3]_2$ (3.235 Å) (A comparison of the Mo-Mo bonds and the Mo-S bonds shown in Table 7). The absence of any metal-metal bonding in **9** is in agreement with the eighteen electron rule.

Table 6. Bond lengths [Å] and angles [deg] for $[\text{CpMo}(\text{CO})_2(\text{SBz})]_2$ (**9**).

Bond lengths			
Mo(1)-C(25)	1.951 (3)	Mo(2)-S(2)	2.516 (6)
Mo(1)-C(26)	1.947 (3)	S(1)-C(11)	1.843 (2)
Mo(1)-S(1)	2.521 (7)	S(2)-C(18)	1.842 (2)
Mo(1)-S(2)	2.512 (7)	O(1)-C(25)	1.162 (3)
Mo(2)-C(27)	1.944 (3)	O(2)-C(26)	1.160 (3)
Mo(2)-C(28)	1.959 (3)	O(3)-C(27)	1.166 (3)
Mo(2)-S(1)	2.522 (6)	O(4)-C(28)	1.148 (3)
Bond angles			
C(1)-Mo(1)-S(2)	116.9 (1)	C(28)-Mo(2)-S(2)	126.5 (1)
C(1)-Mo(1)-S(1)	85.9 (1)	S(1)-Mo(2)-S(2)	69.6 (1)
S(1)-Mo(1)-S(2)	69.7 (1)	C(11)-S(1)-Mo(1)	113.5 (9)
C(8)-Mo(2)-S(1)	88.0 (1)	C(11)-S(1)-Mo(2)	114.1 (8)
C(8)-Mo(2)-S(2)	101.9 (1)	Mo(1)-S(1)-Mo(2)	99.1 (2)
C(9)-Mo(2)-S(1)	101.7 (1)	C(18)-S(2)-Mo(1)	112.2 (8)
C(9)-Mo(2)-S(2)	136.3 (1)	C(18)-S(2)-Mo(2)	112.6 (8)
C(10)-Mo(2)-S(1)	137.4 (1)	Mo(1)-S(2)-Mo(2)	99.5 (2)
C(10)-Mo(2)-S(2)	137.1 (1)	O(1)-C(25)-Mo(1)	176.1 (2)
C(27)-Mo(2)-S(1)	120.1 (1)	O(2)-C(26)-Mo(1)	177.6 (2)
C(27)-Mo(2)-S(2)	83.6 (1)	O(3)-C(27)-Mo(2)	178.1 (2)
C(28)-Mo(2)-S(1)	82.7 (1)	O(4)-C(28)-Mo(2)	176.6 (2)

Symmetry transformations used to generate the equivalent atoms:

Table 7. Comparison of Mo-Mo bonds and Mo-S bonds

Complex	Mo-Mo (Å)	Mo-S (sulfido) (Å)	Mo-S (thiolato) (Å)	Ref.
Cp ₂ Mo ₂ (CO) ₆ (3)	3.235	-	-	7b, 89
[CpMo(CO) ₂ (SBz)] ₂ (9)	-	-	2.512(7) 2.521(7)	90
[CpMo(CO)(SBz)] ₂ S (11)	2.802	2.437(2)	2.460(2) 2.452(2)	91
[CpMo(SBz)S] ₂ (10a)	2.579(7)	2.341(1) 2.355(1)	2.465(1) 2.478(1)	92
[CpMo(SBz)S] ₂ (10b)	2.581(5)	2.352(1) 2.344(1)	2.479(1) 2.476(1)	92
[CpMo(CO) ₂ (SPh)] ₂	3.940(2)	-	2.553(3) 2.530(3)	39
[CpMo(CO) ₂ (S ^t Bu)] ₂	2.616(2)	-	2.422(2) 2.415(4)	39
[CpMo(SPh)(O)(μ-O)] ₂	-	-	2.369(3)	39

[CpMo(SBz)S]₂ (**10a** & **b**)

[CpMo(SBz)S]₂ (**10**) can be obtained as two polymorphous species. **10a** crystallizes in the space group *Pcba* of the orthorhombic system and **10b** in the space group *P2₁/c* of the monoclinic system. The ORTEP plots of **10a** and **10b** are presented in Figure 12 and 13 respectively with the atomic numbering scheme as indicated. The selected bond lengths and angles of **10a** and **10b** are shown in Table 8. Both compounds consist of a Mo₂S₄ framework with the Mo atom possessing a pseudo-pentagonal bipyramidal geometry and features a nearly square-planar arrangement of the four sulfur atoms, perpendicular to the Mo-Mo bond and almost parallel to the two (η⁵-C₅H₅) planes. Their phenyl groups which attached to the thiolato bridges are in an equatorial-axial configuration and are *trans*

to each other. The quadruply thiolato-bridged complex belongs to a well characterized group of structures which contain a $\text{Mo}_2(\mu\text{-S})_4$ residue such as $\text{Cp}^*_2\text{Mo}_2(\mu\text{-SCH}_3)_2(\mu\text{-S})_2$ ($\text{Cp}^* = \eta^5\text{-pentamethylcyclopentadienyl}$) [93], $\text{Cp}_2\text{Mo}_2(\mu_2\text{-SCH}_3)_4$ [94], $\text{Cp}'_2\text{Mo}_2(\mu_2\text{-SCH}_3)_2(\mu_2\text{-S})_2$ ($\text{Cp}' = \eta^5\text{-methylcyclopentadienyl}$) [95] and $\text{Cp}''_2\text{Mo}_2(\mu_2\text{-SCH}_3)_4$ ($\text{Cp}'' = \eta^5\text{-ethyltetramethylcyclopentadienyl}$) [96]. In all these complexes, the formal +4 oxidation state of the Mo atoms would require the existence of a double bond between them, in accordance to the demands of the 18 e rule. Both **10a** and **10b** with the Mo-Mo bond lengths of 2.579(2) and 2.581(5) Å compares very closely to $\text{Cp}^*_2\text{Mo}_2(\mu\text{-SCH}_3)_2(\mu\text{-S})_2$ (2.573(1) Å) and $\text{Cp}'_2\text{Mo}_2(\mu_2\text{-SCH}_3)_2(\mu_2\text{-S})_2$ (2.582(1)) Å bond distances. The four S atoms are bonded in a $\mu\text{-}\eta^2$ -mode. The Mo-S(thiolato) bond distances [average 2.472(1) Å] are significantly longer than the Mo-S(sulfide) distances [average 2.348(1) Å] resulting in a more acute Mo1-S1-Mo1^i angle. It is likely that these observations arise due to greater steric repulsions between the SBz group and an S substituent.

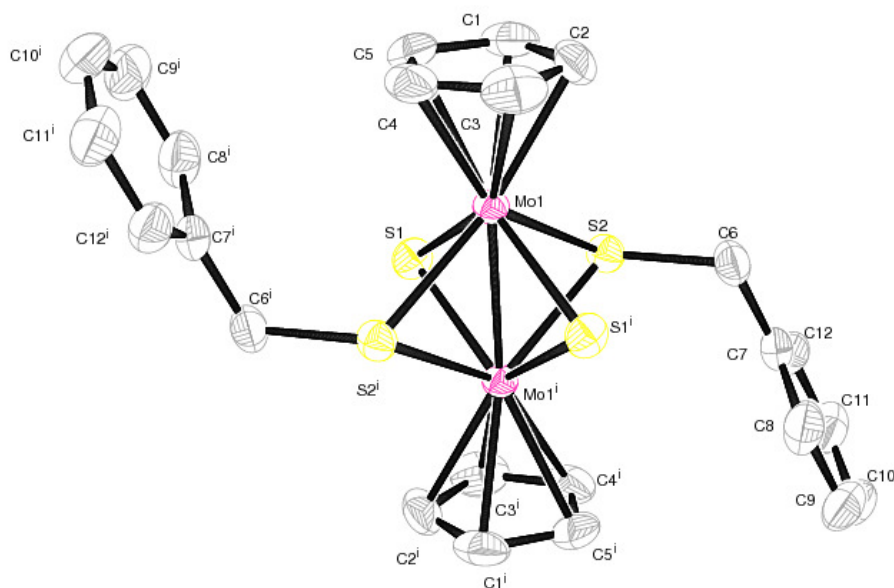


Figure 12. Molecular structure of the orthorhombic modification of $[\text{CpMo}(\text{SBz})\text{S}]_2$ (**10a**)

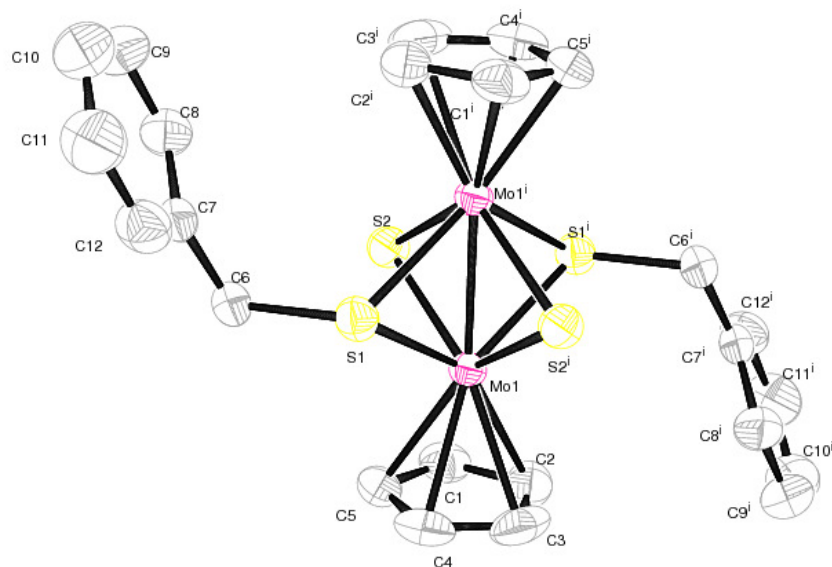


Figure 13. Molecular structure of the monoclinic modification of $[\text{CpMo}(\text{SBz})\text{S}]_2$ (**10b**)

Table 8. Bond lengths (Å) and angles (°) for **10a** and **10b**

<i>Bond lengths (Å)</i>		
	10a	10b
Mo1–C1	2.339(4)	2.325(3)
Mo1–C2	2.346(5)	2.312(4)
Mo1–C3	2.348(5)	2.334(4)
Mo1–C4	2.327(4)	2.350(3)
Mo1–C5	2.315(4)	2.351(3)
Mo1–S1	2.465(1)	2.479(1)
Mo1–S1 ⁱ	2.478(1)	2.476(1)
Mo1–S2	2.341(1)	2.352(1)
Mo1–S2 ⁱ	2.355(1)	2.344(1)
Mo1–Mo1 ⁱ	2.579(2)	2.581(5)
<i>Bond angles (°)</i>		
S1–Mo1–S1 ⁱ	117.1(1)	113.3(1)
S1–Mo1–S2	77.3(1)	69.7(1)
S1–Mo1–S2 ⁱ	69.6(1)	76.8(1)
S1 ⁱ –Mo1–S2	69.6(1)	76.9(1)
S1 ⁱ –Mo1–S2 ⁱ	76.8(1)	69.9(1)
S2–Mo1–S2 ⁱ	113.4(1)	117.2(1)
Mo1–S1–Mo1 ⁱ	62.9(3)	66.7(2)
Mo1–S2–Mo1 ⁱ	66.6(3)	62.8(2)

Symmetry transformation: $i = 1 - x, 1 - y, 1 - z$.

[CpMo(CO)(SBz)]₂S (**11**)

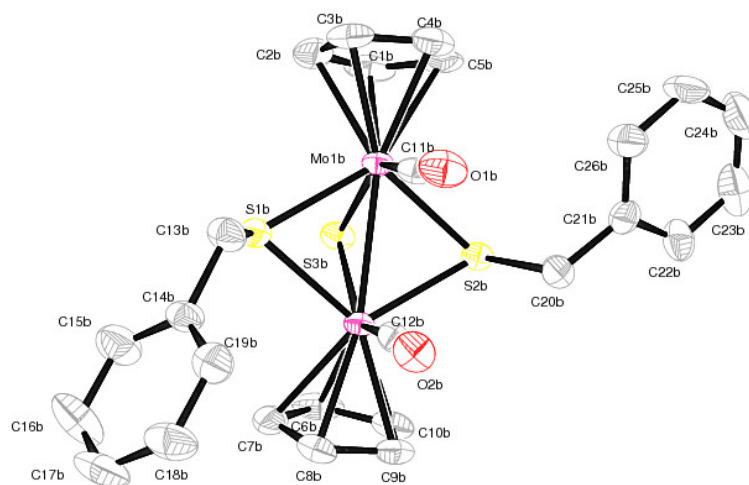


Figure 14. Molecular structure of [CpMo(CO)(SBz)]₂S (**11**)

The product [CpMo(CO)(SBz)]₂S (**11**) (Figure 14), differs from [CpMo(CO)₂(SBz)]₂ (**9**) (Figure 12) by having a sulfide linkage in addition to the two bibenzylthiolate linkages. In the related reaction of [CpCr(CO)₃]₂ with diphenyl disulfide, one of the products is [CpCr(C₆H₅S)]₂S, but the carbonyl ligands was cleaved in the reaction [47] as shown in Scheme 10. In the present structure, if the cyclopentadienyl ring is considered to occupy three sites, then the geometry of the Mo atom is pseudo-pentagonal bipyramidal.

In the collected data, three independent molecules exist in the asymmetric unit of the triclinic unit cell; one is related to another by a false inversion center and is related to the third by a false translation. In each dinuclear entity, each Mo atom is bonded to a cyclopentadienyl anion and a carbon monoxide molecule; the phenylmethanethiolate groups bridge a pair of Mo atoms, as does the sulfide atom. The cyclopentadienyl ring is considered to occupy three sites, hence the geometry of the Mo atom is pseudo-pentagonal bipyramidal. *C* is by an approximate translation of (1/3, 1/3, 1/3). The false

symmetry/translational symmetry necessitated constraining the five-membered rings to be refined as regular pentagons (C-C = 1.42Å) and the six-membered rings as regular hexagons (C-C = 1.39Å) with H atoms placed at calculated positions in the riding-model approximation [aromatic C-H = 0.94Å and aliphatic C-H = 0.98Å; $U_{\text{iso}}(\text{H}) = 1.2U_{\text{eq}}(\text{C})$]. The final difference Fourier had a large peak at about 1.5Å from atom Mo1a and the deepest hole is approximately 1.5Å from atom C11a. The selected bond lengths and angles of [CpMo(CO)(SBz)]₂S (**11**) are shown in Table 9.

Table 9. Bond lengths [Å] and angles [deg] for [CpMo(CO)(SBz)]₂S (**11**)

Bond lengths			
Mo(1a)-C(11a)	1.952 (8)	Mo(2a)-S(3a)	2.443 (2)
Mo(1a)-S(1a)	2.460 (2)	S(1a)-C(13a)	1.842 (8)
Mo(1a)-S(2a)	2.452 (2)	S(2a)-C(20a)	1.834 (8)
Mo(1a)-S(3a)	2.437 (2)	O(1a)-C(11a)	1.181 (9)
Mo(2a)-C(12a)	1.965 (9)	O(2a)-C(12a)	1.160 (10)
Mo(2a)-S(2a)	2.462 (2)	C(20a)-C(21a)	1.517 (8)
Bond angles			
C(1a)-Mo(1a)-C(11a)	134.3(2)	C(6a)-Mo(2a)-C(12a)	134.2(3)
C(1a)-Mo(1a)-S(1a)	115.9(2)	C(6a)-Mo(2a)-S(1a)	112.5(2)
C(1a)-Mo(1a)-S(2a)	112.4(2)	C(6a)-Mo(2a)-S(2a)	115.2(2)
C(1a)-Mo(1a)-S(3a)	82.2(1)	C(6a)-Mo(2a)-S(3a)	81.5(1)
C(2a)-Mo(1a)-C(11a)	112.4(3)	C(7a)-Mo(2a)-C(12a)	111.9(3)
C(2a)-Mo(1a)-S(1a)	94.1(1)	C(7a)-Mo(2a)-S(1a)	147.5(1)
C(2a)-Mo(1a)-S(2a)	147.4(2)	C(7a)-Mo(2a)-S(2a)	93.6(1)
C(2a)-Mo(1a)-S(3a)	100.3(1)	C(7a)-Mo(2a)-S(3a)	99.4(2)
C(3a)-Mo(1a)-C(11a)	78.6(2)	C(8a)-Mo(2a)-C(12a)	78.2(3)
C(3a)-Mo(1a)-S(1a)	106.1(2)	C(8a)-Mo(2a)-S(1a)	141.8(2)
C(3a)-Mo(1a)-S(2a)	141.2(2)	C(8a)-Mo(2a)-S(2a)	105.9(1)
C(3a)-Mo(1a)-S(3a)	135.9(1)	C(8a)-Mo(2a)-S(3a)	135.0(2)
C(4a)-Mo(1a)-C(11a)	76.6(3)	C(9a)-Mo(2a)-C(12a)	76.8(3)
C(4a)-Mo(1a)-S(1a)	141.3(2)	C(9a)-Mo(2a)-S(1a)	105.9(2)
C(4a)-Mo(1a)-S(2a)	105.4(1)	C(9a)-Mo(2a)-S(2a)	141.3(2)
C(4a)-Mo(1a)-S(3a)	136.9(2)	C(9a)-Mo(2a)-S(3a)	136.5(1)
C(5a)-Mo(1a)-C(11a)	109.3(3)	C(10a)-Mo(2a)-C(12a)	109.7(3)
C(5a)-Mo(1a)-S(1a)	150.8(2)	C(10a)-Mo(2a)-S(1a)	91.8(1)
C(5a)-Mo(1a)-S(2a)	91.5(1)	C(10a)-Mo(2a)-S(2a)	150.1(2)
C(5a)-Mo(1a)-S(3a)	101.3(2)	C(10a)-Mo(2a)-S(3a)	101.0(2)
C(11a)-Mo(1a)-S(1a)	90.5(2)	C(12a)-Mo(2a)-S(1a)	90.1(2)
C(11a)-Mo(1a)-S(2a)	89.0(2)	C(12a)-Mo(2a)-S(2a)	90.5(2)
C(11a)-Mo(1a)-S(3a)	143.5(2)	C(12a)-Mo(2a)-S(3a)	144.2(2)

S(1a)-Mo(1a)-S(2a)	110.7(1)	S(1a)-Mo(2a)-S(3a)	70.59(7)
S(1a)-Mo(1a)-S(3a)	70.6(1)	S(1a)-Mo(2a)-S(2a)	110.55(7)
S(2a)-Mo(1a)-S(3a)	70.2(1)	S(2a)-Mo(2a)-S(3a)	69.99(7)
C(13a)-S(1a)-Mo(2a)	112.5(3)	Mo(1a)-S(2a)-Mo(2a)	69.36(5)
C(13a)-S(1a)-Mo(1a)	113.4(3)	Mo(1a)-S(3a)-Mo(2a)	69.90(5)
Mo(2a)-S(1a)-Mo(1a)	69.35(5)	O(1a)-C(11a)-Mo(1a)	173.8(6)
C(20a)-S(2a)-Mo(1a)	112.0(3)	O(2a)-C(12a)-Mo(2a)	174.0(7)
C(20a)-S(2a)-Mo(2a)	113.0(3)	C(14a)-C(13a)-S(1a)	111.1(5)

2.3 Studies of [CpCr(CO)₃]₂ (1) with Bibenzyl Disulfide

2.3.1 Study of [CpCr(CO)₃]₂ (1) with equimolar Bibenzyl Disulfide

A deep green suspension of [CpCr(CO)₃]₂ (1) was reacted with equimolar Bz₂S₂ under rigorous stirring at ambient temperature. The reaction was completed in 13.5 h and the color of the reaction mixture had changed to dirty brown. Isolation of the products *via* column chromatography gave [CpCr(CO)₂(SBz)]₂ (42.6% yield) as the primary products, with [CpCr(CO)₂]₂S (28.8% yield) as the secondary product and [CpCr(SBz)]₂S (11.8% yield) as the total decarbonylated product. A similar reaction at 110 °C for 1 h, yielded only [CpCr(CO)₂]₂S (53.7% yield) and the final thermolyzed product of Cp₄Cr₄S₄ (15.4% yield). No new products were isolated in this reaction when we compared to the previous reported reaction of [CpCr(CO)₃]₂ (1) with an equimolar amount of Bz₂S₃. The expected common product with a framework similar to [CpCr(CO)(EPh)]₂ (E = S, Se, Te) [47-49] was not isolated in this reaction.

2.3.2 Study of [CpCr(CO)₂]₂ (2) with equimolar bibenzyl disulfide

A deep green suspension of [CpCr(CO)₂]₂ (2) was reacted with equimolar bibenzyl disulfide and heated vigorously at 110 °C to completion in 1 h. Two products,

[CpCr(CO)₂]₂S (**5**) (40.3 % yield) and Cp₄Cr₄S₄ (**8**) (10.6 % yield) were eluted out *via* column chromatography. An uncharacterized dark brown fraction which was eluted out with ether/THF solution gave dark brown solids (62 mg) when dried under *vacuo*.

2.3.3 NMR spectral studies

(a) Reaction of [CpCr(CO)₂]₂ (**2**) with equimolar bibenzyl disulfide at 60 °C

The reaction of **2** with equimolar Bz₂S₂ at 60 °C has been monitored *via* ¹H NMR in benzene-*d*₆ at intervals for which the product compositions are given in Table 10. After 2 h, the spectrum showed the presence of [CpCr(CO)₂]₂S (**5**) (4.4% yield), [CpCr(SBz)]₂S (**7**) (5.5% yield), Cp₄Cr₄S₄ (**8**) (5.6% yield) together with unreacted [CpCr(CO)₂]₂ (**2**) (59.5% recovery). After 4 h, the yield for [CpCr(CO)₂]₂S (**5**), [CpCr(SBz)]₂S (**7**) and Cp₄Cr₄S₄ (**8**) increased gradually to 15.9%, 9.2% and 11.2%, respectively. Subsequently, after 6 h, the relative yield of **5** has increased to 28.3%. However, the yield of **7** and **8** has decreased to 3.9% and 19%, together with unreacted [CpCr(CO)₂]₂ (**2**) (9.7% recovery).

Table 10. Variation of product composition^a from the reaction of [CpCr(CO)₂]₂ (**2**) with Bz₂S₂ at 60 °C

Time (h) \ Complexes (%)	[CpCr(CO) ₂] ₂ (2)	[CpCr(CO) ₂] ₂ S (5)	[CpCr(SBz)] ₂ S (7)	Cp ₄ Cr ₄ S ₄ (11)
1	79.4	0.19	0	2.8
2	59.5	4.4	5.5	5.6
3	34.7	8.3	7.5	8.2
4	23.0	15.9	9.2	11.2
5	15.8	25.3	8.0	8.0
6	9.7	28.3	3.9	9.0

^a - Product yields by integration of Cp resonances in ¹H NMR spectrum of products mixture

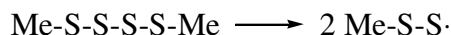
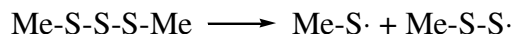
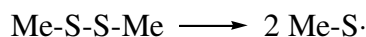
(b) **Reaction of [CpCr(CO)₂]₂S (5) equimolar Bibenzyl Disulfide at 60 °C**

No intermediate product was observed except for Cp₄Cr₄S₄ (8) (6.5 % yield) which is the final thermolytic product of 5 after 5 h.

2.3.4 Mechanistic pathways: Formation of [CpCr(CO)₂(SBz)]₂ (6) and [CpCr(SBz)]₂S (7)

The products isolated from the reaction of [CpCr(CO)_n]₂ (n = 2 or 3) with one equivalent of Bz₂S₂ or Bz₂S₃ are similar but in different yields as mentioned in Section 2.1.

It is assumed that both ligands exhibit different reactivity towards the chromium dimer whereas the disulfide ligand requires a higher thermal energy to initiate the reaction. This finding agrees with the higher dissociation energy of the disulfide ligand (+69 kcal/mole) as compared to the trisulfide ligand (+46 kcal/mole) as reported by Tobolsky *et al* [97] using Me-S_n-Me (n = 2, 3 or 4) as the reference models (Table 11) and it explains why the bond scission between the -S-S- linkage is less facile than that of the -S-S-S- linkage as mentioned by Harpp [80] and Ho [86] in the previous Chapter 2.2.4. As similar hypothesis was also invoked by Gee [98] where it was suggested that fragments containing more than one sulfur atom may be stabilized by resonance interaction of the free electron with the sulfur chain. Using this concept, the preferable fragmentation patterns could be as follows:-



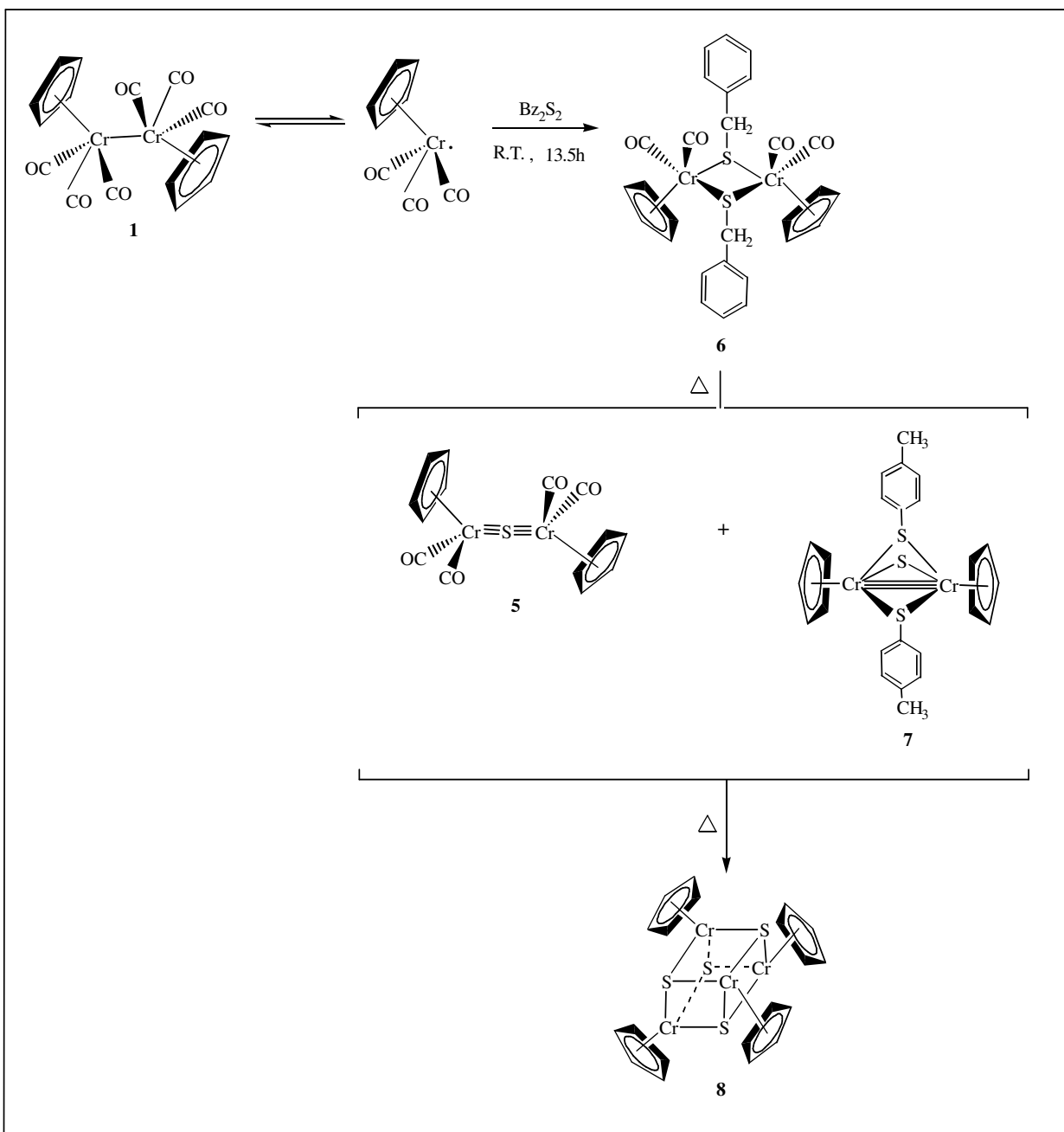
If the Me — S \equiv S fragments are indeed more stable than the Me-S \cdot fragments, then the predicted ease of cleavage of the polysulfide linkage is in the order of disulfide < trisulfide < tetrasulfide \sim S₈ \sim polymeric sulfur.

Table 11. Dissociation Energies of polysulfide [97]

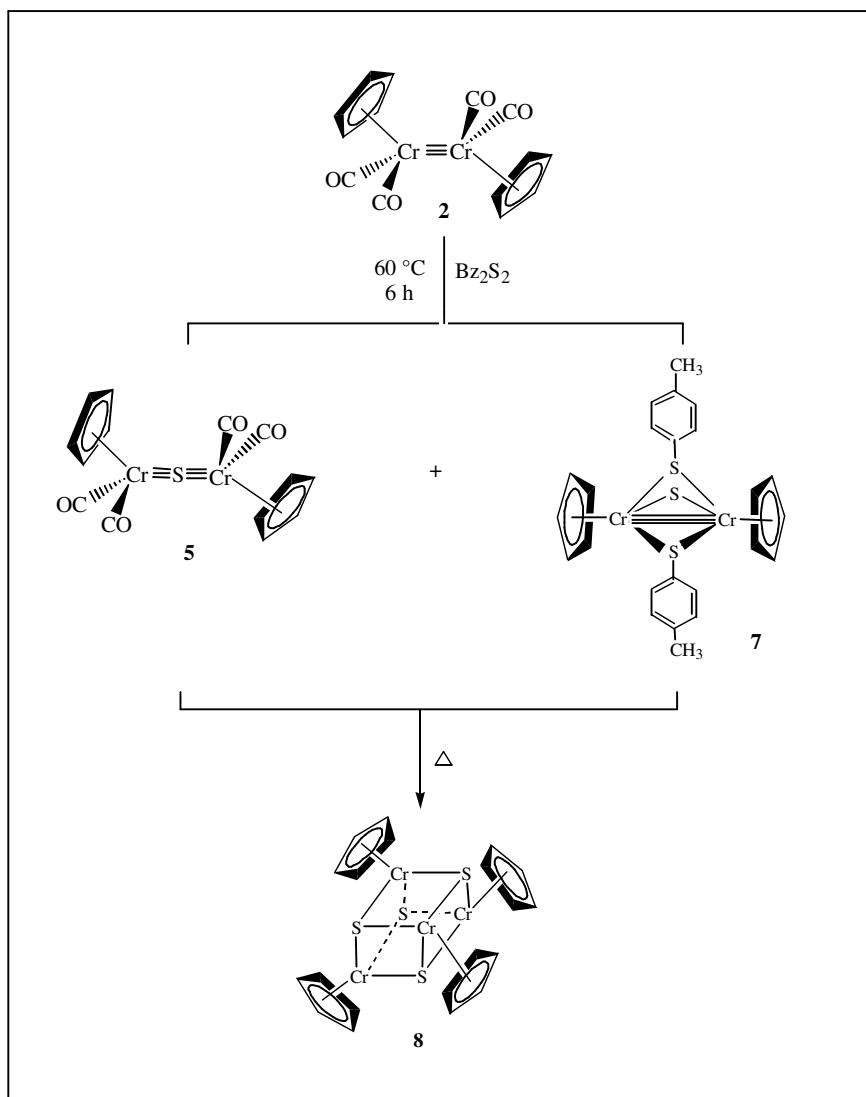
Compound	Dissociation energy (kcal/mole)
Me-S-S-Me	69
Me-S-S-S-Me	46
Me-S-S-S-S-Me	37
S ₈ (ring) \rightleftharpoons \cdot S-S ₆ -S \cdot	33
\cdot S _{x+y} \rightleftharpoons \cdotS_{x} + \cdotS_{y}}}}	33

It was observed that [CpCr(CO)₂(SBz)]₂ (**6**) was only formed in the reaction of [CpCr(CO)₃]₂ (**1**) (Scheme 21) but not of [CpCr(CO)₂]₂ (**2**) (Scheme 22) with Bz₂S₂. This supports the hypothesis that the formation of **6** proceeds *via* the 17e⁻ radical pathway which is generated from **1**. It is theorised that the S-S bond of the ligand is cleaved by these radicals to form a pair of Bz-S \cdot moieties which will further bridge across the two CpCr(CO)₃ \cdot species and decarbonylate to give **6**.

The reduced amount of free sulfur moiety, S \cdot , produced by Bz₂S₂ as compared to Bz₂S₃ has limited the process of sulfur insertion between the Cr dimer to give the triply bonded Cr \equiv S \equiv Cr complex **5** which explains the lower yield of **5** in the reaction with Bz₂S₂. Further thermal degradation of **6** afforded [CpCr(CO)₂]₂S (**5**), [CpCr(SBz)]₂S (**7**) and ultimately the cubane Cp₄Cr₄S₄ (**8**) as the final thermolytic product.



Scheme 21. Proposed synthetic pathway for the reaction of $[\text{CpCr}(\text{CO})_3]_2$ (**1**) with Bz_2S_2



Scheme 22. Proposed synthetic pathway for the reaction of $[\text{CpCr}(\text{CO})_2]_2$ (**2**) with Bz_2S_2

2.3.5 Molecular structure

$[\text{CpCr}(\text{SBz})_2]_2\text{S}$ (**7**)

$[\text{CpCr}(\text{SBz})_2]_2\text{S}$ (**7**) crystallized in monoclinic, space group $C2/c$. A perspective view of **7** is shown in Figure 15 and the bonding parameters are given in Table 12. The structure is very similar to the analogous $[\text{CpCr}(\text{SPh})_2]_2\text{S}$ [47] and bis(μ -*tert*-butylthiolato) complex [99] where the Cr atoms are of +3 oxidation state. The bond distance between

Cr(1)-Cr(2) [2.692 (1) Å] is close to the Cr-Cr distance in the [CpCr(SPh)]₂S [2.676 (1) Å] and bis(μ -*tert*-butylthiolato) complex [2.689 (8) Å] but it is much shorter than the Cr-Cr single bond in [CpCr(CO)₃]₂ [3.281 (1) Å] [3]. This observation indicates that the Cr-Cr bond in **7** is triply-bonded with a 17 e⁻ configuration, which also agrees with the paramagnetic chemical shift found in the ¹H NMR, δ 13.89 (br, Cp, $\nu_{1/2}$ = 57 Hz). Similar to [CpCr(SPh)]₂S, each Cr atom in **7** is in an elongated tetrahedral coordination environment, with the Cp ligand occupying the apical position. The Cr-S (thiolato) bond distance [2.381 (2) Å] in **7** is longer than the Cr-S (sulfido) [2.256 (2) Å] which is possibly due to the partial π -back donation at S(1) which is enhanced by the aromatic ring of the benzyl moiety. The two Cp rings are approximately in an eclipsed configuration about the Cr(1)-Cr(2) bond.

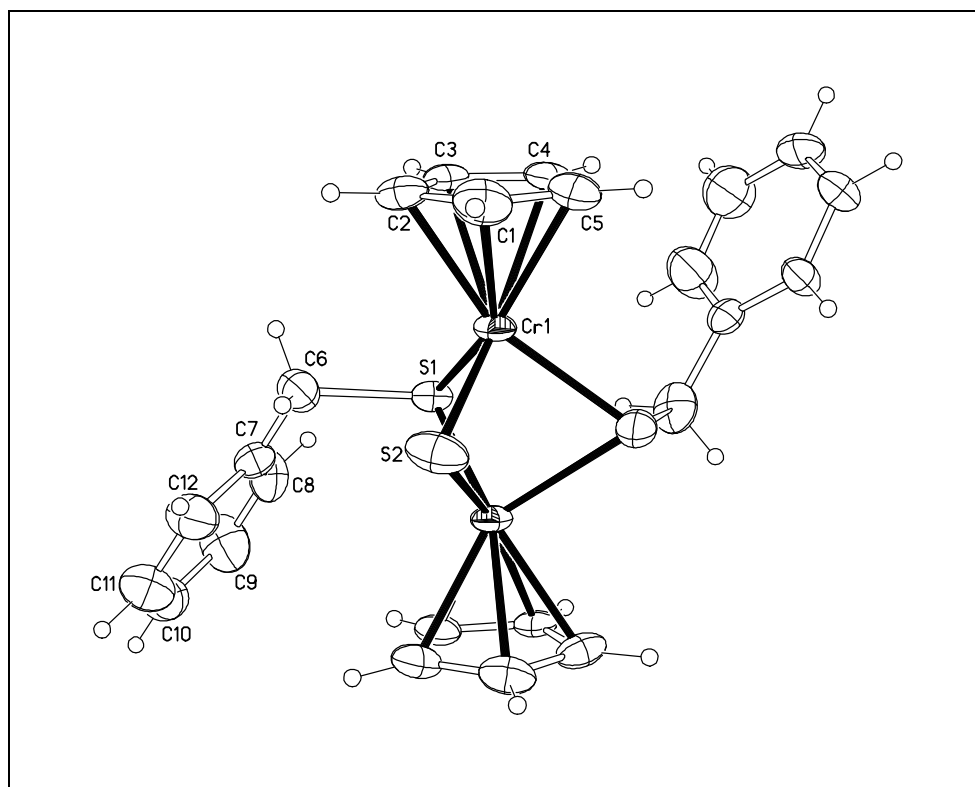


Figure 15. Molecular structure of [CpCr(SBz)]₂S (**7**)

Table 12. Bond lengths [Å] and angles [°] for [CpCr(SBz)]₂S (7)

Bond length			
Cr(1)-Cr(2)	2.692(1)	S(1)-Cr(1)#1	2.328(2)
Cr(1)-S(2)	2.248(2)	S(1')-C(6')	1.931(17)
Cr(1)-S(2)#1	2.256(2)	S(1')-Cr(1)#1	2.381(2)
S(1)-S(1)#1	1.694(4)	S(2)-Cr(1)#1	2.256(2)
S(1)-C(6)	1.933(18)		
Bond angles			
C(1)-Cr(1)-S(2)	95.4(3)	C(1)-Cr(1)-S(2)#1	99.6(2)
C(5)-Cr(1)-S(2)	122.0(4)	C(5)-Cr(1)-S(2)#1	103.0(3)
C(2')-Cr(1)-S(2)	113.8(4)	C(2')-Cr(1)-S(2)#1	139.7(4)
C(3')-Cr(1)-S(2)	150.3(4)	C(3')-Cr(1)-S(2)#1	151.5(4)
C(2)-Cr(1)-S(2)	103.6(2)	C(2)-Cr(1)-S(2)#1	128.7(3)
C(1')-Cr(1)-S(2)	90.8(3)	C(1')-Cr(1)-S(2)#1	103.7(3)
S(2)-Cr(1)-C(4')	139.8(4)	S(2)-Cr(1)-S(2)#1	39.73(15)
S(2)-Cr(1)-C(5')	103.9(3)	C(4')-Cr(1)-S(2)#1	115.3(4)
S(2)-Cr(1)-C(4)	156.9(3)	S(2)#1-Cr(1)-C(5')	91.9(2)
S(2)-Cr(1)-C(3)	137.7(3)	S(2)#1-Cr(1)-C(4)	135.0(4)
		S(2)#1-Cr(1)-C(3)	161.02(18)
S(1)#1-S(1)-C(6)	168.5(7)	C(6')-S(1')-Cr(1)	103.2(7)
S(1)#1-S(1)-Cr(1)#1	69.37(9)	C(6')-S(1')-Cr(1)#1	107.4(10)
C(6)-S(1)-Cr(1)#1	105.5(9)	Cr(1)-S(1')-Cr(1)#1	69.09(7)
S(1)#1-S(1)-Cr(1)	68.14(8)	Cr(1)-S(2)-Cr(1)#1	73.40(8)
C(6)-S(1)-Cr(1)	100.6(6)	C(7)-C(6)-S(1)	108.2(13)
Cr(1)#1-S(1)-Cr(1)	70.31(7)	C(7')-C(6')-S(1')	105.6(14)

Symmetry transformations used to generate equivalent atoms: #1 -x+1,y,-z+1/2

2.4 Studies of $[\text{CpMo}(\text{CO})_2]_2$ (**4**) with Bibenzyl Disulfide

2.4.1 The reaction of $[\text{CpMo}(\text{CO})_2]_2$ (**4**) with equimolar Bibenzyl Disulfide

The reddish brown solution of $[\text{CpMo}(\text{CO})_2]_2$ (**4**) in toluene was reacted with equimolar bibenzyl disulfide at 70 °C for 7.5 h to give a dark yellowish brown reaction mixture from which was isolated a pair of isomeric products, namely *trans-syn* $[\text{CpMo}(\text{CO})(\text{SBz})]_2$ (**12a**) (43.3% yield) and *trans-anti* $[\text{CpMo}(\text{CO})(\text{SBz})]_2$ (**12b**) (34.1% yield), $[\text{CpMo}(\text{SBz})\text{S}]_2$ (**10**) (5.5% yield) and $[\text{CpMo}(\text{CO})(\text{SBz})]_2\text{S}$ (**11**) (3.1% yield). When the same reaction was repeated at 110 °C for 2 h, *trans-syn* $[\text{CpMo}(\text{CO})(\text{SBz})]_2$ (**12a**) (43.58% yield), *trans-anti* $[\text{CpMo}(\text{CO})(\text{SBz})]_2$ (**12b**) (41.4% yield), $[\text{CpMo}(\text{SBz})\text{S}]_2$ (**10**) (5.2% yield) and $[\text{CpMo}(\text{CO})(\text{SBz})]_2\text{S}$ (**11**) (5.3% yield) were isolated. The yield for *trans-anti* $[\text{CpMo}(\text{CO})(\text{SBz})]_2$ was increased dramatically when the reaction was carried out at a higher temperature of 110 °C. The NMR tube thermolytic study of the *trans-anti* $[\text{CpMo}(\text{CO})(\text{SBz})]_2$ (**12b**) showed that it is slowly converting to *trans-syn* $[\text{CpMo}(\text{CO})(\text{SBz})]_2$ (**12a**) together with $[\text{CpMo}(\text{SBz})\text{S}]_2$ (**10**) and $[\text{CpMo}(\text{CO})(\text{SBz})]_2\text{S}$ (**11**) (refer to Figure 16). Another interesting observation was that when *trans-syn* $[\text{CpMo}(\text{CO})(\text{SBz})]_2$ was recrystallized at -28 °C, crystals of *trans-anti* $[\text{CpMo}(\text{CO})(\text{SBz})]_2$ (**12b**) was obtained after 4 days. However, if *trans-syn* $[\text{CpMo}(\text{CO})(\text{SBz})]_2$ was recrystallized at ambient temperature, it will slowly degrade to $[\text{CpMo}(\text{SBz})_2]_2$ (**13**).

2.4.2 NMR spectral studies

(a) Thermolysis of *trans-anti* $[\text{CpMo}(\text{CO})(\text{SBz})]_2$ (**12b**) at 110 °C

The thermolysis of a dark green solution of *trans-anti* $[\text{CpMo}(\text{CO})(\text{SBz})]_2$ (**12b**) in benzene- d_6 at 110 °C was monitored by ^1H NMR at intervals for which the product compositions are given in Table 13 and the time-dependant ^1H NMR spectra changes of *trans-anti* $[\text{CpMo}(\text{CO})(\text{SBz})]_2$ (**12b**) is illustrated in Figure 16. After 2 h, the spectrum

showed the presence of *trans-syn* [CpMo(CO)(SBz)]₂ (**12a**) in 2% yield together with unconverted *trans-anti* [CpMo(CO)(SBz)]₂ (**12b**) (98% recovery). Under thermal condition, **12b** is converted to other secondary products of [CpMo(SBz)S]₂ (**10**) (0.8% yield), [CpMo(SBz)₂]₂ (**13**) (1% yield) together with its *trans-syn* isomer, **12a** (37% yield) and the unconverted **12b** (54% recovery) after 8 h. After 10 h, other than [CpMo(SBz)S]₂ (**10**) (2% yield), *trans-syn* [CpMo(CO)(SBz)]₂ (**12a**) (18% yield) and [CpMo(SBz)₂]₂ (**13**) (2% yield), formation of [CpMo(CO)(SBz)]₂S (**11**) (0.5% yield) and some unidentified Cp-containing complexes (δ 5.16, 5.34, 5.44, 5.47, 5.55, 5.56 and 5.58), was also found together with unconverted **12b** (56% recovery). Subsequently, after 14 h, the relative yield for [CpMo(SBz)S]₂ (**10**) (4% yield), [CpMo(CO)(SBz)]₂S (**11**) (0.8% yield) and [CpMo(SBz)₂]₂ (**13**) (3% yield) were increased slowly but the yield of *trans-syn*[CpMo(CO)(SBz)]₂ (**12a**) (4% yield) was decreased. This observation may be due to slow thermal degradation of **12a** to other secondary products as well.

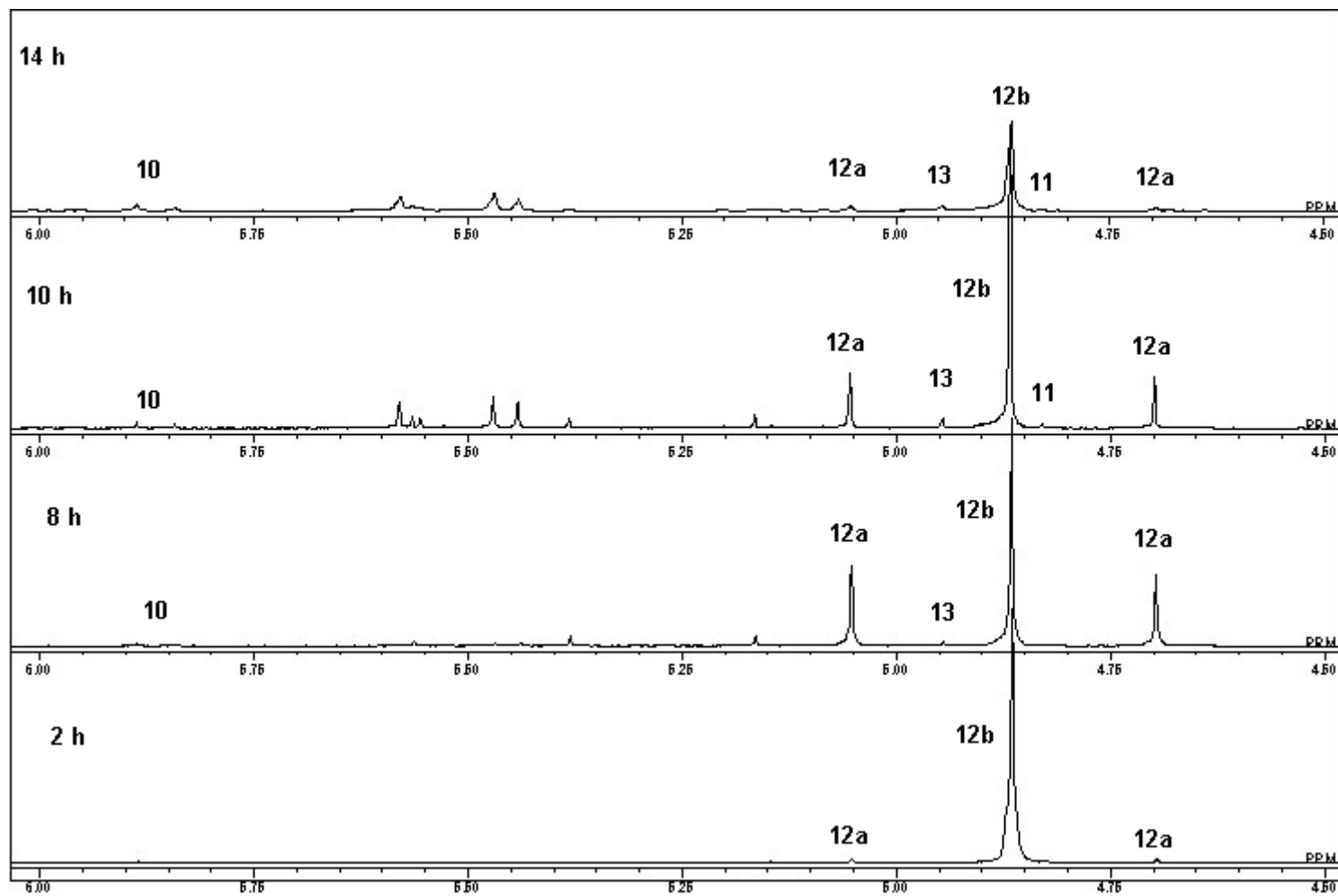
It is significant to note that, the *trans-anti* configuration of **12b** is quite stable in solution even under thermolytic conditions as compared to its *trans-syn* isomer of **12a**, which is easily degraded to other secondary products when under thermolytic condition of 110°C.

Table 13. Time dependent variation of product composition^a from thermolysis study of *trans-anti* [CpMo(CO)(SBz)]₂ (**12b**)

Time/h	Complexes (%)				
	10	11	12a	12b	13
2	-	-	2	98	-
8	0.8	-	37	54	1
10	1.6	0.5	18	56	2
14	4	0.8	4	55	3

^a – Product yields obtained by integration of Cp resonances in ¹H NMR spectrum of product mixture

Figure 16. Time-dependant ^1H NMR spectra changes of *trans-anti*[CpMo(CO)(SBz)]₂ (**12b**) in benzene-*d*₆ at 110 °C



(b) Cothermolysis of *trans-syn* [CpMo(CO)(SBz)]₂ with equimolar Bz₂S₂ at 110 °C

A yellowish green solution of *trans-syn* [CpMo(CO)(SBz)]₂ (**12a**) (16 mg, 0.026 mmol) together with Bz₂S₂ (6 mg, 0.026 mmol) was cothermolized in C₆D₆ (~0.5 mL) at 110 °C and was monitored at regular intervals *via* ¹H NMR. The final spectrum showed the presence of *trans-anti* [CpMo(CO)(SBz)]₂ (8.1% recovery), *trans-syn* [CpMo(CO)(SBz)]₂ (7.0% recovery), [CpMo(CO)(SBz)]₂S (4.6% yield) and [CpMo(SBz)S]₂ (30.9% yield) after 13 h. This observation demonstrates that in the presence of Bz₂S₂, greater amounts of [CpMo(CO)(SBz)]₂S and [CpMo(SBz)S]₂ were produced. The time dependent spectra of these studies are illustrated in Figure 17.

(c) Reaction of [CpMo(CO)₃]₂ (3**) with equimolar Bz₂S₂ at 60 °C**

A reddish purple solution of [CpMo(CO)₃]₂ (**3**) with equimolar Bz₂S₂ in toluene was thermolyzed at 60 °C and followed by ¹H NMR spectral scans at hourly intervals. No reaction was observed even after 21 h. This observation substantiates that the reaction between the molybdenum dimer, **3**, with Bz₂S₂ is initiated by the cleavage of the -S-S- bond in the ligand *via* nucleophilic addition of the 15 electron radical of CpMo(CO)₂.

2.4.3 Cothermolysis study

(a) Reaction of *trans-syn* [CpMo(CO)(SBz)]₂ (12a**) with equimolar bibenzyl disulfide at 110°C**

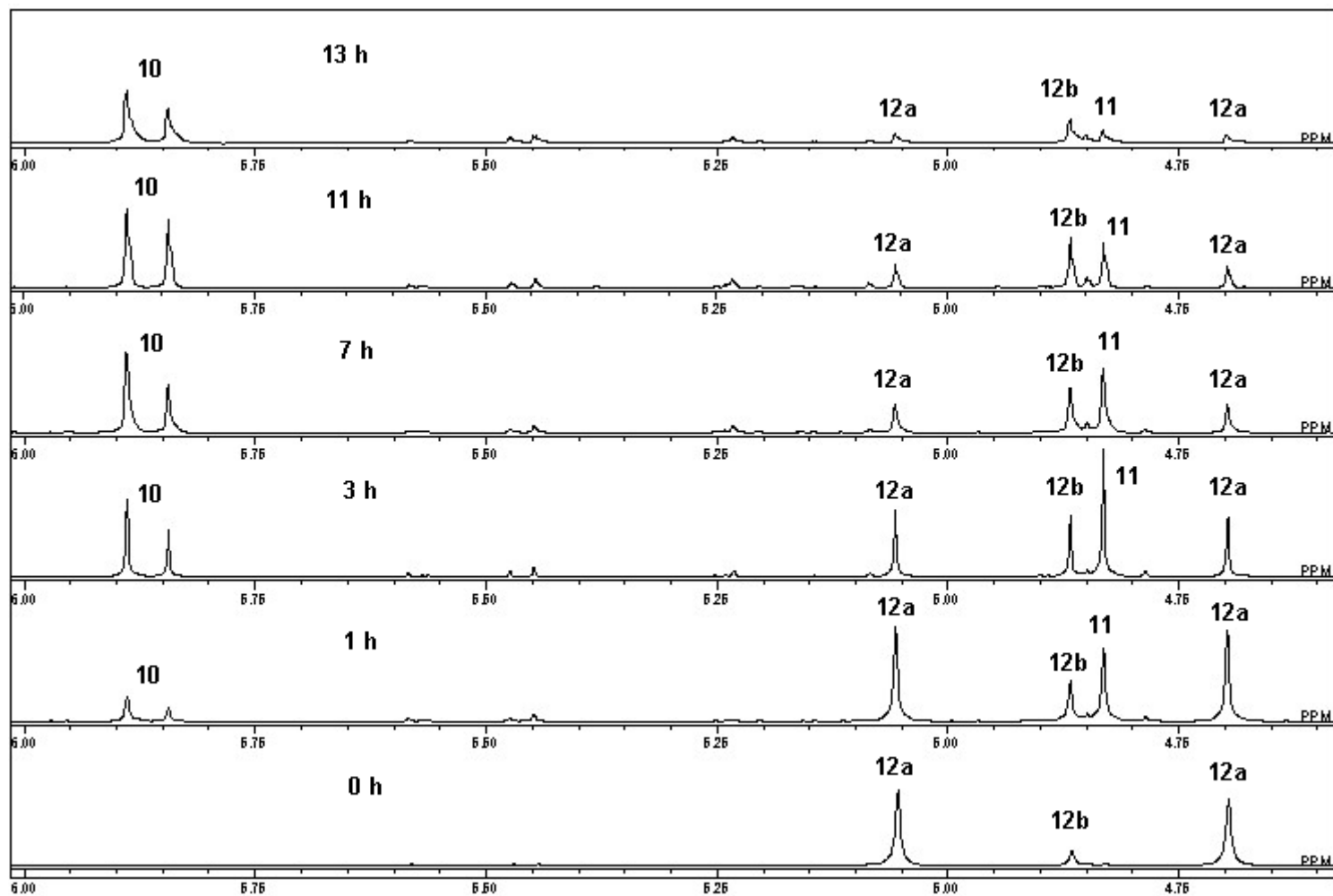
A dark yellowish brown solution of *trans-syn* [CpMo(CO)(SBz)]₂ (**12a**) with equimolar bibenzyl disulfide was stirred at 110 °C for 2 h. Four complexes were isolated as [CpMo(SBz)₂]₂ (**13**), unreacted *trans-syn* [CpMo(CO)(SBz)]₂ (**12a**), *trans-anti* [CpMo(CO)(SBz)]₂ (**12b**) and [CpMo(SBz)S]₂ (**10**) in 33.2%, 26.8, 14.4% and 21.6% yield, respectively. From this observation, it is proposed that *trans-syn* [CpMo(CO)(SBz)]₂ (**12a**)

is the primary product which is less stable as compared to *trans-anti* [CpMo(CO)(SBz)]₂ (**12b**). However, [CpMo(SBz)₂]₂ (**13**) was only isolated in the presence of excess bibenzyl disulfide.

2.4.4 Solventless reaction at 110 °C for 2h

A solventless reaction has been carried out for the reactivity studies of [CpMo(CO)₂]₂ (**4**) with one mole equivalent of Bz₂S₂ at 110 °C for 2 h. The variation of the product composition from the reaction was analyzed by ¹H NMR and the product yields were estimated by integration of Cp resonances in ¹H NMR spectrum of the product mixture. The following products were found to be present :- [CpMo(CO)₂(SBz)]₂ (**9**) (15.3% yield), *trans-syn* [CpMo(CO)(SBz)]₂ (**12a**) (4.5% yield), *trans-anti* [CpMo(CO)(SBz)]₂ (**12b**) (6.1% yield), [CpMo(CO)(SBz)]₂S (**10**) (1.3% yield) and [CpMo(SBz)S]₂ (**13**) (2.4% yield). The higher yield of **9** under solventless condition as compared to solvent reaction (where only trace amounts were detected) indicates that an alternative pathway could exist. The reaction in solid state limits the decarbonylation process as compared to reaction in solution, hence the yield of **9** is considerably higher than the other products which required the loss of more CO to proceed [100].

Figure 17. Time-dependant ^1H NMR spectra changes of cothermolysis of *trans-syn* $[\text{CpMo}(\text{CO})(\text{SBz})]_2$ (**12a**) with 1 mole equivalent of Bz_2S_2 at $110\text{ }^\circ\text{C}$



2.4.5 Mechanistic pathways: Formation of doubly bonded isomers *trans-syn/trans-anti* [CpMo(CO)(SBz)]₂ (**12**) and quadruply bridged [CpMo(SBz)]₄ (**13**)

The E-E linkage in the REER (E = S, Se, Te; R = Me, Et, Ph) [35-39, 42-43, 47-49] are well known to be easily cleaved by nucleophilic, electrophilic or radical processes (Eqn. (11)).

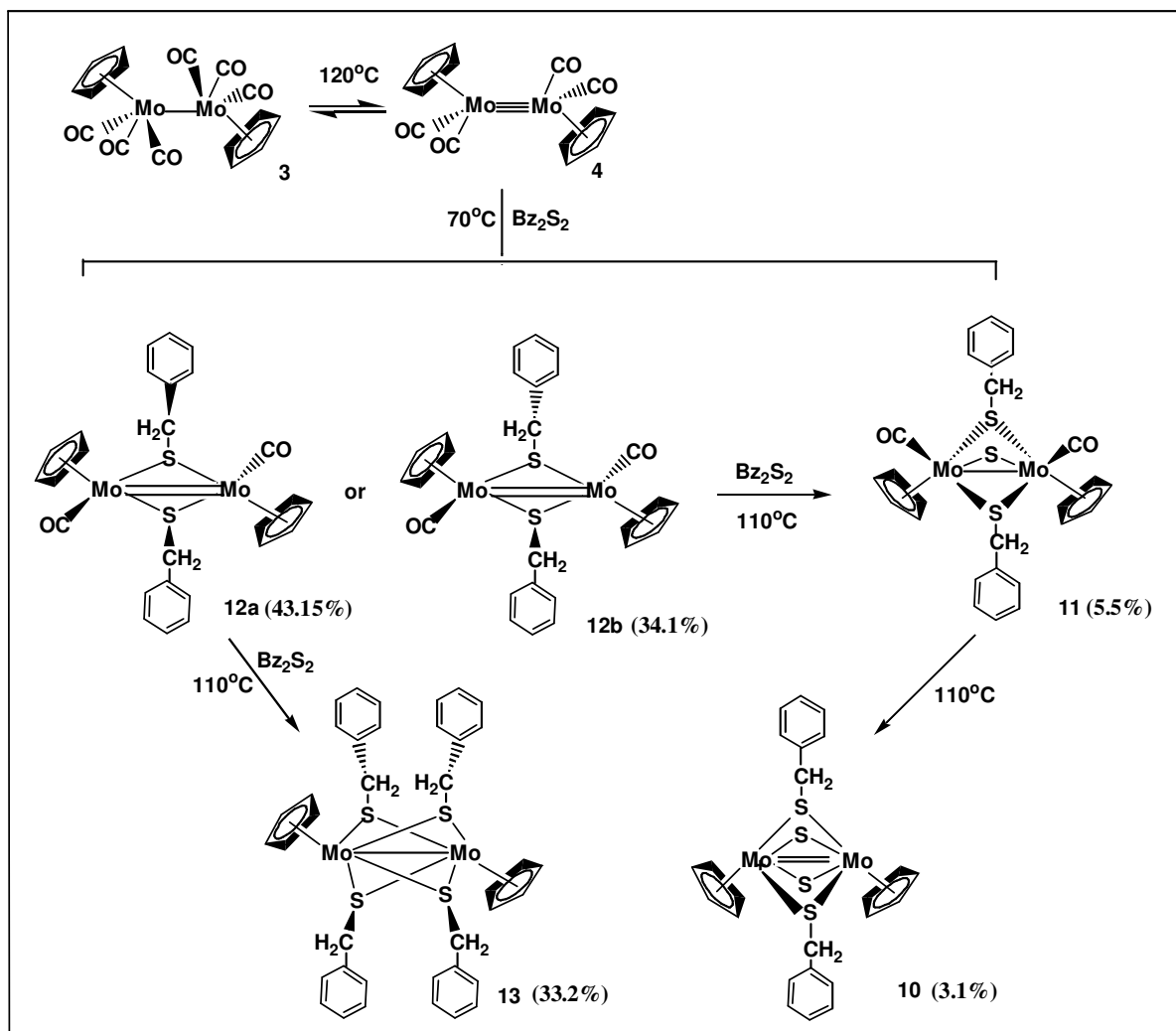


In the reaction of [CpMo(CO)₂]₂ (**4**) with Bz₂S₂, it is postulated that the Bz-S• moiety generated as in Eqn (11) undergoes oxidation addition to the M≡M bonds to form the thiolato-bridged isomers *trans-syn/trans-anti* [CpMo(CO)(SBz)]₂ (**12**). The *trans-syn* isomer converts to the more stable *trans-anti* isomer when it was slowly cooled to -28 °C for a couple of days. Both isomers showed markedly different physical properties. For example the *trans-syn* isomer is yellowish brown in color whereas the *trans-anti* isomer is yellowish green. This phenomenon is also shared by other *trans-syn/trans-anti* complexes of [(RC₅H₄)M(CO)(μ-ER')]₂ [M = Mo or W; E = S, Se or Te; R = H, MeCO, MeO₂C, EtO₂C; R' = Me, Ph, Prⁱ and Bu^t] [42-43].

Thermolytic NMR tube reaction of **12b** in the presence of Bz₂S₂ has shown that the yields of [CpMo(CO)(SBz)S]₂ (**10**) and [CpMo(CO)(SBz)]₂S (**11**) were higher as compared to the thermolysis of **12b** alone. This observation indicates the extra free sulfur moiety S• resulted from the desulfurization process of the Bz₂S₂ which undergoes nucleophilic addition towards the Mo-Mo bond in **12b** to afford **11**. Further decarbonylation of **11** followed by sulfurization will give **10**.

In a similar manner, the formation of [CpMo(SBz)₂]₂ (**13**) from the co-thermolysis of **12a** with Bz₂S₂ at 110 °C was initiated by the decarbonylation of **12a** followed by the insertion of the benzylthiolate moieties across the doubly bonded Mo=Mo dimer.

However, no reaction was observed for $[\text{CpMo}(\text{CO})_3]_2$ (**3**) with Bz_2S_2 even at 60°C as compared to its reaction with Bz_2S_3 . This observation is related to the reactivity of the disulfide and trisulfide ligand as indicated in Sec. 2.3.3 where more thermal energy was needed to cleave the S-S bond in bibenzyl disulfide than the S-S-S bond in bibenzyl trisulfide [97]. The synthetic pathways for products **10**, **11**, **12a**, **12b** and **13** are shown in Scheme 23.



Scheme 23. Synthetic pathways of $[\text{CpMo}(\text{CO})(\text{SBz})\text{S}]_2$ (**10**), $[\text{CpMo}(\text{CO})(\text{SBz})_2]\text{S}$ (**11**) *trans-syn/trans-anti* $[\text{CpMo}(\text{CO})(\text{SBz})_2]$ (**12a** & **b**) and $[\text{CpMo}(\text{SBz})_2]_2$ (**13**)

2.4.6 Physical Properties

***Trans-syn* [CpMo(CO)(SBz)]₂ (12a)**

Trans-syn [CpMo(CO)(SBz)]₂ (**12a**) exists as a dark yellowish brown crystalline solid. In the solids state, it is stable at ambient temperature as well as being stable for a couple of days at ambient temperature in solution. It can be converted to its *trans-anti* isomer when its solution is slowly cooled down to -28 °C. It is soluble in *n*-hexane/toluene mixture to give a yellowish brown solution.

***Trans-anti* [CpMo(CO)(SBz)]₂ (12b)**

Trans-anti [CpMo(CO)(SBz)]₂ (**12b**) exists as a bright yellowish green crystalline solid. It is stable both in the solution and solid state at ambient temperature for couple of days under an inert atmosphere and will convert to its *trans-syn* isomer only at higher temperatures in solution. It is soluble in *n*-hexane/toluene mixture to give a yellowish green solution.

[CpMo(SBz)₂]₂ (13)

[CpMo(SBz)₂]₂ (**13**) exists as a bright yellowish orange crystalline solid. It is stable both in the solution and solid state at ambient temperature under an inert atmosphere. It is soluble in *n*-hexane/toluene mixture to give an orange solution.

2.4.7 Spectral properties

2.4.7.1 IR spectra

***Trans-syn* [CpMo(CO)(SBz)]₂ (12a)**

The IR spectrum in nujol shows $\nu(\text{CO})$ stretching frequencies at 1839s, 1797sh, other peaks at 802m, 764w, 723w, 698m and 476m cm⁻¹ (refer to Appendix I).

***Trans-anti* [CpMo(CO)(SBz)]₂ (12b)**

The IR spectrum in nujol shows $\nu(\text{CO})$ stretching frequencies at 1837vs, 1796sh, other peaks at 800m, 764w, 724vw, 699m, 536w and 491w cm^{-1} (refer to Appendix I).

[CpMo(SBz)₂]₂ (13)

The IR spectrum in nujol shows ν stretching frequencies at 1261w, 1225m, 1199m, 1101sh, 1070s, 1029s, 913vw, 865m, 803w, 766s, 758s, 695vs, 661s, 570m, 564m, 467m, 391w and 384w cm^{-1} (refer to Appendix I).

2.4.7.2 NMR spectra

***Trans-syn* [CpMo(CO)(SBz)]₂ (12a)**

In the ¹H NMR spectrum (benzene-*d*₆), this complex shows two peaks at δ 4.70 and δ 5.05 within the Cp region. This indicates that the two Cp rings are not symmetrical. For the –CH₂-S, their chemical shift were recorded at δ 3.64, δ 3.61 (d, Hz) and δ 3.96, δ 3.93 (d, Hz). Other peaks for the phenyl rings C₆H₅ were recorded as multiplets at δ 7.12-7.08, δ 7.23-7.19 and δ 7.50-7.48. In the ¹³C NMR spectrum (benzene-*d*₆), two Cp peaks at δ 91.6 and δ 91.2 were observed. There is a peak at δ 52.4 which corresponds to –CH₂-S, and four peaks at δ 141.9, 129.8, 129.0, and δ 127.3 which are assigned as the phenyl ring, C₆H₅. For the CO, the chemical shifts were found at δ 250.9 and δ 246.5.

***Trans-anti* [CpMo(CO)(SBz)]₂ (12b)**

In the ¹H NMR spectrum (benzene-*d*₆), only one Cp peak was observed at δ 4.86. This showed that, this complex is very symmetrical. However, there were two doublets recorded for –CH₂-S at δ 3.34, 3.31 (d, Hz) and δ 3.93, δ 3.90 (d, Hz). The first set of chemical shifts of –CH₂-S is different from its *trans-syn* isomer but the later is almost the same as its *trans-syn* isomer. This is an additional indicator with regard to the syn/anti

position of the $-\text{CH}_2\text{-S}$ moiety. In the ^{13}C NMR spectrum (benzene- d_6), the Cp peak was recorded at δ 91.2, and that of $-\text{CH}_2\text{-S}$ was recorded at δ 55.0. Similarly, with its *trans-syn* isomer there were four peaks recorded at δ 132.4, 129.7, 129.0, and 127.3 which are assigned as the phenyl ring, C_6H_5 . Because this complex is symmetrical, there is only one CO peak observed at δ 249.4.

[CpMo(SBz)₂]₂ (**13**)

In the ^1H NMR spectrum (benzene- d_8), one Cp peak at δ 4.92 and one $\text{CH}_2\text{-S}$ peak at δ 3.4 were recorded. In the ^{13}C NMR spectrum (benzene- d_8), the Cp peak was recorded at δ 90.24, and that of $-\text{CH}_2\text{-S}$ was recorded at δ 52.36. Eight phenyl peaks have been recorded as δ 139.07, 138.27, 130.33, 130.09, 129.71, 129.00, 127.88, and 127.45 which indicates that the two pairs of thiol-benzyl moiety are not symmetrical to each other. This observation agrees with the molecular structure of [CpMo(SBz)₂]₂ (**13**) in the single crystal X-ray diffractometry analyses.

2.4.7.3 Mass spectra

Trans-anti [CpMo(CO)(SBz)₂]₂ (**12b**)

The mass spectrum of **12b** with its parent ion at $m/z = 624.9192$ [CpMo(CO)(SBz)₂]₂ and its fragmentation ions are tabulated in Table 14.

Table 14. Electrospray ionization mass spectrum of [CpMo(CO)(SBz)₂]₂ (**12b**)

m/z	Assignments
624	[CpMo(CO)(SBz) ₂] ₂
596	Cp ₂ Mo ₂ (CO)(SBz) ₂
473	Cp ₂ Mo ₂ (SBz)S
256	Mo ₂ S ₂

cis[CpMo(CO)(SBu^t)]₂ (2.616(2) Å) [39] and *trans-syn*[CpMo(CO)(*p*-PhCH₃)]₂ (2.6052(8) Å) and 2.5751(8) Å) [101]. The planar Mo₂S₂ ring of **12b** is also observed in other known analogues as mentioned above.

Table 15. Bond lengths [Å] and angles [deg] for *trans-anti*-[CpMo(CO)(SBz)]₂ (**12b**)

Bond lengths			
Mo(1)-C(6)	1.945(5)	Mo(1)-S(1)#1	2.4106(12)
Mo(1)-C(4)	2.304(5)	Mo(1)-S(1)	2.4226(13)
Mo(1)-C(5)	2.321(5)	Mo(1)-Mo(1)#1	2.5918(8)
Mo(1)-C(1)	2.336(5)	S(1)-C(7)	1.841(5)
Mo(1)-C(3)	2.344(5)	S(1)-Mo(1)#1	2.4106(12)
Mo(1)-C(2)	2.365(5)	O(1)-C(6)	1.153(6)
Bond angles			
C(6)-Mo(1)-S(1)#1	80.99(15)	C(7)-S(1)-Mo(1)#1	112.34(17)
C(6)-Mo(1)-S(1)	87.51(15)	C(7)-S(1)-Mo(1)	111.33(17)
S(1)#1-Mo(1)-S(1)	115.14(3)	Mo(1)#1-S(1)-Mo(1)	64.86(3)
C(6)-Mo(1)-Mo(1)#1	79.26(16)	O(1)-C(6)-Mo(1)	175.0(5)
S(1)#1-Mo(1)-Mo(1)#1	57.79(3)	C(8)-C(7)-S(1)	110.9(3)
S(1)-Mo(1)-Mo(1)#1	57.35(3)		

Symmetry transformations used to generate equivalent atoms: #1 -x+1,-y+1,-z+1

Table 16. Bond lengths [Å] and angles [deg] for [CpMo(SBz)₂]₂ (13)

Bond lengths

Mo(1)-S(1)#1	2.400(18)	S(1)-C(6)	1.866(11)
Mo(1)-S(2')	2.46(2)	S(1)-Mo(1)#1	2.467(3)
Mo(1)-S(2)#1	2.454(3)	S(2)-C(13)	1.845(11)
Mo(1)-S(1)	2.459(3)	S(2)-Mo(1)#1	2.454(3)
Mo(1)-S(2)	2.460(3)	S(1')-C(6)	1.859(14)
Mo(1)-S(1')	2.457(18)	S(1')-Mo(1)#1	2.400(18)
Mo(1)-S(1)#1	2.467(3)	S(2')-C(13)	1.837(14)
Mo(1)-Mo(1)#1	2.623	S(2')-Mo(1)#1	2.50(2)

Bond angles

C(3)-Mo(1)-S(1')#1	110.2(6)	C(3)-Mo(1)-S(2)#1	95.8(4)
C(2)-Mo(1)-S(1')#1	88.4(6)	C(2)-Mo(1)-S(2)#1	92.1(3)
C(1)-Mo(1)-S(1')#1	104.3(6)	C(1)-Mo(1)-S(2)#1	121.6(4)
C(4)-Mo(1)-S(1')#1	146.2(6)	C(4)-Mo(1)-S(2)#1	129.6(4)
C(5)-Mo(1)-S(1')#1	138.0(6)	C(5)-Mo(1)-S(2)#1	150.5(4)
C(3)-Mo(1)-S(2')	153.0(6)	C(3)-Mo(1)-S(1)	97.9(4)
C(2)-Mo(1)-S(2')	119.3(6)	C(2)-Mo(1)-S(1)	132.3(4)
C(1)-Mo(1)-S(2')	93.1(6)	C(1)-Mo(1)-S(1)	152.2(4)
C(4)-Mo(1)-S(2')	131.0(6)	C(4)-Mo(1)-S(1)	93.6(4)
C(5)-Mo(1)-S(2')	98.8(6)	C(5)-Mo(1)-S(1)	122.2(4)
S(1')#1-Mo(1)-S(2')	74.2(5)	S(1')#1-Mo(1)-S(2)#1	30.9(4)
S(1')#1-Mo(1)-S(1)	98.9(4)	S(2')-Mo(1)-S(2)#1	98.9(4)
S(2)#1-Mo(1)-S(1)	73.82(11)	S(2')-Mo(1)-S(1)	107.9(5)
C(3)-Mo(1)-S(2)	142.3(4)	S(1')#1-Mo(1)-S(2)	107.3(5)
C(2)-Mo(1)-S(2)	148.5(4)	S(2')-Mo(1)-S(2)	45.1(4)
C(1)-Mo(1)-S(2)	113.0(4)	S(2)#1-Mo(1)-S(2)	115.53(9)
C(4)-Mo(1)-S(2)	106.3(4)	S(1)-Mo(1)-S(2)	73.32(11)
C(5)-Mo(1)-S(2)	93.6(4)	S(2)#1-Mo(1)-S(1)#1	73.31(11)
C(3)-Mo(1)-S(1')	123.8(5)	S(1)-Mo(1)-S(1)#1	115.70(8)
C(2)-Mo(1)-S(1')	156.6(5)	S(2)-Mo(1)-S(1)#1	73.58(11)
C(1)-Mo(1)-S(1')	132.4(6)	S(1')-Mo(1)-S(1)#1	97.2(4)
C(4)-Mo(1)-S(1')	96.1(5)	C(6)-S(1)-Mo(1)	117.4(4)
C(5)-Mo(1)-S(1')	101.9(6)	C(6)-S(1)-Mo(1)#1	116.4(4)
S(1')#1-Mo(1)-S(1')	114.7(4)	Mo(1)-S(1)-Mo(1)#1	64.30(8)
S(2')-Mo(1)-S(1')	73.4(6)	Mo(1)#1-S(2)-Mo(1)	64.47(9)
S(2)#1-Mo(1)-S(1')	105.7(5)	Mo(1)#1-S(1')-Mo(1)	65.3(4)
S(1)-Mo(1)-S(1')	44.2(4)	Mo(1)-S(2')-Mo(1)#1	63.9(5)
S(2)-Mo(1)-S(1')	30.5(4)		

Symmetry transformations used to generate equivalent atoms: #1 -x+1,-y+1,-z+1

2.5 Studies of $[\text{CpMo}(\text{CO})_3]_2$ (**3**) and $[\text{CpMo}(\text{CO})_2]_2$ (**4**) with 2,4-bis(*p*-tolylthio)1,3-dithia-2,4-diphosphetane-2,4-disulfide (Davy's reagent)

2.5.1 The reaction of $[\text{CpMo}(\text{CO})_3]_2$ (**3**) and $[\text{CpMo}(\text{CO})_2]_2$ (**4**) with equimolar Davy's Reagent (DR)

The reaction of $[\text{CpMo}(\text{CO})_3]_2$ (**3**) with equimolar DR, $[\text{CH}_3\text{C}_6\text{H}_4\text{SP}(\text{S})\text{S}]_2$, at 110 °C for 4 h led to the isolation of greenish brown crystalline solids of $[\text{CpMo}(\text{CO})_2(\text{S}_2\text{P}(\text{SC}_6\text{H}_4\text{Me})_2)]$ (**14**) as the primary product and dark purple crystalline solids of $[\text{Cp}_2\text{Mo}_2(\mu\text{-S})(\mu\text{-S}_2)(\mu\text{-SC}_6\text{H}_4\text{Me})]$ (**16**) as a secondary product in 11.0% and 13.0% yield, respectively. However, in a similar reaction of $[\text{CpMo}(\text{CO})_2]_2$ (**4**) at an elevated temperature of 70 °C for 18 h, a much greater yield of $[\text{CpMo}(\text{CO})_2(\text{S}_2\text{P}(\text{SC}_6\text{H}_4\text{Me})_2)]$ (**14**) (26.1%) was obtained followed by the elution of a pinkish brown fraction of $\text{Cp}_2\text{Mo}_2(\text{CO})_5(\text{S}_2\text{P}(\text{SC}_6\text{H}_4\text{Me}))$ (**15**) (6.0%) and an unidentified dark red precipitate (47 mg). The distribution of components in the mixture formed by the reaction of $[\text{CpMo}(\text{CO})_3]_2$ (**3**) or $[\text{CpMo}(\text{CO})_2]_2$ (**4**) with one mole equivalent of Davy's reagent was observed to vary with temperature. From the NMR tube reaction studies, it was shown that **14** and **15** converted to **16** under thermolytic conditions at 110 °C and 90 °C after 7.5 h (24.6% yield) and 24 h (18.0% yield), respectively. Thermolysis of **14** in the presence of Davy's reagent at 110 °C, resulted in **16** at 16.5% yield together with an unknown product at δ 4.56 (8.0% yield) after 5 h. In contrast, cothermolysis of **14** with $[\text{CpMo}(\text{CO})_2]_2$ (**4**) at 110 °C, resulted in **15** (1.2% yield) and **16** (26.5% yield), together with some unknown products possessing chemical shifts at δ 4.77, 4.96, 5.03, 5.06 and 5.28. This could mean that both **14** and **15** are individual primary products with the totally decarbonylated **16** as the final thermolytic product.

2.5.2 The reaction of $[\text{CpMo}(\text{CO})_2]_2$ (**4**) with 0.5 equivolar Davy's Reagent (DR)

The reaction of $[\text{CpMo}(\text{CO})_2]_2$ (**4**) with 0.5 equivolar amount of DR at 110 °C for 2 h has led to the isolation of the following :- $\text{Cp}_2\text{Mo}_2(\text{CO})_5(\text{S}_2\text{P}(\text{SC}_6\text{H}_4\text{Me}))$ (**15**) (5.2% yield), a greenish brown mixture of *trans-syn/trans-anti*- isomers of $[\text{CpMo}(\text{CO})(\text{SC}_6\text{H}_4\text{Me})]_2$ (**17**) (16.5% yield), yellowish orange crystalline solids of $\text{Cp}_2\text{Mo}_2(\text{CO})_2(\mu\text{-PS})(\mu\text{-SC}_6\text{H}_4\text{Me})_2$ (**18**) (13.6% yield), yellowish brown crystalline solids of $[\text{CpMo}(\text{CO})_2\text{S}]_2$ (**19**) (12.2% yield) and greenish brown fine crystalline solids of $\text{Cp}_3\text{Mo}_3(\mu\text{-S})_2(\mu\text{-S}_2)(\mu_3\text{-S})$ (**20**) (2.6% yield) as an ultimate thermolytic product together with an unknown Cp-containing product ($^1\text{H NMR}$ (benzene- d_6) : δ 4.31, 4.61, 5.14, 14.54) (19mg). When a similar reaction was repeated at 70 °C for 18 h, greenish brown crystalline solids of $[\text{CpMo}(\text{CO})_2(\text{S}_2\text{P}(\text{SC}_6\text{H}_4\text{Me})_2)]$ (**14**) (10.9% yield) and brownish pink crystalline solids of $\text{Cp}_2\text{Mo}_2(\text{CO})_5(\text{S}_2\text{P}(\text{SC}_6\text{H}_4\text{Me}))$ (**15**) (7.6% yield) were isolated as primary products followed by greenish brown crystalline solids of *trans-syn*- $[\text{CpMo}(\text{CO})(\text{SC}_6\text{H}_4\text{Me})]_2$ (**17a**) (6.5% yield), orange crystalline solids of $\text{Cp}_2\text{Mo}_2(\text{CO})_2(\mu\text{-PS})(\mu\text{-SC}_6\text{H}_4\text{Me})_2$ (**18**) (5.4% yield) and yellowish brown crystalline solids of $[\text{CpMo}(\text{CO})_2(\mu\text{-S})]_2$ (**19**) (2.2% yield) isolated as secondary products. Finally, the totally decarbonylated dark purple crystalline solids of $[\text{Cp}_2\text{Mo}_2(\mu\text{-S})(\mu\text{-S}_2)(\mu\text{-SC}_6\text{H}_4\text{Me})]$ (**16**) and greenish brown crystalline solids of $\text{Cp}_3\text{Mo}_3(\mu\text{-S})_2(\mu\text{-S}_2)(\mu_3\text{-S})$ (**20**) were isolated as tertiary products.

2.5.3 NMR thermolytic studies

(a) Thermolysis of $[\text{CpMo}(\text{CO})_2(\text{S}_2\text{P}(\text{SC}_6\text{H}_4\text{Me})_2)]$ (**14**)

Thermolysis of $[\text{CpMo}(\text{CO})_2(\text{S}_2\text{P}(\text{SC}_6\text{H}_4\text{Me})_2)]$ (**14**) (10 mg, 0.018 mmol) in $\text{C}_6\text{D}_5\text{CD}_3$ for 7.5 h gave **16** (24.6% yield) together with some uncharacterized dark brown precipitates.

(b) Thermolysis of $\text{Cp}_2\text{Mo}_2(\text{CO})_5(\text{S}_2\text{P}(\text{SC}_6\text{H}_4\text{Me}))$ (**15**)

Thermolysis of **15** (7 mg, 0.015 mmol) in $\text{C}_6\text{D}_5\text{CD}_3$ for 24 h gave **15** (15% recovery) and **16** (18% yield) together with some uncharacterized dark brown precipitates.

(c) Cothermolysis of $[\text{CpMo}(\text{CO})_2(\text{S}_2\text{P}(\text{SC}_6\text{H}_4\text{Me})_2)]$ with Davy's Reagent (DR) at 110 °C

Cothermolysis of $[\text{CpMo}(\text{CO})_2(\text{S}_2\text{P}(\text{SC}_6\text{H}_4\text{Me})_2)]$ (**14**) with an equimolar amount of DR in $\text{C}_6\text{D}_5\text{CD}_3$ at 110 °C for 5 h gave only $[\text{Cp}_2\text{Mo}_2(\mu\text{-S})(\mu\text{-S}_2)(\mu\text{-SC}_6\text{H}_4\text{Me})]$ (**16**) (16.5% yield).

(d) Cothermolysis of $[\text{CpMo}(\text{CO})_2(\text{S}_2\text{P}(\text{SC}_6\text{H}_4\text{Me})_2)]$ (**14**) with $[\text{CpMo}(\text{CO})_2]_2$ at 110 °C

Cothermolysis of **14** with an equimolar amount of $[\text{CpMo}(\text{CO})_2]_2$ (**4**) in $\text{C}_6\text{D}_5\text{CD}_3$ at 110 °C for 1 h gave $\text{Cp}_2\text{Mo}_2(\text{CO})_5(\text{S}_2\text{P}(\text{SC}_6\text{H}_4\text{Me}))$ (**15**) (1.4% yield), $[\text{CpMo}(\text{CO})_2(\mu\text{-S})]_2$ (**19**) (0.8% yield), *trans-syn* $[\text{CpMo}(\text{CO})(\text{SC}_6\text{H}_4\text{Me})]_2$ (**17a**) (10.6% yield), *trans-anti* $[\text{CpMo}(\text{CO})(\text{SC}_6\text{H}_4\text{Me})]_2$ (**17b**) (5.8% yield), $[\text{Cp}_2\text{Mo}_2(\text{CO})_2(\mu\text{-PS})(\mu\text{-SC}_6\text{H}_4\text{Me})]$ (**18**) (9.8% yield), $[\text{Cp}_2\text{Mo}_2(\mu\text{-S})(\mu\text{-S}_2)(\mu\text{-SC}_6\text{H}_4\text{Me})]$ (**16**) (1.1% yield), $\text{Cp}_3\text{Mo}_3(\mu\text{-S})_2(\mu\text{-S}_2)(\mu_3\text{-S})$ (**20**) (1.3% yield) together with traces of unreacted $[\text{CpMo}(\text{CO})_2(\text{S}_2\text{P}(\text{SC}_6\text{H}_4\text{Me})_2)]$ (**14**) (0.9% recovery) and $[\text{CpMo}(\text{CO})_2]_2$ (**4**) (0.6% recovery). This observation suggests that the complex **14** readily reacts with the excess $\text{CpMo}(\text{CO})_2$ -fragment resulting from

homolytic bond cleavage of **4** to afford **15**, **17(a, b)**, **18** and **19** as the secondary products. Prolonged thermolysis after 2.5 h, gave **16** and **20** as the final products.

(e) Thermolysis of [CpMo(CO)(SC₆H₄Me)]₂ (17**) at 110 °C**

Thermolysis of **17** after 1 h gave only [Cp₂Mo₂(μ-S)(μ-S₂)(μ-SC₆H₄Me)] (**16**) (6.1% yield) together with unreacted **17** (41.0% recovery). Subsequently, after 5 h, the relative amount of **16** increased to 12.3%, while 35.1% of **17** remained in the mixture. After 11 h, the amount of **16** (8.2% yield) together with unreacted **17** (33.6% recovery) was still unchanged. From this study, it indicates that **17** is reasonably stable but degrades slowly to **16** under prolonged thermolytic conditions.

(f) Thermolysis of Cp₂Mo₂(CO)₂(μ-PS)(μ-SC₆H₄Me)₂ (18**) at 110 °C**

Under prolonged thermolysis over 15 h, **18** remains relatively unchanged, with a trace amount of [Cp₂Mo₂(μ-S)(μ-S₂)(μ-SC₆H₄Me)] (**16**) and [CpMo(CO)₂(μ-S)]₂ (**19**) observed in the solution.

(g) Cothermolysis of [CpMo(CO)₂(μ-S)]₂ (19**) with Davy's Reagent (DR)**

Cothermolysis of **19** with DR at 110 °C for 5 h gave [CpMo(CO)₂(μ-S)]₂ (23.8% recovery) and [Cp₂Mo₂(μ-S)(μ-S₂)(μ-SC₆H₄Me)] (43.7 %).

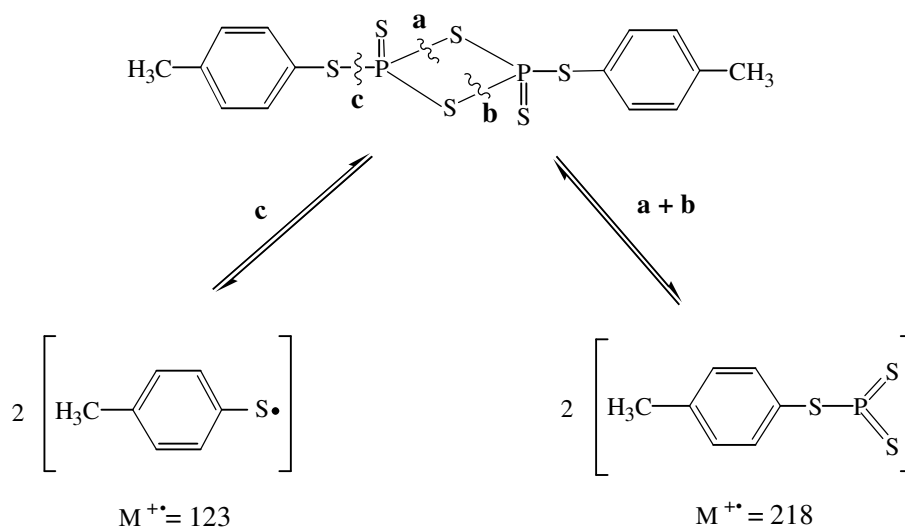
(h) Thermolysis of [Cp₂Mo₂(μ-S)(μ-S₂)(μ-SC₆H₄Me)] (16**)**

Thermolysis of a solution of **16** at 110 °C for 3 h resulted in the total decomposition of **16**. This indicates that **16** is the final thermolyzed product.

2.5.4 Mechanistic pathways

2.5.4.1 Mechanistic pathways of the reaction of $[\text{CpMo}(\text{CO})_2]_2$ (**4**) with an equimolar amount of Davy's Reagent (DR)

The reactivity of the triply bonded **4** with DR resulted in a ring opening of the central P_2S_2 component of the organic substrate. The weak P–S linkage with DR makes it vulnerable to cleavage processes initiated by nucleophiles, electrophiles and radicals as demonstrated by Rauchfuss whereby the reagent undergoes reversible cleavage to give $\text{PhPS}_2\cdot$ radicals [102]. With DR, it was deduced that two types of $\text{RPS}_2\cdot$ and $\text{R}\cdot$ ($\text{R} = \text{SPhCH}_3$) radicals were generated from the cleavage process according to its mass spectrometric analyses by Heimgartner et al [103] (Scheme 24).

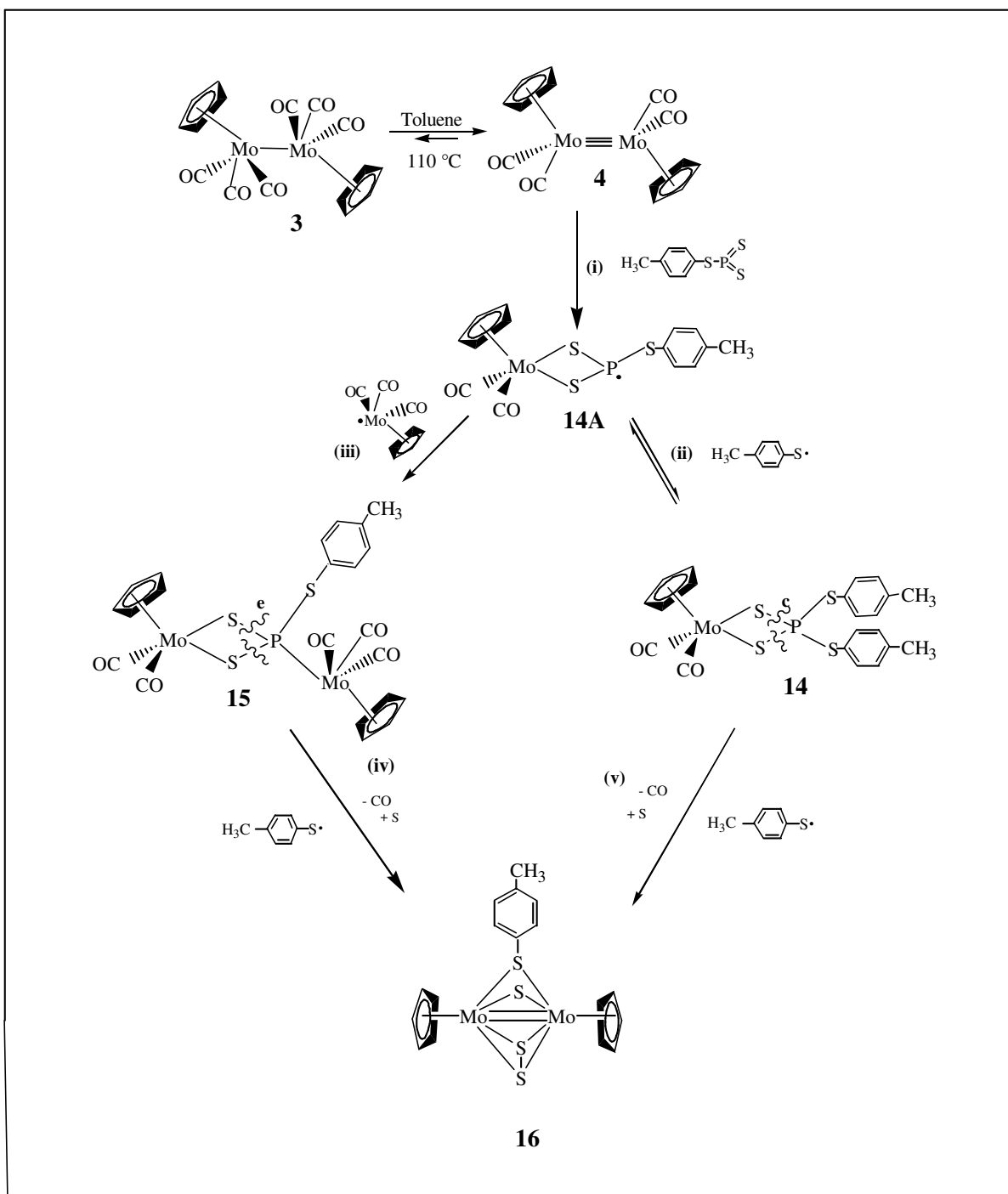


Scheme 24

As perceived earlier from the reaction of LR, $[\text{CH}_3\text{OC}_6\text{H}_4\text{PS}_2]_2$, with the chromium analogue of **3** by Goh *et al.* [56a], a common intermediate radical species, $\text{CpCr}(\text{CO})_3\text{R}'\text{PS}_2\cdot$ ($\text{R}' = \text{PhOCH}_3$), was postulated as a precursor to all the primary

products that were obtained. By analogy, it is anticipated that such a pathway could possibly occur here with the initial formation of $\text{CpMo(CO)}_2\text{RPS}_2\cdot$ ($\text{R} = \text{SC}_6\text{H}_4\text{CH}_3$), **14A**, *via* the coupling of a $\text{CpMo(CO)}_2\cdot$ fragment resulting from homolytic bond cleavage of **4** with a $\text{RPS}_2\cdot$ radical as depicted by pathway (i) (Scheme 25). The detection of the molecular ion (m/z 439) in the mass spectrum of **14** substantiates the existence of **14A**. From the molecular structures of **14** and **15**, it is apparent that formation of **14** is the result of the interaction of **14A** with $\text{R}\cdot$ as depicted in pathway (ii). **15** is likely to be the result of a 17-electron $\text{CpMo(CO)}_3\cdot$ radical attack generated by homolytic cleavage of **3** [104] (pathway (iii)). Indeed, when **14** and **15** are thermolyzed in a NMR tube in toluene- d_8 , **16** is obtained as the only product even after prolonged heating. Formation of **16** (pathways iv and v) which proceeds *via* total decarbonylation, P-S bond cleavage and desulfurization of **14** and **15**, respectively, will normally require drastic conditions.

In conclusion, $[\text{CpMo(CO)}_n]_2$ ($n = 2, 3$) possesses both versatility and a unique pattern of reactivity towards a variety of phosphorus-sulfur containing ligands. The opening of the P_2S_2 ring of the Davy's reagent by means of the 17-electron $\text{CpMo(CO)}_3\cdot$ radical and nucleophilic attack of **14** and **15**, respectively, had led to the formation of complexes with interesting bonding and structural features.

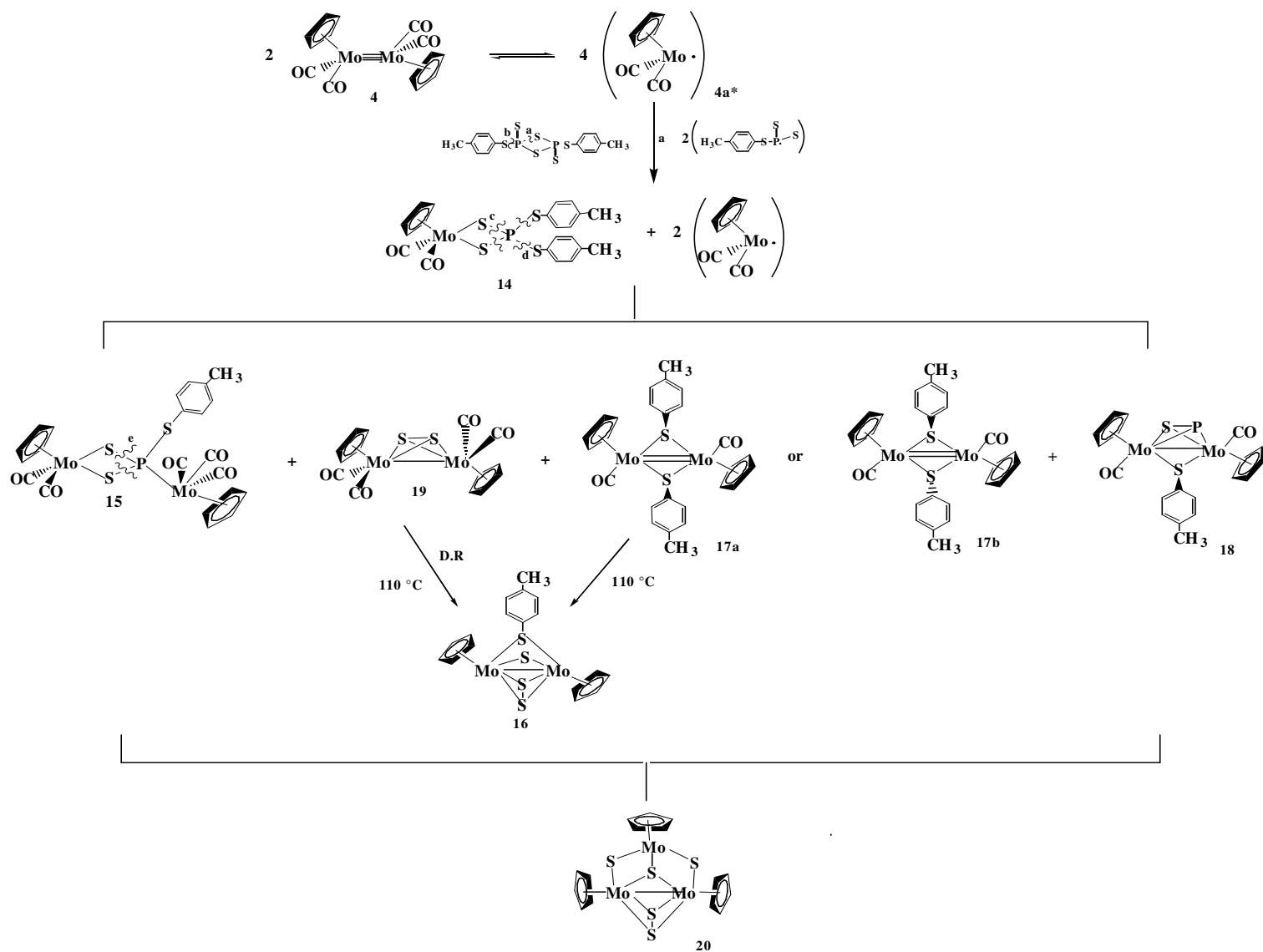


Scheme 25. Synthetic pathways for $[\text{CpMo}(\text{CO})_2(\text{S}_2\text{P}(\text{SC}_6\text{H}_4\text{Me})_2)]$ (**14**), $\text{Cp}_2\text{Mo}_2(\text{CO})_5(\text{S}_2\text{P}(\text{SC}_6\text{H}_4\text{Me}))$ (**15**) and $[\text{Cp}_2\text{Mo}_2(\mu\text{-S})(\mu\text{-S}_2)(\mu\text{-SC}_6\text{H}_4\text{Me})]$ (**16**)

2.5.4.2 Mechanistic pathways of the reaction of $[\text{CpMo}(\text{CO})_2]_2$ (**4**) with 0.5 mole equivalent of Davy's Reagent (DR)

From the previous studies for the reaction of $[\text{CpMo}(\text{CO})_2]_2$ (**4**) with an equimolar amount of DR, only three complexes of $[\text{CpMo}(\text{CO})_2(\text{S}_2\text{P}(\text{SC}_6\text{H}_4\text{Me})_2)]$ (**14**), $\text{Cp}_2\text{Mo}_2(\text{CO})_5(\text{S}_2\text{P}(\text{SC}_6\text{H}_4\text{Me}))$ (**15**) and $[\text{Cp}_2\text{Mo}_2(\mu\text{-S})(\mu\text{-S}_2)(\mu\text{-SC}_6\text{H}_4\text{Me})]$ (**16**) were isolated (Scheme 25) [57a] together with some organic residues. However, when a similar reaction was repeated with equimolar $[\text{CpMo}(\text{CO})_2]_2$ (**4**) and 0.5 mole equivalent of DR, apart from **14**, **15** and **16**, this reaction also afforded the formation of a pair of isomers $[\text{CpMo}(\text{CO})(\text{SC}_6\text{H}_4\text{Me})]_2$ (**17**), $\text{Cp}_2\text{Mo}_2(\text{CO})_2(\mu\text{-PS})(\mu\text{-SC}_6\text{H}_4\text{Me})$ (**18**), $[\text{CpMo}(\text{CO})_2\text{S}]_2$ (**19**) and $\text{Cp}_3\text{Mo}_3(\mu\text{-S})_2(\mu\text{-S}_2)(\mu_3\text{-S})$ (**20**) as final thermolyzed products.

The isolation of these 4 additional products of **17**, **18**, **19** and **20** in the presence of excess **4** can be rationalized by a bond scission process in $[\text{CpMo}(\text{CO})_2(\text{S}_2\text{P}(\text{SC}_6\text{H}_4\text{Me})_2)]$ (**14**) followed by cleavage with extra $\text{CpMo}(\text{CO})_2\cdot$ fragments. It was envisaged that $\text{CpMo}(\text{CO})_2\cdot$ radicals will attack the P-S bond at *d* in **14** to give the monomeric species, $\text{CpMo}(\text{CO})_2(\text{SC}_6\text{H}_4\text{Me})\cdot$, which eventually dimerised with decarbonylation to form $[\text{CpMo}(\text{CO})(\text{SC}_6\text{H}_4\text{Me})]_2$ (**17**) (Scheme 26). From the molecular structure of **18**, this complex is likely to originate from complex **14**. To support this, **18** was detected from the cothermolysis of **14** with one mole equivalent of $[\text{CpMo}(\text{CO})_2]_2$ (**4**) at 110 °C (refer to (2.5.3 (d))). The formation of $[\text{CpMo}(\text{CO})_2\text{S}]_2$ (**19**) could result from two possible pathways emanating from **14** or **15**. Both pathways involved P-S cleavage in both **14** and **15** affording the $\text{CpMo}(\text{CO})_2\text{S}_2$ fragment which subsequently interacts with a $\text{CpMo}(\text{CO})_2\cdot$ radical to form the dithia-bridged complexes. The presence of **19** was confirmed in the reaction of **14** with one mole equivalent of $[\text{CpMo}(\text{CO})_2]_2$ at 110 °C. From the above Section 2.5.1, it was shown that **16** is the final thermolytic product of **14** and **15**. The NMR tube thermolysis of **17** and cothermolysis studies of **19** with one mole equivalent of Davy's reagent have demonstrated that there are alternative pathways to obtain **16**.



Scheme 26. Synthetic pathways for complexes 14 - 20

2.5.5 Physical properties

CpMo(CO)₂{S₂P(SC₆H₄Me)₂} (14)

CpMo(CO)₂{S₂P(SC₆H₄Me)₂} exists as a dark greenish brown crystalline solid. In the solid state, it is stable at ambient temperature under an inert atmosphere. It is slightly soluble in *n*-hexane but soluble in most polar organic solvents to give a greenish brown solution. In solution, it is fairly stable at room temperature under an inert atmosphere for a few days.

Cp₂Mo₂(CO)₅{S₂P(SC₆H₄Me)} (15)

Cp₂Mo₂(CO)₅{S₂P(SC₆H₄Me)} exists as a deep pink solid. In the solid state, it is stable at ambient temperature under an inert atmosphere. It is slightly soluble in *n*-hexane but soluble in most polar organic solvents to give a brownish pink solution. In solution, it is stable at room temperature under an inert atmosphere for a few days.

Cp₂Mo₂(μ-S₂)(μ-S)(μ-SC₆H₄Me) (16)

Cp₂Mo₂(μ-S₂)(μ-S)(μ-SC₆H₄Me) exists as a dark purple crystalline solid. In the solid state, it is stable at ambient temperature under an inert atmosphere. It is soluble in a mixture of *n*-hexane/toluene to give a deep purple solution. In solution, it is stable at room temperature under an inert atmosphere for a few days.

***Trans-syn* [CpMo(CO)(SC₆H₄Me)]₂ (17a)**

Trans-syn [CpMo(CO)(SC₆H₄Me)]₂ exists as a yellowish brown crystalline solid. In the solid state, it is stable at ambient temperature under an inert atmosphere. It is very soluble in a mixture of *n*-hexane/toluene to give a yellowish brown solution. In solution, it is stable at room temperature under an inert atmosphere for a couple of hours but it can be converted slowly to *trans-anti* [CpMo(CO)(SC₆H₄Me)]₂.

***Trans-anti* [CpMo(CO)(SC₆H₄Me)]₂ (17b)**

Trans-anti [CpMo(CO)(SC₆H₄Me)]₂ exists as a yellowish green crystalline solid. In the solid state, it is stable at ambient temperature under an inert atmosphere. It is very soluble in a mixture of *n*-hexane/toluene to give a yellowish green solution. In solution, it is stable at room temperature under an inert atmosphere for a few days.

Cp₂Mo₂(CO)₂(μ-PS)(μ-SC₆H₄Me) (18)

Cp₂Mo₂(CO)₂(μ-PS)(μ-SC₆H₄Me) exists as an orange amorphous solid. In the solid state, it is stable at ambient temperature under an inert atmosphere. It is soluble in a mixture of *n*-hexane/ toluene to give a yellowish orange solution. In solution, it is stable at room temperature under an inert atmosphere for a couple of days.

[CpMo(CO)₂S]₂ (19)

[CpMo(CO)₂S]₂ exists as a reddish brown crystalline solid. In the solid state, it is stable at ambient temperature under an inert atmosphere. It is soluble in a mixture of *n*-hexane/toluene to give a reddish brown solution. In solution, it is stable at room temperature for 1-2 days under an inert atmosphere.

Cp₃Mo₃(μ-S)₂(μ-S₂)(μ₃-S) (20)

Cp₃Mo₃(μ-S)₂(μ-S₂)(μ₃-S) exists as a greenish brown fine crystalline solid. In the solid state, it is stable at ambient temperature under an inert atmosphere. It is soluble in toluene and other more polar organic solvents. In solution, it is stable at room temperature for 1-2 days under an inert atmosphere.

2.5.6 Spectral properties

2.5.6.1 IR spectra

CpMo(CO)₂{S₂P(SC₆H₄Me)₂} (14)

The IR spectrum of **14** in nujol shows ν_{CO} stretching frequencies at 1949vs, 1861vs, 1833sh cm^{-1} and P-S stretching at 806s and 600s cm^{-1} (refer to Appendix I).

Cp₂Mo₂(CO)₅{S₂P(SC₆H₄Me)} (15)

The IR spectrum of **15** in nujol shows ν_{CO} stretching frequencies at 2035vs, 1970s, 1949vs, 1924vs, 1917vs and 1826vs cm^{-1} ; P-S stretching at 804 m and another band at 727m cm^{-1} (refer to Appendix I).

Cp₂Mo₂(μ -S₂)(μ -S)(μ -SC₆H₄Me) (16)

The IR spectrum of **16** in nujol shows stretching frequencies at 1299vw, 1261vw, 1156vw, 1101w, 1062w, 1009w, 836vw, 803w 733.54vw, 721.77vw cm^{-1} (refer to Appendix I).

***Trans-syn/trans-anti* [CpMo(CO)(SC₆H₄Me)]₂ (17a & b)**

Mixture of *trans-syn/trans-anti* [CpMo(CO)(SC₆H₄Me)]₂ in nujol exhibits ν_{CO} stretching frequencies at 1911s, 1854vs, 1836vs cm^{-1} ; other bands at 1178vw, 1156w, 1105m, 1062m, 1016m, 836vw, 816vw, 802m, 722vw, 499vw and 480vw (refer to Appendix I).

Cp₂Mo₂(CO)₂(μ -PS)(μ -SC₆H₄Me) (18)

The IR spectrum of **18** in nujol shows ν_{CO} stretching frequencies at 1882vs, 1863vs cm^{-1} and P-S stretching at 804m cm^{-1} , other bands at 1159w, 1105m, 1058m, 1032sh, 1015m and 839w cm^{-1} (refer to Appendix I).

[CpMo(CO)₂S]₂ (19)

The IR spectrum of **19** shows ν_{CO} stretching frequencies at 1988s, 1947vs, 1902vs, 1865s cm^{-1} in nujol and other bands at 1260s, 803s 572w, 544vw, 530w, 496w, 461w cm^{-1} (refer to Appendix I).

Cp₃Mo₃(μ -S)₂(μ -S₂)(μ ₃-S) (20)

The I. R. spectrum of **20** shows ν_{CO} stretching frequencies at 1158w, 1112m, 1058m, 1002m, 805s, 722vw, 599vw, 547vw cm^{-1} (refer to Appendix I).

2.5.6.2 NMR spectra

CpMo(CO)₂{S₂P(SC₆H₄Me)₂} (14)

The complex is monomeric and the Cp ring appears as a singlet in both of the ¹H and ¹³C NMR spectra in benzene-*d*₆. In the ¹H NMR spectrum, the Cp signal was recorded at δ 4.50, two -CH₃ peaks at δ 2.09 and δ 1.92 and the aromatic protons as multiplets at δ 7.73-6.80. In the ¹³C NMR spectrum, the Cp peak was recorded at δ 95.98, the -CH₃ peaks at δ 21.55 and δ 21.30, the aromatic carbons at δ 137.36, 137.33, 137.15, 137.11, 130.84, 130.82, 130.38, 130.35 and the two CO peaks at δ 256.46, 256.39. In the ³¹P NMR spectrum, the phosphorus peak was recorded at δ 125.18 (refer to Appendix II). The results obtained from these NMR spectra are consistent with the molecular structure of **14**.

Cp₂Mo₂(CO)₅{S₂P(SC₆H₄Me)} (15)

The complex **15** is an unsymmetrical and diamagnetic compound. In the ¹H NMR spectrum in benzene-*d*₆, the Cp signals were recorded at δ 5.08 and δ 4.62, the -CH₃ peak at δ 1.99 and the -C₆H₄ peaks as multiplets at δ 7.72-6.89. In the ¹³C NMR spectrum in benzene-*d*₆, the Cp peaks were recorded at δ 97.06 and 96.34, the -CH₃ peak at δ 21.31, the

$-\text{C}_6\text{H}_4$ peaks at δ 137.41, 132.51, 130.16, 129.84 and the CO peaks at δ 260.40, 260.34, 255.88, 233.38, 226.14. In the ^{31}P NMR spectrum of **15** in benzene- d_6 , the phosphorus peak was recorded at δ 187.60 (refer to Appendix II).

$\text{Cp}_2\text{Mo}_2(\mu\text{-S}_2)(\mu\text{-S})(\mu\text{-SC}_6\text{H}_4\text{Me})$ (16)

Complex **16** is diamagnetic and highly symmetrical where only one Cp ring signal was observed in both the ^1H and ^{13}C NMR spectra in benzene- d_6 . The proton signal for Cp was recorded at δ 5.91, a $-\text{CH}_3$ peak was recorded at δ 2.03 and the $-\text{C}_6\text{H}_4$ peaks were recorded as multiplets at δ 7.52-6.75. In the ^{13}C NMR spectrum, the Cp peak was recorded at δ 98.55 and the $-\text{CH}_3$ peak was recorded at δ 26.19.

***Trans-syn* [$\text{CpMo}(\text{CO})(\text{SC}_6\text{H}_4\text{Me})$] $_2$ (17a)**

Trans-syn [$\text{CpMo}(\text{CO})(\text{SC}_6\text{H}_4\text{Me})$] $_2$ is an unsymmetrical diamagnetic compound. Two Cp signals were observed in both the ^1H and ^{13}C NMR spectra in benzene- d_6 . In the ^1H NMR spectrum, Cp signals were recorded at δ 5.26, 4.96; a $-\text{CH}_3$ peak at δ 2.07 and the $-\text{C}_6\text{H}_4$ peaks as multiplets at δ 6.97-6.96, δ 7.35-7.33 and δ 7.44-7.42. In the ^{13}C NMR spectrum, the Cp peaks were recorded at δ 92.35 and 92.03, a $-\text{CH}_3$ peak at δ 21.27, the $-\text{C}_6\text{H}_4$ peaks at δ 145.96, 136.62, 136.48, 131.63, 131.27, 129.67, 129.50, 129.41.

$\text{Cp}_2\text{Mo}_2(\text{CO})_2(\mu\text{-PS})(\mu\text{-SC}_6\text{H}_4\text{Me})$ (18)

Complex **18** is an unsymmetrical diamagnetic compound. Two Cp signals were observed in both ^1H and ^{13}C NMR spectra in benzene- d_6 . In the ^1H NMR spectrum, the Cp signal was recorded at δ 5.02, 4.77; a $-\text{CH}_3$ peak at δ 1.98 and the $-\text{C}_6\text{H}_4$ peaks as multiplets at δ 7.18-6.80. In the ^{13}C NMR spectrum, the Cp peaks were recorded at δ 94.77 and δ 88.83, a $-\text{CH}_3$ peak at δ 21.10, the $-\text{C}_6\text{H}_4$ peaks at δ 136.64, 130.96, 130.92, 129.65,

128.90 and two CO peaks at δ 239.73, 233.81. The ^{31}P NMR spectrum of **18** in benzene- d_6 was illustrated in Appendix II. In the ^{31}P NMR spectrum, the phosphorus peak was recorded at δ -99.45. The results obtained from these NMR spectra are consistent with the molecular structure of **18**.

[CpMo(CO)₂S]₂ (19)

Complex **19** is diamagnetic and highly symmetrical with one Cp ring signal observed in both ^1H and ^{13}C NMR spectra in benzene- d_6 . In the ^1H NMR spectrum, Cp signal was recorded at δ 4.54. In the ^{13}C NMR spectrum, the Cp peak was recorded at δ 86.65 and one CO peak at δ 227.25. As compared to its isostructural compound of [CpMo(CO)₂P]₂ [105], the chemical shifts in both ^1H and ^{13}C NMR spectra are very similar (^1H NMR (benzene- d_6): δ 4.54 (s, Cp); ^{13}C NMR (benzene- d_6): δ 86.5 (Cp) and δ 226.2 (CO)).

Cp₃Mo₃(μ -S)₂(μ -S₂)(μ_3 -S) (20)

Complex **20** is a trinuclear cluster with only one Cp ring signal observed in ^1H NMR spectrum (benzene- d_6) at δ 5.15, but two Cp signals were recorded in ^{13}C NMR spectrum at (benzene- d_6) δ 94.85 and δ 92.96.

2.5.6.3 Mass spectra

CpMo(CO)₂{S₂P(SC₆H₄Me)₂} (14)

The ESI mass spectrum shows the parent ion $m/z = 559.1300$ CpMo(CO)₂{S₂P(SC₆H₄Me)₂} as well as [CpMo(CO)₂(S₂P(SC₆H₄Me))] (**14A**) and Cp₃Mo₃(μ -S)₂(μ -S₂)(μ_3 -S), which are consistent with our proposal about the formation of the common intermediate of **14A** during the reaction. (Table 17).

Table 17. Electrospray ionization mass spectrum of $\text{CpMo}(\text{CO})_2\{\text{S}_2\text{P}(\text{SC}_6\text{H}_4\text{Me})_2\}$ (**14**)

m/z	Assignments
560	$[\text{CpMo}(\text{CO})_2(\text{S}_2\text{P}(\text{SC}_6\text{H}_4\text{Me})_2)]$
504	$[\text{CpMo}(\text{S}_2\text{P}(\text{SC}_6\text{H}_4\text{Me})_2)]$
439	$[\text{CpMo}(\text{CO})_2(\text{S}_2\text{P}(\text{SC}_6\text{H}_4\text{Me}))]$
373	$[\text{CpMo}(\text{CO})_2(\text{PS}_4)]$
341	$[\text{CpMo}(\text{CO})_2(\text{PS}_3)]$
313	$[\text{CpMo}(\text{CO})_2(\text{PS}_2)]$
289	$[\text{CpMo}(\text{CO})(\text{PS}_2)]$
256	$[\text{CpMo}(\text{PS}_2)]$

$\text{Cp}_2\text{Mo}_2(\text{CO})_5\{\text{S}_2\text{P}(\text{SC}_6\text{H}_4\text{Me})\}$ (15**)**

The mass spectrum of **15** shows the parent ion $m/z = 680.4208$ $[\text{Cp}_2\text{Mo}_2(\text{CO})_5(\text{S}_2\text{P}(\text{SC}_6\text{H}_4\text{Me}))]$ and its fragmentation ions as listed in Table 18.

Table 18. Electrospray ionization mass spectrum of $[\text{Cp}_2\text{Mo}_2(\text{CO})_5(\text{S}_2\text{P}(\text{SC}_6\text{H}_4\text{Me}))]$ (**15**)

m/z	Assignments
680	$[\text{Cp}_2\text{Mo}_2(\text{CO})_5(\text{S}_2\text{P}(\text{SC}_6\text{H}_4\text{Me}))]$
589	$[\text{Cp}_2\text{Mo}_2(\text{CO})_5(\text{PS}_3)]$
401	$[\text{CpMo}(\text{P}(\text{SC}_6\text{H}_4\text{Me}))]$
341	$[\text{CpMo}(\text{CO})_2(\text{PS}_3)]$
315	$[\text{CpMo}(\text{CO})_2(\text{PS}_2)]$
247	$[\text{CpMo}(\text{CO})_3]$
215	$[\text{CpMo}(\text{CO})_2]$

Cp₂Mo₂(μ-S₂)(μ-S)(μ-SC₆H₄Me) (16)

The mass spectrum of **16** shows the parent ion $m/z = 545.3670$ Cp₂Mo₂(μ-S₂)(μ-S)(μ-SC₆H₄Me) and its fragmentation ions as listed in Table 19.

Table 19. Electrospray ionization mass spectrum of Cp₂Mo₂(μ-S₂)(μ-S)(μ-SC₆H₄Me) (**16**)

m/z	Assignments
545	[Cp ₂ Mo ₂ (μ-S)(μ-S ₂)(SC ₆ H ₄ Me)]
419	[Cp ₂ Mo ₂ (μ-S)(μ-S ₂)]
386	[Cp ₂ Mo ₂ (S ₂)]
256	[Mo ₂ S ₂]

***Trans-syn* [CpMo(CO)(SC₆H₄Me)]₂ (17a)**

The mass spectrum of **17a** shows the parent ion $m/z = 627.2100$ [CpMo(CO)(SC₆H₄Me)]₂ and its fragmentation ions as listed in Table 20.

Table 20. Electrospray ionization mass spectrum of [CpMo(CO)(SC₆H₄Me)]₂ (**17a**)

m/z	Assignments
628	[Cp ₂ Mo ₂ (CO) ₂ (SC ₆ H ₄ Me) ₂]
599	[Cp ₂ Mo ₂ (CO)(SC ₆ H ₄ Me) ₂]
557	[Cp ₂ Mo ₂ (SC ₆ H ₄ Me)(SC ₆ H ₄)]

Cp₂Mo₂(CO)₂(μ-PS)(μ-SC₆H₄Me) (18)

The mass spectrum of **18** shows the parent ion $m/z = 564.3400$ Cp₂Mo₂(CO)₂(μ-PS)(μ-SC₆H₄Me) and its fragmentation ions as listed in Table 21.

Table 21. Electrospray ionization mass spectrum of Cp₂Mo₂(CO)₂(μ-PS)(μ-SC₆H₄Me) (**18**)

m/z	Assignments
564	[Cp ₂ Mo ₂ (CO) ₂ (μ-PS)(μ-SC ₆ H ₄ Me) ₂]
541	[Cp ₂ Mo ₂ (μ-S)(μ-S ₂)(SC ₆ H ₄ Me)]
536	[Cp ₂ Mo ₂ (CO)(μ-PS)(μ-SC ₆ H ₄ Me) ₂]
508	[Cp ₂ Mo ₂ (μ-PS)(μ-SC ₆ H ₄ Me) ₂]

[CpMo(CO)₂S]₂ (19)

The mass spectrum of **19** shows the parent ion $m/z = 501.3554$ [CpMo(CO)₂S]₂ and its fragmentation ions as listed in Table 22.

Table 22. Electrospray ionization mass spectrum of [CpMo(CO)₂S]₂ (**19**)

m/z	Assignments
501	[CpMo(CO) ₂ S] ₂
473	[Cp ₂ Mo ₂ (CO) ₃ S ₂]
445	[Cp ₂ Mo ₂ (CO) ₂ S ₂]
389	[Cp ₂ Mo ₂ S ₂]
357	[Cp ₂ Mo ₂ S]

$\text{Cp}_3\text{Mo}_3(\mu\text{-S})_2(\mu\text{-S}_2)(\mu_3\text{-S})$ (**20**)

The mass spectrum of **20** shows the parent ion $m/z = 643.3697$ $\text{Cp}_3\text{Mo}_3(\mu\text{-S})_2(\mu\text{-S}_2)(\mu_3\text{-S})$ and its fragmentation ions as listed in Table 23.

Table 23. Electrospray ionization mass spectrum of $\text{Cp}_3\text{Mo}_3(\mu\text{-S})_2(\mu\text{-S}_2)(\mu_3\text{-S})$ (**20**)

m/z	Assignment
643	$\text{Cp}_3\text{Mo}_3(\mu\text{-S})_2(\mu\text{-S}_2)(\mu_3\text{-S})$
446	Mo_3S_5
386	$\text{Cp}_2\text{Mo}_2\text{S}_2$
355	Mo_2S_5
289	Mo_2S_3
256	Mo_2S_2

2.5.7 Molecular structures

$\text{CpMo}(\text{CO})_2\{\text{S}_2\text{P}(\text{SC}_6\text{H}_4\text{Me})_2\}$ (**14**)

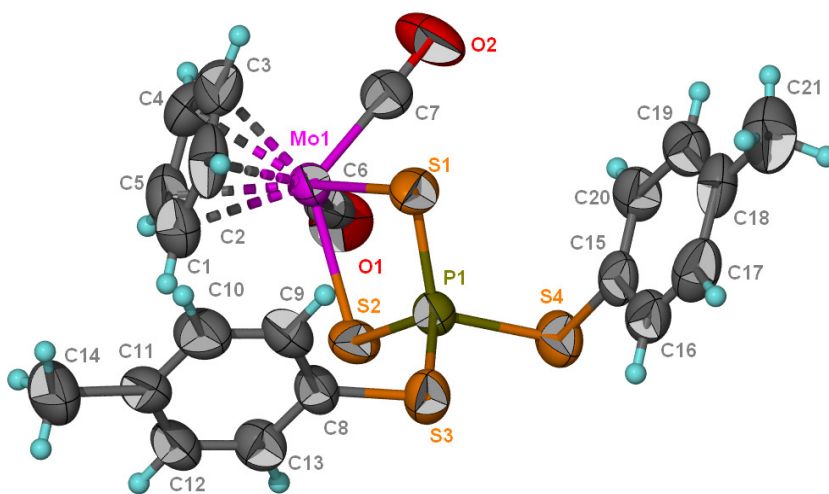


Figure 20. Molecular structure of $\text{CpMo}(\text{CO})_2\{\text{S}_2\text{P}(\text{SC}_6\text{H}_4\text{Me})_2\}$ (**14**)

$\text{CpMo}(\text{CO})_2\{\text{S}_2\text{P}(\text{SC}_6\text{H}_4\text{Me})_2\}$ (**14**) crystallized in orthorhombic, space group $Pbca$. The molecular structure of **14** is shown in Figure 20 and the bond lengths and bond angles are tabulated in Table 24. The monomeric structure **14** possesses a four-legged piano-stool configuration about Mo, coordinated to a bidentate di-*p*-tolylthiophosphetane fragment and two CO ligands and is structurally similar to that of $\text{Cp}^*\text{Mo}(\text{CO})_2(\text{S}_2\text{P}(\text{OPr}^i)_2)$ ($\text{Cp}^* = \eta^5\text{-C}_5\text{H}_4\text{Me}$) [105] and the analogous Cr complex $\text{CpCr}(\text{CO})_2(\text{S}_2\text{PR}_2)$ ($\text{R} = \text{Ph}$ [106a], OPr^i [106b]). The average distance of 2.555 Å for Mo1-S1 and -S2 in $\text{Cp}^*\text{Mo}(\text{CO})_2(\text{S}_2\text{P}(\text{OPr}^i)_2)$ is slightly shorter than **14** (average 2.561 Å) is possibly due to the Cp^* ring stabilization effect. Both $\text{Cp}^*\text{Mo}(\text{CO})_2(\text{S}_2\text{P}(\text{OPr}^i)_2)$ and **14** have almost identical ligand bite angles (S(1)-Mo-S(2)) which are $76.50(4)^\circ$ and $76.65(4)^\circ$, respectively. However, **14** could be the first metal complex with a S_2PS_2 center framework that has been synthesized.

$\text{Cp}_2\text{Mo}_2(\text{CO})_5\{\text{S}_2\text{P}(\text{SC}_6\text{H}_4\text{Me})\}$ (**15**)

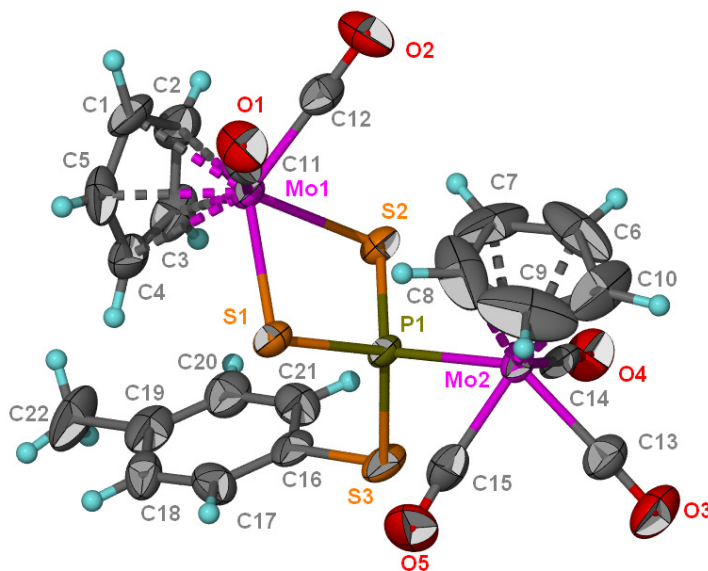


Figure 21. Molecular structure of $\text{Cp}_2\text{Mo}_2(\text{CO})_5\{\text{S}_2\text{P}(\text{SC}_6\text{H}_4\text{Me})\}$ (**15**)

$\text{Cp}_2\text{Mo}_2(\text{CO})_5\{\text{S}_2\text{P}(\text{SC}_6\text{H}_4\text{Me})\}$ (**15**) crystallized in monoclinic, space group $P2_1/a$. The molecular structure of $\text{Cp}_2\text{Mo}_2(\text{CO})_5\{\text{S}_2\text{P}(\text{SC}_6\text{H}_4\text{Me})\}$ (**15**) is shown in Figure 21 and

its bond lengths and bond angles are tabulated in Table 24. The molecular structure of **15** is almost similar to **14** with the exception that one of the *p*-tolythiodithiaphosphetane fragment is replaced by a CpMo(CO)₃ moiety at P1. This bulkier replacement has an elongation effect on the MoPS₂ ring, as indicated by the Mo1-P1 distances for **14** and **15** which have increased from 3.206 Å to 3.283 Å, respectively. The position of the two η⁵-coordinated Cp rings is located almost perpendicular to each other. The dicarbonylated Mo1 is coordinated to the monodentate tolydithiaphosphetane at S1 and S2, while the other tricarbonylated Mo2 is coordinated to the ligand at P1. The distances between both bridging sulfides in **14** and **15** (3.176 and 3.143 Å, respectively) are relatively too far apart to be bonded when compared to that of **16** (S2-S3) (2.117(1) Å).

Cp₂Mo₂(μ-S₂)(μ-S)(μ-SC₆H₄Me) (**16**)

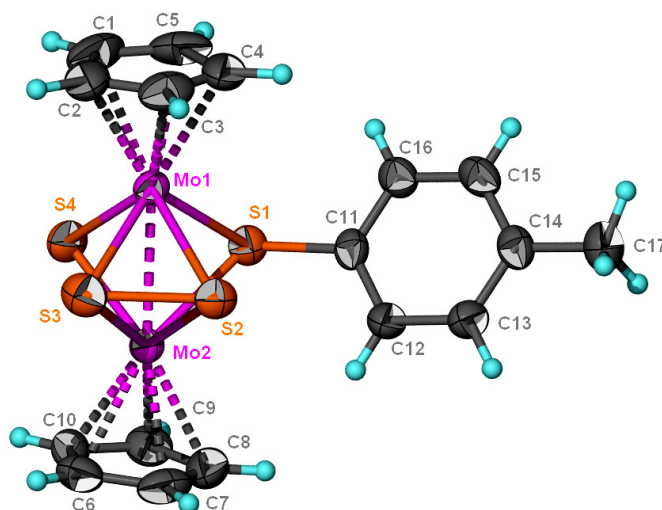


Figure 22. Molecular structure of Cp₂Mo₂(μ-S₂)(μ-S)(μ-SC₆H₄Me) (**16**)

Cp₂Mo₂(μ-S₂)(μ-S)(μ-SC₆H₄Me) (**16**) crystallized in monoclinic, space group P2₁/n. The molecular structure of Cp₂Mo₂(μ-S₂)(μ-S)(μ-SC₆H₄Me) (**16**) is illustrated in Figure 22 and its bond lengths and bond angles are tabulated in Table 24. The quadruply thiolato bridged complex **16** belongs to a well characterized group of structures which contain a

Mo₂(μ-S)₄ residue such as Cp*₂Mo₂(μ-SCH₃)₂(μ-S)₂ (Cp* = η⁵-pentamethyl-cyclopentadienyl) [107a], Cp₂Mo₂(μ₂-SCH₃)₄ [107b], Cp'₂Mo₂(μ₂-SCH₃)₂(μ₂-S)₂ (Cp' = η⁵-methyl-cyclopentadienyl) [107c] and Cp''₂Mo₂(μ₂-SCH₃)₄ (Cp'' = η⁵-ethyltetramethylcyclopentadienyl) [107d]. **16** features a Mo₂S₄ framework with a near square-planar arrangement of the four μ-η²-S atoms, perpendicular to the Mo-Mo bond and almost parallel to the two (η⁵-C₅H₅) planes. The greater steric effects of the *p*-tolylthio group results in longer Mo-S(thiolato) bond distances of Mo1-S1 and Mo2-S2 [average 2.472(1) Å] as compared to the other Mo-S(sulfido) distances [average 2.348(1) Å].

Interestingly, the four S atoms are bonded in 3 different modes comprising a μ₂-dithiolato (S2-S3), a μ₂-thiolato (S4) and a μ₂-*p*-tolylthiolato (S1). The electron withdrawing *p*-tolylthiolate ligand reduces the electron density in S1 hence resulting in an extended Mo-S (average 2.486(1) Å) bond length as compared to the other μ₂-sulfido (S4) (average 2.312(1) Å) and μ₂-disulfido ligand (S2-S3) (average 2.422(1) Å). The Mo-Mo distance of 2.652(4) Å indicates a double bond in accordance to the demand of the 18 e rule and is comparable with the distance in [CpMo(SBz)S]₂ (average 2.58(6)) [92].

Table 24. Bond lengths (Å) and angles (°) for **14**, **15** and **16**

<i>Bond lengths</i>	14	15	16
Mo1—Mo2			2.652(5)
Mo1—S1	2.588(1)	2.538(3)	2.483(1)
Mo1—S2	2.564(1)	2.537(3)	2.425(1)
Mo1—S3			2.419(1)
Mo1—S4			2.315(1)
Mo2—P1		2.524(3)	
Mo2—S1			2.488(1)
Mo2—S2			2.418(1)
Mo2—S3			2.424(1)
Mo2—S4			2.309(1)
P1—S1	1.990(1)	2.036(4)	
P1—S2	1.992(1)	2.043(4)	
P1—S3	2.090(1)	2.110(4)	

P1—S4	2.105(1)		
S2—S3			2.117(1)
<i>Bond angles</i>			
Mo1-S1-P1	88.74(6)	91.04(12)	
Mo1-S2-P1	88.52(6)	90.91(12)	
Mo1-S1-Mo2			64.50(3)
Mo1-S2-Mo2			66.42(3)
Mo1-S3-Mo2			66.40(3)
Mo1-S4-Mo2			69.99(3)
Mo2-P1-S1		115.41(13)	
Mo2-P1-S2		115.22(14)	
Mo2-P1-S3		104.48(13)	
Mo2-S2-S3			64.23(4)
P1-S3-C8	100.48(17)		
P1-S4-C15	101.00(17)		
P1-S3-C16		102.2(4)	
S1-P1-S2	105.78(8)	100.76(15)	
S1-P1-S3	114.95(9)	110.58(17)	
S1-P1-S4	109.63(8)		
S2-Mo1-S1	76.65(4)	76.52(19)	
S2-P1-S3	113.84(9)	110.55(16)	
S2-P1-S4	109.63(8)		
S3-P1-S4	99.39(8)		
S3-P1-Mo2		104.48(13)	
S3-S2-Mo1			69.99(3)
S3-S2-Mo2			64.23(4)

Cp₂Mo₂(CO)₂(μ-PS)(μ-SC₆H₄Me) (18)

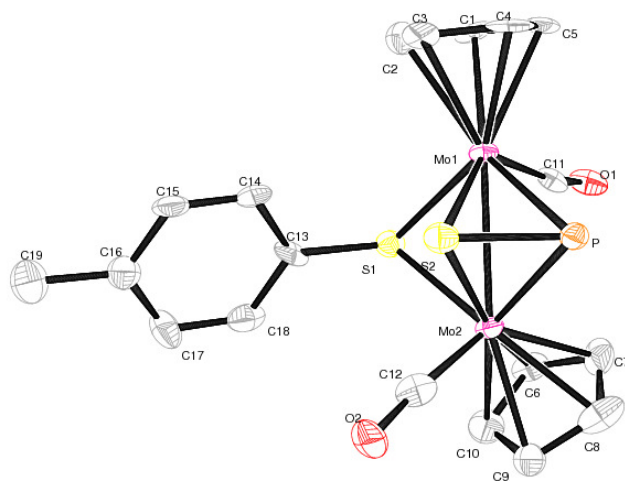


Figure 23. Molecular structure of Cp₂Mo₂(CO)₂(μ-PS)(μ-SC₆H₄Me) (**18**)

The molecular structure of **18** is shown in Figure 23. The selected bond lengths (Å) and bond angles (°) of **18** are shown in Table 25. $\text{Cp}_2\text{Mo}_2(\text{CO})_2(\mu\text{-PS})(\mu\text{-SC}_6\text{H}_4\text{Me})$ (**18**) crystallized in triclinic, space group P-1. The complex **18** features a $\text{Mo}_2\text{S}_2\text{P}$ framework with two CO ligands in the *trans* orientation. The Cp ring coordinated at Mo1 is at the apical position while the Cp ring coordinated at Mo2 is tilted away from C(12)-O(2) and the $-\text{SC}_6\text{H}_4\text{Me}$ fragment to reduce the steric hindrance generated by those ligands. The dihedral angle between Mo(1)-S(1)-Mo(2) plane and Mo(1)-P-Mo(2) plane is $167.47(16)^\circ$ which forms a near square-planar arrangement. The bond distance of Mo-S (thiolato) [2.458(5) Å] in **18** is shorter than that found in $\text{Cp}_2\text{Mo}_2(\mu\text{-S}_2)(\mu\text{-S})(\mu\text{-SC}_6\text{H}_4\text{Me})$ (**16**) [2.486(1) Å] while the bond distance of Mo-S (μ_2 -sulfido) [2.455(5) Å] in **18** is longer than a similar bond in **16** [2.312(1) Å]. The Mo-Mo distance of 2.852(4) Å indicates a single bond and is comparable with the distance in $[\text{CpMo}(\text{CO})(\text{SBz})]_2\text{S}$ (**11**) [2.802 Å] which is also in accordance to the 18 e rule.

Table 25. Bond lengths [Å] and angles [°] for $\text{Cp}_2\text{Mo}_2(\text{CO})_2(\mu\text{-PS})(\mu\text{-SC}_6\text{H}_4\text{Me})$ (**18**)

Bond lengths			
Mo(1)-C(11)	1.991(17)	Mo(2)-C(12)	1.922(18)
Mo(1)-S(1)	2.451(5)	Mo(2)-S(1)	2.465(5)
Mo(1)-S(2)	2.441(5)	Mo(2)-S(2)	2.468(5)
Mo(1)-P	2.474(5)	Mo(2)-P	2.462(5)
Mo(1)-Mo(2)	2.852 (4)	C(11)-O(1)	1.142(18)
S(2)-P	2.078(6)	C(12)-O(2)	1.205(19)
Bond angles			
C(11)-Mo(1)-S(2)	130.7(5)	C(12)-Mo(2)-P	103.1(13)
C(11)-Mo(1)-S(1)	84.2(5)	C(12)-Mo(2)-S(1)	99.6(5)
C(11)-Mo(1)-P	92.2(5)	C(12)-Mo(2)-S(2)	68.1(5)
C(11)-Mo(1)-Mo(2)	78.3(4)	C(12)-Mo(2)-Mo(1)	118.3(5)
S(2)-Mo(1)-S(1)	80.97(15)	S(1)-Mo(2)-S(2)	80.15(15)
S(2)-Mo(1)-P	50.00(14)	S(1)-Mo(2)-Mo(1)	54.31(11)
S(1)-Mo(1)-P	108.32(16)	S(2)-Mo(2)-Mo(1)	54.05(11)

S(2)-Mo(1)-Mo(2)	54.93(11)	P-Mo(2)-S(1)	108.28(16)
S(1)-Mo(1)-Mo(2)	54.78(10)	P-Mo(2)-S(2)	49.85(14)
P-Mo(1)-Mo(2)	54.50(11)	P-Mo(2)-Mo(1)	54.92(10)
O(2)-C(12)-Mo(2)	173.9(13)	S(2)-P-Mo(2)	65.24(16)
O(1)-C(11)-Mo(1)	169.1(13)	S(2)-P-Mo(1)	64.17(16)
P-S(2)-Mo(1)	65.83(17)	Mo(2)-P-Mo(1)	70.58(15)
P-S(2)-Mo(2)	64.91(17)	C(13)-S(1)-Mo(2)	109.3(5)
Mo(1)-S(2)-Mo(2)	71.02(15)	C(13)-S(1)-Mo(1)	114.1(5)
		Mo(2)-S(1)-Mo(1)	71.02(15)

Torsion angles

S(2)-Mo(1)-Mo(2)-S(1)	105.11(18)
P-Mo(1)-Mo(2)-S(1)	167.47(16)

Cp₃Mo₃(μ-S)₂(μ-S₂)(μ₃-S) (20)

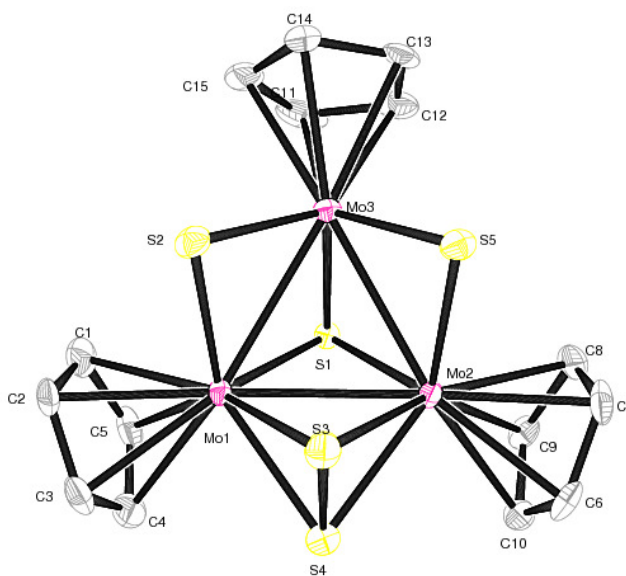


Figure 24. Molecular structure of Cp₃Mo₃(μ-S)₂(μ-S₂)(μ₃-S) (**20**)

The molecular structure of **20** is shown in Figure 24. The selected bond lengths (Å) and bond angles (°) of **20** are shown in Table 26. Cp₃Mo₃(μ-S)₂(μ-S₂)(μ₃-S) (**20**) crystallized in P2₁/c and consists of a Mo₃S₅ core. The three Mo atoms are connected by two μ₂-sulfido, one μ₃-sulfido and one μ₃-disulfido ligands in a highly symmetrical arrangement which is in accordance with the observed Cp chemical shifts in the ¹H NMR.

The bond lengths and bond angles of **20** are shown in Table 26. The Mo- μ_2 -S distance (average 2.3902(13) Å) is slightly longer than the Mo- μ_3 -S (average 2.3447(12) Å) but is shorter than Mo- μ_3 -S₂ (average 2.4612(14) Å). The differences in bond lengths between the different modes of the Mo-S bond depend on the distribution of the electrons at each sulfur atom. However, the bond length between each Mo-Mo bond is very similar (average 2.8881(6) Å) and is comparable to that in other Mo-Mo single bond complexes [7b, 89].

Table 26. Bond lengths [Å] and angles [°] for Cp₃Mo₃(μ -S)₂(μ -S₂)(μ_3 -S) (**20**)

Mo(1)-S(1)	2.3460(12)	Mo(2)-S(1)	2.3433(12)
Mo(1)-S(2)	2.3932(13)	Mo(2)-S(5)	2.3871(13)
Mo(1)-S(3)	2.4743(14)	Mo(2)-S(4)	2.4528(15)
Mo(1)-S(4)	2.4492(15)	Mo(2)-S(3)	2.4685(14)
Mo(1)-Mo(2)	2.8807(6)	Mo(2)-Mo(3)	2.8879(6)
Mo(1)-Mo(3)	2.8957(6)	Mo(3)-S(5)	2.2664(13)
S(3)-S(4)	2.055(2)	Mo(3)-S(2)	2.2724(14)
		Mo(3)-S(1)	2.3383(12)
Bond angles			
S(1)-Mo(1)-S(2)	100.20(5)	S(5)-Mo(2)-Mo(3)	49.79(3)
S(1)-Mo(1)-S(4)	89.52(5)	S(4)-Mo(2)-Mo(3)	113.95(4)
S(2)-Mo(1)-S(4)	132.65(5)	S(3)-Mo(2)-Mo(3)	88.46(4)
S(1)-Mo(1)-S(3)	106.14(5)	Mo(1)-Mo(2)-Mo(3)	60.262(14)
S(2)-Mo(1)-S(3)	83.67(5)	S(5)-Mo(3)-S(2)	99.64(5)
S(4)-Mo(1)-S(3)	49.33(5)	S(5)-Mo(3)-S(1)	104.20(5)
S(1)-Mo(1)-Mo(2)	52.05(3)	S(2)-Mo(3)-S(1)	104.10(5)
S(2)-Mo(1)-Mo(2)	96.97(4)	S(5)-Mo(3)-Mo(2)	53.54(3)
S(4)-Mo(1)-Mo(2)	54.07(4)	S(2)-Mo(3)-Mo(2)	99.63(4)
S(3)-Mo(1)-Mo(2)	54.26(3)	S(1)-Mo(3)-Mo(2)	51.99(3)
S(1)-Mo(1)-Mo(3)	51.70(3)	S(5)-Mo(3)-Mo(1)	99.58(4)
S(2)-Mo(1)-Mo(3)	49.79(3)	S(2)-Mo(3)-Mo(1)	53.53(3)
S(4)-Mo(1)-Mo(3)	113.79(4)	S(1)-Mo(3)-Mo(1)	51.94(3)
S(3)-Mo(1)-Mo(3)	88.18(4)	Mo(2)-Mo(3)-Mo(1)	59.747(14)
Mo(2)-Mo(1)-Mo(3)	59.991(14)	Mo(3)-S(1)-Mo(2)	76.17(4)
S(1)-Mo(2)-S(5)	100.37(5)	Mo(3)-S(1)-Mo(1)	76.37(4)
S(1)-Mo(2)-S(4)	89.50(5)	Mo(2)-S(1)-Mo(1)	75.81(4)
S(5)-Mo(2)-S(4)	132.64(5)	Mo(3)-S(2)-Mo(1)	76.68(4)
S(1)-Mo(2)-S(3)	106.41(4)	S(4)-S(3)-Mo(2)	64.92(6)
S(5)-Mo(2)-S(3)	83.65(5)	S(4)-S(3)-Mo(1)	64.70(6)
S(4)-Mo(2)-S(3)	49.35(5)	Mo(2)-S(3)-Mo(1)	71.30(4)

S(1)-Mo(2)-Mo(1)	52.14(3)	S(3)-S(4)-Mo(1)	65.97(6)
S(5)-Mo(2)-Mo(1)	97.14(4)	S(3)-S(4)-Mo(2)	65.72(6)
S(4)-Mo(2)-Mo(1)	53.95(4)	Mo(1)-S(4)-Mo(2)	71.98(4)
S(3)-Mo(2)-Mo(1)	54.44(3)	Mo(3)-S(5)-Mo(2)	76.67(4)
S(1)-Mo(2)-Mo(3)	51.83(3)		

2.6 Studies of [CpCr(CO)₃]₂ (**1**) with 2,4-bis(phenyl)-1,3-diselenadiphosphetane-2,4-diselenide (Woollins' Reagent)

2.6.1 The reaction of [CpCr(CO)₃]₂ (**1**) with an equimolar amount of Woollins' Reagent (WR)

The facile reaction of [CpCr(CO)₃]₂ (**1**) with one mole equivalent of WR, [PhP(Se)Se]₂ at ambient temperature completed in 0.5 h leads to the isolation of Cp₂Cr₂(CO)₄Se (**21**) as the main product together with traces of *trans*-[CpCr(CO)₂(SePPh)]₂ (**22**), CpCr(CO)₂{SeP(H)Ph} (**23**) and an uncharacterized insoluble green residue resulting from decomposed WR.

This observation is comparable to the reaction of **1** with elemental selenium [46c-d] and the mixed ligand P₄Se₃ [15-17] affording **21** as the main product. It is envisaged that the labile monomeric species CpCr(CO)₃[•] (**1A**) or CpCr(CO)₂[•] (**2A**) [3, 5, 108] generated from the dissociation of **1** reacts with excess WR resulting in its cleavage and the subsequent abstraction of the Se atom to form **21** as depicted in route (i) in Scheme 28. However, a similar reaction of **1** with 0.125 equivalent of WR gave Cp₂Cr₂(CO)₄Se (58% yield), unreacted Cp₂Cr₂(CO)₆ (**1**) (17% recovery) and *trans*-[CpCr(CO)₂(SePPh)]₂ (**22**) (25% yield). It was observed WR was completely consumed since **1** was in excess and noticeably the uncharacterized insoluble green residue was not formed.

2.6.2 The reaction of $[\text{CpCr}(\text{CO})_2]_2$ (**4**) with equimolar Woollins' Reagent

The reaction of the triply bonded congener $\text{Cp}_2\text{Cr}_2(\text{CO})_4$ (**2**) with an equivalent of WR required a longer time of 3 h and at an elevated temperature of 60 °C to yield **23** (18%), **22** (3%), **24** (2%) and an uncharacterized insoluble green precipitate (361 mg). It is worthy to note that $\text{Cp}_2\text{Cr}_2(\text{CO})_4\text{Se}$ (**21**) was not formed here which agrees with previous reports involving selenation agents such as Se_8 [46c-d] and Ph_2Se_2 [48].

During the thermolysis of **22** which was monitored by ^1H NMR at 110 °C, the emergence of a species at δ 4.26 together with the formation of **24** (δ 5.04) was observed. It is proposed that this species (δ 4.26) is $\text{CpCr}(\text{CO})_2(\text{SePPh})$ (**23A**) which results from the loss of a hydrogen since the ^1H chemical shifts for **23** are δ 4.26 (Cp) and δ 5.72 (P-H) (route v). The formation of this phosphinoselenoylidene product, **23A** is believed to be the common intermediate species which acts as a precursor to the formation of **22** and **24**. This postulation agrees with the NMR tube thermolysis study of **23** at 110 °C for 14 h which gave **22** (38% yield) and **24** (11% yield) and also from the ESI ms data of **23** which shows the presence of *trans*- $[\text{CpCr}(\text{CO})_2(\text{SePPh})]_2$ ($m/e = 722$). These observations suggest that the thermally unstable **23** is likely to be the primary product which slowly converts to the secondary product **22** via **23A** (route iv and vi). Under similar conditions, cothermolysis of **23** with WR gave unreacted **23** (19% recovered), **22** (6% yield), **24** (31% yield) and some uncharacterized Cp-containing compounds. As expected, in the presence of WR more Se atoms will be available for the formation of **24**, hence prolonged thermolysis ultimately resulted in the isolation of the eight-membered ring complex $[\text{CpCr}(\text{Se}_2\text{P}(\text{O})\text{Ph})]_2$ (**24**) as the final thermolytic product (route vii).

2.6.3 NMR spectral studies

(a) Thermolysis of CpCr(CO)₂(SeP(H)Ph) (**23**)

Thermolysis of CpCr(CO)₂(SeP(H)Ph) (**23**) (20 mg, 0.055 mmol) in toluene-*d*₈ (~0.5 mL) at 110 °C was monitored *via* ¹H NMR at regular intervals. A time-dependent variation of product composition from the thermolysis study of CpCr(CO)₂(SeP(H)Ph) (**23**) is given in Table 27. The study was completed in 14 h, giving **22** (38%) as the main product together with **24** (11%) as the final thermolyzed product. This observation suggested that **23** is the primary product and **22** is the secondary product.

Table 27. Time dependent variation of product composition^a from thermolysis study of CpCr(CO)₂(SeP(H)Ph) (**23**)

Complexes (%) Time/h	<i>trans</i> - [CpCr(CO) ₂ (SePPh)] ₂ (22)	CpCr(CO) ₂ (SeP(H)Ph) (23)	Cp ₂ Cr ₂ (Se ₂ P(O)Ph) ₂ (24)
0	2	94	-
1	2	65	7
4	2.5	37	9
14	38	-	11

^a – Products yields obtained by integration of Cp resonances in ¹H NMR spectra of product mixture.

(b) Thermolysis of *trans*-[CpCr(CO)₂(SePPh)]₂ (**22**)

Thermolysis of *trans*-[CpCr(CO)₂(SePPh)]₂ (**22**) (13 mg, 0.018 mmol) in toluene-*d*₈ (~0.5 mL) at 110 °C was monitored *via* ¹H NMR at regular intervals. A time-dependent variation of product composition from the thermolysis study of CpCr(CO)₂(SeP(H)Ph) (**23**) is given in Table 28. The results obtained from this study showed the presence of an intermediate **23A** during thermal degradation of **22** to give **24**.

Table 28. Time dependent variation of product composition^a from the thermolysis study of *trans*-[CpCr(CO)₂(SePPh)]₂ (**22**)

Complexes (%) Time/h	<i>trans</i> - [CpCr(CO) ₂ (SePPh)] ₂ (22)	CpCr(CO) ₂ (SePPh) (23A)	Cp ₂ Cr ₂ (Se ₂ P(O)Ph) ₂ (24)
0	36	-	-
1	25	16	8
2	23	16	12
3	14	8	19
5	-	10	34

^a – Products yields obtained by integration of Cp resonances in ¹H NMR spectra of product mixture

(c) Thermolysis of Cp₂Cr₂(Se₂P(O)Ph)₂ (24**)**

Thermolysis of Cp₂Cr₂(Se₂P(O)Ph)₂ (**24**) (22 mg, 0.013 mmol) in toluene-*d*₈ (~0.5 mL) at 110 °C was monitored *via* ¹H NMR at regular intervals. After 14 h, complex **24** was completely decomposed in the solution.

(d) Cothermolysis of CpCr(CO)₂(SeP(H)Ph) (23**) and Woollins' Reagent**

The ¹H NMR spectral observation of the co-thermolysis study of CpCr(CO)₂(SeP(H)Ph) (**23**) (20 mg, 0.055 mmol) with an equimolar amount of Woollins' reagent (29 mg, 0.055 mmol) in toluene-*d*₈ (~0.5 mL) at 110 °C is summarized in Table 29. The spectra were examined at intervals of 0.5 h, 2 h, 4 h, 5 h and 14 h. The recorded spectra showed that in the presence of Woollins' Reagent which acts as a selenium transfer agent, the rate of the formation of **24** will increase.

Table 29. Time dependent variation of product composition^a from co-thermolysis study of CpCr(CO)₂(SeP(H)Ph) (**23**) with Woollins' reagent

Time/h \ Complexes (%)	<i>trans</i> - [CpCr(CO) ₂ (SePPh)] ₂ (22)	CpCr(CO) ₂ (SeP(H)Ph) (23)	Cp ₂ Cr ₂ (Se ₂ P(O)Ph) ₂ (24)
0	3.3	85	-
0.5	2	47	16
2	1	45	23
5	1	37	26
14	6	19	31

^a – Product yields obtained by integration of Cp resonances in ¹H NMR spectra of product mixture.

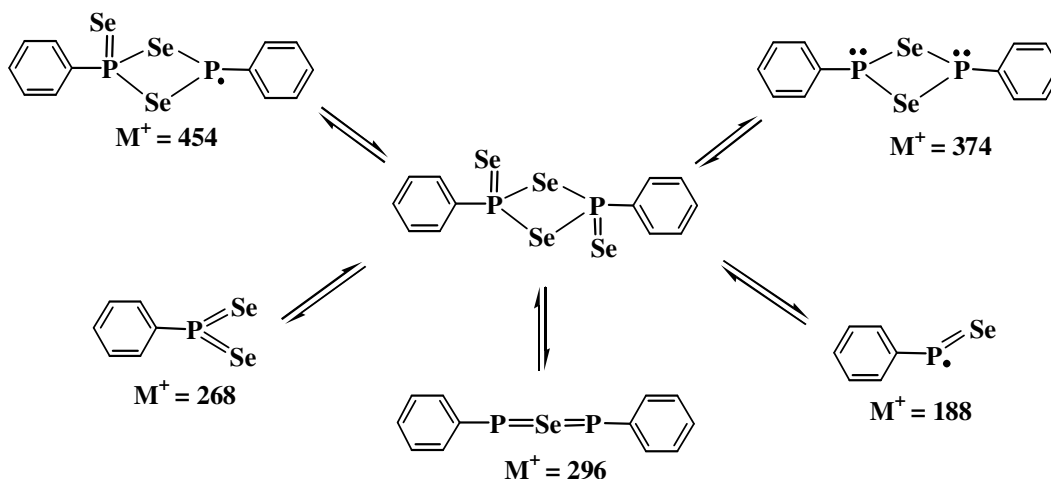
2.6.3 Mechanistic Pathway: Formation of Cp₂Cr₂(CO)₄Se (**21**), *trans*-[CpCr(CO)₂(SePPh)]₂ (**22**), CpCr(CO)₂(SeP(H)Ph) (**23**) and [CpCr(Se₂P(O)Ph)]₂ (**24**)

Similar to its sulfur analogue of LR [56a, b], WR also undergoes P₂Se₂ ring opening mechanism with a propensity to give several types of fragments as detected by mass spectrometry [109] (Scheme 27). The molecular structure of **23** suggested that its formation is likely to result from the attack of CpCr(CO)_n• (n = 2 (**2A**) or 3 (**1A**)) radical at the P₂Se₂ central ring of the WR to generate the PhPSe• fragment. Further interaction of **1A** or **2A** with a PhPSe• fragment followed by the subsequent abstraction of H afforded **23** (route ii and iii). The source of hydrogen is believed to be the coordinated Cp, as proposed by Goh *et al* in a similar reaction with LR [56a] which explained the presence of several unassigned peaks in the Cp region encountered in the product solutions. Such observation was also present especially in reaction mixtures of **1** and **2** with WR and some chromatographed fractions as weak intensity Cp resonances between δ 5.55 and 4.07. However, the unstable **23** undergoes thermolytic degradation with the loss of hydrogen to

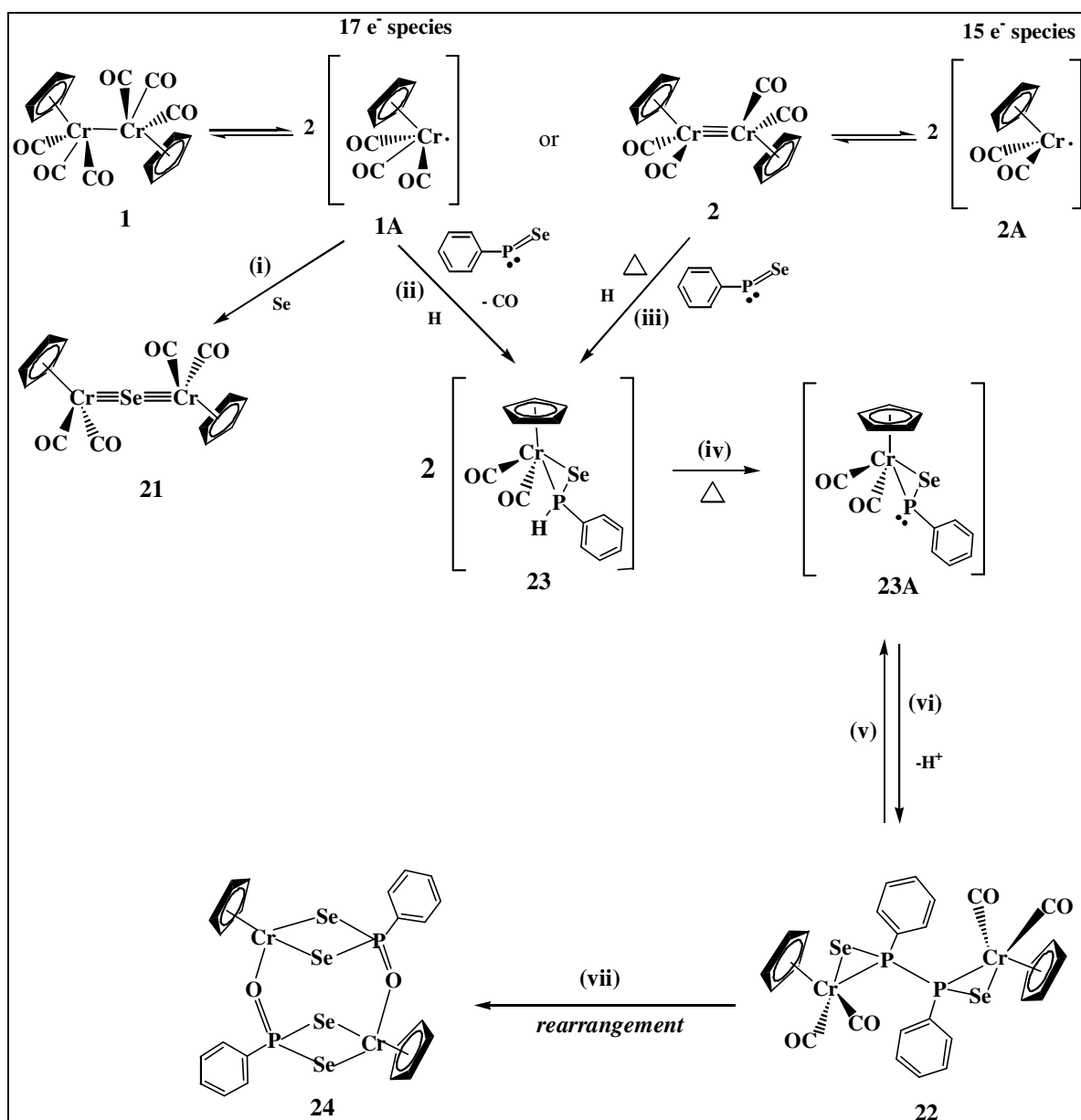
give **23A** (route iv). From the thermolysis study, it is proposed that the formation of **22** is reversible which proceeds with dimerization of **23A** via P-P bond coupling and decoupling (route v and vi). The similarities in both P-Se (2.1487(14) Å) and Cr-Se (2.6389(9) Å) bond lengths for CpCr(CO)₂(SeP(H)Ph) (**23**) as compared to those in **22** (2.1425(17) Å and 2.6309(12) Å, respectively) provides further supportive evidence.

Selenation of **22** from the WR ligand with concomitant bond formation and cleavage followed by intramolecular bond rearrangements with dimerization, decarbonylation and oxygen abstraction results in the formation of **24** (route vii). From the experiment carried out in the absence of water and oxygen, the potential source of oxygen in **24** is still inconclusive.

The ease of fragmentation of the P-Se heterocyclic ligand which leads to ring opening in WR is similar to that of its P-S analogue, Lawesson's reagent, [CH₃OC₆H₄PS₂]₂. Indeed, both ligands showed similar patterns of reactivity yielding some structurally analogous products with **1** [56a].



Scheme 27. Fragmentation pattern of Woollins' reagent [109]



Scheme 28. Synthetic pathway of $\text{Cp}_2\text{Cr}_2(\text{CO})_4\text{Se}$ (**21**), $\text{trans}-[\text{CpCr}(\text{CO})_2(\text{SePPh})]_2$ (**22**), $\text{CpCr}(\text{CO})_2(\text{SeP}(\text{H})\text{Ph})$ (**23**) and $[\text{CpCr}(\text{Se}_2\text{P}(\text{O})\text{Ph})]_2$ (**24**) from the reaction of $\text{Cp}_2\text{Cr}_2(\text{CO})_6$ (**1**) with 0.5 mole equivalent of Woollins' reagent

2.6.4 Physical properties

Trans- $[\text{CpCr}(\text{CO})_2(\text{SePPh})]_2$ (**22**)

Trans- $[\text{CpCr}(\text{CO})_2(\text{SePPh})]_2$ exists as a brown precipitate. It is stable both in the solid state and solution for a couple of hours at ambient temperature under an inert

atmosphere. It is partially soluble in *n*-hexane and very soluble in toluene to form a brown solution.

CpCr(CO)₂(SeP(H)Ph) (23)

CpCr(CO)₂(SeP(H)Ph) exists as a dark purple crystalline solid. In the solid state, it is stable for a couple of hours at ambient temperature under an inert atmosphere. It is soluble in toluene to give a deep purple solution. In solution, it is stable at low temperature but will decompose after a few hours at ambient temperature.

[CpCr(Se₂P(O)Ph)]₂ (24)

[CpCr(Se₂P(O)Ph)]₂ exists as a green precipitate on drying. It is stable both in the solid state and solution for a couple of hours at ambient temperature under an inert atmosphere. It is only soluble in ether and THF to give a green solution.

2.6.5 Spectral properties

2.6.5.1 IR spectra

***Trans*-[CpCr(CO)₂(SePPh)]₂ (22)**

The IR spectrum of **22** in nujol shows ν_{CO} at 1962vs, 1951vs, 1899vs cm⁻¹; other peaks at 1086m, 1063m, 1016m, 860vw, 844vw, 828w, 803w, 741w, 690w, 664vw cm⁻¹ (refer to Appendix I).

CpCr(CO)₂(SeP(H)Ph) (23)

The IR spectrum of **23** in nujol shows ν_{CO} at 1954vs, 1942vs, 1871vs, 1853sh, and 1847sh cm⁻¹ and other peaks at 1159m, 1110m, 1093m, 1067m, 1055m, 1014m, 921m, 912m, 846m, 82 m, 748m, 727w, 706vw, 690m, 685m, 639.48m, 590.79m, 550m cm⁻¹ (refer to Appendix I).

[CpCr(Se₂P(O)Ph)]₂ (24)

The IR spectrum of **24** in nujol shows stretching frequencies at 1157w, 1106m, 1084m, 1058m, 1026m, 998m, 815m, 741w, 728sh, 686w cm⁻¹ (refer to Appendix I).

2.6.5.2 NMR spectra

***Trans*-[CpCr(CO)₂(SePPh)]₂ (22)**

The complex **22** is a symmetrical Cr dimer, and one Cp ring signal appeared in both the ¹H and ¹³C NMR spectra in benzene-*d*₆. In the ¹H NMR spectrum, one Cp signal was recorded at δ 4.01 and the -C₆H₅ peaks were recorded as multiplets at δ 7.72-7.02. In the ¹³C NMR spectrum, the Cp peak was recorded at δ 89.52 and proton resonances of the Ph ring peaks, -C₆H₅, were recorded at δ 138.65, 138.23, 130.56, 129.65, 128.89, 126.02 and the CO peaks were recorded at δ 254.22, 249.79.

CpCr(CO)₂(SeP(H)Ph) (23)

The complex **23** is a monomeric species with one hydride bonded to the phosphorus atom. One Cp signal was recorded both in the ¹H and ¹³C NMR spectra in benzene-*d*₆. In the ¹H NMR spectrum, the Cp signal was recorded at δ 4.26, the P-H signal was recorded at δ 5.72 and the -C₆H₅ were recorded as multiplets at δ 7.37-6.68. In the ¹³C NMR spectrum, the Cp peak was recorded at δ 89.53, the -C₆H₅ peaks were recorded at δ 132.71, 132.59, 131.37, 129.67, 129.62, 129.50 and the CO peaks were recorded at δ 254.22, 249.79. In the ³¹P NMR proton coupled spectrum (refer to Appendix II), the signals were recorded at δ 48.26, 45.84 with $J = 387.6$ Hz. However in the ³¹P NMR proton decoupled spectrum (refer to Appendix II), the signals were recorded at δ 47.27 and 46.68.

[CpCr(Se₂P(O)Ph)]₂ (**24**)

The complex **24** is a dimeric arylthioxophosphane chromium complex. One Cp signal was recorded in both ¹H and ¹³C NMR spectra in benzene-*d*₆. In the ¹H NMR spectrum, the Cp signal was recorded at δ 5.13 and the -C₆H₅ signals were recorded as multiplets at δ 7.71-7.03. In the ¹³C NMR spectrum, the Cp signal was recorded at δ 126.02 and the -C₆H₅ signals were recorded at δ 138.63, 138.20, 132.46, 130.56, 129.67. In the ³¹P NMR spectrum (refer to Appendix II), one peak was recorded at the high field region, δ -123.34 which was due to the presence of the oxygen in the complex.

2.6.5.3 Mass spectra

Trans-[CpCr(CO)₂(SePPh)]₂ (**22**)

The mass spectrum of **22** shows the parent ion $m/z = 722.4748$ *trans*-[CpCr(CO)₂(SePPh)]₂ and its fragmentation ions as listed in Table 30.

Table 30. Electrospray ionization mass spectrum of *trans*-[CpCr(CO)₂(SePPh)]₂ (**22**)

m/z	Assignments
802	Cp ₂ Cr ₂ (Se ₂ (O)PPh) ₂
722	Cp ₂ Cr ₂ (CO) ₄ (SePPh) ₂
666	Cp ₂ Cr ₂ (CO) ₂ (SePPh) ₂
589	Cp ₂ Cr ₂ (CO) ₂ (SePPh)(SeP-)
533	Cp ₂ Cr ₂ (SePPh)(SeP-)
502	Cp ₂ Cr ₂ (Se ₂ PPh)(Se)
451	Cp ₂ Cr ₂ (CO)(SePPh)
401	CpCr(Se ₂ (O)PPh)
385	CpCr(Se ₂ PPh)
228	CpCrSeP

CpCr(CO)₂(SeP(H)Ph) (23)

The mass spectrum of **23** shows the parent ion $m/z = 362.2380$ CpCr(CO)₂(SeP(H)Ph) and its fragmentation ions as listed in Table 31.

Table 31. Electrospray ionization mass spectrum of CpCr(CO)₂(SeP(H)Ph) (**23**)

m/z	Assignments
723	Cp ₂ Cr ₂ (CO) ₄ (SePPh) ₂
695	Cp ₂ Cr ₂ (CO) ₃ (SePPh) ₂
666	Cp ₂ Cr ₂ (CO) ₂ (SePPh) ₂

[CpCr(Se₂P(O)Ph)]₂ (24)

The mass spectrum of **24** shows the parent ion $m/z = 801.5744$ [CpCr(Se₂P(O)Ph)]₂ and its fragmentation ions as listed in Table 32.

Table 32. Electrospray ionization mass spectrum of [CpCr(Se₂P(O)Ph)]₂ (**24**)

m/z	Assignments
802	Cp ₂ Cr ₂ (Se ₂ (O)PPh) ₂
401	[CpCr(Se ₂ P(O)Ph)]
308	[CpCr(Se ₂ P)]
277	[CpCrSe ₂]

2.6.6 Molecular structures

Trans-[CpCr(CO)₂(SePPh)]₂ (**22**)

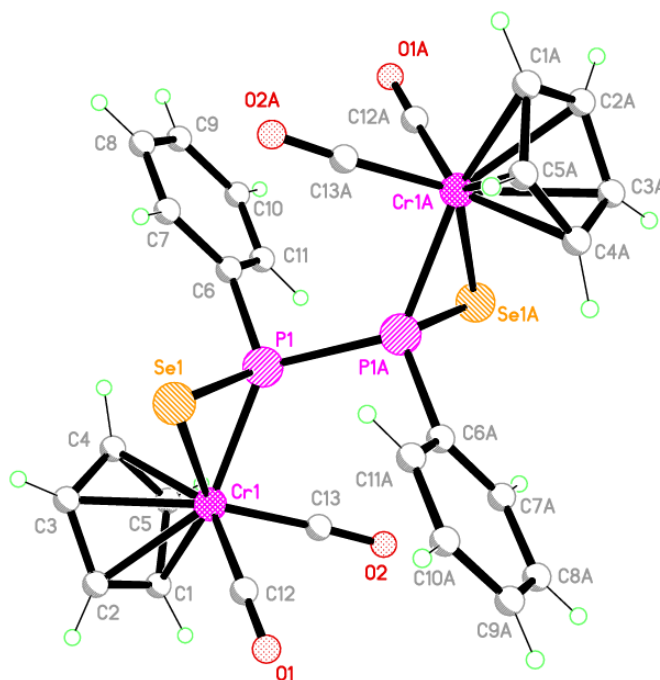


Figure 25. Molecular structure of *trans*-[CpCr(CO)₂(SePPh)]₂ (**22**)

The molecular structure of *trans*-[CpCr(CO)₂(SePPh)]₂ (**22**) is illustrated in Figure 25 and its bond lengths and bond angles are shown in Table 33. *trans*-[CpCr(CO)₂(SePPh)]₂ (**22**) crystallized in monoclinic, space group P2(1)/c. **22** consists of a framework similar to that of its sulfur analogue, *trans*-[CpCr(CO)₂(SPhOMe)]₂ [56a]. The dimer molecule is bridged by a P-P bond (2.212(3) Å) with both CpCr(CO)₂ moieties and the bridged [-SePAr]₂ ligand in a *trans* orientation which is comparable to that of *trans*-[CpCr(CO)₂(SPhOMe)]₂ (2.219(2) Å). The C(6)-P(1)-P(1)#1 angle (104.5(2)°) is more than 90° indicating that the phenyl ring is experiencing steric repulsion from the CpCr(CO)₂ moiety. The P-Se (2.1425(17) Å) and Cr-Se bond (2.6309(12) Å) distances of **22** are longer than the P-S (2.0003(15) Å) and Cr-S bonds (2.4962(15) Å) found in *trans*-

[CpCr(CO)₂(SPhPhOMe)]₂ which is possibly due to the larger atomic radii of Se as compared to S.

Table 33. Bond lengths [Å] and angles [°] for *trans*-[CpCr(CO)₂(SePPh)]₂ (**22**)

Bond lengths

Cr(1)-C(13)	1.833(7)	Se(1)-P(1)	2.1425(17)
Cr(1)-C(12)	1.854(7)	P(1)-C(6)	1.823(6)
Cr(1)-P(1)	2.2700(18)	P(1)-P(1)#1	2.212(3)
Cr(1)-Se(1)	2.6309(12)	O(1)-C(12)	1.140(8)
Cr(1)-Cr(1)#1	6.1018(19)	O(2)-C(13)	1.148(8)

Bond angles

C(13)-Cr(1)-P(1)	86.7(2)	P(1)-Se(1)-Cr(1)	55.66(5)
C(12)-Cr(1)-P(1)	110.7(2)	C(6)-P(1)-Se(1)	114.2(2)
C(13)-Cr(1)-Se(1)	124.4(2)	C(6)-P(1)-P(1)#1	104.5(2)
C(12)-Cr(1)-Se(1)	82.3(2)	Se(1)-P(1)-P(1)#1	108.70(11)
P(1)-Cr(1)-Se(1)	51.20(5)	C(6)-P(1)-Cr(1)	124.6(2)
C(13)-Cr(1)-Cr(1)#1	73.60(19)	Se(1)-P(1)-Cr(1)	73.14(6)
C(12)-Cr(1)-Cr(1)#1	97.4(2)	P(1)#1-P(1)-Cr(1)	125.74(11)
P(1)-Cr(1)-Cr(1)#1	17.11(4)	O(1)-C(12)-Cr(1)	178.4(7)
Se(1)-Cr(1)-Cr(1)#1	56.34(2)	O(2)-C(13)-Cr(1)	177.2(6)

Symmetry transformations used to generate equivalent atoms: #1 -x+1,-y+1,-z

CpCr(CO)₂(SeP(H)Ph) (**23**)

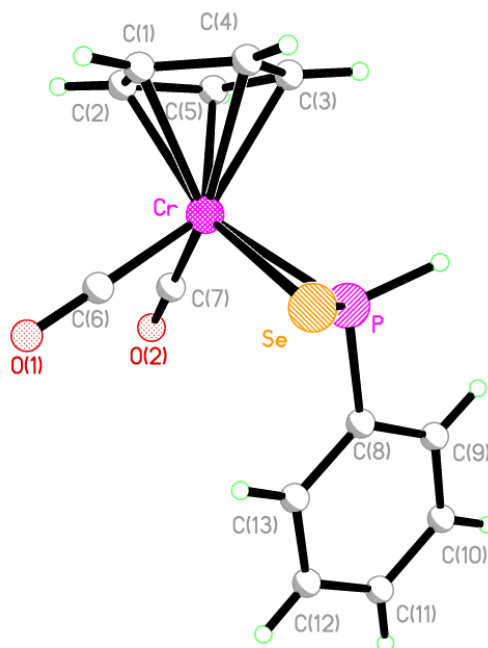


Figure 26. Molecular structure of CpCr(CO)₂(SeP(H)Ph) (**23**)

The molecular structure of CpCr(CO)₂(SeP(H)Ph) (**23**) is illustrated in Figure 26 and its bond lengths and bond angles are tabulated in Table 34. CpCr(CO)₂(SeP(H)Ph) (**23**) which crystallizes in monoclinic, space group $P2_1/n$ possesses a four-legged piano-stool configuration at Cr. **23** contains a Cp moiety at the apical position while is bonded to two CO groups and a η^2 -arylselenaphosphetane ligand. The complex is isostructural to CpCr(CO)₂(SP(H)Ar) (Ar = C₆H₄OMe) which is obtained from the reaction of **1** with LR [104] and [MoCp{ κ^2 -OP(OC₆H₄OH)R*}(CO)₂] (R* = 2,4,6-C₆H₂^tBu₃) from *p*-benzoquinone oxidation of [[MoCp(CO)₂{P(O)R*}]⁻ [110].

The Cr-P bond is indicative of a single bond as the bond distance of 2.2643(15) Å is similar with some of the reported complexes such as CpCr(CO)₂(SP(H)Ar) (2.2607(8) Å) [56a]; CpCr(CO)₂(SPR₂) (R = Me, 2.2704(6) Å; Et, 2.2738 (18) Å) [67]. The Cr-Se bond

distance of 2.6389(9) Å possesses a single Cr-Se bond which is longer than those observed in the (μ - η^2 -Se₂) complexes of both [CpCr(CO)₂]₂Se₂ (2.277 Å) [46d] and Cp₄Cr₄(CO)₈(P₂Se₂) (2.566(2) Å and 2.575(2) Å) [55c]. However, both the C=O bonds (1.361(4) and 1.420(5) Å) for CpCr(CO)₂(SP(H)Ar) are longer than those in **23** (1.150(6) and 1.147(6) Å). The hydrogen atom bonded to phosphorus is confirmed by ³¹P proton coupled NMR ($J = 387.6$ Hz).

Table 34. Bond lengths [Å] and angles [°] for CpCr(CO)₂(SeP(H)Ph) (**23**)

Bond lengths

Cr(1)-C(7)	1.837(5)	Se(1)-P(1)	2.1487(14)
Cr(1)-C(6)	1.837(5)	P(1)-C(8)	1.802(5)
Cr(1)-P(1)	2.2643(15)	O(1)-C(6)	1.150(6)
Cr(1)-Se(1)	2.6389(9)	O(2)-C(7)	1.147(6)

Bond angles

C(7)-Cr(1)-C(6)	81.0(2)	P(1)-Se(1)-Cr(1)	55.31(4)
C(7)-Cr(1)-P(1)	83.68(16)	Se(1)-P(1)-Cr(1)	73.40(5)
C(6)-Cr(1)-P(1)	112.14(16)	O(1)-C(6)-Cr(1)	177.2(5)
C(7)-Cr(1)-Se(1)	118.84(15)	O(2)-C(7)-Cr(1)	178.9(4)
C(6)-Cr(1)-Se(1)	81.36(16)	C(9)-C(8)-P(1)	119.9(4)
P(1)-Cr(1)-Se(1)	51.29(4)		

[CpCr(Se₂P(O)Ph)]₂ (**24**)

The molecular structure of [CpCr(Se₂P(O)Ph)]₂ (**24**) is illustrated in Figure 27 and its bond lengths and bond angles are shown in Table 35. [CpCr(Se₂P(O)Ph)]₂ (**24**) crystallizes in monoclinic, space group P2₁/n. **24** is isostructural with [CpCr(S₂P(O)PhOMe)]₂ isolated from the reaction of **1** with Lawesson's reagent [56a]. The molecule consists of two CpCr and two [SeP(O)Ar] moieties attached to an eight-membered ring center. The almost equivalent bond lengths of Cr(1)-Se(1) and Cr(1)-Se(2) (2.4957(6) and 2.5089(6) Å, respectively) are significantly longer than the Cr-S bond distance (2.3862(10) and 2.3951(10) Å) of the sulfur analogue. Such observation is likely due to the lower electronegativity of Se, compared to S, resulting in the lower electron density at the metal centre, hence reducing the π back-bonding effect which therefore becomes less strongly bonded to the metal.

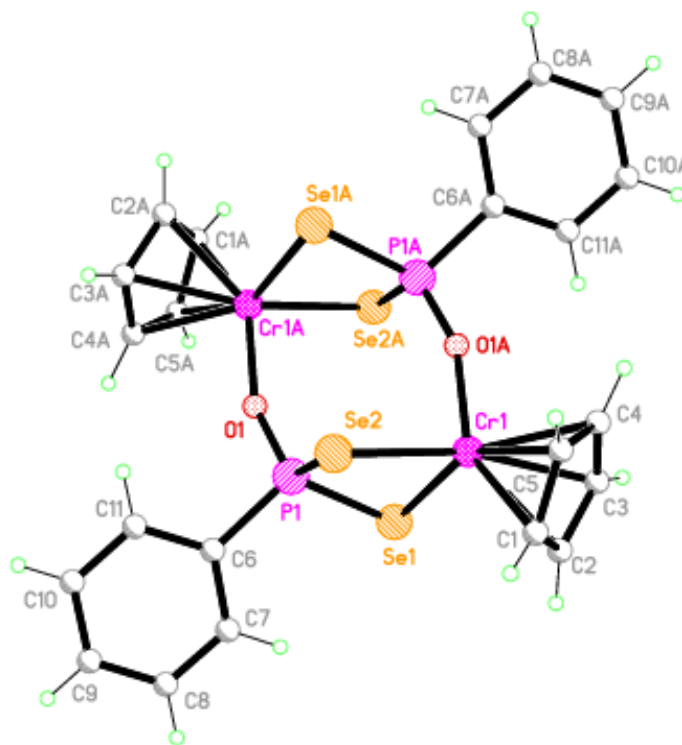


Figure 27. Molecular structure of [CpCr(Se₂P(O)Ph)]₂ (**24**)

Table 35. Bond lengths [Å] and angles [°] for [CpCr(Se₂P(O)Ph)]₂ (**24**)

Bond lengths

Cr(1)-O(1)#1	1.954(2)	Se(1)-Se(1)#1	5.3724(7)
Cr(1)-Se(1)	2.4957(6)	Se(2)-P(1)	2.1842(8)
Cr(1)-Se(2)	2.5089(6)	Se(2)-Se(2)#1	5.3978(7)
Cr(1)-Cr(1)#1	5.0598(10)	P(1)-O(1)	1.514(2)
Se(1)-P(1)	2.1785(8)	P(1)-C(6)	1.804(3)
Se(1)-Se(2)	3.4112(4)	O(1)-Cr(1)#1	1.954(2)
Se(1)-Se(2)#1	4.1669(5)		

Bond angles

O(1)#1-Cr(1)-C(1)	146.64(18)	P(1)-Se(1)-Se(1)#1	48.13(2)
O(1)#1-Cr(1)-C(5)	110.24(18)	Cr(1)-Se(1)-Se(1)#1	58.308(12)
O(1)#1-Cr(1)-C(2)	139.9(2)	Se(2)-Se(1)-Se(1)#1	50.859(8)
O(1)#1-Cr(1)-C(3)	103.8(2)	Se(2)#1-Se(1)-Se(1)#1	39.416(6)
O(1)#1-Cr(1)-C(4)	90.22(15)	P(1)-Se(2)-Cr(1)	81.66(3)
O(1)#1-Cr(1)-Se(1)	97.00(7)	P(1)-Se(2)-Se(1)	38.50(2)
O(1)#1-Cr(1)-Se(2)	97.53(7)	Cr(1)-Se(2)-Se(1)	46.868(14)
O(1)#1-Cr(1)-Cr(1)#1	45.70(6)	P(1)-Se(2)-Se(2)#1	47.90(2)
Se(1)-Cr(1)-Se(2)	85.941(19)	Cr(1)-Se(2)-Se(2)#1	57.992(13)
Se(1)-Cr(1)-Cr(1)#1	64.617(14)	Se(1)-Se(2)-Se(2)#1	50.530(8)
Se(2)-Cr(1)-Cr(1)#1	64.771(14)	O(1)-P(1)-C(6)	104.41(14)
P(1)-Se(1)-Cr(1)	82.08(2)	O(1)-P(1)-Se(1)	114.98(10)
P(1)-Se(1)-Se(2)	38.62(2)	C(6)-P(1)-Se(1)	110.03(10)
P(1)-Se(1)-Se(2)#1	77.23(2)	O(1)-P(1)-Se(2)	114.43(10)
Cr(1)-Se(1)-Se(2)	47.191(14)	C(6)-P(1)-Se(2)	110.22(11)
Cr(1)-Se(1)-Se(2)#1	83.049(14)	Se(1)-P(1)-Se(2)	102.87(3)
Se(2)-Se(1)-Se(2)#1	90.275(10)	P(1)-O(1)-Cr(1)#1	158.80(14)

Symmetry transformations used to generate equivalent atoms: #1 -x,-y,-z

2.7 Studies of $[\text{CpMo}(\text{CO})_2]_2$ (**4**) with Woollins' Reagent

2.7.1 The reaction of $[\text{CpMo}(\text{CO})_2]_2$ (**4**) with equimolar Woollins' Reagent

The reaction of $[\text{CpMo}(\text{CO})_2]_2$ (**4**) with Woollins' reagent at 110 °C for 4 h, resulted in a dark purplish brown reaction mixture. Column chromatography of the reaction mixture with silica gel led to the isolation of unreacted $\text{Cp}_2\text{Mo}_2(\text{CO})_4$ (**4**) (10.5%), $[\text{Cp}_2\text{Mo}_2\{(\mu\text{-Se})_2(\text{PPh}(\text{Se}))\}\{(\mu\text{-Se})(\text{PPh})_3\}]$ (**25**) as dark reddish brown crystals (17.5%), $\text{Cp}_4\text{Mo}_4(\text{CO})_3\text{Se}_4$ (**26**) as dark greenish blue crystals (3.1%), a pair of polymorphic products of $\text{Cp}_3\text{Mo}_3(\text{CO})_4[\text{Se}_3(\text{PPh})_2]$ (**27a**) as pink crystals (2.1%) and dark purplish pink crystalline solids (**27b**) (2.8%) together with an uncharacterized brown amorphous solid (42 mg). When a similar reaction was repeated at 70 °C for 2 h, unreacted $\text{Cp}_2\text{Mo}_2(\text{CO})_6$ (11.5%), unreacted $\text{Cp}_2\text{Mo}_2(\text{CO})_4$ (5.6%), **27a** (2.0%) and **27b** (4.9%) together with an uncharacterized Cp containing red precipitate (49 mg) were isolated.

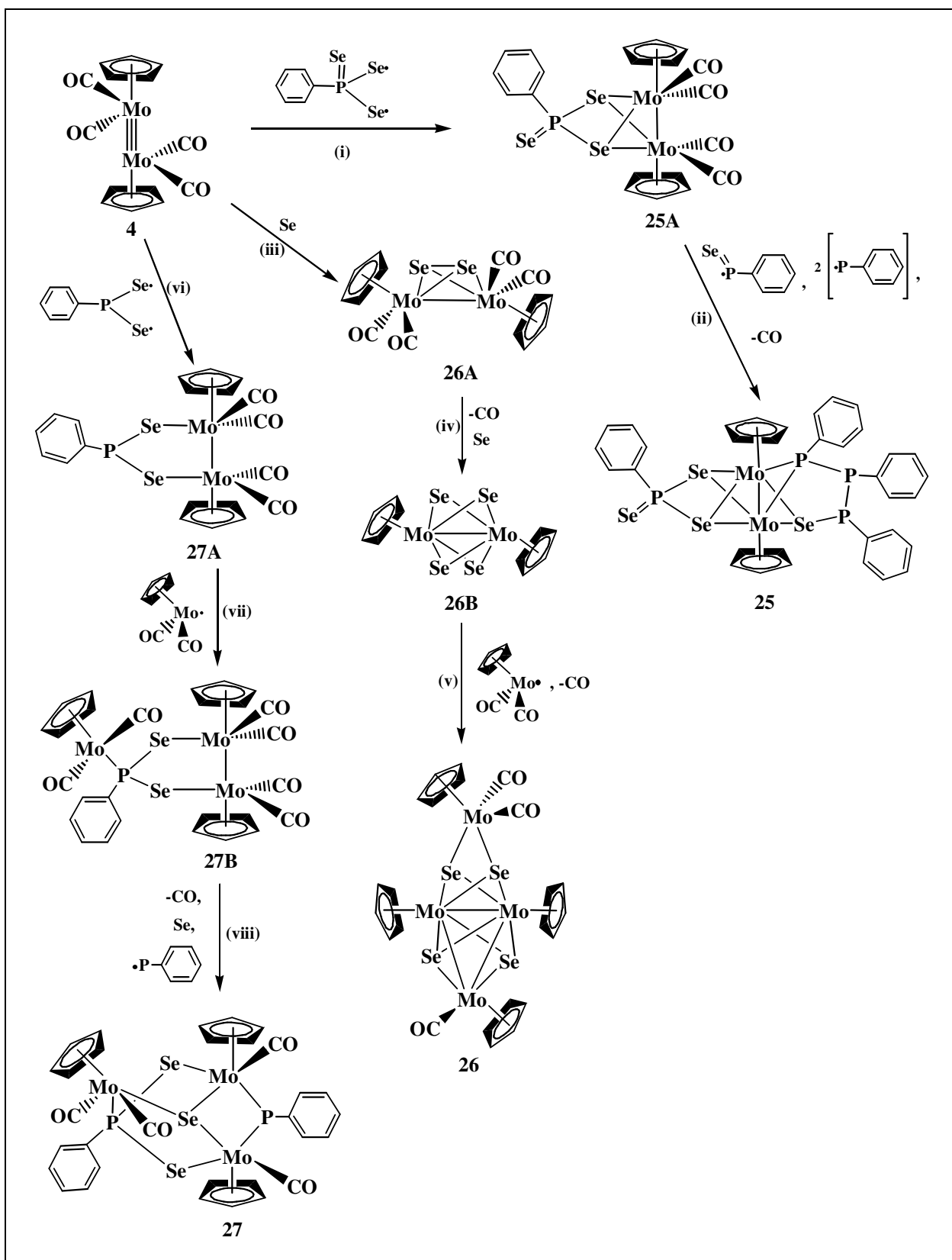
2.7.2 Mechanistic pathways : Formation of $[\text{Cp}_2\text{Mo}_2\{(\mu\text{-Se})_2(\text{PPh}(\text{Se}))\}\{(\mu\text{-Se})(\text{PPh})_3\}]$ (**25**), $\text{Cp}_4\text{Mo}_4(\text{CO})_3\text{Se}_4$ (**26**) and $\text{Cp}_3\text{Mo}_3(\text{CO})_4[\text{Se}_3(\text{PPh})_2]$ (**27a & b**)

From the molecular structures obtained for **25**, **26** and **27**, it is postulated that the formation of these three complexes proceeds *via* individual pathways as illustrated in Scheme 29. The mixed phosphorus-selenium dimeric compound of $[\text{Cp}_2\text{Mo}_2\{(\mu\text{-Se})_2(\text{PPh}(\text{Se}))\}\{(\mu\text{-Se})(\text{PPh})_3\}]$ (**25**) contained a PhPSe_3 fragment, probably initiated by homolytic cleavage of both the P-Se bonds in Woollins' reagent (Scheme 29). This type of fragment was also observed in another Woollins reagent derivative complex of *cis*- $\text{Pt}(\text{Se}_3\text{PPh})(\text{PR}_3)_2$ ($\text{PR}_3 = \frac{1}{2}$ dppe, PEt_3 , PMe_2Ph , or PPh_2Me) [111], suggesting a plausible mechanism which could involve an initial oxidative addition of PhPSe_3 to the Mo≡Mo bond of **4** to generate the intermediate $\text{Cp}_2\text{Mo}_2(\text{CO})_4\{\text{Se}_2\text{PPh}(\text{Se})\}$, **25A** (route i). Subsequent

decarbonylation followed by nucleophilic addition of $\text{PhPSe}\cdot$ and $\text{PhP}\cdot$ into **25A** afforded complex **25** (route ii).

26 was only isolated from the reaction at 110 °C but not at 70 °C. This probably suggests that the availability of free Se atoms resulting from higher thermal degradation of the ligand undergo oxidative addition towards the $\text{Mo}\equiv\text{Mo}$ bonds to form seleno-bridges as the intermediate in $\text{Cp}_2\text{Mo}_2(\text{CO})_4\text{Se}_2$ (**26A**) (route iii). The detection of the molecular ion ($m/z = 590$) in the mass spectrum of **26** substantiates the existence of this proposed intermediate **26A**. Subsequent decarbonylation followed by addition of seleno-bridged atoms on **26A** then generates **26B** ($m/z = 636$) which was also detected in the mass spectrum of **26**. Further attack of $15 e^-$ radical species of $\text{CpMo}(\text{CO})_2\cdot$ towards the free seleno complex **26B** followed by concomitant loss of CO will then yield the tetranuclear molybdenum cluster **26** (route v).

The mixed phosphorus-selenium trimolybdenum cluster of $\text{Cp}_3\text{Mo}_3(\text{CO})_4[\text{Se}_3(\text{PPh})_2]$ (**27**) is the result of the attack of $15e^-$ radical species of $\text{CpMo}(\text{CO})_2\cdot$ towards the PhPSe_2 fragment to give $\text{Cp}_2\text{Mo}_2(\text{CO})_4(\text{Se}_2\text{PPh})$ (**27A**) as the intermediate (route vi). The phosphorus atom in **27A** consisting of an unpaired electron, is further attacked by another $\text{CpMo}(\text{CO})_2\cdot$ radical to form $\text{Cp}_3\text{Mo}_3(\text{CO})_6(\text{Se}_2\text{PPh})$ (**27B**) (route vii). Subsequent decarbonylation followed by nucleophilic addition of a Se moiety and a PPh radical then afforded $\text{Cp}_3\text{Mo}_3(\text{CO})_4[\text{Se}_3(\text{PPh})_2]$ (**27**) (route viii).



Scheme 29. Synthetic pathways of $[\text{Cp}_2\text{Mo}_2\{(\mu\text{-Se})_2(\text{PPh}(\text{Se}))\}\{(\mu\text{-Se})(\text{PPh})_3\}]$ (**25**), $\text{Cp}_4\text{Mo}_4(\text{CO})_3\text{Se}_4$ (**26**) and $\text{Cp}_3\text{Mo}_3(\text{CO})_4[\text{Se}_3(\text{PPh})_2]$ (**27**)

2.7.3 Physical properties

[Cp₂Mo₂{(μ-Se)₂(PPh(Se))}{(μ-Se)(PPh)₃}] (25)

[Cp₂Mo₂{(μ-Se)₂(PPh(Se))}{(μ-Se)(PPh)₃}] exists as a dark reddish brown crystalline solid. It is stable both in the solution and solid state at ambient temperature under an inert atmosphere. It is soluble in a mixture of *n*-hexane-toluene to give an orange brown solution.

Cp₄Mo₄(CO)₃Se₄ (26)

Cp₄Mo₄(CO)₃Se₄ exists as a deep greenish blue oily solid. In the solid state, it is stable at ambient temperature under an inert atmosphere. It is soluble in a mixture of *n*-hexane-toluene to give a dark blue solution. In the solution, **26** is very stable at temperature below -28 °C but will slowly decompose to an uncharacterized green fraction after 1-2 days.

Cp₃Mo₃(CO)₄[Se₃(PPh)₂] (27a)

Cp₃Mo₃(CO)₄[Se₃(PPh)₂] exists as a pink crystalline solid. In the solid state, it is stable at ambient temperature under an inert atmosphere. It is soluble in toluene to give a dark pink solution. In the solution, **27a** is very stable at -28 °C but only stable for a couple of days at ambient temperature under an inert atmosphere.

Cp₃Mo₃(CO)₄[Se₃(PPh)₂] (27b)

27b is the other polymorphic product with **27a**. It exists as a dark purplish pink crystalline solid. In the solid state, it is stable at ambient temperature as well as being stable for a couple of days at ambient temperature in solution and indefinitely at -28 °C under an inert atmosphere. It is soluble in toluene to give a dark purplish pink solution.

2.7.4 Spectral characteristics

2.7.4.1 IR spectra

[Cp₂Mo₂{(μ-Se)₂(PPh(Se))}{(μ-Se)(PPh)₃}] (25)

The IR spectrum in nujol shows the stretching frequencies at 1158w, 1104m, 1088m, 1061m, 803w, 740m, 722w, 690w, 668w, 533m, 468w, 389m cm⁻¹ (refer to Appendix I).

Cp₄Mo₄(CO)₃Se₄ (26)

The IR spectrum in nujol shows the ν_{CO} stretching frequencies at 1933vs, 1870s cm⁻¹ and other peaks at 804m, 738w, 722.39w, 551vw, 533w, 510vw cm⁻¹ (refer to Appendix I).

Cp₃Mo₃(CO)₄[Se₃(PPh)₂] (27a)

The IR spectrum in nujol shows the ν_{CO} stretching frequencies at 1973s, 1921vs, 1844s cm⁻¹; other peaks at 1156m, 1095m, 1021m, 820w, 794w, 748vw, 738vw, 724w, 697vw, 554vw, 511vw, 489w, 474w, 465w, 448w, 422w, 407vw cm⁻¹ (refer to Appendix I).

Cp₃Mo₃(CO)₄[Se₃(PPh)₂] (27b)

The IR spectrum in nujol shows the ν_{CO} stretching frequencies at 1960.52m, 1925.64s, 1846.69m, 1156.19m, 1105.86m, 1050.12m, 1020.89m, 875.87w, 817.99w, 743.20vw, 728.24vw, 693.12vw, 669.05vw, 550.69vw, 525.32vw, 517.52vw, 472.64vw, 466.14vw, 457.68vw, 442.07vw cm⁻¹ (refer to Appendix I). Most of the chemical stretching frequencies of **27b** are similar to **27a** which is evidence that both of them are polymorphic in nature.

2.7.4.2 NMR spectra

[Cp₂Mo₂{(μ-Se)₂(PPh(Se))}{(μ-Se)(PPh)₃}] (**25**)

25 is a non-symmetrical dimolybdenum dimer. In ¹H NMR spectrum (benzene-*d*₆), it exhibits four Cp signals at δ 5.60, 5.34, 4.72, 4.39 and the C₆H₅- protons appear as multiplets at δ 7.95-6.78. In ¹³C NMR spectrum (benzene-*d*₆), four Cp signals were recorded at δ 90.37, 89.54, 89.43, 88.47 and the phenyl ring carbon was recorded at δ 132.43, 130.57, 129.67, 128.90, 126.04. Two extra Cp signals were recorded in both ¹H and ¹³C NMR which may be caused by the fluxional behavior of the complex when it is in solution. The ³¹P NMR spectrum is illustrated in Figure 28 and 29. Owing to a lack of symmetry, 4 clusters of resonances are observed ranging between δ 167.29 and δ -8.44 as detailed in Table 36. Similar observation was found in the ³¹P NMR in which the fluxional behavior of the complex has caused an extra set reading was recorded (label as * in Figure 29 and 30). The assignments of the chemical shifts for individual phosphorus atoms were done by considering the electron density of their substituents according to their electronegativity.

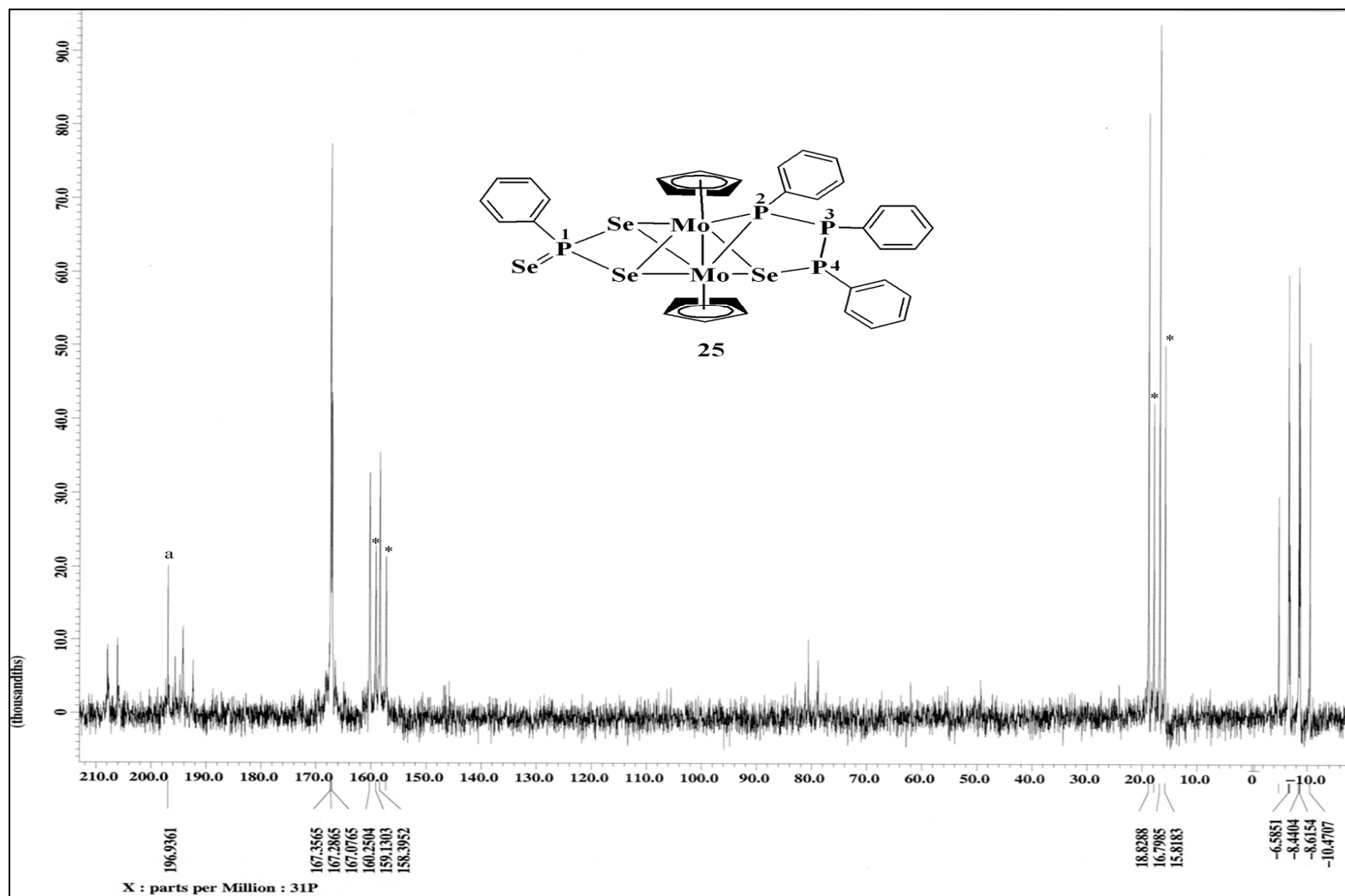
Table 36. ³¹P{¹H} NMR Resonances of [Cp₂Mo₂{(μ-Se)₂(PPh(Se))}{(μ-Se)(PPh)₃}] (**25**)

Chemical shift δ(ppm) (±0.01ppm)	Assignment	Multiplicity [<i>J</i> coupling, Hz]
167.29	P1	----
158.40	P4	d (297)
16.80	P2	d (382)
-8.44	P3	dd (297, 903)

Cp₄Mo₄(CO)₃Se₄ (26)

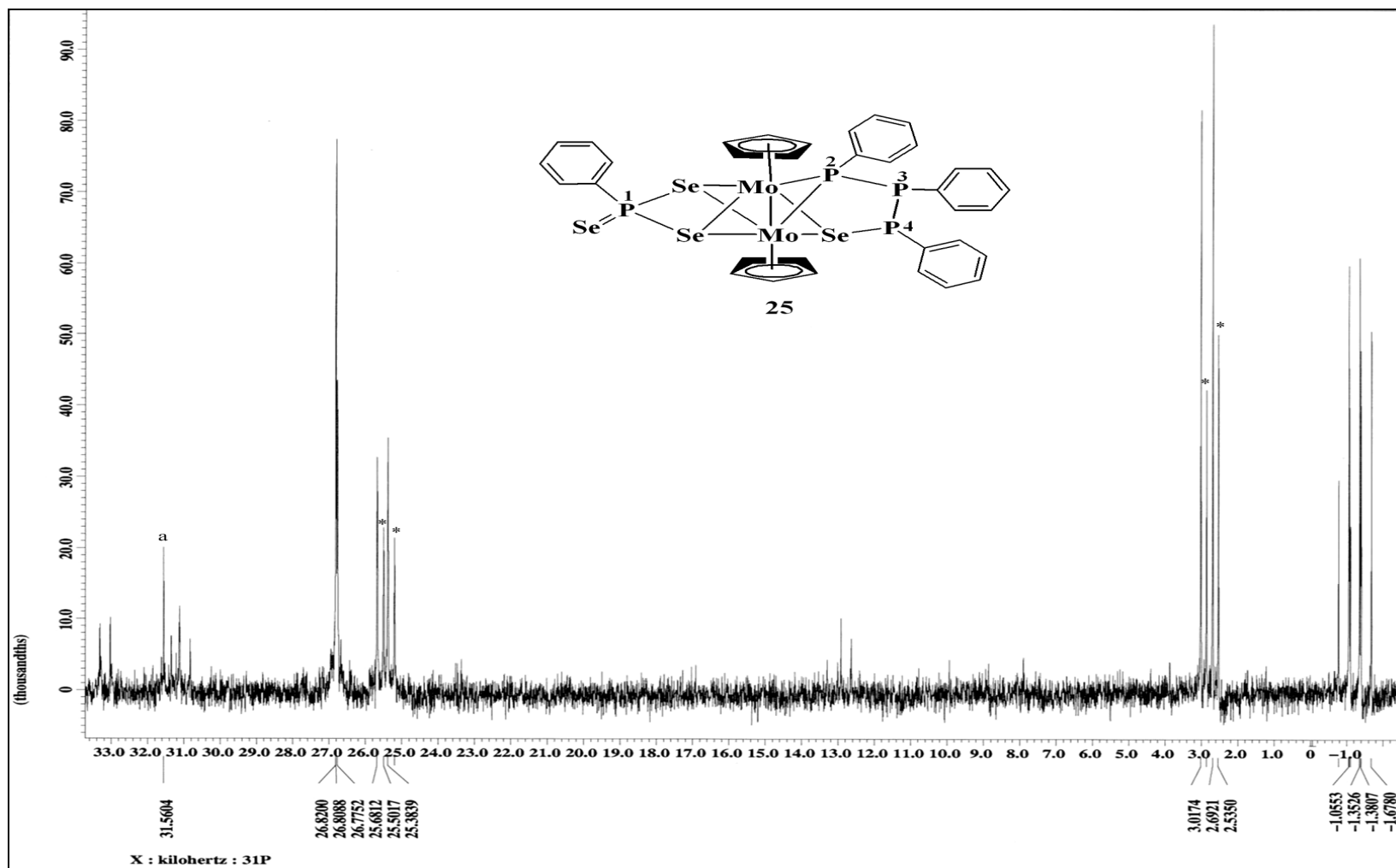
Complex **26** is an unsymmetrical tetramolybdenum cluster with more than four Cp signals recorded in both of its ¹H and ¹³C NMR spectra. In the ¹H NMR spectrum in C₆D₆, the complex shows δ(Cp) resonances at δ 5.63, 5.52, 5.49, 5.43, 4.71, 4.57, 4.56, 4.55, 4.53, 4.49 and 4.48. In the ¹³C NMR spectrum (benzene-*d*₆), the δ(Cp) resonances were recorded at δ 92.59, 92.43, 92.07, 92.01, 91.73, 91.64, 91.09, 91.01, 90.77, 90.73, 89.86, 89.76 and CO signals at δ 230.02, 196.02. Such observation might be due to the fluxional behavior of the Cp rings in solution. A low temperature ¹H NMR study carried out in toluene-*d*₈ from -60 °C to room temperature (RT) has substantiate our proposal (refer to Figure 30). At ambient temperature, the Cp signals in C₆D₅CD₃ were recorded at δ 5.56, 5.55, 5.46, 5.45, 5.44, 5.42, 5.38, 5.36, 4.64, 4.63, 4.57, 4.55, 4.54, 4.53, 4.51, 4.49, 4.47 and 4.46. The rapid vibration of the Cp rings begin to slow down at 0 °C and below. Finally, at -60°C all the multiplets have coalesced to give singlets at δ 5.59, 5.49, 5.36, 4.56, 4.43, 4.38, 4.36, and 4.33.

Figure 28. ^{31}P NMR proton-decouple spectrum of $[\text{Cp}_2\text{Mo}_2\{(\mu\text{-Se})_2(\text{PPh}(\text{Se}))\}\{(\mu\text{-Se})(\text{PPh})_3\}]$ (**25**) measured in ppm



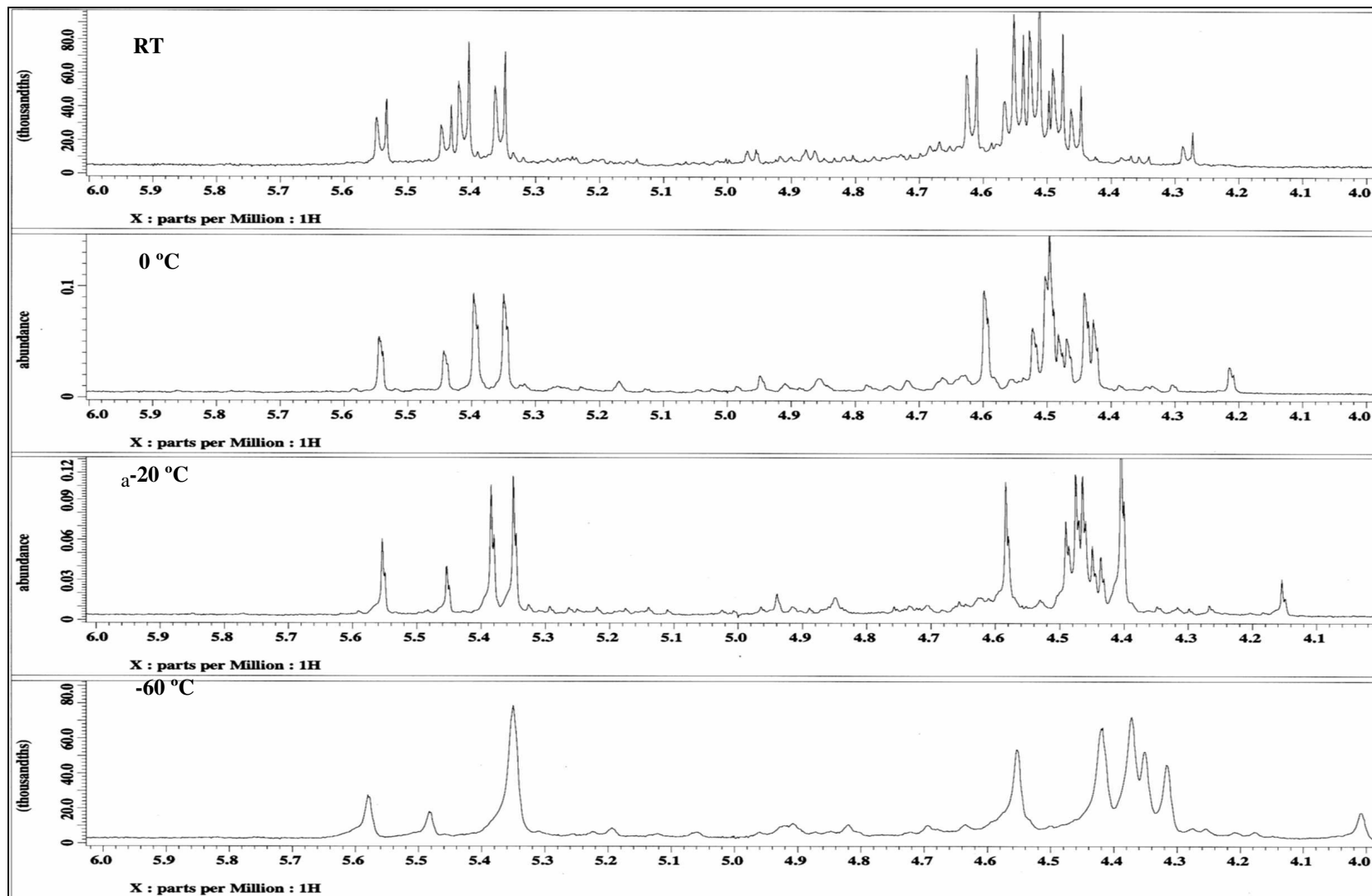
^a - From unknown impurity

Figure 29. ^{31}P NMR proton-decouple spectrum of $[\text{Cp}_2\text{Mo}_2\{(\mu\text{-Se})_2(\text{PPh}(\text{Se}))\}\{(\mu\text{-Se})(\text{PPh})_3\}]$ (**25**) measured in KHz



^a - From unknown impurity.

Figure 30. Temperature-dependent ^1H NMR spectra of $\text{Cp}_4\text{Mo}_4(\text{CO})_3\text{Se}_4$ (**26**) in toluene- d_8



Cp₃Mo₃(CO)₄[Se₃(PPh)₂] (27a)

Complex **27a** is a trimolybdenum cluster with three Cp signals recorded in both of its ¹H and ¹³C NMR spectra in benzene-*d*₆. In the ¹H NMR spectrum, the δ(Cp) resonances were recorded at δ4.82, 4.78 and 4.57 with δ(C₆H₅) resonances as multiplets at δ8.95-8.91 and 7.13-7.01. In the ¹³C NMR spectrum, both δ(Cp) and δ(C₆H₅) resonances were recorded at δ94.04, 91.15, 90.55 and δ138.23, 129.67, 128.90, 126.03, respectively. In the ³¹P NMR, two resonances were recorded at δ120.49 and 118.55 (refer to Appendix II).

Cp₃Mo₃(CO)₄[Se₃(PPh)₂] (27b)

Complex **27b** is a polymorphic product with **27a**. However, **27b** possesses different chemical shifts as compared to **27a**. The ¹H NMR spectrum (benzene-*d*₆), shows δ(Cp) resonances at δ 4.85, 4.77 and 4.58 together with δ(C₆H₅) resonances as multiplets at δ 7.14-7.01. In the ¹³C NMR spectrum (benzene-*d*₆), the δ(Cp) peaks were recorded at δ 94.27, 90.72 and 90.16 together with δ(C₆H₅) peaks at δ 133.45, 129.67, 128.90 and 126.03. In the ³¹P NMR, two resonances were recorded at δ 120.71 and 118.73 (refer to Appendix II).

2.7.4.3 Mass Spectra

[Cp₂Mo₂{(μ-Se)₂(PPh(Se))}{(μ-Se)(PPh)₃}] (25)

The mass spectrum of **25** shows the parent ion $m/z = 1073.6073$ [Cp₂Mo₂{(μ-Se)₂(PPh(Se))}{(μ-Se)(PPh)₃}] and its fragmentation ions as listed in Table 37.

Table 37. Electrospray ionization mass spectrum of [Cp₂Mo₂{(μ-Se)₂(PPh(Se))}{(μ-Se)(PPh)₃}] (25)

m/z	Assignments
1074	[Cp ₂ Mo ₂ {(μ-Se) ₂ (PPh(Se))}{(μ-Se)(PPh) ₃ }]
970	[Cp ₂ Mo ₂ {(μ-Se) ₂ (PPh(Se))}{(μ-Se)(PPh) ₂ }]

Cp₄Mo₄(CO)₃Se₄ (26)

The mass spectrum of **26** shows the parent ion $m/z = 1056.0000$ Cp₄Mo₄(CO)₃Se₄ and its fragmentation ions as listed in Table 38.

Table 38. Electrospray ionization mass spectrum of Cp₄Mo₄(CO)₃Se₄ (26)

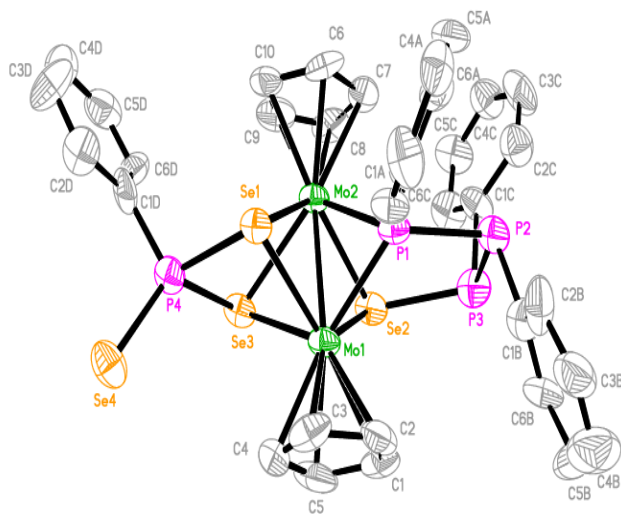
m/z	Assignments
1056	Cp ₄ Mo ₄ (CO) ₃ Se ₄
1028	Cp ₄ Mo ₄ (CO) ₂ Se ₄
1000	Cp ₄ Mo ₄ (CO)Se ₄
972	Cp ₄ Mo ₄ Se ₄
809	Cp ₃ Mo ₃ Se ₄
677	Cp ₃ Mo ₃ (CO)Se ₂
649	Cp ₃ Mo ₃ Se ₂
644	Mo ₃ Se ₄
534	Mo ₃ Se ₃

Cp₃Mo₃(CO)₄[Se₃(PPh)₂] (27a)

The mass spectrum of **27a** shows the parent ion $m/z = 1057.0000$ Cp₃Mo₃(CO)₄[Se₃(PPh)₂] and its fragmentation ions as listed in Table 39.

Table 39. Electrospray ionization mass spectrum of Cp₃Mo₃(CO)₄[Se₃(PPh)₂] (**27**)

m/z	Assignments
1057	Cp ₃ Mo ₃ (CO) ₄ [Se ₃ (PPh) ₂]
894	Cp ₃ Mo ₃ (CO) ₂ [Se ₃ (PPh)]
785	Cp ₃ Mo ₃ (CO) ₂ Se ₃
678	Cp ₃ Mo ₃ (CO)Se ₂
662	Cp ₂ Mo ₃ (CO)Se ₂

2.7.5 Molecular structures**[Cp₂Mo₂{(μ-Se)₂(PPh(Se))}{(μ-Se)(PPh)₃}] (25)**Figure 31. Molecular structure of [Cp₂Mo₂{(μ-Se)₂(PPh(Se))}{(μ-Se)(PPh)₃}] (**25**)

The molecular structure of $[\text{Cp}_2\text{Mo}_2\{(\mu\text{-Se})_2(\text{PPh}(\text{Se}))\}\{(\mu\text{-Se})(\text{PPh})_3\}]$ (**25**) is shown in Figure 31 and its bond lengths and bond angles are tabulated in Table 40. **25** was crystallized from a mixture of *n*-hexane/toluene (1:3) in space group $\text{C}_{2/c}$. The asymmetrical molecule **25** consists of a $\text{Mo}_2\text{Se}_3\text{P}$ framework with one phenylphosphinetriselenato fragment coordinated to both the Mo atoms at Se1 and Se3, respectively. The Mo-Mo bond distance of 2.684(2) Å indicates a singly bonded 36 electron molecule. Both Mo atoms are in a pentagonal pyramidal coordination environment with each metal bonded to a Cp group occupying the axial position. The Mo1-Mo2 bond is bridged by three interlinked phenylphosphine fragments *via* a μ_2 -selenido ligand (Se2). The three phenyl rings of the phenylphosphine ligands are positioned in a zig-zag configuration to minimize steric hindrance.

Table 40. Bond lengths [Å] and angles [°] for $[\text{Cp}_2\text{Mo}_2\{(\mu\text{-Se})_2(\text{PPh}(\text{Se}))\}\{(\mu\text{-Se})(\text{PPh})_3\}]$ (**25**)

Bond lengths

Mo(1)-P(1)	2.407(5)	Se(1)-P(4)	2.307(5)
Mo(1)-Se(2)	2.561(2)	Se(2)-P(3)	2.361(6)
Mo(1)-Se(1)	2.573(2)	Se(3)-P(4)	2.286(5)
Mo(1)-Se(3)	2.592(3)	Se(4)-P(4)	2.096(5)
Mo(1)-Mo(2)	2.684(2)	P(1)-C(1A)	1.807(16)
Mo(2)-P(1)	2.396(5)	P(1)-P(2)	2.241(7)
Mo(2)-Se(1)	2.552(2)	P(2)-C(1B)	1.76(2)
Mo(2)-Se(2)	2.557(2)	P(2)-P(3)	2.162(7)
Mo(2)-Se(3)	2.610(2)	P(3)-C(1C)	1.856(17)
		P(4)-C(1D)	1.83(2)

Bond angles

P(1)-Mo(1)-Se(2)	75.37(11)	P(3)-Se(2)-Mo(2)	111.01(14)
P(1)-Mo(1)-Se(1)	72.70(12)	P(3)-Se(2)-Mo(1)	112.81(15)
Se(2)-Mo(1)-Se(1)	116.25(8)	Mo(2)-Se(2)-Mo(1)	63.26(6)
P(1)-Mo(1)-Se(3)	115.10(13)	P(4)-Se(3)-Mo(1)	91.01(14)
Se(2)-Mo(1)-Se(3)	71.93(7)	P(4)-Se(3)-Mo(2)	92.55(13)

Se(1)-Mo(1)-Se(3)	74.15(7)	Mo(1)-Se(3)-Mo(2)	62.12(6)
P(1)-Mo(1)-Mo(2)	55.84(12)	C(1A)-P(1)-P(2)	99.1(6)
Se(2)-Mo(1)-Mo(2)	58.29(6)	C(1A)-P(1)-Mo(2)	122.0(6)
Se(1)-Mo(1)-Mo(2)	58.05(5)	P(2)-P(1)-Mo(2)	121.2(2)
Se(3)-Mo(1)-Mo(2)	59.27(6)	C(1A)-P(1)-Mo(1)	125.7(6)
P(1)-Mo(2)-Se(1)	73.24(11)	P(2)-P(1)-Mo(1)	121.2(2)
P(1)-Mo(2)-Se(2)	75.64(12)	Mo(2)-P(1)-Mo(1)	67.95(14)
Se(1)-Mo(2)-Se(2)	117.16(8)	C(1B)-P(2)-P(3)	101.2(7)
P(1)-Mo(2)-Se(3)	114.83(12)	C(1B)-P(2)-P(1)	100.7(6)
Se(1)-Mo(2)-Se(3)	74.19(7)	P(3)-P(2)-P(1)	98.5(3)
Se(2)-Mo(2)-Se(3)	71.71(7)	C(1C)-P(3)-P(2)	100.4(6)
P(1)-Mo(2)-Mo(1)	56.21(11)	C(1C)-P(3)-Se(2)	100.2(7)
Se(1)-Mo(2)-Mo(1)	58.79(6)	P(2)-P(3)-Se(2)	103.3(2)
Se(2)-Mo(2)-Mo(1)	58.46(6)	C(1D)-P(4)-Se(4)	110.8(6)
Se(3)-Mo(2)-Mo(1)	58.61(6)	C(1D)-P(4)-Se(3)	109.6(6)
P(4)-Se(1)-Mo(2)	93.55(13)	Se(4)-P(4)-Se(3)	120.9(2)
P(4)-Se(1)-Mo(1)	91.02(13)	C(1D)-P(4)-Se(1)	109.5(6)
Mo(2)-Se(1)-Mo(1)	63.16(6)	Se(4)-P(4)-Se(1)	118.2(2)
		Se(3)-P(4)-Se(1)	85.38(17)

Cp₄Mo₄(CO)₃Se₄ (**26**)

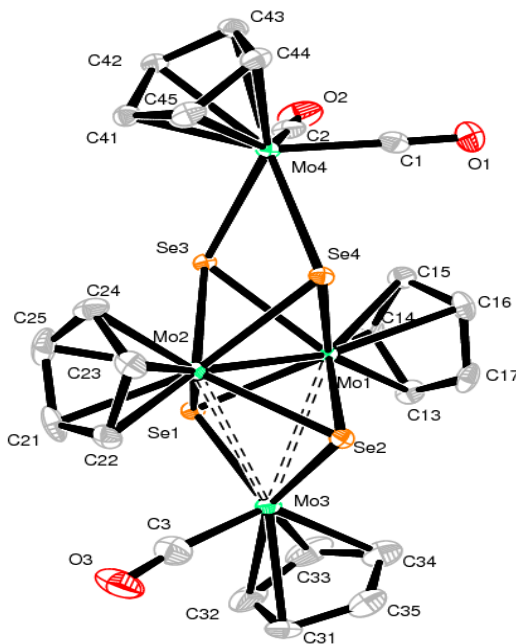


Figure 32. Molecular structure of Cp₄Mo₄(CO)₃Se₄ (**26**)

The molecular structure of Cp₄Mo₄(CO)₃Se₄ (**26**) is illustrated in Figure 32 and its bond lengths and bond angles are tabulated in Table 41. **26** crystallized from a mixture of

n-hexane/toluene (1:3) in space group P2₁/n. The molecular structure of **26** consists of a Mo₃Se₄ framework without the presence of a P atom. The Mo(1) and Mo(2) atoms are in a pentagonal bipyramid coordination environment with the Cp ring occupying the axial position while the other two Cp rings are coordinated at Mo(3) and Mo(4) in a *trans* orientation. The four μ₃-Se atoms are located at the center of the molecule with each forming a seleno bridge between the two Mo moieties, together with one and two CO ligands, respectively. The short bond distance of Mo(1)-Mo(2) (2.6127(4) Å) indicates a Mo=Mo double bond which is comparable to [CpMo(SBz)S]₂ (**10a** & **b**) and [CpMo(CO)₂(SBU¹)]₂ (refer Table 7). However, the Mo(1)-Mo(3) (3.0262(4) Å) and Mo(2)-Mo(3) (3.0476(4) Å) bond distances are similar with the Mo-Mo bond found in Cp₂Mo₂(CO)₆ [7b, 89]. The Se(3)-Mo(4) (2.6395(5) Å) and Se(4)-Mo(4) (2.6504(4) Å) bond distances are longer than the Se(1)-Mo(3) (2.4399(4) Å) and Se(2)-Mo(3) (2.4411(5) Å), respectively. The difference in bond distances can be attributed to Mo(4) which contains an extra CO group as compared to Mo(3). Consequently, the π-back donation to the two CO groups has lessened the electron density at Mo(4) as compared to Mo(3) resulting in the Se(1)-Mo(3) and Se(2)-Mo(3) bonds being stronger and shorter.

Table 41. Bond lengths [Å] and angles [°] for Cp₄Mo₄(CO)₃Se₄ (**26**)

Bond lengths			
Se(1) – Mo(3)	2.4399(4)	Se(4) – Mo(4)	2.6504(4)
Se(1) – Mo(2)	2.5409(5)	Mo(1)- Mo(2)	2.6127(4)
Se(1) – Mo(1)	2.5419(4)	Mo(1)- Mo(3)	3.0262(4)
Se(2) – Mo(3)	2.4411(5)	Mo(2) –Mo(3)	3.0476(4)
Se(2) – Mo(2)	2.5539(4)	C(1) – O(1)	1.159(5)
Se(2) – Mo(1)	2.5656(4)	C(2) – O(2)	1.159(5)
Se(3) – Mo(1)	2.6080(4)	C(3) – O(3)	1.140(5)
Se(3) – Mo(2)	2.6200(4)	C(1) – Mo(4)	1.935(4)
Se(3) – Mo(4)	2.6395(5)	C(2) – Mo(4)	1.950(4)
Se(4) – Mo(1)	2.6113(4)	C(3) – Mo(3)	1.957(5)

Se(4) – Mo(2) 2.6189(4)

Bond angles

Mo3-Se1-Mo2	75.419(13)	Se1-Mo2-Se4	116.538(15)
Mo3-Se1-Mo1	74.781(13)	Se2-Mo2-Se4	69.216(12)
Mo2-Se1-Mo1	61.864(12)	Mo1-Mo2-Se4	59.887(11)
Mo3-Se2-Mo2	75.162(13)	Se1-Mo2-Se3	69.156(13)
Mo3-Se2-Mo1	74.330(13)	Se2-Mo2-Se3	116.821(14)
Mo2-Se2-Mo1	61.372(11)	Mo1-Mo2-Se3	59.790(11)
Mo1-Se3-Mo2	59.965(11)	Se4-Mo2-Se3	66.911(12)
Mo1-Se3-Mo4	102.926(14)	Se1-Mo2-Mo3	50.787(11)
Mo2-Se3-Mo4	107.062(15)	Se2-Mo2-Mo3	50.738(11)
Mo1-Se4-Mo2	59.937(11)	Mo1-Mo2-Mo3	64.100(10)
Mo1-Se4-Mo4	102.536(14)	Se4-Mo2-Mo3	112.258(12)
Mo2-Se4-Mo4	106.770(14)	Se3-Mo2-Mo3	112.370(14)
Se1-Mo1-Se2	93.387(14)	O3-C3-Mo3	174.0(4)
Se1-Mo1-Se3	69.332(12)	C3-Mo3-Se1	100.09(14)
Se2-Mo1-Se3	116.833(15)	C3-Mo3-Se2	98.62(14)
Se1-Mo1-Se4	116.782(14)	Se1-Mo3-Se2	99.189(15)
Se2-Mo1-Se4	69.160(13)	C3-Mo3-Mo1	130.71(13)
Se3-Mo1-Se4	67.196(12)	Se1-Mo3-Mo1	54.144(11)
Se1-Mo1-Mo2	59.051(12)	Se2-Mo3-Mo1	54.714(11)
Se2-Mo1-Mo2	59.092(11)	C3-Mo3-Mo2	79.76(13)
Se3-Mo1-Mo2	60.245(11)	Se1-Mo3-Mo2	53.794(11)
Se4-Mo1-Mo2	60.176(11)	Se2-Mo3-Mo2	54.100(11)
Se1-Mo1-Mo3	51.075(11)	Mo1-Mo3-Mo2	50.953(9)
Se2-Mo1-Mo3	50.956(11)	O1-C1-Mo4	178.6(4)
Se3-Mo1-Mo3	113.406(13)	O2-C2-Mo4	177.0(3)
Se4-Mo1-Mo3	113.161(13)	C1-Mo4-C2	77.72(17)
Mo2-Mo1-Mo3	64.948(10)	C1-Mo4-Se3	114.56(12)
Se1-Mo2-Se2	93.690(14)	C2-Mo4-Se3	78.13(12)
Se1-Mo2-Mo1	59.085(11)	C1-Mo4-Se4	76.68(11)
Se2-Mo2-Mo1	59.535(11)	C2-Mo4-Se4	120.94(11)
		Se3-Mo4-Se4	66.183(12)

$\text{Cp}_4\text{Mo}_4(\text{CO})_3\text{Se}_4$ (**27a**)

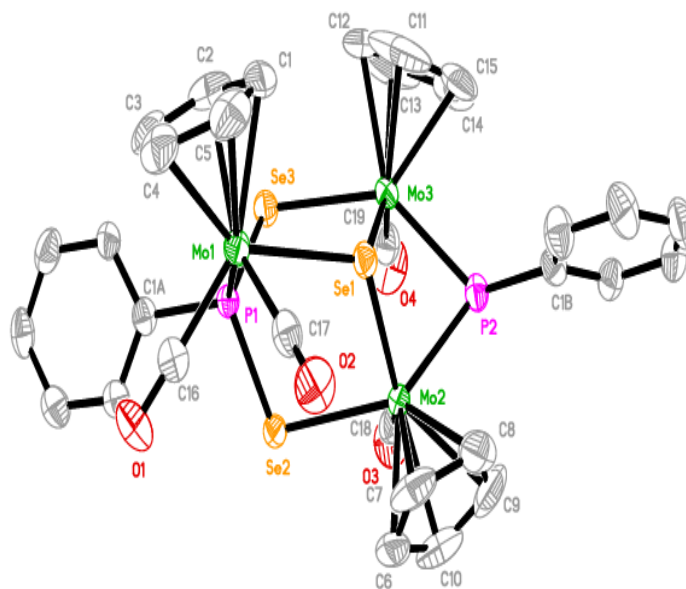


Figure 33. Molecular structure of $\text{Cp}_3\text{Mo}_3(\text{CO})_4[\text{Se}_3(\text{PPh})_2]$ (**27a**)

The molecular structure of $\text{Cp}_3\text{Mo}_3(\text{CO})_4[\text{Se}_3(\text{PPh})_2]$ (**27a**) is shown in Figure 33 and its bond lengths and bond angles are tabulated in Table 42. **27a** was crystallized from a mixture of THF/ether (1:3) in space group $P2_1/n$. The asymmetrical trinuclear complex of **27a** consists of a $\text{Mo}_3\text{Se}_3\text{P}_2$ cage framework of a μ_3 -selenido ligand (Se1) bridging across three metal atoms of Mo1, Mo2 and Mo3. Each Mo atom has a η^5 -coordinated Cp ring located almost perpendicular to each other. Mo(2) and Mo(3) possesses a four-legged piano-stool geometry with the Cp rings at the apical position, whereas Mo(1) possesses a three legged piano-stool geometry with a Cp ring at the apical position, two CO groups and a $[\text{Se}_2\text{PPh}]$ fragment at the lower positions.

Table 42. Bond lengths [Å] and angles [°] for Cp₃Mo₃(CO)₄[Se₃(PPh)₂] (**27a**)

Bond lengths

Mo(1)-C(16)	1.956(7)	Mo(3)-Se(3)	2.5983(9)
Mo(1)-C(17)	1.968(6)	Mo(3)-Se(1)	2.5990(9)
Mo(1)-P(1)	2.4498(15)	Se(2)-P(1)	2.2159(15)
Mo(1)-Se(1)	2.6792(8)	Se(3)-P(1)	2.2290(16)
Mo(2)-C(18)	1.984(6)	P(1)-C(1A)	1.836(6)
Mo(2)-P(2)	2.4014(17)	P(2)-C(1B)	1.818(6)
Mo(2)-Se(1)	2.5760(9)	O(1)-C(16)	1.160(7)
Mo(2)-Se(2)	2.6121(8)	O(2)-C(17)	1.150(7)
Mo(3)-C(19)	1.976(7)	O(3)-C(18)	1.157(7)
Mo(3)-P(2)	2.4069(16)	O(4)-C(19)	1.145(7)

Bond angles

C(16)-Mo(1)-C(17)	78.3(2)	P(2)-Mo(3)-Se(1)	79.13(4)
C(16)-Mo(1)-P(1)	75.64(16)	Se(3)-Mo(3)-Se(1)	87.43(2)
C(17)-Mo(1)-P(1)	118.68(18)	Mo(2)-Se(1)-Mo(3)	77.78(2)
C(16)-Mo(1)-Se(1)	123.00(17)	Mo(2)-Se(1)-Mo(1)	120.58(3)
C(17)-Mo(1)-Se(1)	75.72(18)	Mo(3)-Se(1)-Mo(1)	120.09(3)
P(1)-Mo(1)-Se(1)	74.13(4)	P(1)-Se(2)-Mo(2)	102.52(4)
C(18)-Mo(2)-P(2)	82.8(2)	P(1)-Se(3)-Mo(3)	103.33(4)
C(18)-Mo(2)-Se(1)	133.70(18)	Se(2)-P(1)-Se(3)	104.86(6)
P(2)-Mo(2)-Se(1)	79.69(4)	Se(2)-P(1)-Mo(1)	115.74(6)
C(18)-Mo(2)-Se(2)	77.18(18)	Se(3)-P(1)-Mo(1)	115.51(6)
P(2)-Mo(2)-Se(2)	137.54(4)	Mo(2)-P(2)-Mo(3)	85.03(5)
Se(1)-Mo(2)-Se(2)	87.67(2)	O(1)-C(16)-Mo(1)	177.7(5)
C(19)-Mo(3)-P(2)	80.64(18)	O(2)-C(17)-Mo(1)	175.7(5)
C(19)-Mo(3)-Se(3)	79.43(18)	O(3)-C(18)-Mo(2)	175.0(6)
P(2)-Mo(3)-Se(3)	136.35(4)	O(4)-C(19)-Mo(3)	174.7(6)
C(19)-Mo(3)-Se(1)	133.8(2)		

2.8 Studies with $P(C_6H_4SMe-p)_3$

2.8.1 Reaction of $Cp_2Cr_2(CO)_6$ (**1**) and $Cp_2Cr_2(CO)_4$ (**2**) with $P(C_6H_4SMe-p)_3$

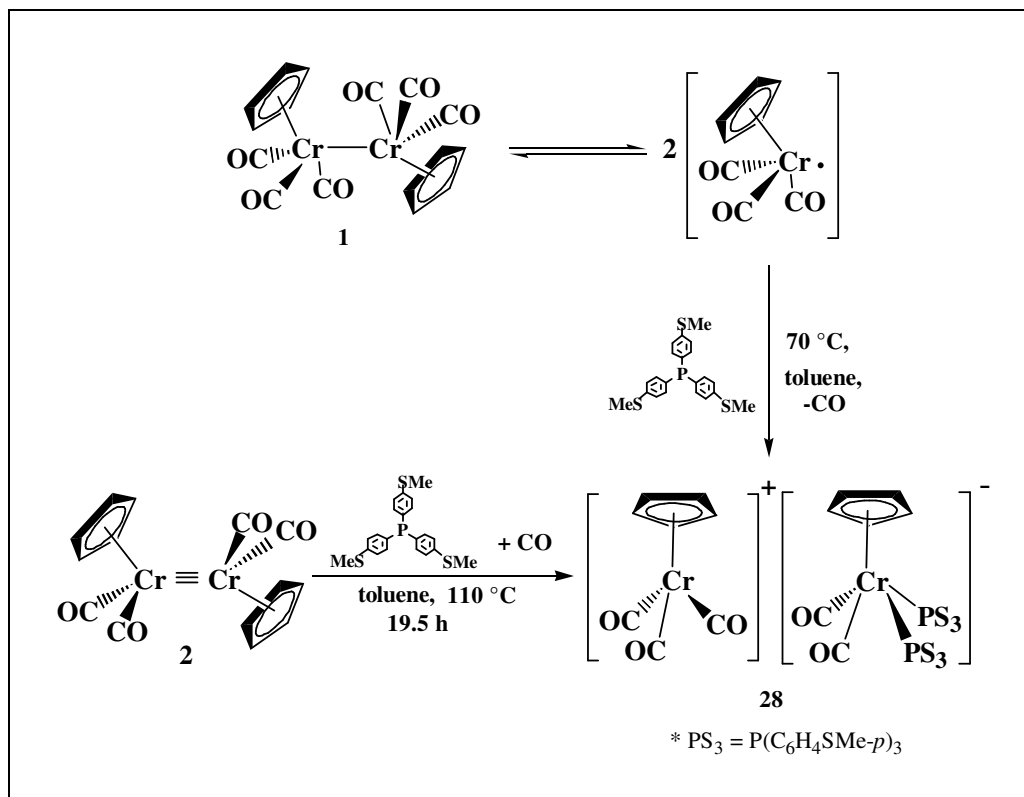
A deep green solution of $Cp_2Cr_2(CO)_6$ (**1**) was reacted with one mole equivalent of *p*-P(PhSMe)₃ in toluene at 70 °C for 12 h. Column chromatography of the deep dirty green reaction mixture led to the isolation of $Cp_2Cr_2(CO)_4$ (**2**) (77.9% yield) as dark green crystalline solids and $[CpCr(CO)_2\{P(C_6H_4SMe-p)_3\}_2][CpCr(CO)_3]$ (**28**) (16.7% yield) as a bright yellowish green residue. No reaction was observed after 24 h of stirring at ambient temperature. It was observed that a large proportion of **2** which was converted from its congener **1** remained unreacted.

The reaction of $[CpCr(CO)_2]_2$ (**2**) with one mole equivalent of $P(C_6H_4SMe-p)_3$ at an elevated temperature of 110 °C for 19.5 h in toluene gave a deep brownish green reaction mixture. The products isolated were unreacted $[CpCr(CO)_2]_2$ (21.1% recovery) and $[CpCr(CO)_2\{P(C_6H_4SMe-p)_3\}_2][CpCr(CO)_3]$ (**28**) (40.5% yield).

2.8.2 Proposed Structure for **28**

28 is not structurally elucidated because attempts to obtain a suitable crystal for x-ray diffractometry were not successful. However, a structure for **28** was proposed by comparison with spectroscopic data of analogous products especially $[CpCr(CO)_2(dppe)][CpCr(CO)_3]$ [108] and $[CpMo(CO)_2(PPh_3)_2][CpMo(CO)_3]$ [76]. It is proposed that the reaction of **1** with $P(C_6H_4SMe-p)_3$ proceeds *via* both the 17-electron radical and triply-bonded $[CpCr(CO)_2]_2$ (**2**) pathways as shown in Scheme 30. Apparently, this monodentate tertiary phosphine reacts with **1** to afford **28** which is a product of CO substitution, as well as a product of disproportionation. The IR spectrum of the yellow salt-like **28** contains four bands in the C-O stretching region with two high frequency bands typical of the cation, $[CpCr(CO)_2\{P(C_6H_4SMe-p)_3\}_2]$, and two bands, at lower frequencies, typical of the anion, $[CpCr(CO)_3]$. **28** exhibited ν_{CO} at $\approx 1961s$ and $\approx 1887vs\text{ cm}^{-1}$, as

expected by analogy with similar complexes of $[\text{CpMo}(\text{CO})_2(\text{PPh}_3)_2][\text{CpMo}(\text{CO})_3]$ (1966s, 1883s, 1776s and 1738s cm^{-1}) as well as two strong ν_{CO} at $\approx 1863\text{vs}$ and $\approx 1770\text{vs}$ cm^{-1} , attributed to the $[\text{CpCr}(\text{CO})_3]^-$ carbonylate anion.



Scheme 30

2.8.3 Physical properties

$[\text{CpCr}(\text{CO})_2\{\text{P}(\text{C}_6\text{H}_4\text{SMe-}p)_3\}_2][\text{CpCr}(\text{CO})_3]$ (**28**)

28 exists as a bright yellowish green salt-like solid when it is concentrated to dryness under *vacuo*. In the solid state, it is stable at ambient temperature under an inert atmosphere for a few hours and stable at $-28\text{ }^\circ\text{C}$ for a prolonged period. It is very soluble in toluene and other more polar solvents to give a yellowish green solution. In solution, it is only stable for 1-2 hours at ambient temperature but it can be kept longer at $-28\text{ }^\circ\text{C}$.

2.8.4 Spectral characteristics

2.8.4.1 IR spectrum

[CpCr(CO)₂{P(C₆H₄SMe-*p*)₃}₂][CpCr(CO)₃] (**28**)

28 showed four CO stretching frequencies, ν_{CO} , at 1961s, 1887vs, 1863vs, 1769vs cm^{-1} in nujol and other peaks at 1658vs, 1598s, 1578vs, 1543s, 1277vs, 1260vs, 1194s, 1079vs, 807vs, 763w, 746s, 719s, 703s, 571m, 545m, 501w cm^{-1} (refer to Appendix I).

2.8.4.2 NMR spectrum

[CpCr(CO)₂{P(C₆H₄SMe-*p*)₃}₂][CpCr(CO)₃] (**28**)

28 showed two $\delta(\text{Cp})$ resonances in its ¹H NMR spectrum (benzene-*d*₆) at δ 9.94 and 4.33 (br, Cp, $\nu_{1/2} = 72$ Hz), $\delta(\text{CH}_3)$ at δ 1.88 and $\delta(\text{C}_6\text{H}_4)$ as multiplets at δ 7.40-6.94. In the ¹³C NMR, one $\delta(\text{Cp})$ resonances was recorded at δ 91.69, three $\delta(\text{CH}_3)$ peaks at δ 21.77, 15.68 and 15.11 together with $\delta(\text{C}_6\text{H}_4)$ as multiplets at δ 140.99, 138.22, 134.91, 134.71, 130.57, 129.67, 128.90, 126.79, 126.73 and 126.04. In the ³¹P NMR, the phosphorus resonance was recorded at δ -8.74 (refer to Appendix II).

2.8.4.3 Mass spectrum

$[\text{CpCr}(\text{CO})_2\{\text{P}(\text{C}_6\text{H}_4\text{SMe-}p)_3\}_2][\text{CpCr}(\text{CO})_3]$ (**28**)

The mass spectrum of **28** shows the parent ion $m/z = 1175.3844$ $[\text{CpCr}(\text{CO})_2\{\text{P}(\text{C}_6\text{H}_4\text{SMe-}p)_3\}_2][\text{CpCr}(\text{CO})_3]$ and its fragmentation ions as listed in Table 43.

Table 43. Electrospray ionization mass spectrum of $[\text{CpCr}(\text{CO})_2\{\text{P}(\text{C}_6\text{H}_4\text{SMe-}p)_3\}_2][\text{CpCr}(\text{CO})_3]$ (**28**)

m/z	Assignments
1119	$[\text{Cp}_2\text{Cr}_2(\text{CO})_3\{\text{P}(\text{C}_6\text{H}_4\text{SMe-}p)_3\}_2]^+$
1063	$[\text{Cp}_2\text{Cr}_2(\text{CO})\{\text{P}(\text{C}_6\text{H}_4\text{SMe-}p)_3\}_2]^+$
1035	$[\text{Cp}_2\text{Cr}_2\{\text{P}(\text{C}_6\text{H}_4\text{SMe-}p)_3\}_2]^+$
973	$[\text{CpCr}(\text{CO})_2\{\text{P}(\text{C}_6\text{H}_4\text{SMe-}p)_3\}_2]^+$
852	$[\text{Cr}\{\text{P}(\text{C}_6\text{H}_4\text{SMe-}p)_3\}_2]^+$
545	$[\text{CpCr}(\text{CO})\{\text{P}(\text{C}_6\text{H}_4\text{SMe-}p)_3\}]^+$
517	$[\text{CpCr}\{\text{P}(\text{C}_6\text{H}_4\text{SMe-}p)_3\}]^+$
502	$[\text{CpCr}\{\text{P}(\text{C}_6\text{H}_4\text{SMe-}p)_2(\text{C}_6\text{H}_4\text{S})\}]^+$
487	$[\text{CpCr}\{\text{P}(\text{C}_6\text{H}_4\text{SMe-}p)(\text{C}_6\text{H}_4\text{S})_2\}]^+$
402	$[\text{Cp}_2\text{Cr}_2(\text{CO})_6]^+$
400	$[\text{P}(\text{C}_6\text{H}_4\text{SMe-}p)_3]^+$

2.9 Studies of $\text{Cp}_2\text{Mo}_2(\text{CO})_6$ (**3**) and $\text{Cp}_2\text{Mo}_2(\text{CO})_4$ (**4**) with $\text{P}(\text{C}_6\text{H}_4\text{SMe-}p)_3$

2.9.1 Reaction of $\text{Cp}_2\text{Mo}_2(\text{CO})_6$ (**3**) and $\text{Cp}_2\text{Mo}_2(\text{CO})_4$ (**4**) with $\text{P}(\text{C}_6\text{H}_4\text{SMe-}p)_3$

A reddish brown solution of $\text{Cp}_2\text{Mo}_2(\text{CO})_6$ (**3**) undergoes reaction with one mole equivalent of $\text{P}(\text{C}_6\text{H}_4\text{SMe-}p)_3$ in toluene at 70 °C for 74 h. Column chromatography of the deep reddish brown reaction mixture led to the isolation of $\text{Cp}_2\text{Mo}_2(\text{CO})_6$ (**3**) (49.0% recovered) as reddish purple crystalline solids and $[\text{Cp}_2\text{Mo}_2(\text{CO})_5\{\text{P}(\text{C}_6\text{H}_4\text{SMe-}p)_3\}_2]$ (**29**) (18.6% yield) as a deep pink crystalline residue. It is worthy to note that the reaction requires a prolonged reaction time of 74 h in order to get half of the amount of **3** reacted.

The reaction of $\text{Cp}_2\text{Mo}_2(\text{CO})_4$ (**4**) with one mole equivalent of $\text{P}(\text{C}_6\text{H}_4\text{SMe-}p)_3$ at 110 °C took only 6.5 h to complete. Column chromatography of the resultant dark brownish pink reaction mixture gave $\text{Cp}_2\text{Mo}_2(\text{CO})_6$ (**3**) (3.5% recovery), $\text{Cp}_2\text{Mo}_2(\text{CO})_4$ (**4**) (13.9% recovery), $\text{Cp}_2\text{Mo}_2(\text{CO})_5\{\text{P}(\text{C}_6\text{H}_4\text{SMe-}p)_3\}$ (**29**) (37.4% yield), $\text{Cp}_2\text{Mo}_2(\text{CO})(\mu\text{-CO})_2\{\text{P}(\text{C}_6\text{H}_4\text{SMe-}p)_3\}$ (**30**) (20% yield) and a side product of $\text{Cp}_4\text{Mo}_4(\text{CO})_4(\mu_3\text{-O})(\mu_2\text{-O})_2(\text{O})$ (**31**) (2.6% yield).

2.9.2 Mechanistic pathways : Formation of $\text{Cp}_2\text{Mo}_2(\text{CO})_5\{\text{P}(\text{C}_6\text{H}_4\text{SMe-}p)_3\}$ (**29**), $\text{Cp}_2\text{Mo}_2(\text{CO})(\mu\text{-CO})_2\{\text{P}(\text{C}_6\text{H}_4\text{SMe-}p)_3\}$ (**30**) and $\text{Cp}_4\text{Mo}_4(\text{CO})_4(\mu_3\text{-O})(\mu_2\text{-O})_2(\text{O})$ (**31**)

The reactivity of $\text{Cp}_2\text{Mo}_2(\text{CO})_4$ towards $\text{P}(\text{C}_6\text{H}_4\text{SMe-}p)_3$ had led to the isolation of two monosubstituted dimers, pentacarbonyl $\text{Cp}_2\text{Mo}_2(\text{CO})_5\{\text{P}(\text{C}_6\text{H}_4\text{SMe-}p)_3\}$ (**29**) and tricarbonyl $\text{Cp}_2\text{Mo}_2(\text{CO})(\mu\text{-CO})_2\{\text{P}(\text{C}_6\text{H}_4\text{SMe-}p)_3\}$ (**30**). In addition, a molybdenum oxo complex of $\text{Cp}_4\text{Mo}_4(\text{CO})_4(\mu_3\text{-O})(\mu_2\text{-O})_2(\text{O})$ (**31**) was isolated as a side product in this reaction. The formation of **31** is likely to be a result from the oxidation with traces of oxygen in the atmosphere during the manipulation of the reaction mixture [39] or in the absence of oxygen or water, the oxygen atom could originate from a CO ligand [103].

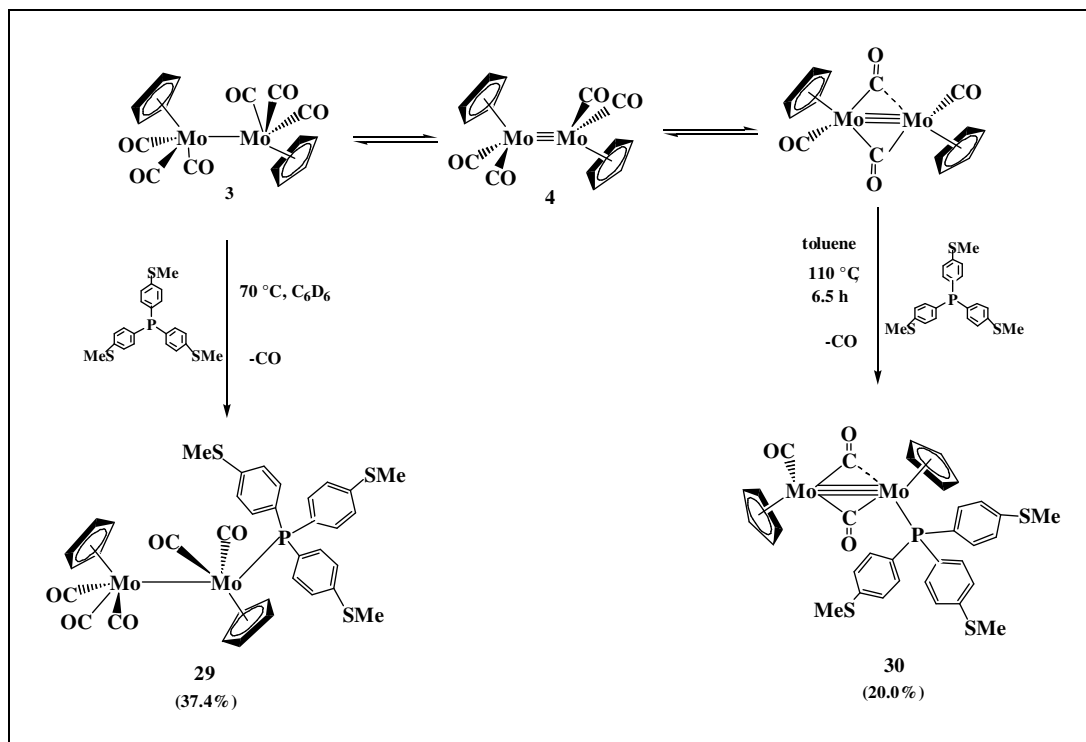
To deduce the formation of $\text{Cp}_2\text{Mo}_2(\text{CO})_5\{\text{P}(\text{C}_6\text{H}_4\text{SMe-}p)_3\}$ (**29**) from $\text{Cp}_2\text{Mo}_2(\text{CO})_4$ (**4**) as the starting complex, it is postulated that the formation of **29**

originates from $\text{Cp}_2\text{Mo}_2(\text{CO})_6$ (**3**) whereby one of the CO is substituted by a $\text{P}(\text{C}_6\text{H}_4\text{SMe-}p)_3$ moiety. The possible formation of $\text{Cp}_2\text{Mo}_2(\text{CO})_6$ in the reaction mixture is due to reversible CO transfer process between **3** and **4** particularly in toluene as reported by Curtis [11] (Eqn. (4)).

This postulation is substantiated by the reaction of $\text{Cp}_2\text{Mo}_2(\text{CO})_6$ with $\text{P}(\text{C}_6\text{H}_4\text{SMe-}p)_3$ in which **29** was isolated as the only product after 74 h. Similar observation was also reported by P.M. Treichel and co-worker [74] whereby only one monosubstituted product of $\text{Cp}_2\text{Mo}_2(\text{CO})_5(\text{PPh})_3$ was afforded from the reaction of **3** with PPh_3 . Haines *et al.* [76] have pointed out that when substituent groups attached to the phosphorus atom are more electronegative, such as $\text{P}(\text{O}i\text{Bu})_3$ and $\text{P}(\text{OPh})_3$, substitution of CO groups without rupture of the Mo-Mo bond can occur. Such phosphines are expected to be more CO-like exhibiting properties as good d_π electron acceptors from the metal. In this study, the bulky unsymmetrical $\text{Cp}_2\text{Mo}_2(\text{CO})_5\{\text{P}(\text{C}_6\text{H}_4\text{SMe-}p)_3\}$ is stable enough to be isolated because of the stabilizing effect of the more electronegative $-S\text{Me}$ substituents in the phosphine ligand.

The presence of the bridged $\mu\text{-CO}$ in the structure of $\text{Cp}_2\text{Mo}_2(\text{CO})(\mu\text{-CO})_2\{\text{P}(\text{C}_6\text{H}_4\text{SMe-}p)_3\}$ (**30**), indicates that **4** probably exists as the species $\text{Cp}_2\text{Mo}_2(\text{CO})_2(\mu\text{-CO})_2$ prior to nucleophilic addition (refer to Eqn. (5)). It is envisaged that formation of **4** is initiated by the attack of the lone pair electrons in $\text{P}(\text{C}_6\text{H}_4\text{SMe-}p)_3$ towards the $\text{Mo}\equiv\text{Mo}$ bond followed by decarbonylation (Scheme 31). Hence, one of the weaker terminal CO will preferentially undergo decarbonylation rather than the stronger bridging CO. Since phosphine is a weaker π acceptor as compared to CO, metal π -back donation towards CO is preferred.

In this study, the results indicated that *para* substituents in phosphines do not take part in metal coordination.



Scheme 31. Synthetic pathways for the formation of $\text{Cp}_2\text{Mo}_2(\text{CO})_5\{\text{P}(\text{C}_6\text{H}_4\text{SMe-}p)_3\}$ (**29**) and $\text{Cp}_2\text{Mo}_2(\text{CO})(\mu\text{-CO})_2\{\text{P}(\text{C}_6\text{H}_4\text{SMe-}p)_3\}$ (**30**)

2.9.3 Physical properties

$\text{Cp}_2\text{Mo}_2(\text{CO})_5\{\text{P}(\text{C}_6\text{H}_4\text{SMe-}p)_3\}$ (**29**)

$\text{Cp}_2\text{Mo}_2(\text{CO})_5\{\text{P}(\text{C}_6\text{H}_4\text{SMe-}p)_3\}$ exists as deep pink crystalline solids. In the solid state, it is stable at ambient temperature under an inert atmosphere. It is soluble in *n*-hexane: toluene mixture and very soluble in toluene to give a reddish pink solution. In solution, it is stable at ambient temperature for couple of days under an inert atmosphere and very stable if kept at -28°C .

$\text{Cp}_2\text{Mo}_2(\text{CO})(\mu\text{-CO})_2\{\text{P}(\text{C}_6\text{H}_4\text{SMe-}p)_3\}$ (**30**)

$\text{Cp}_2\text{Mo}_2(\text{CO})(\mu\text{-CO})_2\{\text{P}(\text{C}_6\text{H}_4\text{SMe-}p)_3\}$ exists as brownish pink crystalline solids. In the solid state, it is stable at ambient temperature under an inert atmosphere. It is sparingly soluble in toluene and very soluble in ether and THF to give a brownish pink

solution. In solution, it is stable at ambient temperature for couple of days under an inert atmosphere and very stable if kept at -28 °C.

Cp₄Mo₄(CO)₄(μ₃-O)(μ₂-O)₂(O) (31)

Cp₄Mo₄(CO)₄(μ₃-O)(μ₂-O)₂(O) exists as brown crystalline solids. In the solid state, it is stable at ambient temperature under an inert atmosphere. It is soluble in THF to give a brown solution. In solution, it is stable at ambient temperature for couple of days under an inert atmosphere and very stable if kept at -28 °C.

2.9.4 Spectral characteristics

2.9.4.1 IR spectra

Cp₂Mo₂(CO)₅{P(C₆H₄SMe-*p*)₃} (29)

The IR spectrum of **29** in nujol shows ν_{CO} stretching frequencies at 1965s, 1896s, 1871vs, 1812s cm⁻¹ and other peaks at 1152sh, 1094s, 1073s, 878vw, 808m, 746vw, 721vw, 668vw, 537w, 466w cm⁻¹ (refer to Appendix I).

Cp₂Mo₂(CO)(μ-CO)₂{P(C₆H₄SMe-*p*)₃} (30)

The IR spectrum of **30** in nujol shows ν_{CO} stretching frequencies at 1866s, 1786s, 1763vs cm⁻¹ and other peaks at 836vw, 811m, 798m, 745m, 576vw, 552m, 540m, 494vw, 467w cm⁻¹ (refer to Appendix I).

2.9.4.2 NMR spectra

Cp₂Mo₂(CO)₅{P(C₆H₄SMe-*p*)₃} (29)

29 is an unsymmetrical pentacarbonyl dimer. Two Cp peaks were recorded in its ¹H NMR spectrum (benzene-*d*₆) at δ 4.92, 4.85, one -CH₃ peak at δ 1.82 as singlet and the aromatic protons were recorded at δ 7.65-6.90 as multiplets. In the ¹³C NMR spectrum (benzene-*d*₆), two Cp peaks were recorded at δ 93.34, 91.84, one -CH₃ peak at δ 1.75 and the aromatic carbon were recorded at δ 133.15, 133.05, 129.67, 128.90, 125.71 (C₆H₄). In

the ^{31}P NMR spectrum, the phosphorus peak was recorded at δ 72.83 (refer to Appendix II). The results obtained from these NMR spectra are consistent with the molecular structure of **29**.

$\text{Cp}_2\text{Mo}_2(\text{CO})(\mu\text{-CO})_2\{\text{P}(\text{C}_6\text{H}_4\text{SMe-}i>p\text{)}_3\}$ (30**)**

30 is an unsymmetrical Mo dimer. Two Cp peaks were recorded in its ^1H NMR spectrum (benzene- d_6) at δ 4.67, 4.57, one $-\text{CH}_3$ peak at δ 1.89 and the aromatic protons as multiplets at δ 7.79-6.97. In the ^{13}C NMR spectrum (benzene- d_6), two Cp peaks were recorded at δ 93.09, 92.46, one CH_3 peak at δ 15.92 and aromatic carbons were recorded at δ 134.81, 134.70, 129.67, 128.91, 125.45, 125.35 (C_6H_4). In the ^{31}P NMR spectrum, the phosphorus peak was recorded at δ 25.09 (refer to Appendix II). The results obtained from these NMR spectra are consistent with the molecular structure of **30**. When compared to **29**, the chemical shifts in the ^{31}P NMR for **30** is in a lower frequency which could be due to the lesser number of CO ligands in **30**. Therefore, the electron density at Mo is higher and the deshielding effect is stronger for **30** as compared to **29**.

$\text{Cp}_4\text{Mo}_4(\text{CO})_4(\mu_3\text{-O})(\mu_2\text{-O})_2(\text{O})$ (31**)**

31 is an unsymmetrical tetramolybdenum complex. Four Cp peaks were recorded in its ^1H NMR spectrum at δ 5.70, 4.98, 4.87 and 4.72.

2.9.4.3 Mass spectra

Cp₂Mo₂(CO)₅{P(C₆H₄SMe-*p*)₃} (29)

The mass spectrum of **29** shows the parent ion $m/z = 863.0550$ Cp₂Mo₂(CO)₅{P(C₆H₄SMe-*p*)₃} and its fragmentation ions as listed in Table 44.

Table 44. Electrospray ionization mass spectrum of Cp₂Mo₂(CO)₅{P(C₆H₄SMe-*p*)₃} (**29**)

m/z	Assignments
863	Cp ₂ Mo ₂ (CO) ₅ {P(C ₆ H ₄ SMe- <i>p</i>) ₃ }
617	CpMo(CO) ₂ {P(C ₆ H ₄ SMe- <i>p</i>) ₃ }
589	CpMo(CO){P(C ₆ H ₄ SMe- <i>p</i>) ₃ }
561	CpMo{P(C ₆ H ₄ SMe- <i>p</i>) ₃ }
546	CpMo{P(C ₆ H ₄ SMe- <i>p</i>) ₂ (C ₆ H ₄ S)}
531	CpMo{P(C ₆ H ₄ SMe- <i>p</i>)(C ₆ H ₄ S) ₂ }
516	CpMo{P(C ₆ H ₄ S) ₃ }
399	P(C ₆ H ₄ SMe- <i>p</i>) ₃

Cp₂Mo₂(CO)(μ-CO)₂{P(C₆H₄SMe-*p*)₃} (30)

The mass spectrum of **30** shows the parent ion $m/z = 809.5274$ Cp₂Mo₂(CO)(μ-CO)₂{P(C₆H₄SMe-*p*)₃} and its fragmentation ions as listed in Table 45.

Table 45. Electrospray ionization mass spectrum of Cp₂Mo₂(CO)(μ-CO)₂{P(C₆H₄SMe-*p*)₃} (**30**)

m/z	Assignments
863	Cp ₂ Mo ₂ (CO) ₅ {P(C ₆ H ₄ SMe- <i>p</i>) ₃ }
810	Cp ₂ Mo ₂ (CO) ₂ (μ-CO) ₂ {P(C ₆ H ₄ SMe- <i>p</i>) ₃ }
795	Cp ₂ Mo ₂ (CO)(μ-CO)(μ-C){P(C ₆ H ₄ SMe- <i>p</i>) ₃ }
782	Cp ₂ Mo ₂ (CO)(μ-CO){P(C ₆ H ₄ SMe- <i>p</i>) ₃ }
765	Cp ₂ Mo ₂ (CO)(μ-C){P(C ₆ H ₄ SMe- <i>p</i>) ₃ }

645	$\text{Cp}_2\text{Mo}_2\{\text{P}(\text{C}_6\text{H}_4\text{S})_2(\text{C}_6\text{H}_4)\}$
616	$\text{CpMo}(\text{CO})_2\{\text{P}(\text{C}_6\text{H}_4\text{SMe-}p)_3\}$
589	$\text{CpMo}(\text{CO})\{\text{P}(\text{C}_6\text{H}_4\text{SMe-}p)_3\}$
561	$\text{CpMo}\{\text{P}(\text{C}_6\text{H}_4\text{SMe-}p)_3\}$
545	$\text{CpMo}\{\text{P}(\text{C}_6\text{H}_4\text{SMe-}p)_2(\text{C}_6\text{H}_4\text{S})\}$
531	$\text{CpMo}\{\text{P}(\text{C}_6\text{H}_4\text{SMe-}p)(\text{C}_6\text{H}_4\text{S})_2\}$

2.9.5 Molecular structures

$\text{Cp}_2\text{Mo}_2(\text{CO})_5\{\text{P}(\text{C}_6\text{H}_4\text{SMe-}p)_3\}$ (**29**)

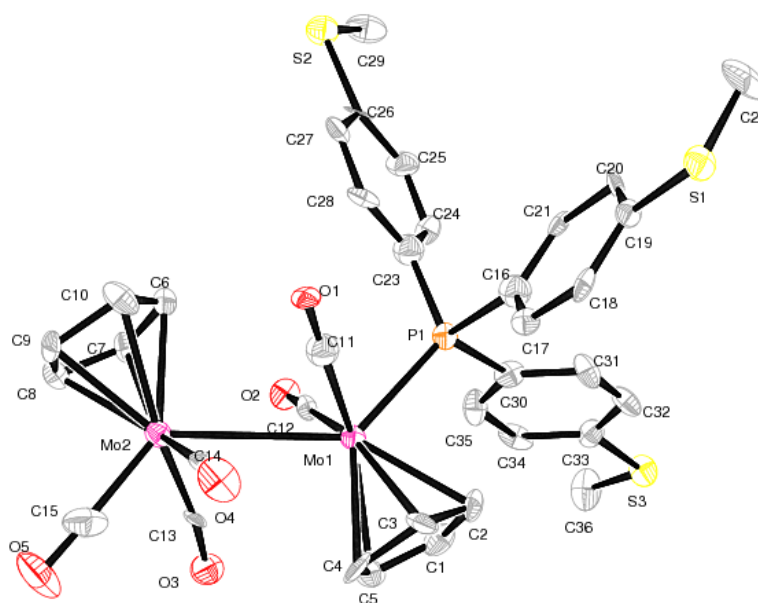


Figure 34. Molecular structure of $\text{Cp}_2\text{Mo}_2(\text{CO})_5\{\text{P}(\text{C}_6\text{H}_4\text{SMe-}p)_3\}$ (**29**)

The molecular structure of **29** is shown in Figure 34. The selected bond lengths (Å) and bond angles (°) are shown in Table 46. The dimeric product of $\text{Cp}_2\text{Mo}_2(\text{CO})_5\{\text{P}(\text{C}_6\text{H}_4\text{SMe-}p)_3\}$ (**29**) possesses a four-legged piano-stool configuration both at Mo1 and Mo2. Each metal has a η^5 -coordinated Cp ring located almost perpendicular to each other in a *trans* arrangement. Mo2 is tricarbonylated while the

dicarbonylated Mo1 has a substituted $P(C_6H_4SMe-p)_3$ ligand which is coordinated *via* the P atom. Half of the molecule **29**, $[CpMo(CO)_2\{P(C_6H_4SMe-p)_3\}]$ is isostructural with $CpM(CO)_2(PPh_3)$ (M = Cr [112], Mn [113]). Both of the molecules **29** and $CpCr(CO)_2(PPh_3)$ were crystallized in a P-1 space group. The bond distance of Mo(1)-Mo(2) (3.251 Å) indicates a single bond which is comparable to $Cp_2Mo_2(CO)_6$ (**3**) (3.235 Å). Apparently, the replacement of $P(C_6H_4SMe-p)_3$ instead of a CO ligand does not affect the electron donor effect in the complex.

Table 46. Bond lengths [Å] and angles [°] for $Cp_2Mo_2(CO)_5\{P(C_6H_4SMe-p)_3\}$ (**29**)

Bond lengths			
Mo(1)-C(12)	1.917(10)	C(15)-O(5)	1.155(13)
Mo(1)-C(11)	1.949(12)	P(1)-C(23)	1.806(10)
Mo(1)-P(1)	2.443(3)	P(1)-C(16)	1.842(9)
Mo(1)-Mo(2)	3.251(14)	P(1)-C(30)	1.852(10)
Mo(2)-C(13)	1.936(13)	C(19)-S(1)	1.758(10)
Mo(2)-C(15)	1.952(13)	S(1)-C(22)	1.773(11)
Mo(2)-C(14)	2.023(11)	C(26)-S(2)	1.764(11)
C(11)-O(1)	1.169(12)	S(2)-C(29)	1.793(10)
C(12)-O(2)	1.176(10)	C(33)-S(3)	1.750(10)
C(13)-O(3)	1.191(12)	S(3)-C(36)	1.747(10)
C(14)-O(4)	1.133(11)		
Bond angles			
C(12)-Mo(1)-C(11)	104.4(4)	O(2)-C(12)-Mo(1)	174.5(9)
C(12)-Mo(1)-P(1)	80.7(3)	O(3)-C(13)-Mo(2)	171.6(9)
C(11)-Mo(1)-P(1)	80.1(3)	O(4)-C(14)-Mo(2)	170.5(10)
C(12)-Mo(1)-Mo(2)	69.5(3)	O(5)-C(15)-Mo(2)	178.0(13)
C(11)-Mo(1)-Mo(2)	71.4(3)	C(23)-P(1)-C(16)	99.5(4)
P(1)-Mo(1)-Mo(2)	131.1(8)	C(23)-P(1)-C(30)	103.0(4)
C(13)-Mo(2)-C(15)	79.1(5)	C(16)-P(1)-C(30)	102.8(4)
C(13)-Mo(2)-C(14)	103.2(5)	C(23)-P(1)-Mo(1)	119.9(3)
C(15)-Mo(2)-C(14)	77.1(4)	C(16)-P(1)-Mo(1)	117.3(3)
C(13)-Mo(2)-Mo(1)	70.2(3)	C(30)-P(1)-Mo(1)	112.1(4)
C(15)-Mo(2)-Mo(1)	126.5(4)	C(19)-S(1)-C(22)	101.9(5)
C(14)-Mo(2)-Mo(1)	69.2(3)	C(26)-S(2)-C(29)	103.1(5)
O(1)-C(11)-Mo(1)	175.1(9)	C(36)-S(3)-C(33)	106.5(5)

Cp₂Mo₂(CO)(μ-CO)₂{P(C₆H₄SMe-*p*)₃} (30)

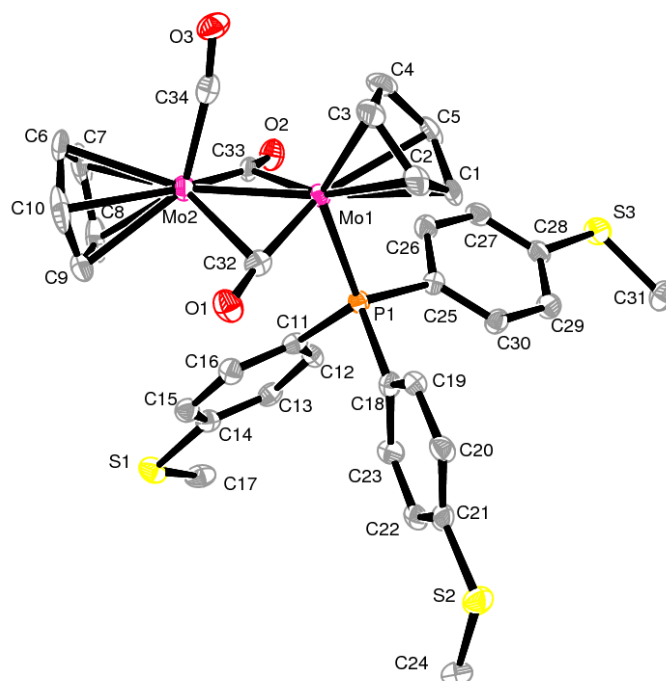


Figure 35. Molecular structure of Cp₂Mo₂(CO)(μ-CO)₂{P(C₆H₄SMe-*p*)₃} (**30**)

The molecular structure of **30** is shown in Figure 35. The selected bond lengths (Å) and bond angles (°) are shown in Table 47. Cp₂Mo₂(CO)(μ-CO)₂{P(C₆H₄SMe-*p*)₃} (**30**) crystallizes in triclinic, space group P-1. **30** consists of two μ₂-CO semi-bridging across two Mo atoms, one terminal CO at Mo(2) and a P(C₆H₄SMe-*p*)₃ ligand coordinated at Mo(1). Both C=O bonds distances in the two μ₂-CO have an average distance of 1.175(6) Å which is close to the terminal CO (1.166(6) Å). The phosphine ligand is in a *trans*-configuration to the terminal CO. Both Mo atoms are in a tetragonal-pyramidal coordination environment, with their Cp rings occupying the axial position. The Cp ring coordinated at Mo(1) is tilted to reduce steric hindrance resulting from the bulky phosphine ligand. The bond distance of Mo(1)-Mo(2) (2.514(9) Å) indicates the presence of a double bond and is comparable to the Mo=Mo bond found in [CpMo(SBz)S]₂ (**10a & b**) (average 2.58 (6) Å). The Mo(1)-P(1) bond distance of 2.465(15) Å is slightly longer as compared to the bond distance in Cp₂Mo₂(CO)₅{P(C₆H₄SMe-*p*)₃} (**29**) (2.443(3) Å).

Table 47. Bond lengths [\AA] and angles [$^\circ$] for $\text{Cp}_2\text{Mo}_2(\text{CO})(\mu\text{-CO})_2\{\text{P}(\text{C}_6\text{H}_4\text{SMe-}p)_3\}$ (**30**)

Bond lengths			
Mo(1)-C(32)	1.931(6)	S(2)-C(24)	1.801(6)
Mo(1)-P(1)	2.465(15)	S(3)-C(28)	1.758(5)
Mo(1)-C(33)	2.504(6)	S(3)-C(31)	1.805(6)
Mo(1)-Mo(2)	2.514(9)	P(1)-C(25)	1.829(5)
Mo(2)-C(33)	1.946(6)	P(1)-C(11)	1.828(5)
Mo(2)-C(34)	1.942(6)	P(1)-C(18)	1.828(5)
Mo(2)-C(32)	2.492(5)	O(1)-C(32)	1.180(6)
S(1)-C(14)	1.764(5)	O(2)-C(33)	1.170(6)
S(1)-C(17)	1.805(6)	O(3)-C(34)	1.166(6)
S(2)-C(21)	1.758(6)		
Bond angles			
C(32)-Mo(1)-P(1)	88.3(15)	C(14)-S(1)-C(17)	102.4(3)
C(32)-Mo(1)-C(33)	106.6(2)	C(21)-S(2)-C(24)	103.2(3)
P(1)-Mo(1)-C(33)	82.5(12)	C(28)-S(3)-C(31)	103.3(3)
C(32)-Mo(1)-Mo(2)	66.7(16)	C(25)-P(1)-Mo(1)	114.3(17)
P(1)-Mo(1)-Mo(2)	102.4(4)	C(11)-P(1)-Mo(1)	119.6(17)
C(33)-Mo(1)-Mo(2)	45.6(13)	C(18)-P(1)-Mo(1)	116.7(17)
C(33)-Mo(2)-C(34)	88.2(2)	O(1)-C(32)-Mo(1)	170.0(4)
C(33)-Mo(2)-C(10)	148.6(2)	O(1)-C(32)-Mo(2)	121.3(4)
C(34)-Mo(2)-C(10)	103.9(2)	Mo(1)-C(32)-Mo(2)	67.9(16)
C(33)-Mo(2)-C(32)	106.6(2)	O(2)-C(33)-Mo(2)	164.9(4)
C(34)-Mo(2)-C(32)	97.1(2)	O(2)-C(33)-Mo(1)	127.6(4)
C(33)-Mo(2)-Mo(1)	66.9(16)	Mo(2)-C(33)-Mo(1)	67.4(17)
C(34)-Mo(2)-Mo(1)	74.9(16)	O(3)-C(34)-Mo(2)	171.5(5)
C(32)-Mo(2)-Mo(1)	45.4(13)		

Cp₄Mo₄(CO)₄(μ₃-O)(μ₂-O)₂(O) (31)

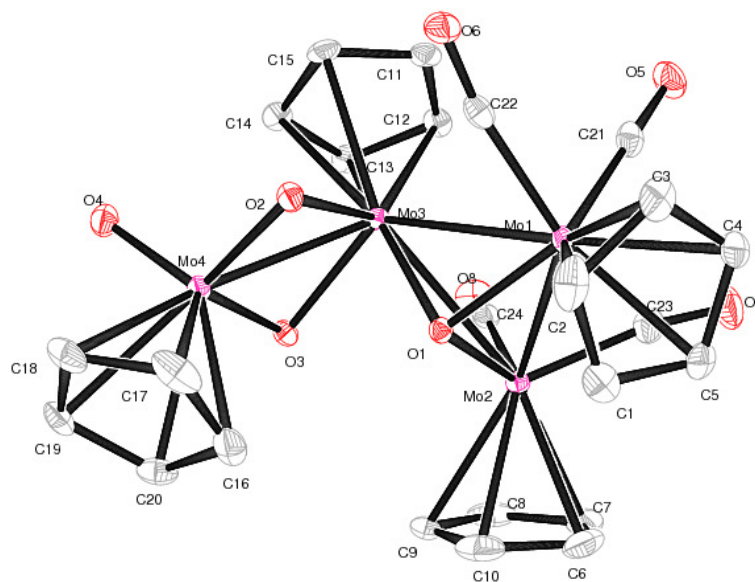


Figure 36. Molecular structure of Cp₄Mo₄(CO)₄(μ₃-O)(μ₂-O)₂(O) (**31**)

The molecular structure of **31** is shown in Figure 36. The selected bond lengths (Å) and bond angles (°) are shown in Table 48. Cp₄Mo₄(CO)₄(μ₃-O)(μ₂-O)₂(O) (**31**) crystallizes in monoclinic, space group P2₁/c. **31** is a tetramolybdenum oxo cluster which consists of four terminal CO, one μ₃-O, two μ₂-O and a free oxo ligand. The μ₃-O connects the Mo(1), Mo(2) and Mo(3) atoms together while the two μ₂-O connect both Mo(3) and Mo(4) atoms. The bond distances of Mo(1)-Mo(2) (2.923(3) Å), Mo(1)-Mo(3) (2.936(4) Å) and Mo(2)-Mo(3) (2.943(3) Å) are very similar and indicate the existence of a single bond when compared to other singly bonded Mo complexes (refer Table 7). However, the bond distance of Mo(3)-Mo(4) (2.653(3) Å) is much shorter and is comparable to other Mo=Mo double bond (refer Table 7). The electron count for Mo(1) and Mo(2) are similar and obeys the 18 e rule. Similarly for Mo(3), each atom O(2) and O(3) contributes one electron for it to obey the octet rule. In the case of Mo(4), both O(2) and O(3) have to donate a total of three electrons in order to attain the 18 e rule. This postulation is supported by the observed bond distances of Mo(3)-O(2) and Mo(3)-O(3)

(2.069(19) Å and 2.048(19) Å, respectively) which are longer than the bond distances of Mo(4)-O(2) and Mo(4)-O(3) (1.861(2) Å and 1.874(19) Å, respectively).

Table 48. Bond lengths [Å] and angles [°] for Cp₄Mo₄(CO)₄(μ₃-O)(μ₂-O)₂(O) (**31**)

Bond lengths			
Mo(1)-C(22)	1.969(3)	Mo(3)-O(3)	2.048(19)
Mo(1)-C(21)	1.974(3)	Mo(3)-O(2)	2.069(19)
Mo(1)-O(1)	2.023(19)	Mo(3)-Mo(4)	2.653(3)
Mo(1)-Mo(2)	2.923(3)	Mo(4)-O(4)	1.710(2)
Mo(1)-Mo(3)	2.936(4)	Mo(4)-O(2)	1.861(2)
Mo(2)-C(24)	1.938(3)	Mo(4)-O(3)	1.874(19)
Mo(2)-C(23)	1.950(3)	O(5)-C(21)	1.155(4)
Mo(2)-O(1)	2.011(19)	O(6)-C(22)	1.159(4)
Mo(2)-Mo(3)	2.943(3)	O(7)-C(23)	1.163(4)
Mo(3)-O(1)	1.987(2)	O(8)-C(24)	1.166(4)
Bond angles			
C(22)-Mo(1)-O(1)	96.41(10)	O(1)-Mo(3)-Mo(1)	43.43(5)
C(21)-Mo(1)-O(1)	124.38(11)	O(3)-Mo(3)-Mo(1)	123.72(6)
C(22)-Mo(1)-Mo(2)	127.62(9)	O(2)-Mo(3)-Mo(1)	86.28(6)
C(21)-Mo(1)-Mo(2)	95.24(9)	Mo(4)-Mo(3)-Mo(1)	116.78(11)
O(1)-Mo(1)-Mo(2)	43.41(5)	O(1)-Mo(3)-Mo(2)	42.93(5)
C(22)-Mo(1)-Mo(3)	67.33(9)	O(3)-Mo(3)-Mo(2)	78.24(6)
C(21)-Mo(1)-Mo(3)	89.14(9)	O(2)-Mo(3)-Mo(2)	123.30(6)
O(1)-Mo(1)-Mo(3)	42.46(6)	Mo(4)-Mo(3)-Mo(2)	110.57(11)
Mo(2)-Mo(1)-Mo(3)	60.31(8)	Mo(1)-Mo(3)-Mo(2)	59.64(8)
C(24)-Mo(2)-O(1)	113.39(10)	O(4)-Mo(4)-O(2)	109.96(10)
C(23)-Mo(2)-O(1)	112.61(11)	O(4)-Mo(4)-O(3)	107.66(9)
C(24)-Mo(2)-Mo(1)	113.17(9)	O(2)-Mo(4)-O(3)	99.84(8)
C(23)-Mo(2)-Mo(1)	68.90(9)	O(4)-Mo(4)-Mo(3)	110.17(7)
O(1)-Mo(2)-Mo(1)	43.74(5)	O(2)-Mo(4)-Mo(3)	50.97(6)
C(24)-Mo(2)-Mo(3)	71.27(9)	O(3)-Mo(4)-Mo(3)	50.28(6)
C(23)-Mo(2)-Mo(3)	107.89(10)	Mo(3)-O(1)-Mo(2)	94.79(8)
O(1)-Mo(2)-Mo(3)	42.28(6)	Mo(3)-O(1)-Mo(1)	94.10(8)
Mo(1)-Mo(2)-Mo(3)	60.06(8)	Mo(2)-O(1)-Mo(1)	92.85(8)
O(1)-Mo(3)-O(3)	80.39(8)	Mo(4)-O(2)-Mo(3)	84.71(8)
O(1)-Mo(3)-O(2)	80.78(8)	Mo(4)-O(3)-Mo(3)	84.99(8)
O(3)-Mo(3)-O(2)	87.89(8)	O(5)-C(21)-Mo(1)	174.70(3)
O(1)-Mo(3)-Mo(4)	84.86(5)	O(6)-C(22)-Mo(1)	169.10(3)
O(3)-Mo(3)-Mo(4)	44.73(5)	O(7)-C(23)-Mo(2)	167.60(3)
O(2)-Mo(3)-Mo(4)	44.31(5)	O(8)-C(24)-Mo(2)	165.90(3)

2.10 Studies of $[\text{CpCr}(\text{CO})_3]_2$ (**1**) with $\text{PPh}_2(\text{C}_6\text{H}_4\text{SMe-}o)$

2.10.1 The reaction of $[\text{CpCr}(\text{CO})_3]_2$ (**1**) with 2.5 mole equivalent of $\text{PPh}_2(\text{C}_6\text{H}_4\text{SMe-}o)$

When a deep green suspension of $\text{Cp}_2\text{Cr}_2(\text{CO})_6$ with $\text{PPh}_2(\text{C}_6\text{H}_4\text{SMe-}o)$ in toluene was stirred at 60 °C for 20 h at ambient temperature, a dark brownish pink reaction mixture was obtained. Chromatography *via* silica gel column led to the isolation of $\text{CpCr}(\text{CO})_2(\text{C}_6\text{H}_4\text{S-}o)\text{PPh}_2$ (**32**) (66.3% yield) as fine red crystalline solids.

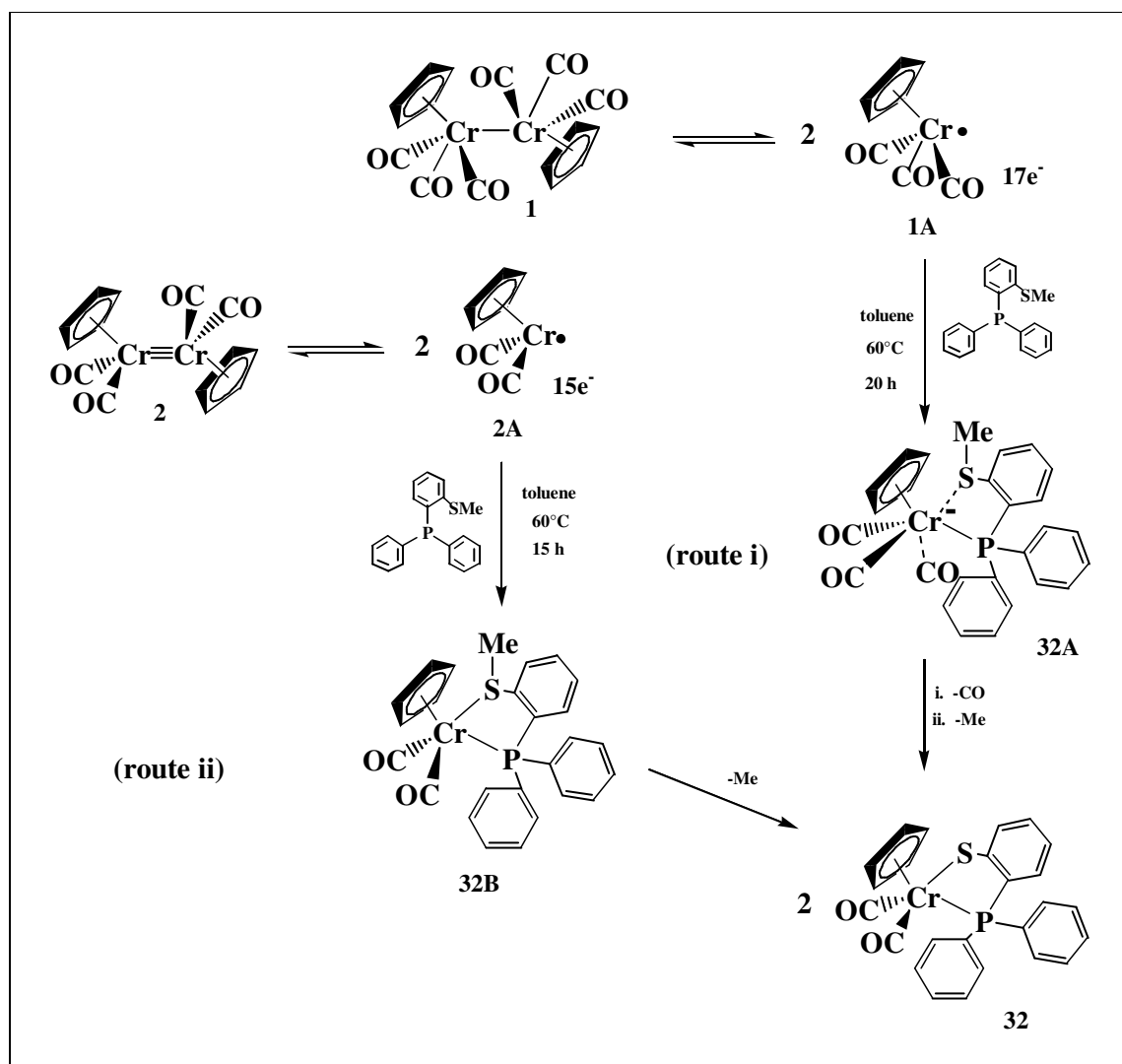
2.10.2 NMR tube reaction of $[\text{CpCr}(\text{CO})_2]_2$ (**2**) with 2.5 mole equivalent of $\text{PPh}_2(\text{C}_6\text{H}_4\text{SMe-}o)$

A mixture of deep green solids of $\text{Cp}_2\text{Cr}_2(\text{CO})_4$ and 2.5 mole equivalent of $\text{PPh}_2(\text{C}_6\text{H}_4\text{SMe-}o)$ in a 5 mm septum capped NMR tube in C_6D_6 (~ 0.5 mL) was thermolyzed at 60 °C with regular interval monitoring *via* ^1H NMR showed only $\text{CpCr}(\text{CO})_2\{(\text{C}_6\text{H}_4\text{S-}o)\text{PPh}_2\}$ (**32**) (42.4% yield) after 15 h.

2.10.3 Mechanistic pathways: Formation of $\text{CpCr}(\text{CO})_2\{(\text{C}_6\text{H}_4\text{S-}o)\text{PPh}_2\}$ (**32**)

During the reaction of $\text{Cp}_2\text{Cr}_2(\text{CO})_6$ (**1**) with $\text{PPh}_2(\text{C}_6\text{H}_4\text{SMe-}o)$ at 60 °C in toluene, only one monomeric product of $\text{CpCr}(\text{CO})_2\{(\text{C}_6\text{H}_4\text{S-}o)\text{PPh}_2\}$ (**32**) was isolated. The formation pathway to **32** is purportedly initiated by the $17e^-$ radical species, $\text{CpCr}(\text{CO})_3\cdot$ (**1A**), which is a result from the homolytic bond cleavage of Cr dimer **1** in solution. The electron deficient **1A** attacks the lone pair electrons of the phosphine resulting in the formation of a $19e^-$ intermediate, **32A**. This can proceed by decarbonylation of a CO ligand followed by concomitant coordination of the $-\text{SMe}$ substituent at the *ortho* position of the phenyl ring resulting in the formation of **32A** (Scheme 32). Subsequently, partial π -back donation of metal electrons into an S-C π^* orbital leads to homolytic S-C bond cleavage to give a Cr-P-S ring complex of $\text{CpCr}(\text{CO})_2\{(\text{C}_6\text{H}_4\text{S-}o)\text{PPh}_2\}$, **32**, as the final product (route i). Demethylation process of this type is quite common for first-row transition metals and low oxidation state metals [114a-b].

It is conceivable that the pathway proposed for the reaction of **2** with $\text{PPh}_2(\text{C}_6\text{H}_4\text{SMe-}o)$ involves the $15e^-$ species, **2A**, resulting from the homolytic cleavage of **2**. The electron deficient **2A** can be attracted to the lone pair electrons in the phosphine to form an intermediate **32B**. Subsequently, **32B** undergoes demethylation process to afford **32** (route ii). Unlike route (i), decarbonylation step is not necessary for route (ii) hence the time taken for the reaction to completion requires only 15 h as compared to 20 h *via* route (i).



Scheme 32. Synthetic pathways of $\text{CpCr(CO)}_2\{(\text{C}_6\text{H}_4\text{S-}o)\text{PPh}_2\}$ (**32**)

2.10.4 Physical Properties



$\text{CpCr(CO)}_2\{(\text{C}_6\text{H}_4\text{S-}o)\text{PPh}_2\}$ exists as orange red crystalline solids. It is fairly soluble in toluene but more soluble in ether, THF and CH_2Cl_2 to give an orange red solution. In the solid state, it is stable at room temperature under an inert atmosphere for a few hours. In solution, it is reasonably stable at a low temperature of $-28\text{ }^\circ\text{C}$.

2.10.5 Spectral Characteristics

2.10.5.1 IR spectrum



The IR spectrum of **32** in nujol shows ν_{CO} stretching frequencies at 1938vs, 1878vs, 1843sh cm^{-1} and other peaks at 1376m, 1245w, 1161w, 1099m, 1093m, 1069m, 1043m, 828w, 732w, 719w, 703m, 693m, 639w, 590w, 563m, 528m, 509w, 470m, 386m cm^{-1} (refer to Appendix I).

2.10.5.2 NMR spectrum



Complex **32** is a mononuclear complex. Therefore, only one Cp peak was recorded in its ^1H NMR spectrum (benzene- d_6) at δ 4.26 and two types of aromatic protons, C_6H_5 and C_6H_4 were recorded as multiplets overlapping each other at δ 6.74-6.68, 6.88-6.82, 6.96-6.92, 7.05-7.02, 7.33-7.29, 7.43-7.39, 7.68-7.63. In the ^{13}C NMR spectrum (benzene- d_6), one Cp peak was observed at δ 92.8, and two types of aromatic carbon, C_6H_5 and C_6H_4 were recorded at δ 158.74, 158.38, 137.37, 133.62, 133.51, 132.20, 132.12, 130.40, 129.69, 122.18, 122.12; two CO were recorded at δ 257.91, 253.33. In the ^{31}P NMR spectrum, the phosphorus peak was recorded at δ 108.46 (refer to Appendix II). All

the NMR chemical shifts agreed with its molecular structure obtained from single crystal X-ray diffraction analysis.

2.10.5.3 Mass spectrum

CpCr(CO)₂{(C₆H₄S-*o*)PPh₂} (32)

The mass spectrum of **32** shows the parent ion $m/z = 466.5188$ CpCr(CO)₂{(C₆H₄S-*o*)PPh₂} and its fragmentation ions as listed in Table 49.

Table 49. Electrospray ionization mass spectrum of CpCr(CO)₂{(C₆H₄S-*o*)PPh₂} (**32**)

m/z	Assignments
932	Cp ₂ Cr ₂ (CO) ₄ {(C ₆ H ₄ S- <i>o</i>)PPh ₂ } ₂
876	Cp ₂ Cr ₂ (CO) ₂ {(C ₆ H ₄ S- <i>o</i>)PPh ₂ } ₂
849	Cp ₂ Cr ₂ (CO){(C ₆ H ₄ S- <i>o</i>)PPh ₂ } ₂
821	Cp ₂ Cr ₂ {(C ₆ H ₄ S- <i>o</i>)PPh ₂ } ₂
667	[CpCr(CO) ₃][CpCr(CO) ₂ {(C ₆ H ₄ S- <i>o</i>)PPh ₂ }]
466	CpCr(CO) ₂ {(C ₆ H ₄ S- <i>o</i>)PPh ₂ }
410	CpCr{(C ₆ H ₄ S- <i>o</i>)PPh ₂ }

2.10.6 Molecular structure

$\text{CpCr}(\text{CO})_2\{(\text{C}_6\text{H}_4\text{S-}o)\text{PPh}_2\}$ (**32**)

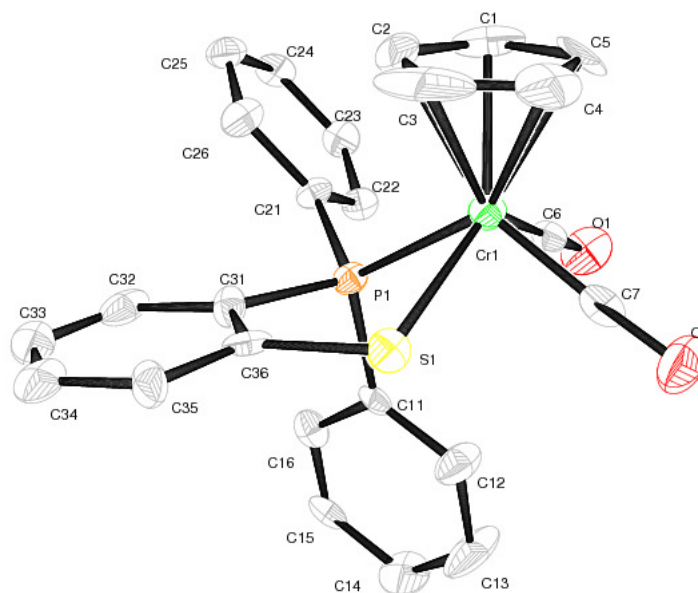


Figure 37. Molecular structure of $\text{CpCr}(\text{CO})_2\{(\text{C}_6\text{H}_4\text{S-}o)\text{PPh}_2\}$ (**32**)

The molecular structure of **32** is shown in Figure 37. The selected bond lengths (Å) and bond angles (°) are shown in Table 50. The monomeric compound of $\text{CpCr}(\text{CO})_2\{(\text{C}_6\text{H}_4\text{S-}o)\text{PPh}_2\}$ (**32**) crystallizes in monoclinic, space group $P2_1/n$ and possesses a four-legged piano-stool configuration at Cr with the Cp ring occupying the apical position. The bidentate heterodonor phosphine is coordinated to both P and S atoms at the Cr metal to form a five membered, Cr-P-C-C-S chelate ring. Both C6 and C7 together with P1 and S1 atoms lie on a nearly square-planar plane which is parallel with the phenyl ring (C31 to C36) but is perpendicular with the CpCr fragment. The Cr-S bond distance of 2.446(3) Å is longer than that found in $\text{Cr}(\text{CO})_4\{(\text{C}_6\text{H}_4\text{SMe-}o)\text{PPh}_2\}$ (2.394(2) Å) [115]. The lengthening effect of the Cr-S bond can be rationalized by the presence of two lone pair electrons at the S atom resulting in electronic repulsion from the Cp ring.

Table 50. Bond lengths [Å] and angles [°] for CpCr(CO)₂{(C₆H₄S-*o*)PPh₂} (**32**)

Bond lengths			
Cr(1)-C(7)	1.818(7)	C(7)-O(2)	1.164(8)
Cr(1)-C(6)	1.838(9)	P(1)-C(31)	1.785(8)
Cr(1)-P(1)	2.325(2)	P(1)-C(11)	1.836(7)
Cr(1)-S(1)	2.446(3)	P(1)-C(21)	1.848(7)
C(6)-O(1)	1.144(9)	S(1)-C(36)	1.748(7)
Bond angles			
C(7)-Cr(1)-C(6)	77.4(3)	C(31)-P(1)-C(11)	103.0(3)
C(7)-Cr(1)-P(1)	118.1(2)	C(31)-P(1)-C(21)	106.8(3)
C(6)-Cr(1)-P(1)	77.0(2)	C(11)-P(1)-C(21)	103.2(3)
C(7)-Cr(1)-S(1)	78.6(3)	C(31)-P(1)-Cr(1)	110.4(2)
C(6)-Cr(1)-S(1)	128.6(3)	C(11)-P(1)-Cr(1)	117.2(2)
P(1)-Cr(1)-S(1)	75.5(8)	C(21)-P(1)-Cr(1)	115.1(3)
O(1)-C(6)-Cr(1)	178.6(6)	C(36)-S(1)-Cr(1)	105.4(3)
O(2)-C(7)-Cr(1)	175.8(7)		

2.11 Studies of [CpCr(CO)₃]₂ (**1**) with PPh(C₆H₄SMe-*o*)₂

2.11.1 The reaction of [CpCr(CO)₃]₂ (**1**) with PPh(C₆H₄SMe-*o*)₂

A deep green solution of [CpCr(CO)₃]₂ (**1**) with PPh(C₆H₄SMe-*o*)₂ in toluene (~20mL) under rigorous stirring at 110 °C for 5 h resulted in the formation of a reddish brown reaction mixture. Separation of the reaction mixture by column chromatography led to the isolation of [CpCr(CO)₂]₂ (**2**) as dark green solids (82.5% yield), [Cp₂Cr₂(CO){(μ-C₆H₄S)₂PPh}] (**33**) as dark pink crystalline solids (4.3% yield) and CpCr{(μ-C₆H₄S)₂PPh} (**34**) (8.2% yield) as fine brownish pink crystalline solids.

2.11.2 The reaction of [CpCr(CO)₂]₂ (**2**) with PPh(C₆H₄SMe-*o*)₂

A deep green suspension of [CpCr(CO)₂]₂ (**2**) with PPh(C₆H₄SMe-*o*)₂ in toluene (~20mL) under rigorous stirring at 110 °C for 3 h resulted in a reddish brown reaction mixture. Chromatography of the reaction mixture *via* a silica gel column led to the isolation of unreacted [CpCr(CO)₂]₂ (**2**) (44.4% recovery), an orange red crystalline solids

of $[\text{Cp}_2\text{Cr}_2(\text{CO})\{\mu\text{-C}_6\text{H}_4\text{S}\}_2\text{PPh}]$ (**33**) (42.4% yield) and fine brownish pink crystalline solid of $\text{CpCr}\{\mu\text{-C}_6\text{H}_4\text{S}\}_2\text{PPh}$ (**34**) (4.9% yield).

2.11.3 NMR Tube Reaction

(a) The reaction of $[\text{CpCr}(\text{CO})_3]_2$ (**1**) with $\text{PPh}(\text{C}_6\text{H}_4\text{SMe-}o)_2$

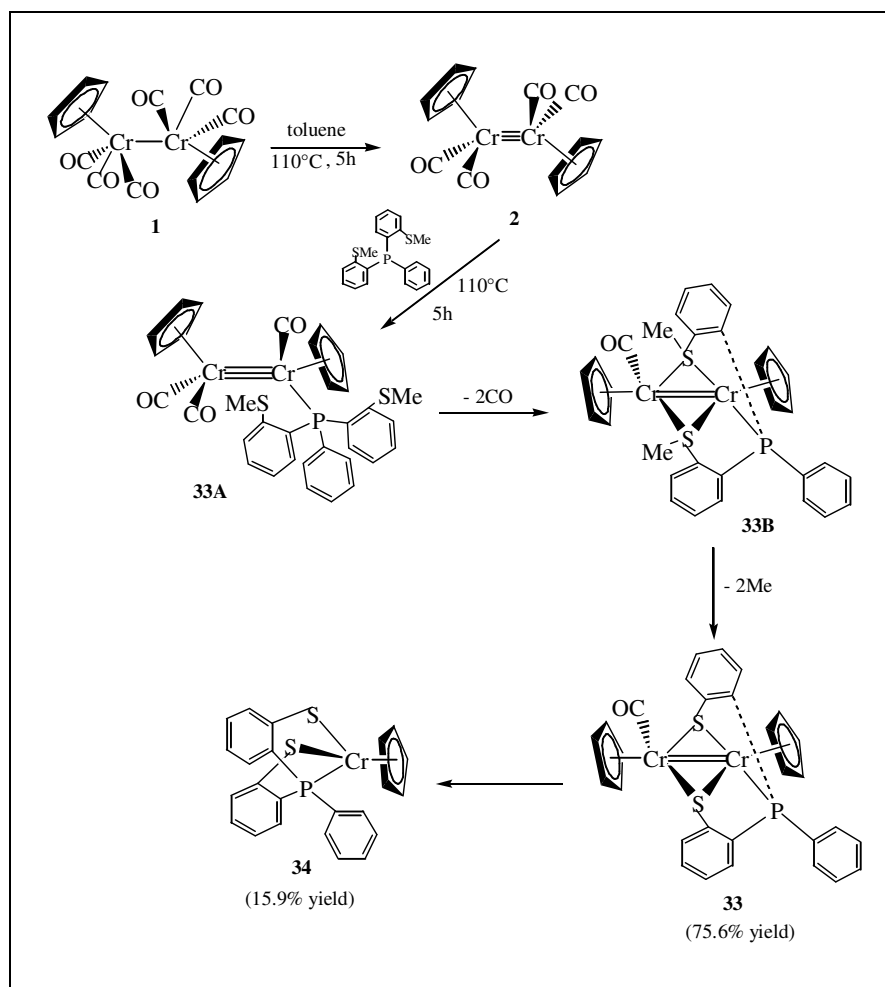
A time-dependent variation of products composition from the reaction of $[\text{CpCr}(\text{CO})_3]_2$ (**1**) with one mole equivalent of $\text{PPh}(\text{C}_6\text{H}_4\text{SMe-}o)_2$ at 110 °C has been monitored *via* ^1H NMR spectra scans which are illustrated in Figure 40. The conversion of $[\text{CpCr}(\text{CO})_3]_2$ (**1**) to its thermolytic congener, **2**, occurred after 4 to 7.5 h of reaction. After 13 h, the main product formed is **2** together with a small amount of $[\text{Cp}_2\text{Cr}_2(\text{CO})\{\mu\text{-C}_6\text{H}_4\text{S}\}_2\text{PPh}]$ (**33**). Over 15 h, a gradual increase of the products **33** and $\text{CpCr}\{\mu\text{-C}_6\text{H}_4\text{S}\}_2\text{PPh}$ (**34**) was observed. Finally, after 25 h of reaction, most of **2** will be converted to **33** and **34**. The above observation is represented in Scheme 33 which indicates that the synthetic pathway of complex **33** proceeds *via* the triply bonded Cr dimer.

2.11.4 Mechanistic pathways: Formation of $[\text{Cp}_2\text{Cr}_2(\text{CO})\{\mu\text{-C}_6\text{H}_4\text{S}\}_2\text{PPh}]$ (**33**) and $\text{CpCr}\{\mu\text{-C}_6\text{H}_4\text{S}\}_2\text{PPh}$ (**34**)

From the above experimental findings, it is postulated that the reaction of $[\text{CpCr}(\text{CO})_3]_2$ (**1**) with $\text{PPh}(\text{C}_6\text{H}_4\text{SMe-}o)_2$ is most likely to proceed *via* the $15e^-$ radical species generated from $[\text{CpCr}(\text{CO})_2]_2$ (**2**) to afford $[\text{Cp}_2\text{Cr}_2(\text{CO})\{\mu\text{-C}_6\text{H}_4\text{S}\}_2\text{PPh}]$ (**33**) and $\text{CpCr}\{\mu\text{-C}_6\text{H}_4\text{S}\}_2\text{PPh}$ (**34**). This postulation was made by referring to the observation during the NMR tube reaction of **1** with $\text{PPh}(\text{C}_6\text{H}_4\text{SMe-}o)_2$ at 110 °C where conversion of **1** to **2** is necessary before formation of products **33** and **34** occurred. $\text{PPh}(\text{C}_6\text{H}_4\text{SMe-}o)_2$ which acts as an electrophile will attack the electron-rich $\text{Cr}\equiv\text{Cr}$ bond in **2** and substitute one CO ligand to give an intermediate of **33A** (Scheme 33).

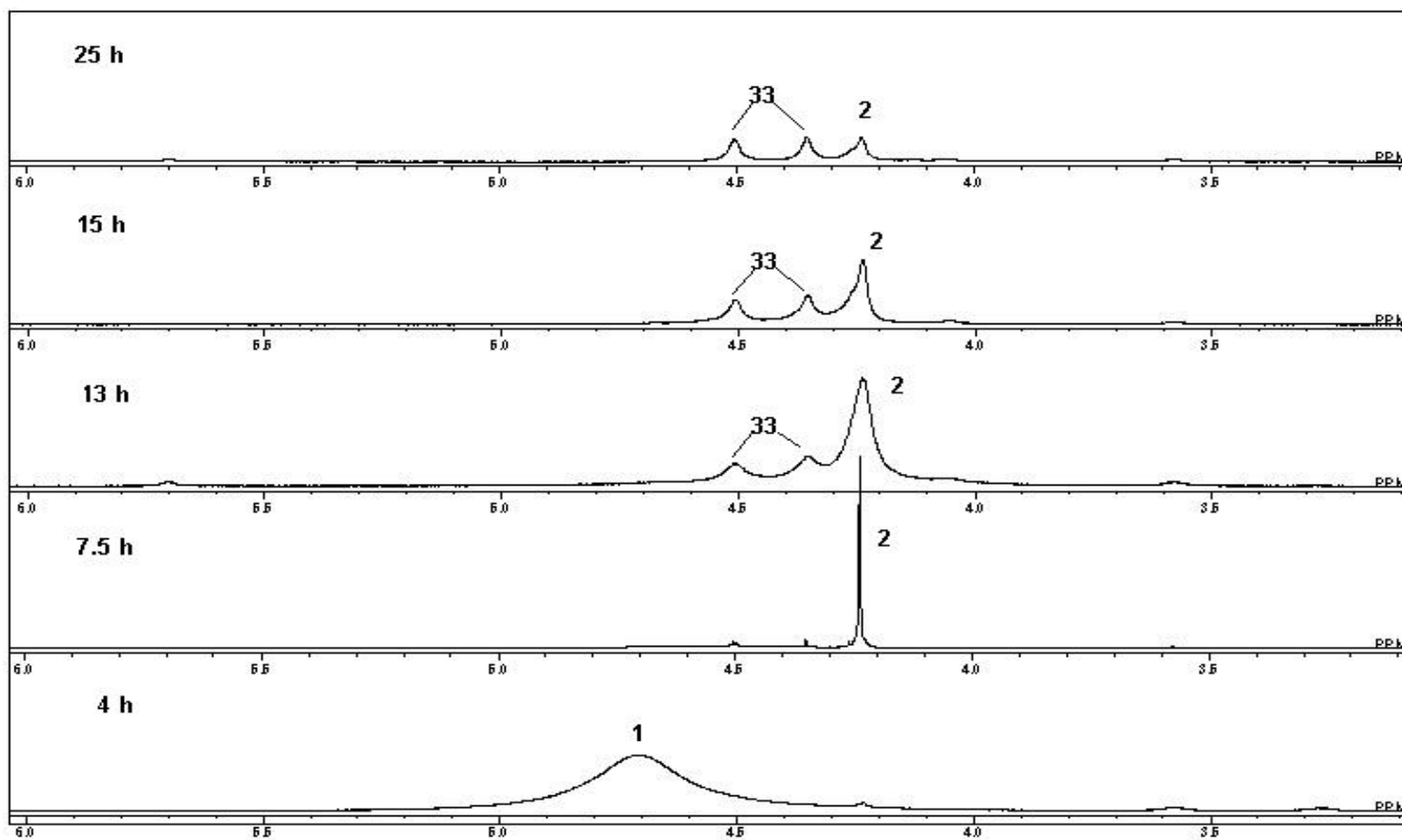
The electronic and steric effects of the $-SMe$ groups in $PPh(C_6H_4SMe-o)_2$ are different from the $P(C_6H_4SMe-p)_3$ [116]. Both the $-SMe$ groups in the ligand will bridge between the two Cr atoms forming two thiolate bridges accompanied by the loss of two CO ligands in a concerted manner to give **33B**. Consequently, the partial π -back donation effect of the metal electrons into the S-C π^* orbitals can induce homolytic S-C bond cleavage to give **33**.

The formation of the paramagnetic mononuclear complex of $CpCr\{(\mu-C_6H_4S)_2PPh\}$ (**34**) has been postulated to be the result from the thermal degradation of $[Cp_2Cr_2(CO)\{(\mu-C_6H_4S)_2PPh\}]$ (**33**). The steps involve total decarbonylation followed by molecular rearrangement to afford $CpCr\{(\mu-C_6H_4S)_2PPh\}$ (**34**).



Scheme 33. Synthetic pathways for $[Cp_2Cr_2(CO)\{(\mu-C_6H_4S)_2PPh\}]$ (**33**) and $CpCr\{(\mu-C_6H_4S)_2PPh\}$ (**34**)

Figure 38. Time-dependant ^1H NMR spectra of $[\text{CpCr}(\text{CO})_3]_2$ (**1**) with one mole equivalent of $\text{PPh}(\text{C}_6\text{H}_4\text{SMe-}o)_2$ at $110\text{ }^\circ\text{C}$



Chemical shift for product 34 was not included in multi-spectrum for clarity reason.

2.11.5 Physical Properties

$[\text{Cp}_2\text{Cr}_2(\text{CO})\{\mu\text{-C}_6\text{H}_4\text{S}\}_2\text{PPh}]$ (33)

The complex exists as an orange red crystalline solid which is stable for several hours at ambient temperature under an inert atmosphere and can be stored for an indefinite period at $-28\text{ }^\circ\text{C}$. It is insoluble in *n*-hexane but can be dissolved in toluene to give an orange red solution. The solution of the complex is stable at room temperature for several hours and fairly stable at $-28\text{ }^\circ\text{C}$ under an inert atmosphere for a few weeks.

$\text{CpCr}\{\mu\text{-C}_6\text{H}_4\text{S}\}_2\text{PPh}$ (34)

The complex exists as brown crystalline solids and is stable for a couple of hours at ambient temperature under an inert atmosphere and can be stored at $-28\text{ }^\circ\text{C}$ for a prolonged period. The complex is soluble in ether and THF to give an unstable brown solution.

2.11.6 Spectral Characteristics

2.11.6.1 IR spectra

$[\text{Cp}_2\text{Cr}_2(\text{CO})\{\mu\text{-C}_6\text{H}_4\text{S}\}_2\text{PPh}]$ (33)

The IR spectrum of **33** in nujol shows ν_{CO} stretching frequencies at 1836vs cm^{-1} and other peaks at 1316w , 1270sh , 1160w , 1096m , 1069vw , 1043m , 1029sh , 998w , 966w , 946w , 807w , 746vs , 732sh , 719w and 697m cm^{-1} (refer to Appendix I).

$\text{CpCr}\{\mu\text{-C}_6\text{H}_4\text{S}\}_2\text{PPh}$ (34)

The IR analysis for complex **34** could not be obtained owing to its instability.

2.11.6.2 NMR spectra

[Cp₂Cr₂(CO){(μ-C₆H₄S)₂PPh}] (33)

Complex **33** is an unsymmetrical dimeric compound, and both the ¹H and ¹³C NMR showed two Cp signals. The recorded ¹H NMR spectrum in benzene-*d*₆ showed the Cp signals at δ 4.51, 4.36, and aromatic protons of C₆H₅ and C₆H₄ as multiplets at δ 7.71-6.45. In the ¹³C NMR spectrum in benzene-*d*₆, the Cp signals were recorded at δ 94.0, 92.7, aromatic carbons of C₆H₅ and C₆H₄ at δ 145.33, 145.05, 138.63, 135.28, 135.07, 134.27, 132.43, 130.56, 129.81, 129.30, 127.78, 126.02 together with a CO peak at δ 196.02. In the ³¹P NMR spectrum, the phosphorus peak was recorded at δ 153.50 (Figure 99).

CpCr{(μ-C₆H₄S)₂PPh} (34)

Complex **34** is a monomeric 15e⁻ compound. A broad Cp peak was recorded in the ¹H NMR spectrum (benzene-*d*₆) at δ 11.37 (br, Cp, *v*_{1/2} = 96 Hz) with the aromatic protons of C₆H₅ and C₆H₄ as multiplets at δ 7.71-7.03. In the ¹³C NMR spectrum (benzene-*d*₆), the Cp signal was too weak to be recorded but the aromatic carbons of C₆H₅ and C₆H₄ were recorded at δ 138.21, 132.43, 130.56, 129.67, 128.90, 126.03.

2.11.6.3 Mass spectra

[Cp₂Cr₂(CO){(μ-C₆H₄S)₂PPh}] (33)

The mass spectrum of **33** shows the parent ion *m/z* = 587.4015 [Cp₂Cr₂(CO){(μ-C₆H₄S)₂PPh}] and its fragmentation ions as listed in Table 51.

Table 51. Electrospray ionization mass spectrum of [Cp₂Cr₂(CO){(μ-C₆H₄S)₂PPh}] (33)

<i>m/z</i>	Assignments
882	Cp ₂ Cr ₂ {(μ-C ₆ H ₄ S) ₂ PPh} ₂
469	CpCr(CO){(μ-C ₆ H ₄ S)PPh}

2.11.7 Molecular Structures

[Cp₂Cr₂(CO){(μ-C₆H₄S)₂PPh}] (33)

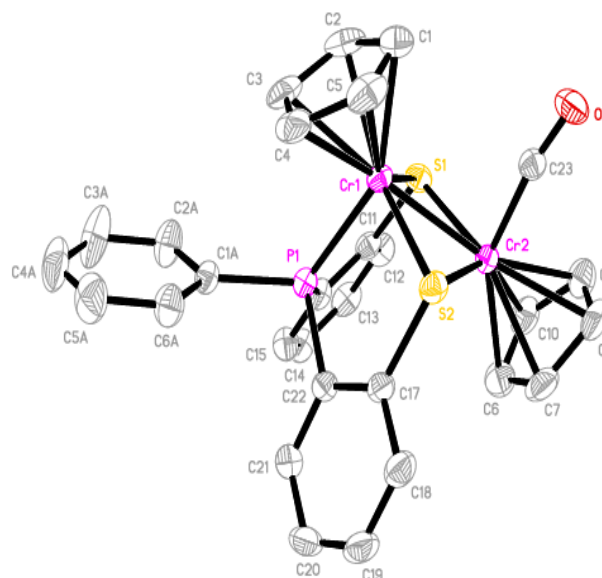


Figure 39. Molecular structure of [Cp₂Cr₂(CO){(μ-C₆H₄S)₂PPh}] (33)

The molecular structure of **33** is as shown in Figure 39. The selected bond lengths (Å) and bond angles (°) for [Cp₂Cr₂(CO){(μ-C₆H₄S)₂PPh}] are shown in Table 52. [Cp₂Cr₂(CO){(μ-C₆H₄S)₂PPh}] (**33**) crystallizes in monoclinic, space group P2₁/n. In [Cp₂Cr₂(CO){(μ-C₆H₄S)₂PPh}], the dihedral angle for Cr(1)-S(2)-Cr(2)-S(1) core is -12.6° which shows that this core is nearly co-planar. The Cr(1)-Cr(2) separation of 2.471(8) Å indicates that it is a double bond and is related to the Cr=Cr complexes of Cp₂Cr₂(CO)₂(μ₂-P(H)PhOMe)₂ (2.579(11) Å) [116] and Cp₂Cr₂(CO)₂(μ-PMe₂)₂ (2.578(7)) [117]. Both Cr1 and Cr2 atoms are in a tetragonal pyramidal coordination environment, with the Cp groups occupying the axial position but Cr1 maintains a distortion due to steric repulsion of the thioaryl group leading to the axial displacement of the Cp group. In addition, the effect also increases the bond angles of C(22)-P(1)-Cr(1) (110.29(12)°) by 12° as compared to those of C(16)-P(1)-Cr(1) and C(22)-P(1)-Cr(1). The average distance of the four Cr-S bond is 2.291(11) Å which is shorter than the similar bond found in [CpCr(SPh)]₂S (aveg. 2.371(1) Å) [47].

Table 52. Bond lengths [Å] and bond angles [°] for complex **33**

Bond lengths

Cr(1)-Cr(2)	2.471(8)	P(1)-C(16)	1.822(4)
Cr(1)-P(1)	2.276(11)	P(1)-C(22)	1.826(4)
Cr(1)-S(2)	2.277(10)	P(1)-C(1A)	1.830(4)
Cr(1)-S(1)	2.286(11)	O(1)-C(23)	1.164(4)
Cr(2)-C(23)	1.819(4)	S(1)-C(11)	1.791(4)
Cr(2)-S(2)	2.294(11)	S(2)-C(17)	1.783(4)
Cr(2)-S(1)	2.305(10)		

Bond angles

S(2)-Cr(1)-S(1)	114.11(4)	C(16)-P(1)-C(22)	107.24(17)
P(1)-Cr(1)-S(2)	84.96(4)	C(16)-P(1)-C(1A)	104.47(16)
P(1)-Cr(1)-S(1)	84.97(4)	C(16)-P(1)-Cr(1)	110.42(13)
P(1)-Cr(1)-Cr(2)	91.55(3)	C(22)-P(1)-Cr(1)	110.29(12)
S(1)-Cr(1)-Cr(2)	57.82(3)	C(1A)-P(1)-Cr(1)	121.94(12)
S(2)-Cr(1)-Cr(2)	57.61(3)	C(11)-S(1)-Cr(1)	108.60(13)
C(23)-Cr(2)-S(2)	88.71(12)	Cr(1)-S(1)-Cr(2)	65.10(3)
C(23)-Cr(2)-S(1)	90.28(11)	Cr(1)-S(2)-Cr(2)	65.44(3)
S(2)-Cr(2)-S(1)	112.74(4)	C(17)-S(2)-Cr(1)	108.92(12)
S(2)-Cr(2)-Cr(1)	56.95(3)		
S(1)-Cr(2)-Cr(1)	57.08(3)		

Dihedral angle

Cr(1)-S(2)-Cr(2)-S(1)	-12.6
-----------------------	-------

CpCr{(μ -C₆H₄S)₂PPh} (34)

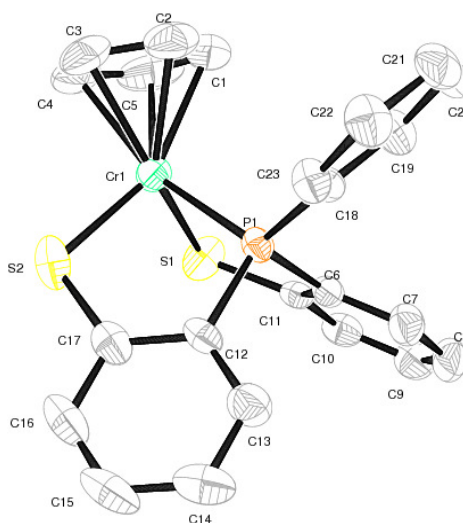


Figure 40. Molecular structure of CpCr{(μ -C₆H₄S)₂PPh} (**34**)

The molecular structure of **34** is as shown in Figure 40. The selected bond lengths (Å) and bond angles (°) for **34** are shown in Table 53. CpCr{(μ-C₆H₄S)₂PPh} (**34**) crystallizes in monoclinic, space group P2₁/c. **34** is a tridentate chelate complex with two S atoms and one P atom coordinated to the metal center. Similar to Ga^tBu{PPh(2-SPh)₂-κ³S,S',P} [118], **34** contains a PS₂²⁻ ligand which coordinates in a pincer-like manner. The bond angles of P(1)-Cr(1)-S(1) (82.81(3)°) and P(1)-Cr(1)-S(2) (86.07(4)°) which is close to 90° indicates **33** is in a three-legged piano-stool configuration with the Cp ring coordinated at the apical position of Cr.

Table 53. Bond lengths [Å] and bond angles [°] for complex CpCr{(μ-C₆H₄S)₂PPh} (**34**)

Bond lengths			
Cr(1)-C(5)	2.199(4)	S(1)-C(11)	1.755(3)
Cr(1)-C(4)	2.206(4)	S(2)-C(17)	1.767(4)
Cr(1)-S(1)	2.331(10)	P(1)-C(6)	1.803(3)
Cr(1)-S(2)	2.332(12)	P(1)-C(12)	1.807(3)
Cr(1)-P(1)	2.370(10)	P(1)-C(18)	1.811(3)
Bond angles			
C(4)-Cr(1)-S(1)	113.65(18)	C(11)-S(1)-Cr(1)	107.48(11)
C(1)-Cr(1)-S(1)	104.68(15)	C(17)-S(2)-Cr(1)	105.74(12)
C(2)-Cr(1)-S(1)	139.75(16)	C(6)-P(1)-C(12)	106.60(15)
C(3)-Cr(1)-S(1)	150.49(16)	C(6)-P(1)-Cr(1)	107.57(11)
C(2)-Cr(1)-S(2)	118.85(16)	C(18)-P(1)-Cr(1)	120.75(10)
C(3)-Cr(1)-S(2)	92.76(14)	C(7)-C(6)-P(1)	124.1(3)
S(1)-Cr(1)-S(2)	101.40(4)	C(11)-C(6)-P(1)	115.6(2)
C(5)-Cr(1)-P(1)	137.38(18)	C(6)-C(11)-S(1)	121.9(2)
C(4)-Cr(1)-P(1)	159.54(13)	C(10)-C(11)-S(1)	119.4(3)
C(1)-Cr(1)-P(1)	105.04(13)	C(13)-C(12)-P(1)	122.4(3)
C(2)-Cr(1)-P(1)	98.75(11)	C(17)-C(12)-P(1)	117.2(3)
C(3)-Cr(1)-P(1)	124.28(16)		
S(1)-Cr(1)-P(1)	82.81(3)		
S(2)-Cr(1)-P(1)	86.07(4)		

2.12 Studies of $[\text{CpCr}(\text{CO})_3]_2$ (**1**) with $\text{P}(\text{C}_6\text{H}_4\text{SMe-}o)_3$

2.12.1 The reaction of $[\text{CpCr}(\text{CO})_3]_2$ (**1**) with $\text{P}(\text{C}_6\text{H}_4\text{SMe-}o)_3$

A deep green solution of $[\text{CpCr}(\text{CO})_3]_2$ (**1**) with one mole equivalent of *o*- $\text{P}(\text{PhSMe})_3$ undergoes complete reaction in refluxing toluene after 5 h. Column chromatography of the reddish brown reaction mixture led to the isolation of $[\text{CpCr}(\text{CO})_2]_2$ (**2**) (58.2% recovery) as fine dark green crystalline solids and $[\text{Cp}_2\text{Cr}_2(\text{CO})\{(\mu\text{-C}_6\text{H}_4\text{SMe})_2(\text{C}_6\text{H}_4\text{SMe-}o)\text{P}\}]$ (**35**) (12.7% yield) as dark red crystalline solids.

2.12.2 The reaction of $[\text{CpCr}(\text{CO})_2]_2$ (**2**) with $\text{P}(\text{C}_6\text{H}_4\text{SMe-}o)_3$

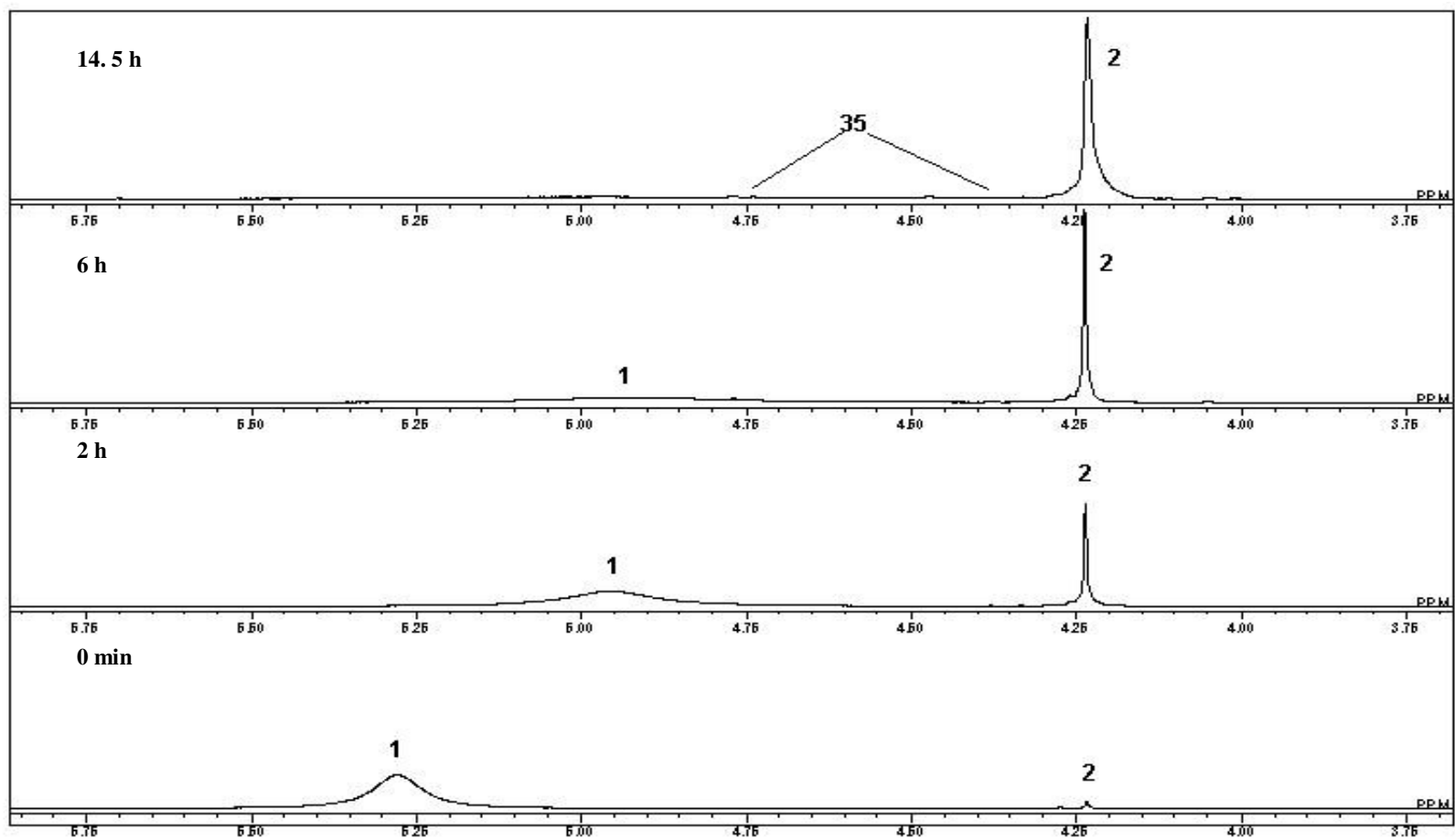
The reaction of $[\text{CpCr}(\text{CO})_2]_2$ (**2**) with $\text{P}(\text{C}_6\text{H}_4\text{SMe-}o)_3$ in refluxing toluene for 5 h gave unreacted **2** (36.3% recovery) and $[\text{Cp}_2\text{Cr}_2(\text{CO})\{(\mu\text{-C}_6\text{H}_4\text{SMe})_2(\text{C}_6\text{H}_4\text{SMe-}o)\text{P}\}]$ (**35**) (40.5% yield).

2.12.3 NMR Tube Reaction

The reaction of $[\text{CpCr}(\text{CO})_3]_2$ (**1**) with $\text{P}(\text{C}_6\text{H}_4\text{SMe-}o)_3$ at 80 °C in C_6D_6

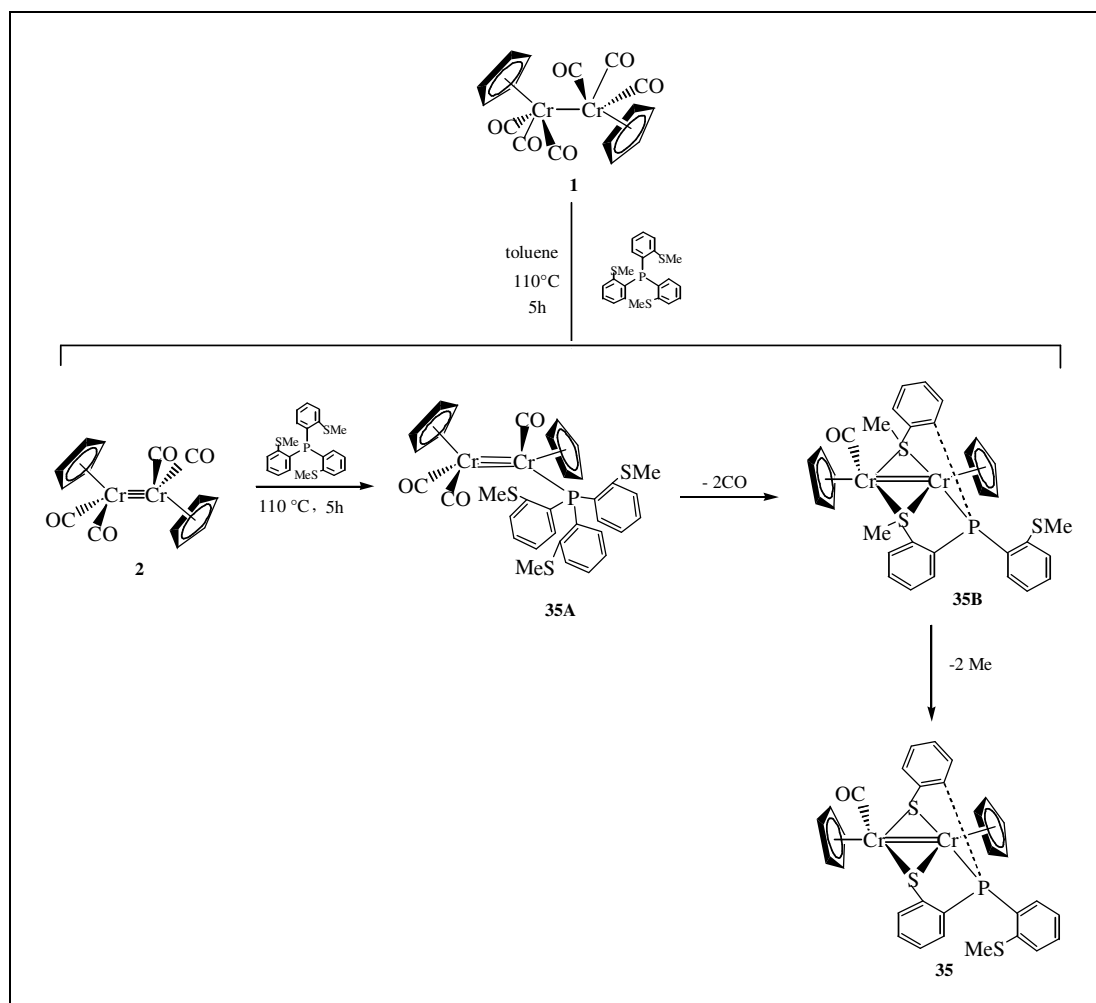
A time-dependent variation of product composition from the reaction of $[\text{CpCr}(\text{CO})_3]_2$ (**1**) with one mole equivalent of $\text{P}(\text{C}_6\text{H}_4\text{SMe-}o)_3$ at 80 °C was monitored *via* ^1H NMR spectra scans which are illustrated in Figure 41. The conversion of $[\text{CpCr}(\text{CO})_3]_2$ (**1**) to its thermolytic congener, **2**, took place after 1 to 6 h of reaction. After 14.5 h, the main product formed is **2** together with traces of $[\text{Cp}_2\text{Cr}_2(\text{CO})\{(\mu\text{-C}_6\text{H}_4\text{SMe})_2(\text{C}_6\text{H}_4\text{SMe-}o)\text{P}\}]$ (**35**). The above observation is represented in Scheme 34 which indicates that the synthetic pathway of complex **35** proceeds *via* the triply bonded Cr dimer.

Figure 41. Time-dependant ^1H NMR spectra of $[\text{CpCr}(\text{CO})_3]_2$ (**1**) with one mole equivalent of $\text{P}(\text{C}_6\text{H}_4\text{SMe-}o)_3$ at $80\text{ }^\circ\text{C}$



2.12.4 Mechanistic pathway: Formation of $[\text{Cp}_2\text{Cr}_2(\text{CO})\{\mu\text{-C}_6\text{H}_4\text{SMe}\}_2\text{-}(\text{C}_6\text{H}_4\text{SMe-}o)\text{P}\}]$ (**35**)

The reaction of $[\text{CpCr}(\text{CO})_3]_2$ (**1**) with tetradentate ligand of $\text{P}(\text{C}_6\text{H}_4\text{SMe-}o)_3$ at 110 °C is proposed to proceed *via* the $\text{Cr}\equiv\text{Cr}$ triply bonded complex **2**. This postulation is substantiated from the NMR tube reaction study of **1** with $\text{P}(\text{C}_6\text{H}_4\text{SMe-}o)_3$ at 110 °C which indicates that complete conversion of **1** to **2** occurred prior to the formation of product **35**. The electrophilic $\text{P}(\text{C}_6\text{H}_4\text{SMe-}o)_3$ attacks the electron rich $\text{Cr}\equiv\text{Cr}$ bond in **2** and substitutes one of the CO ligand to give an intermediate of **35A** (Scheme 34). The thiomethyl groups in the ligand will form two thiolate bridges between the two Cr atoms. Decarbonylation will happen in a concerted manner to give **35B**. Subsequent partial π -back donation from the metals into the S-C π^* orbitals will cause the homolytic S-C bond cleavage to give **35**.



Scheme 34. Synthetic pathway of $[\text{Cp}_2\text{Cr}_2(\text{CO})\{\mu\text{-C}_6\text{H}_4\text{SMe}\}_2(\text{C}_6\text{H}_4\text{SMe-}o)\text{P}\}]$ (**35**)

2.12.5 Physical properties

$[\text{Cp}_2\text{Cr}_2(\text{CO})\{\mu\text{-C}_6\text{H}_4\text{SMe}\}_2(\text{C}_6\text{H}_4\text{SMe-}o)\text{P}]$ (35)

$[\text{Cp}_2\text{Cr}_2(\text{CO})\{\mu\text{-C}_6\text{H}_4\text{SMe}\}_2(\text{C}_6\text{H}_4\text{SMe-}o)\text{P}]$ exists as dark orange pink crystalline solids. In the solid state, it is stable for a couple of hours at ambient temperature under an inert atmosphere and can be kept longer at $-28\text{ }^\circ\text{C}$. It is soluble in toluene to give an orange pink solution. The solution is stable at room temperature under inert atmosphere for a few hours.

2.12.6 Spectral characteristics

2.12.6.1 IR spectrum

$[\text{Cp}_2\text{Cr}_2(\text{CO})\{\mu\text{-C}_6\text{H}_4\text{SMe}\}_2(\text{C}_6\text{H}_4\text{SMe-}o)\text{P}]$ (35)

$[\text{Cp}_2\text{Cr}_2(\text{CO})\{\mu\text{-C}_6\text{H}_4\text{SMe}\}_2(\text{C}_6\text{H}_4\text{SMe-}o)\text{P}]$ exhibits ν_{CO} stretching frequencies at 1833 s cm^{-1} in nujol and other peaks at 1317m , 1276sh , 1253m , 1161m , 1100s , 1058sh , 1042vs , 1034sh , 966w , 948w , 918vw , 873vw , 807m , 748vs , 721m , 705m , 694w , 665vw , 638w cm^{-1} (refer to Appendix I).

2.12.6.2 NMR spectrum

$[\text{Cp}_2\text{Cr}_2(\text{CO})\{\mu\text{-C}_6\text{H}_4\text{SMe}\}_2(\text{C}_6\text{H}_4\text{SMe-}o)\text{P}]$ (35)

The complex **35** is an unsymmetrical dimeric product. Similar with **33**, two Cp signals were recorded in both of the ^1H and ^{13}C NMR spectra. In the ^1H NMR spectrum (benzene- d_6), the Cp signals were recorded at δ 4.74, 4.38, one $-\text{SCH}_3$ signal was recorded at δ 1.97 and the signals for $-\text{C}_6\text{H}_4$ were recorded as multiplets at δ 7.73-6.48. In the ^{13}C NMR spectrum (benzene- d_6), the Cp signals were recorded at δ 94.24, 93.77, the $-\text{SCH}_3$ signal was recorded at δ 17.29, the signals for $-\text{C}_6\text{H}_4$ were recorded at δ 146.69, 146.23, 145.60, 145.31, 144.10, 144.02, 138.61, 138.21, 137.52, 137.40, 134.46, 132.42, 132.08, 131.40, 130.55, 127.90, 127.86, 127.25, 127.19, 126.11, 126.02, 125.05, 124.67 and one

CO signal was recorded at δ 262.72. In the ^{31}P NMR spectrum, the phosphorus peak was recorded at δ 153.80 (refer to Appendix II).

2.12.6.3 Mass spectrum

$[\text{Cp}_2\text{Cr}_2(\text{CO})\{\mu\text{-C}_6\text{H}_4\text{SMe}_2(\text{C}_6\text{H}_4\text{SMe-}o)\text{P}\}]$ (**35**)

The mass spectrum of **35** shows the parent ion $m/z = 632$ $[\text{Cp}_2\text{Cr}_2(\text{CO})\{\mu\text{-C}_6\text{H}_4\text{SMe}_2(\text{C}_6\text{H}_4\text{SMe-}o)\text{P}\}]$ and its fragmentation ions as listed in Table 54.

Table 54. Electrospray ionization mass spectrum of $[\text{Cp}_2\text{Cr}_2(\text{CO})\{\mu\text{-C}_6\text{H}_4\text{SMe}_2(\text{C}_6\text{H}_4\text{SMe-}o)\text{P}\}]$ (**35**)

m/z	Assignments
632	$[\text{Cp}_2\text{Cr}_2(\text{CO})\{\mu\text{-C}_6\text{H}_4\text{SMe}_2(\text{C}_6\text{H}_4\text{SMe-}o)\text{P}\}]$
487	$\text{CpCr}\{\mu\text{-C}_6\text{H}_4\text{S}\}_2(\text{C}_6\text{H}_4\text{SMe-}o)\text{P}$

2.12.7 Molecular structure

$[\text{Cp}_2\text{Cr}_2(\text{CO})\{\mu\text{-C}_6\text{H}_4\text{SMe}_2(\text{C}_6\text{H}_4\text{SMe-}o)\text{P}\}]$ (**35**)

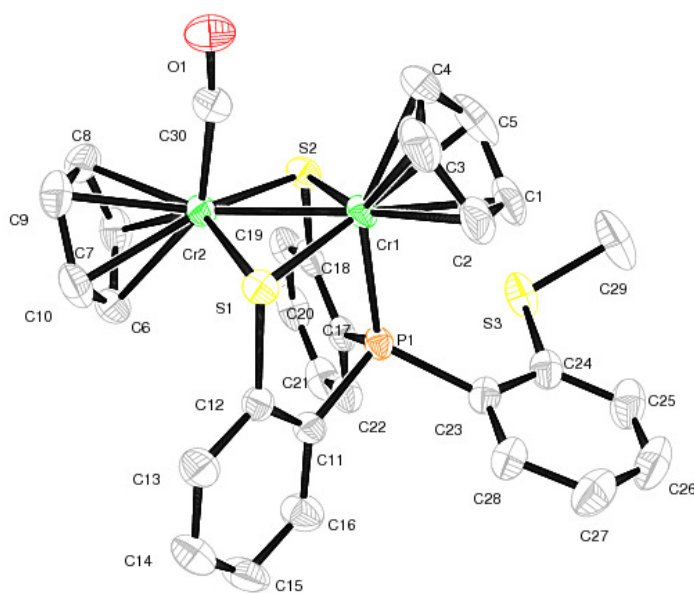


Figure 42. Molecular structure of $[\text{Cp}_2\text{Cr}_2(\text{CO})\{\mu\text{-C}_6\text{H}_4\text{SMe}_2(\text{C}_6\text{H}_4\text{SMe-}o)\text{P}\}]$ (**35**)

[Cp₂Cr₂(CO){(μ-C₆H₄SMe)₂(C₆H₄SMe-*o*)P}] (**35**) crystallizes in monoclinic, space group P2₁/c. In complex **35**, the Cr2-S2 fragment is nearly co-planar and the dihedral angle between Cr(1)-S(1)-Cr(2) and Cr(1)-S(2)-Cr(2) is 163.22° (Figure 42). The Cr(1)-Cr(2) separation of 2.470(6) Å is shorter than the single bond found in the related dinuclear complex **33**. Both Cr1 and Cr2 atoms are in a tetragonal pyramidal coordination environment, with the Cp groups occupying the axial position but Cr1 maintains a distortion due to steric repulsion of the thiolaryl group leading to the axial displacement of the Cp group. In addition, the effect also increases the bond angles of C(23)-P(1)-Cr1 by 10° as compared to C(11)-P(1)-Cr(1) and C(17)-P(1)-Cr(1). **35** exhibits a single tridentate phosphinothiolate ligand bridging through two thiolate donor groups across the two metal atoms. The selected bond lengths (Å) and bond angles (°) for **35** are shown in Table 55.

Table 55. Bond lengths [Å] and angles [°] for [Cp₂Cr₂(CO){(μ-C₆H₄SMe)₂(C₆H₄SMe-*o*)P}] (**35**)

Bond lengths			
Cr(1)-Cr(2)	2.470(6)	S(1)-C(12)	1.793(3)
Cr(1)-P(1)	2.287(8)	S(2)-C(18)	1.797(3)
Cr(1)-S(1)	2.274(8)	S(3)-C(24)	1.779(3)
Cr(1)-S(2)	2.282(9)	S(3)-C(29)	1.801(4)
Cr(2)-C(30)	1.823(3)	P(1)-C(17)	1.825(3)
Cr(2)-S(1)	2.291(8)	P(1)-C(11)	1.831(3)
Cr(2)-S(2)	2.303(8)	P(1)-C(23)	1.837(3)
		O(1)-C(30)	1.168(4)
Bond angles			
S(1)-Cr(1)-S(2)	113.49(3)	Cr(1)-S(1)-Cr(2)	65.51(3)
P(1)-Cr(1)-S(1)	84.79(3)	Cr(1)-S(2)-Cr(2)	65.20(3)
P(1)-Cr(1)-S(2)	84.53(3)	C(24)-S(3)-C(29)	101.99(19)
S(1)-Cr(2)-S(2)	112.04(3)	C(17)-P(1)-C(11)	104.97(13)
S(1)-Cr(1)-Cr(2)	57.59(2)	C(17)-P(1)-C(23)	106.56(14)
S(2)-Cr(1)-Cr(2)	57.81(2)	C(11)-P(1)-C(23)	102.65(14)
P(1)-Cr(1)-Cr(2)	93.20(3)	C(17)-P(1)-Cr(1)	110.69(10)
C(30)-Cr(2)-Cr(1)	78.65(10)	C(11)-P(1)-Cr(1)	110.00(10)
S(1)-Cr(2)-Cr(1)	56.90(2)	C(23)-P(1)-Cr(1)	120.67(10)
S(2)-Cr(2)-Cr(1)	56.99(2)	O(1)-C(30)-Cr(2)	172.8(3)

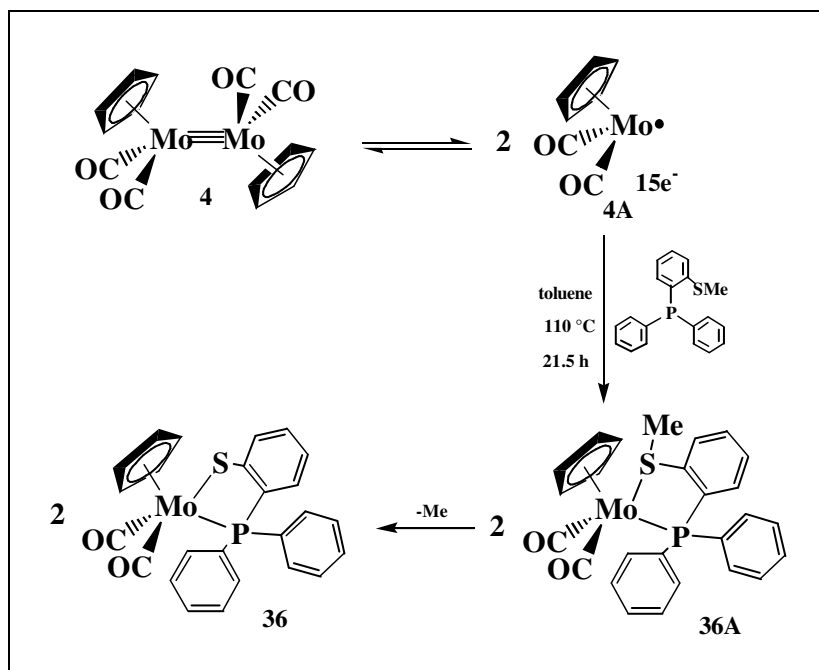
2.13 Studies of $[\text{CpMo}(\text{CO})_2]_2$ (**4**) with $\text{PPh}_2(\text{C}_6\text{H}_4\text{SMe-}o)$

2.13.1 The reaction of $[\text{CpMo}(\text{CO})_2]_2$ (**4**) with $\text{PPh}_2(\text{C}_6\text{H}_4\text{SMe-}o)$

A reddish brown solution of $[\text{CpMo}(\text{CO})_2]_2$ (**4**) underwent reaction with one mole equivalent of $\text{PPh}_2(\text{C}_6\text{H}_4\text{SMe-}o)$ at 110 °C after 21.5 h. Column chromatography of the yellowish brown reaction mixture had led to the isolation of a monomeric complex of $\text{CpMo}(\text{CO})_2\{o\text{-(C}_6\text{H}_4\text{S)PPh}_2\}$ (**36**) (42.5%) as orange red crystals together with unreacted $[\text{CpMo}(\text{CO})_2]_2$ (47.7%).

2.13.2 Mechanistic pathways: Formation of $\text{CpMo}(\text{CO})_2\{o\text{-(C}_6\text{H}_4\text{S)PPh}_2\}$ (**36**)

The reaction of $[\text{CpMo}(\text{CO})_2]_2$ (**4**) with $\text{PPh}_2(\text{C}_6\text{H}_4\text{SMe-}o)$ at 110 °C is initiated with the attack of the lone pair electrons in $\text{PPh}_2(\text{C}_6\text{H}_4\text{SMe-}o)$ by a 15e^- radical species generated from **4** to form **36A** as an intermediate. Similar with its Cr analogue, partial π -back donation from Mo to S will weaken the S-C bond. A concomitant demethylation process occurs to give a Mo-P-S ring complex of $\text{CpMo}(\text{CO})_2\{o\text{-(C}_6\text{H}_4\text{S)PPh}_2\}$. The synthetic pathway for complex **36** is shown in Scheme 35.



Scheme 35. Synthetic pathways for $\text{CpMo}(\text{CO})_2\{o\text{-(C}_6\text{H}_4\text{S)PPh}_2\}$ (**36**)

2.13.3 Physical Properties

CpMo(CO)₂{*o*-(C₆H₄S)PPh₂} (36)

CpMo(CO)₂{*o*-(C₆H₄S)PPh₂} exists as an orange red crystalline solid. It is fairly soluble in toluene and very soluble in ether, THF and CH₂Cl₂ to give an orange red solution. In the solid state, it is stable at room temperature under an inert atmosphere. In solution, it is stable at ambient temperature for a few days under an inert atmosphere.

2.13.4 Spectral Characteristics

2.13.4.1 IR spectrum

CpMo(CO)₂{*o*-(C₆H₄S)PPh₂} (36)

The I.R. spectrum of **36** shows ν_{CO} stretching frequencies at 1944vs, 1873vs, 1841sh cm⁻¹ in nujol and other peaks at 1159w, 1092m, 1044m, 1025m, 814m, 734w, 720w, 703m, 693m, 553m, 528m, 520m, 501w, 469w, 458w, 387w cm⁻¹ (refer to Appendix I).

2.13.4.2 NMR spectrum

CpMo(CO)₂{*o*-(C₆H₄S)PPh₂} (36)

In the ¹H NMR spectrum (benzene-*d*₆), **36** shows a sharp singlet at δ 4.59 which indicates a Cp signal. The disappearance of the methyl signal compared to the ligand confirms that demethylation has taken place to enable the sulfur to bond to the molybdenum. The phenyl protons were recorded as multiplets at δ 7.80-7.78, 7.69-7.65, 7.61-7.56, 7.28-7.25, 7.02-7.01, 6.98-6.94, 6.89-6.87, 6.78-6.75 and 6.66-6.63. In the ¹³C NMR spectrum (benzene-*d*₆), only one Cp signal was recorded at δ 95.21 which agrees with the observation in the ¹H NMR. The phenyl carbons were recorded at δ 133.22, 133.10, 132.14, 132.06, 131.04, 131.01, 130.83, 130.71, 130.33, 130.31, 130.15, 129.25, 129.14, 129.07, 128.97, 122.11 and 122.05. In the ³¹P NMR spectrum, there was only one sharp peak recorded at δ 90.88 (refer to Appendix II). The results obtained from these NMR spectra are consistent with the molecular structure of **36**.

2.13.4.3 Mass spectrum

CpMo(CO)₂{*o*-(C₆H₄S)PPh₂} (**36**)

The mass spectrum of **36** shows the parent ion $m/z = 510.9933$ CpMo(CO)₂{*o*-(C₆H₄S)PPh₂} and its fragmentation ions as listed in Table 56.

Table 56. Electrospray ionization mass spectrum of CpMo(CO)₂{*o*-(C₆H₄S)PPh₂} (**36**)

m/z	Assignments
512	CpMo(CO) ₂ { <i>o</i> -(C ₆ H ₄ S)PPh ₂ }
483	CpMo(CO){ <i>o</i> -(C ₆ H ₄ S)PPh ₂ }
457	CpMo{ <i>o</i> -(C ₆ H ₄ S)PPh ₂ }

2.13.5 Molecular structure

CpMo(CO)₂{*o*-(C₆H₄S)PPh₂} (**36**)

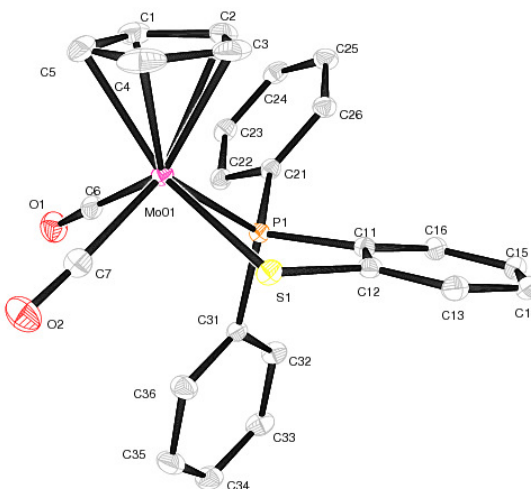


Figure 43. Molecular structure of CpMo(CO)₂{*o*-(C₆H₄S)PPh₂} (**36**)

The molecular structure of **36** is shown in Figure 43. The selected bond lengths (Å) and bond angles (°) of **36** are shown in Table 57. **36** is isostructural with its Cr analogue, CpCr(CO)₂{*o*-(C₆H₄S)PPh₂} (**31**) and both of them crystallize in monoclinic, space group P2₁/n. **36** possesses a four-legged piano-stool configuration at Mo with a Cp ring occupying at the apical position. The phosphine ligand is bonded to the Mo atom through

atom P1 and S1 where it forms a five-membered Mo-P-C-C-S chelate ring. Atom P1, S1, C6 and C7 form a pseudo-square planar plane perpendicular to the CpMo fragment. The Mo-P bond distance of 2.444(6) Å is slightly shorter than that found in Mo(CO)₄{(C₆H₄SMe)PPh₂} (2.498(14) Å) [116]. The Mo-S bond distance in **36**, 2.512(8) Å is longer than a similar bond found in Mo(CO)₄{(C₆H₄SMe)PPh₂} (2.394(2) Å).

Table 57. Bond lengths [Å] and angles [°] for CpMo(CO)₂{*o*-(C₆H₄S)PPh₂} (**36**)

Bond lengths			
Mo(01)-C(6)	1.964(18)	C(7)-O(2)	1.151(2)
Mo(01)-C(7)	1.968(18)	P(1)-C(11)	1.811(17)
Mo(01)-P(1)	2.444(6)	P(1)-C(21)	1.822(16)
Mo(01)-S(1)	2.512(8)	P(1)-C(31)	1.829(16)
C(6)-O(1)	1.149(2)	S(1)-C(12)	1.767(17)
Bond angles			
C(6)-Mo(01)-P(1)	75.92(5)	C(11)-P(1)-C(21)	106.36(7)
C(7)-Mo(01)-P(1)	114.40(5)	C(11)-P(1)-C(31)	102.56(7)
C(6)-Mo(01)-S(1)	128.50(6)	C(21)-P(1)-C(31)	104.15(7)
C(7)-Mo(01)-S(1)	78.93(5)	C(11)-P(1)-Mo(01)	109.76(5)
P(1)-Mo(01)-S(1)	74.85(18)	C(21)-P(1)-Mo(01)	114.35(6)
O(1)-C(6)-Mo(01)	178.54(16)	C(31)-P(1)-Mo(01)	118.43(5)
O(2)-C(7)-Mo(01)	176.77(17)	C(12)-S(1)-Mo(01)	106.94(5)

2.14 Studies of $[\text{CpMo}(\text{CO})_2]_2$ (**4**) with $\text{PPh}(\text{C}_6\text{H}_4\text{SMe-}o)_2$

2.14.1 The reaction of $[\text{CpMo}(\text{CO})_2]_2$ (**4**) with an equimolar amount of $\text{PPh}(\text{C}_6\text{H}_4\text{SMe-}o)_2$

A reddish brown solution of $[\text{CpMo}(\text{CO})_2]_2$ underwent reaction with one mole equivalent of $\text{PPh}(\text{C}_6\text{H}_4\text{SMe-}o)_2$ in toluene at 110 °C for 14 h to give an orange brown reaction mixture. Isolation *via* chromatography using a florisil column gave $\text{CpMo}(\text{CO})_3\text{H}$ (**37**) (35.7% yield) [119], $[\text{Cp}_2\text{Mo}_2(\text{CO})\{\mu\text{-C}_6\text{H}_4\text{S}\}_2\text{PPh}]$ (**38**) (24.5% yield) and $\text{CpMo}(\text{CO})\{\mu\text{-C}_6\text{H}_4\text{S}\}(\mu\text{-C}_6\text{H}_4\text{SMe})\text{PPh}$ (**39**) (14.3% yield).

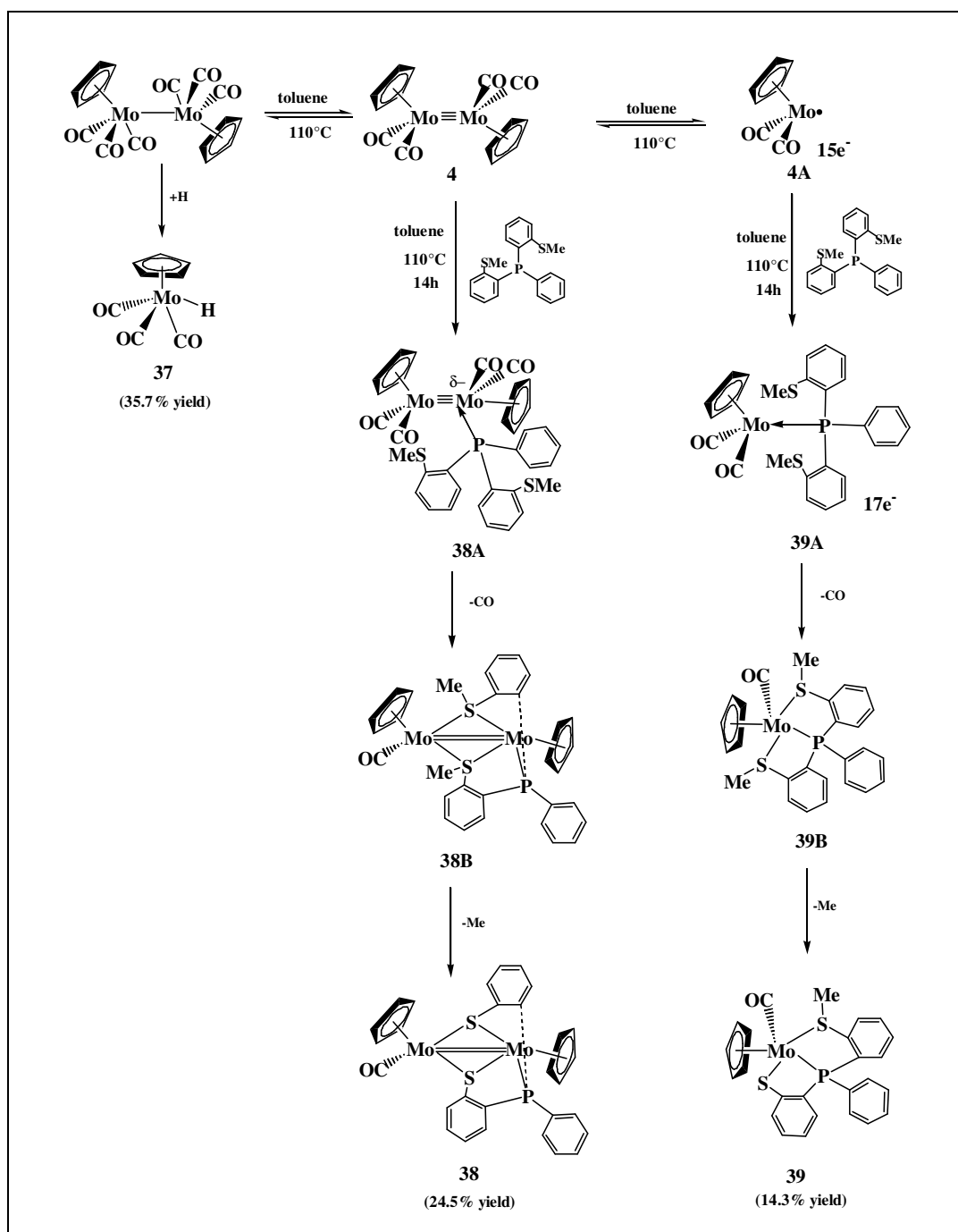
A NMR tube thermolytic study of **39** in C_6D_6 at 110 °C for 14 h indicates that complex **39** decomposed slowly to an uncharacterized product.

2.14.2 Mechanistic pathways: Formation of $\text{CpMo}(\text{CO})_3\text{H}$ (**37**), $[\text{Cp}_2\text{Mo}_2(\text{CO})\{\mu\text{-C}_6\text{H}_4\text{S}\}_2\text{PPh}]$ (**38**) and $\text{CpMo}(\text{CO})\{\mu\text{-C}_6\text{H}_4\text{S}\}(\mu\text{-C}_6\text{H}_4\text{SMe})\text{PPh}$ (**39**)

The formation of the Cr analogue of hydride **37** has been observed in previous reactions of **1** with a number of substrates [54a-b, 55c, 56a]. The source of the hydridic H has been ruled out by experimental evidence. According to Goh *et al.*, it is probable that the source is coordinated Cp [56a], which agrees with their observation of low-intensity unassignable peaks between δ 4.17 and 5.37, compared to several unassignable peaks at δ 5.25, 5.12, 4.84 and 4.68 which were observed in the crude product solution.

The initiation step for the formation of **38** was proposed to proceed *via* an oxidation addition mechanism where the tridentate phosphine readily donates its lone pair electrons to the triply bonded $\text{Mo}\equiv\text{Mo}$ to form Mo-P bond as illustrated in **38A** in Scheme 36. The electron rich phosphine bonded to the Mo atom can π -back donate from the Mo atom to the CO groups. Hence, **38A** undergoes decarbonylation and the $-\text{SMe}$ groups at the *ortho* position will form thiolate-bridges between the two Mo in a concerted manner to give an intermediate, **38B**. Partial π -back donation from the Mo atoms to the $-\text{SMe}$ groups results in demethylation at both sulfur atoms to give **38**.

Similar with $\text{CpMo(CO)}_2\{o\text{-(C}_6\text{H}_4\text{S)PPh}_2\}$ (**36**), it is proposed that the formation of the monomeric complex of $\text{CpMo(CO)}\{(\mu\text{-C}_6\text{H}_4\text{S})(\mu\text{-C}_6\text{H}_4\text{SMe)PPh}\}$ (**39**) proceeds with the attack of the lone pair electrons in $\text{PPh}_2(\text{C}_6\text{H}_4\text{SMe-}o)$ by a $15 e^-$ radical species, **4A**, generated from **4** to form **39A** as an intermediate. To conform with the $18e^-$ rule, **39A** with the $-\text{SMe}$ groups at the *ortho* position will form bonds with the Mo atom and together with concomitant elimination of one CO group to give an intermediate, **39B**. Further partial π -back donation from the Mo atom to the $-\text{SMe}$ groups will caused demethylation to occur on one of the sulfur atoms and to give **39**.



Scheme 36. Synthetic pathways for CpMo(CO)₃H (**37**), [Cp₂Mo₂(CO){(μ-C₆H₄S)₂PPh}] (**38**) and CpMo(CO){(μ-C₆H₄S)(μ-C₆H₄SMe)PPh} (**39**)

2.14.3 Physical properties

CpMo(CO)₃H (37)

CpMo(CO)₃H exists as a yellowish brown crystalline solid which is soluble in *n*-hexane: toluene mixture to give a greenish yellow solution. In the solid state, it is stable at ambient temperature under an inert atmosphere. The solution is stable at ambient temperature for a few days under an inert atmosphere.

[Cp₂Mo₂(CO){(μ-C₆H₄S)₂PPh}] (38)

[Cp₂Mo₂(CO){(μ-C₆H₄S)₂PPh}] exists as a dark brown crystalline solid which is soluble in toluene to give a dark brown solution. In the solid state, it is stable at ambient temperature under an inert atmosphere. The solution is stable at ambient temperature for a few days under an inert atmosphere.

CpMo(CO){(μ-C₆H₄S)(μ-C₆H₄SMe)PPh} (39)

CpMo(CO){(μ-C₆H₄S)(μ-C₆H₄SMe)PPh} exists as a crystalline brownish orange solid which is soluble in toluene: ether mixture. In solid state, it is stable at ambient temperature under an inert atmosphere. The solution is stable at ambient temperature for a few days under an inert atmosphere.

2.14.4 Spectral characteristics

2.14.4.1 IR spectrum

[Cp₂Mo₂(CO){(μ-C₆H₄S)₂PPh}] (38)

[Cp₂Mo₂(CO){(μ-C₆H₄S)₂PPh}] showed the ν_{CO} stretching frequency at 1814 vs cm^{-1} in nujol and other peaks at 1251w, 1091m, 793m, 768m, 741w, 729w, 696w, 537w, 531w, 501vw cm^{-1} (refer to Appendix I).

2.14.5.2 NMR spectra

CpMo(CO)₃H (37)

The spectral data for **37** were found to match closely to those of a synthesised authentic sample of CpMo(CO)₃H, viz ¹H NMR (benzene-*d*₆): δ 4.45 (s, Cp), δ 0.39 (Mo-H). ¹³C NMR (benzene-*d*₆): δ 92.77 (Cp), δ -21.64 (Mo-H) [119].

[Cp₂Mo₂(CO){(μ-C₆H₄S)₂PPh}] (38)

Complex **38** is an unsymmetrical dimeric complex and two Cp peaks were observed in both of their ¹H and ¹³C NMR spectra. In the ¹H NMR spectrum (benzene-*d*₆), the Cp peaks were recorded at δ 4.57 and 4.55 and the aromatic protons of -C₆H₅ and -C₆H₄ were recorded as a multiplet at δ 7.85 - 7.01. In the ¹³C NMR spectrum (benzene-*d*₆), the Cp peaks were recorded at δ 92.93, 89.99 and the aromatic carbons of -C₆H₅ and -C₆H₄ were recorded at δ 129.67, 128.90, 126.03. In the ³¹P NMR spectrum, the phosphorus peak was recorded at δ 125.96 (refer to Appendix II).

CpMo(CO){(μ-C₆H₄S)(μ-C₆H₄SMe)PPh} (39)

Complex **39** is a monomeric complex, consistent with the observation of only one Cp peak in both their ¹H and ¹³C NMR spectra. In the ¹H NMR spectrum (benzene-*d*₆), the Cp peak was recorded at δ 4.51, the -CH₃ peak was recorded at δ 2.36 and aromatic proton of -C₆H₅ and -C₆H₄ were recorded as a multiplet at δ 8.11 - 6.80. In the ¹³C NMR spectrum (benzene-*d*₆), the Cp peak was recorded at δ 92.05, the -CH₃ peak was recorded at δ 15.92 and aromatic carbons of -C₆H₅ and -C₆H₄ were recorded at δ 132.43 - 126.03 and a CO peak at δ 247.13. In the ³¹P NMR spectrum, the phosphorus peak was recorded at δ 82.18 (refer to Appendix II).

2.14.5.3 Mass spectra

[Cp₂Mo₂(CO){(μ-C₆H₄S)₂PPh}] (38)

The mass spectrum of **38** shows the parent ion $m/z = 677.4500$ [Cp₂Mo₂(CO){(μ-C₆H₄S)₂PPh}] and its fragmentation ions as listed in Table 58.

Table 58. Electrospray ionization mass spectrum of [Cp₂Mo₂(CO){(μ-C₆H₄S)₂PPh}] (**38**)

m/z	Assignments
678	[Cp ₂ Mo ₂ (CO){(μ-C ₆ H ₄ S) ₂ PPh}]
573	Cp ₂ Mo ₂ {(μ-C ₆ H ₄ S) ₂ P-}
487	CpMo(C ₆ H ₄ S) ₂ PPh

CpMo(CO){(μ-C₆H₄S)(μ-C₆H₄SMe)PPh} (39)

The mass spectrum of **39** shows the parent ion $m/z = 530.0001$ CpMo(CO){(μ-C₆H₄S)(μ-C₆H₄SMe)PPh} and its fragmentation ions as listed in Table 59.

Table 59. Electrospray ionization mass spectrum of CpMo(CO){(μ-C₆H₄S)(μ-C₆H₄SMe)PPh} (**39**)

m/z	Assignments
530	CpMo(CO){(μ-C ₆ H ₄ S)(μ-C ₆ H ₄ SMe)PPh}
515	CpMo(CO){(μ-C ₆ H ₄ S) ₂ PPh}
502	CpMo{(μ-C ₆ H ₄ S)(μ-C ₆ H ₄ SMe)PPh}
487	CpMo{(μ-C ₆ H ₄ S) ₂ PPh}
435	Mo{(μ-C ₆ H ₄ S)(μ-C ₆ H ₄ SMe)PPh}
422	Mo{(μ-C ₆ H ₄ S) ₂ PPh}

2.14.5 Molecular structures

[Cp₂Mo₂(CO){(μ-C₆H₄S)₂PPh}] (38)

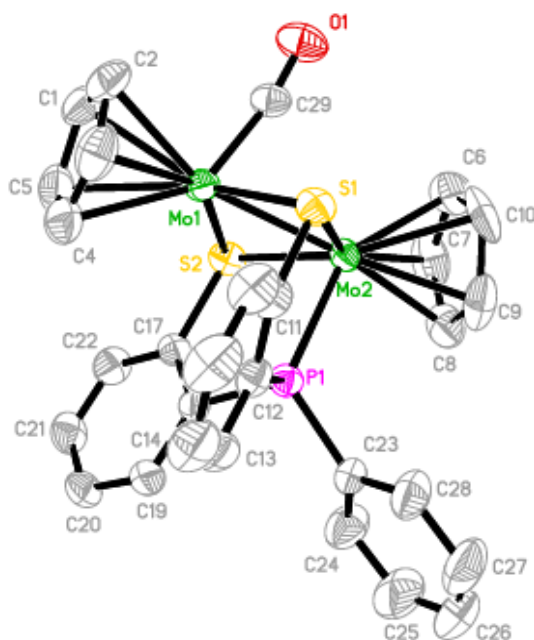


Figure 44. Molecular structure of [Cp₂Mo₂(CO){(μ-C₆H₄S)₂PPh}] (38)

The molecular structure of **38** is shown in Figure 44. The selected bond lengths (Å) and bond angles (°) for [Cp₂Mo₂(CO){(μ-C₆H₄S)₂PPh}] are shown in Table 60. **38** crystallizes in monoclinic, space group P2₁/n and is isostructural with its Cr analogue of [Cp₂Cr₂(CO){(μ-C₆H₄S)₂PPh}] (**32**). The Mo2-S2 plane is nearly co-planar with the dihedral angle between the Mo(1)-S(1)-Mo(2) plane and Mo(1)-S(2)-Mo(2) plane being 167.4° which is similar to the dihedral angle [Cr(1)-S(1)-Cr(2)-S(2), 167.4°] found in [Cp₂Cr₂(CO){(μ-SPh)₂PPh}] (**32**). Both the Mo atoms are in a tetragonal pyramidal coordination environment with the Cp groups occupying the axial position but the Cp group attached to Mo(2) maintains a distortion due to steric repulsion of the thioaryl group leading to the axial displacement of the Cp group. The bond distance of Mo(1)-Mo(2) is 2.598(4) Å which indicates it as a double bond is comparable to the Mo=Mo bond in [CpMo(SBz)S]₂ (**10a & b**) (average 2.58 (6) Å).

Table 60. Bond lengths [\AA] and angles [$^\circ$] for $[\text{Cp}_2\text{Mo}_2(\text{CO})\{(\mu\text{-C}_6\text{H}_4\text{S})_2\text{PPh}\}]$ (**38**)

Bond lengths

Mo(1)-C(29)	1.912(4)	P(1)-C(12)	1.832(3)
Mo(1)-S(1)	2.405(10)	P(1)-C(18)	1.831(3)
Mo(1)-S(2)	2.418(9)	P(1)-C(23)	1.834(4)
Mo(1)-Mo(2)	2.598(4)	S(1)-C(11)	1.795(4)
Mo(2)-P(1)	2.354(9)	S(2)-C(17)	1.797(3)
Mo(2)-S(1)	2.397(9)	O(1)-C(29)	1.171(4)
Mo(2)-S(2)	2.408(9)		

Bond angles

C(29)-Mo(1)-S(1)	87.28(11)	S(1)-Mo(2)-S(2)	113.72(3)
C(29)-Mo(1)-S(2)	87.52(11)	P(1)-Mo(2)-Mo(1)	86.58(2)
S(1)-Mo(1)-S(2)	113.07(3)	S(1)-Mo(2)-Mo(1)	57.39(2)
C(29)-Mo(1)-Mo(2)	74.78(11)	S(2)-Mo(2)-Mo(1)	57.61(2)
S(1)-Mo(1)-Mo(2)	57.10(2)	Mo(2)-S(1)-Mo(1)	65.51(3)
S(2)-Mo(1)-Mo(2)	57.23(2)	Mo(2)-S(2)-Mo(1)	65.16(2)
P(1)-Mo(2)-S(1)	82.49(3)	O(1)-C(29)-Mo(1)	170.2(3)
P(1)-Mo(2)-S(2)	82.27(3)		

Symmetry transformations used to generate equivalent atoms:

$\text{CpMo}(\text{CO})\{(\mu\text{-C}_6\text{H}_4\text{S})(\mu\text{-C}_6\text{H}_4\text{SMe})\text{PPh}\}$ (**39**)

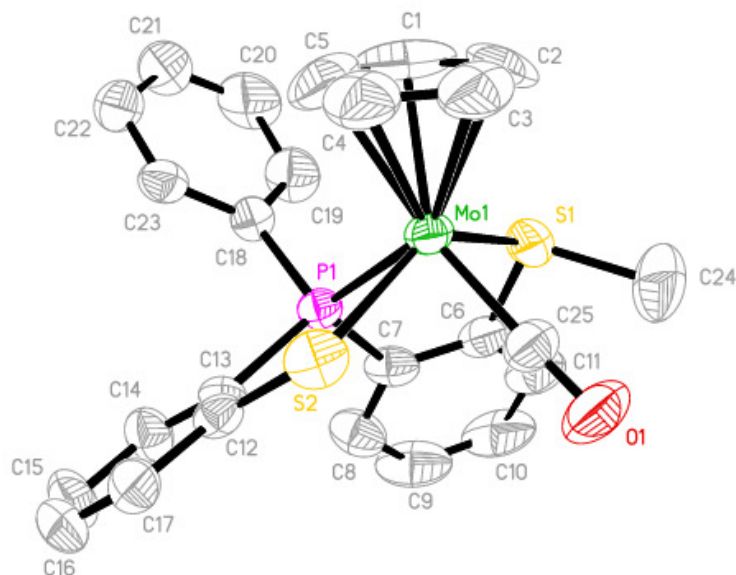


Figure 45. Molecular structure of $\text{CpMo}(\text{CO})\{(\mu\text{-C}_6\text{H}_4\text{S})(\mu\text{-C}_6\text{H}_4\text{SMe})\text{PPh}\}$ (**39**)

The molecular structure of **39** is shown in Figure 45. The selected bond lengths (Å) and bond angles (°) for CpMo(CO){(μ-C₆H₄S)(μ-C₆H₄SMe)PPh} are shown in Table 61. CpMo(CO){(μ-C₆H₄S)(μ-C₆H₄SMe)PPh} (**39**) crystallizes in monoclinic, space group Cc with two independent molecules found in its asymmetric unit. **39** is a tridentate chelate complex with two S atoms and one P atom coordinated to the metal center. Similar to the molecular structure of Ga^tBu{PPh(2-SPh)₂-κ³S,S',P} [118], the PS₂²⁻ ligand in **39**, is coordinated in a pincer-like manner. The P(1)-Mo(1)-S(1) (76.63(6)°), P(1)-Mo(1)-S(2) (78.99(5)°) and C(25)-Mo(1)-S(2) (75.5(2)°) bond angles indicates that **39** is in a tetrahedral coordination with the Cp ring coordinated at the apical position of Mo.

Table 61. Bond lengths [Å] and angles [°] for CpMo(CO){(μ-C₆H₄S)(μ-C₆H₄SMe)PPh}(**39**)

Bond lengths

Mo(1)-C(25)	1.946(7)	S(2)-C(12)	1.756(6)
Mo(1)-P(1)	2.380(16)	P(1)-C(13)	1.809(6)
Mo(1)-S(1)	2.453(18)	P(1)-C(18)	1.808(6)
Mo(1)-S(2)	2.487(18)	P(1)-C(7)	1.832(7)
S(1)-C(6)	1.798(7)	O(1)-C(25)	1.159(8)
S(1)-C(24)	1.818(8)		

Bond angles

C(25)-Mo(1)-P(1)	106.9(2)	C(24)-S(1)-Mo(1)	114.4(3)
P(1)-Mo(1)-S(1)	76.63(6)	C(12)-S(2)-Mo(1)	109.38(18)
C(25)-Mo(1)-S(2)	75.5(2)	C(7)-P(1)-Mo(1)	111.3(2)
P(1)-Mo(1)-S(2)	78.99(5)	C(13)-P(1)-Mo(1)	114.32(19)
S(1)-Mo(1)-S(2)	139.35(6)	C(18)-P(1)-Mo(1)	112.88(19)
C(6)-S(1)-C(24)	100.9(4)	O(1)-C(25)-Mo(1)	176.7(6)
C(6)-S(1)-Mo(1)	109.7(2)		

2.15 Studies of $[\text{CpMo}(\text{CO})_2]_2$ (**4**) with $\text{P}(\text{C}_6\text{H}_4\text{SMe-}o)_3$

2.15.1 The reaction of $[\text{CpMo}(\text{CO})_2]_2$ (**4**) with one mole equivalent of $\text{P}(\text{C}_6\text{H}_4\text{SMe-}o)_3$

A reddish brown solution of $[\text{CpMo}(\text{CO})_2]_2$ (**4**) with $\text{P}(\text{C}_6\text{H}_4\text{SMe-}o)_3$ in toluene was refluxed overnight. Column chromatography of the resultant dark reddish brown reaction mixture led to the isolation of unreacted $\text{Cp}_2\text{Mo}_2(\text{CO})_4$ (**4**) (28.2% recovery), $[\text{Cp}_2\text{Mo}_2(\text{CO})\{(\mu\text{-C}_6\text{H}_4\text{S})_2(\text{C}_6\text{H}_4\text{SCH}_2)\text{P}\}]$ (**40**) (19.1% yield) as dark brown crystalline solids, $[\text{Cp}_2\text{Mo}_2(\text{CO})\{(\mu\text{-C}_6\text{H}_4\text{S})_2(\text{C}_6\text{H}_4\text{SMe-}o)\text{P}\}]$ (**41**) (26.5% yield) as dark brown crystalline solids, $\text{Mo}(\text{CO})_3\{\text{P}(\text{C}_6\text{H}_4\text{SMe-}o)_3\}$ (**42**) (15.8% yield) as bright yellow crystalline solids and $\text{CpMo}_2(\text{CO})_3(\mu\text{-S})\{(\mu\text{-C}_6\text{H}_4\text{S})_2(\text{C}_6\text{H}_4\text{SMe-}o)\text{P}\}$ (**43**) (6.3% yield) as orange crystalline solids.

2.15.2 NMR Tube Reactions

(a) Thermolysis of $[\text{Cp}_2\text{Mo}_2(\text{CO})\{(\mu\text{-C}_6\text{H}_4\text{S})_2(\text{C}_6\text{H}_4\text{SMe-}o)\text{P}\}]$ (**41**)

A dark reddish brown solution of $[\text{Cp}_2\text{Mo}_2(\text{CO})\{(\mu\text{-C}_6\text{H}_4\text{S})_2(\text{C}_6\text{H}_4\text{SMe-}o)\text{P}\}]$ (**41**) in $\text{C}_6\text{D}_5\text{CD}_3$ (~0.5 mL) in a 5mm septum capped NMR tube was thermolyzed at 110 °C. The reaction was monitored by ^1H NMR at periodic intervals. **41** was slowly decomposed in the solution but no formation of new product was observed even after prolonged thermolysis for 64 h.

(b) Thermolysis of $\text{Mo}(\text{CO})_3\{\text{P}(\text{C}_6\text{H}_4\text{SMe-}o)_3\}$ (**42**)

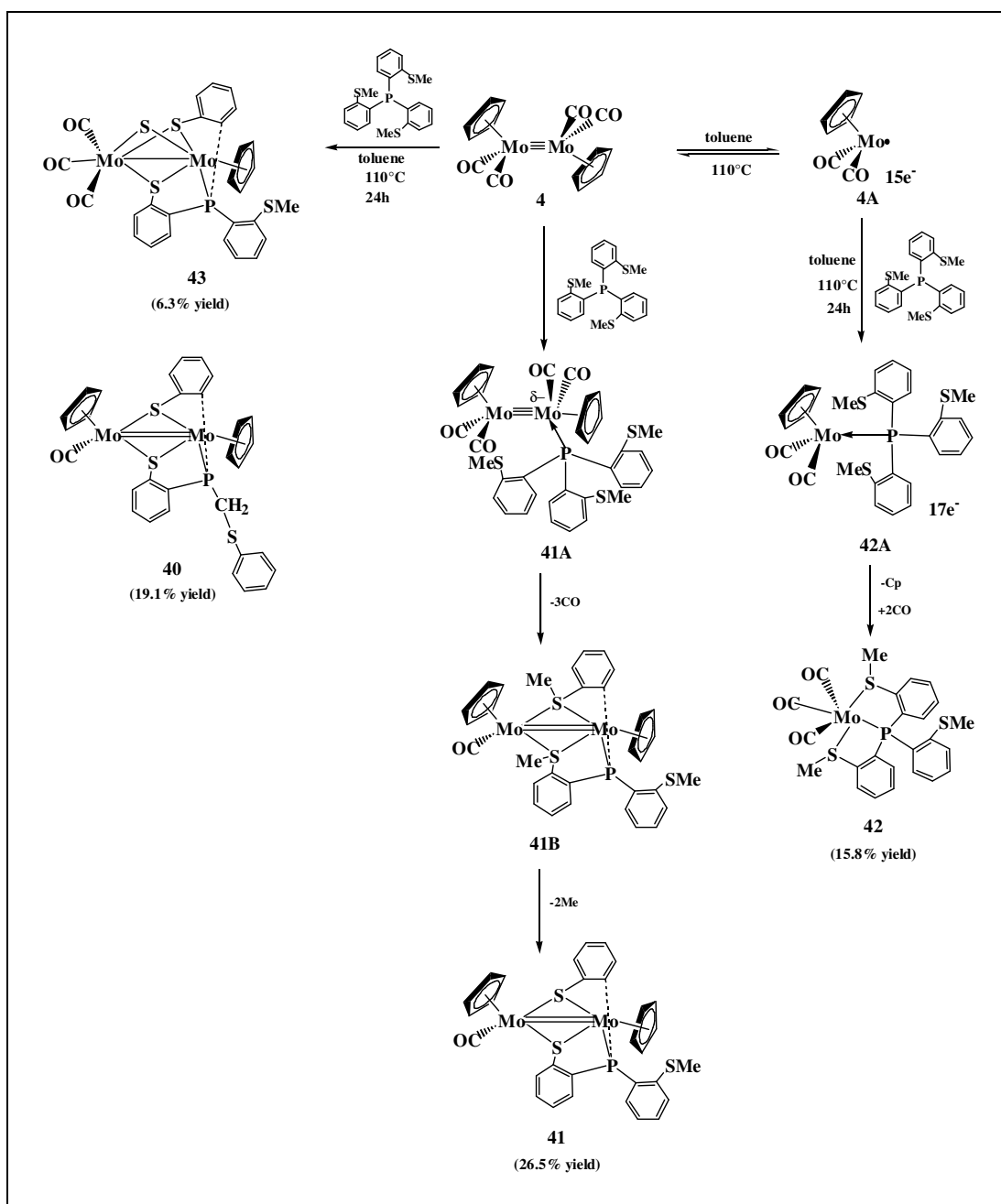
A brownish yellow solution of $\text{Mo}(\text{CO})_3\{\text{P}(\text{C}_6\text{H}_4\text{SMe-}o)_3\}$ (**42**) in $\text{C}_6\text{D}_5\text{CD}_3$ (~0.5 mL) in a 5mm septum capped NMR tube was thermolyzed at 110 °C for 20 h. The reaction was monitored by ^1H NMR at periodic intervals. **42** was slowly decomposed in solution and gave rise to a peak at δ 1.99 which could be due to the organic residue breakup from the metal carbonyl.

2.15.3 Mechanistic pathways : Formation of $[\text{Cp}_2\text{Mo}_2(\text{CO})\{\mu\text{-C}_6\text{H}_4\text{S}\}_2(\text{C}_6\text{H}_4\text{SCH}_2)\text{P}]$ (40), $[\text{Cp}_2\text{Mo}_2(\text{CO})\{\mu\text{-C}_6\text{H}_4\text{S}\}_2(\text{C}_6\text{H}_4\text{SMe-}o)\text{P}]$ (41), $\text{Mo}(\text{CO})_3\{\text{P}(\text{C}_6\text{H}_4\text{SMe-}o)_3\}$ (42) and $\text{CpMo}_2(\text{CO})_3(\mu\text{-S})\{\mu\text{-C}_6\text{H}_4\text{S}\}_2(\text{C}_6\text{H}_4\text{SMe-}o)\text{P}$ (43)

$[\text{Cp}_2\text{Mo}_2(\text{CO})\{\mu\text{-C}_6\text{H}_4\text{S}\}_2(\text{C}_6\text{H}_4\text{SMe-}o)\text{P}]$ (41) is isostructural with $[\text{Cp}_2\text{Mo}_2(\text{CO})\{\mu\text{-C}_6\text{H}_4\text{S}\}_2\text{PPh}]$ (38). Therefore, it is proposed that the synthetic pathways for the formation of 41 is similar to that of 38 via the initial oxidation addition of $\text{P}(\text{C}_6\text{H}_4\text{SMe-}o)_3$ to $[\text{CpMo}(\text{CO})_2]_2$ (4) to form an intermediate of 41A (Scheme 37). Subsequent decarbonylation and formation of thiolate-bridges across the two Mo atoms gave 41B. Concomitant demethylation resulting from the partial π -back donation from the Mo atoms to -SMe groups yields 41 as a pentadentate chelate.

The formation of $\text{Mo}(\text{CO})_3\{\text{P}(\text{C}_6\text{H}_4\text{SMe-}o)_3\}$ (42), does not proceed via 41 because no new product was observed from the NMR tube thermolysis reaction of 41 even after prolonged thermolysis. It is postulated that 42 is the result from the oxidation addition of $\text{P}(\text{C}_6\text{H}_4\text{SMe-}o)_3$ towards the $15e^-$ species, $\text{CpMo}(\text{CO})_2\cdot$ (4A), to give 42A as an intermediate. Further formation of Mo-S bonds with Cp-Mo bond cleavage and carbonylation afforded 42. In this context, the Cp-Mo bond cleavage could be due to the prolonged thermolysis (24 h) at higher temperature (110 °C). A similar observation was reported by Pétilion *et al.* in the formation of $[\text{Cp}^*\text{Mo}(\text{CO})(\mu\text{-SMe})_3\text{Mo}(\text{CO})_2(\mu\text{-SMe})\text{Mo}(\text{CO})_2\text{Cp}^*]$ [120].

However, the formation of $[\text{Cp}_2\text{Mo}_2(\text{CO})\{\mu\text{-C}_6\text{H}_4\text{S}\}_2(\text{C}_6\text{H}_4\text{SCH}_2)\text{P}]$ (40) and $\text{CpMo}_2(\text{CO})_3(\mu\text{-S})\{\mu\text{-C}_6\text{H}_4\text{S}\}_2(\text{C}_6\text{H}_4\text{SMe-}o)\text{P}$ (43) remains unclear. Complex 40 was only isolated once and it was not repeatable while complex 43 was easily isolated repeatedly after the reaction was complete.



Scheme 37. Synthetic pathways for the formation of $[\text{Cp}_2\text{Mo}_2(\text{CO})\{\mu\text{-C}_6\text{H}_4\text{S}\}_2(\text{C}_6\text{H}_4\text{SCH}_2)\text{P}]$ (**40**), $[\text{Cp}_2\text{Mo}_2(\text{CO})\{\mu\text{-C}_6\text{H}_4\text{S}\}_2(\text{C}_6\text{H}_4\text{SMe-}o)\text{P}]$ (**41**), $\text{Mo}(\text{CO})_3\{\text{P}(\text{C}_6\text{H}_4\text{SMe-}o)_3\}$ (**42**) and $\text{CpMo}_2(\text{CO})_3(\mu\text{-S})\{\mu\text{-C}_6\text{H}_4\text{S}\}_2(\text{C}_6\text{H}_4\text{SMe-}o)\text{P}$ (**43**)

2.15.4 Physical properties

[Cp₂Mo₂(CO){(μ-C₆H₄S)₂(C₆H₄SCH₂)P}] (40)

[Cp₂Mo₂(CO){(μ-C₆H₄S)₂(C₆H₄SCH₂)P}] exists as a dark brown crystalline solid which is soluble in *n*-hexane-toluene mixture to give a golden brown solution. At ambient temperature under an inert atmosphere, it is stable as a solid but it is only stable in solution for approximately 5-7 hours.

[Cp₂Mo₂(CO){(μ-C₆H₄S)₂(C₆H₄SMe-*o*)P}] (41)

[Cp₂Mo₂(CO){(μ-C₆H₄S)₂(C₆H₄SMe-*o*)P}] exists as a dark brown crystalline solid which is soluble in *n*-hexane-toluene mixture to give a reddish brown solution. In the solid state, it is stable at ambient temperature under an inert atmosphere and in solution, it is stable for a couple of days under an inert atmosphere.

Mo(CO)₃{P(C₆H₄SMe-*o*)₃} (42)

Mo(CO)₃{P(C₆H₄SMe-*o*)₃} exists as a bright yellow crystalline solid which is soluble in toluene to give a yellowish brown solution. In the solid state, it is stable at ambient temperature under an inert atmosphere. The solution is stable at ambient temperature for a few days under an inert atmosphere.

CpMo₂(CO)₃(μ-S){(μ-C₆H₄S)₂(C₆H₄SMe-*o*)P} (43)

CpMo₂(CO)₃(μ-S){(μ-C₆H₄S)₂(C₆H₄SMe-*o*)P} exists as a orange crystalline solid which is soluble in ether to give a brownish orange solution. In the solid state, it is stable at ambient temperature under an inert atmosphere. The solution is stable at ambient temperature for a few days under an inert atmosphere.

2.15.5 Spectral properties

2.15.5.1 IR spectra

[Cp₂Mo₂(CO){(μ-C₆H₄S)₂(C₆H₄SCH₂)P}] (40)

[Cp₂Mo₂(CO){(μ-C₆H₄S)₂(C₆H₄SCH₂)P}] showed the ν_{CO} stretching frequency at 1815vs cm⁻¹ in nujol and other peaks at 1158m, 1098s, 1051s, 876w, 794w, 769vw, 742vw, 728vw, 713vw, 695vw, 669vw, 537vw, 477vw, and 466vw cm⁻¹ (refer to Appendix I).

[Cp₂Mo₂(CO){(μ-C₆H₄S)₂(C₆H₄SMe-*o*)P}] (41)

[Cp₂Mo₂(CO){(μ-C₆H₄S)₂(C₆H₄SMe-*o*)P}] showed the ν_{CO} stretching frequencies at 1805vs cm⁻¹ in nujol and other peaks at 1254m, 1162m, 1100m, 1042m, 966w, 948w, 795w, 748m, 543w and 483w cm⁻¹ (refer to Appendix I).

Mo(CO)₃{P(C₆H₄SMe-*o*)₃} (42)

Mo(CO)₃{P(C₆H₄SMe-*o*)₃} showed the ν_{CO} stretching frequencies at 1837vs, 1828sh and 1796sh cm⁻¹ in nujol and other peaks at 1152w, 1061w, 1005w, 799w, 763w, 723vw, 698w, 560vw, 549vw, 535vw, 529vw, 490vw and 474vw cm⁻¹ (refer to Appendix I).

CpMo₂(CO)₃(μ-S){(μ-C₆H₄S)₂(C₆H₄SMe-*o*)P} (43)

CpMo₂(CO)₃(μ-S){(μ-C₆H₄S)₂(C₆H₄SMe-*o*)P} showed the ν_{CO} stretching frequencies at 1953s, 1864s and 1829sh cm⁻¹ in nujol and other peaks at 1317w, 1276m, 1258w, 1106m, 1075m, 1029m, 974w, 942w, 921w, 809w, 750m, 729sh, 702m, 667vw, 639vw, 548w, 481vw and 466vw cm⁻¹ (refer to Appendix I).

2.15.5.2 NMR spectra

[Cp₂Mo₂(CO){(μ-C₆H₄S)₂(C₆H₄SCH₂)P}] (40)

Complex **39** is an unsymmetrical dimeric complex and two Cp peaks were observed in both of their ¹H and ¹³C NMR spectra. In the ¹H NMR spectrum (benzene-*d*₆), the Cp peaks were recorded at δ 4.57 and 4.55, the CH₂- peak was recorded as a singlet at δ 1.42 and the aromatic protons of -C₆H₅ and -C₆H₄ were recorded as multiplets at δ 7.14 - 6.58, 7.52 - 7.48 and 7.86 - 7.84. In the ¹³C NMR spectrum (benzene-*d*₆), the Cp peaks were recorded at δ 92.92 and 89.97, the CH₂- peak was recorded at δ 15.92 and the aromatic carbons of -C₆H₅ and -C₆H₄ were recorded at δ 138.23-126.02. In the ³¹P NMR spectrum, the phosphorus peak was recorded at δ 127.29 (refer to Appendix II).

[Cp₂Mo₂(CO){(μ-C₆H₄S)₂(C₆H₄SMe-*o*)P}] (41)

Complex **41** is an unsymmetrical dimeric complex and two Cp peaks were observed in both of their ¹H and ¹³C NMR spectra. In the ¹H NMR spectrum (benzene-*d*₆), the Cp peaks were recorded at δ 4.80 and 4.57, the CH₃- peak was recorded as singlet at δ 1.97 and the aromatic protons of -C₆H₄ were recorded as multiplets at δ 7.85 - 7.83, 7.72 - 7.70, 7.63 - 7.60, 7.55 - 7.51 and 7.13 - 6.53. In the ¹³C NMR spectrum (benzene-*d*₆), the Cp peaks were recorded at δ 93.07 and 90.75, the CH₃- peak was recorded at δ 17.12 and the aromatic carbons of -C₆H₄ were recorded at δ 144.05-124.45. In the ³¹P NMR spectrum, the phosphorus peak was recorded at δ 127.67 (refer to Appendix II) which is similar with [Cp₂Mo₂(CO){(μ-C₆H₄S)₂(C₆H₄SMe-*o*)P}] (**39**).

Mo(CO)₃{P(C₆H₄SMe-*o*)₃} (42)

Complex **42** is a monomeric product consisting of three carbonyl and one phosphine ligand. In the ¹H NMR spectrum (benzene-*d*₆), the CH₃- peak was recorded at δ 2.45 and 2.07 together with the aromatic protons of -C₆H₄ as multiplets at δ 7.60, 7.45, 7.29 - 7.24 and 7.11 - 6.70. In the ¹³C NMR spectrum (benzene-*d*₆), the CH₃- peaks were recorded at δ 26.15, 21.76 and 19.54, the aromatic carbons of -C₆H₄ were recorded at δ 130.85, 129.66, 128.89, 126.03 and one CO peak was recorded at δ 223.07. In the ³¹P NMR spectrum, the phosphorus peak was recorded at δ 79.81 (refer to Appendix II) which is at a much lower field than the dimeric complexes of [Cp₂Mo₂(CO){(μ-C₆H₄S)₂(C₆H₄SCH₂)P}] (**40**) and [Cp₂Mo₂(CO){(μ-C₆H₄S)₂(C₆H₄SMe-*o*)P}] (**41**).

CpMo₂(CO)₃(μ-S){(μ-C₆H₄S)₂(C₆H₄SMe-*o*)P} (43)

Complex **43** is an unsymmetrical product with only one Cp peak bonded to one Mo atom, together three carbonyls bonded to another Mo atom and a phosphine ligand bonded in between two Mo atoms. In the ¹H NMR spectrum (benzene-*d*₆), the Cp peak was recorded at δ 4.70, the CH₃- peak was recorded as a singlet at δ 2.42 and the aromatic protons of -C₆H₄ were recorded as multiplets at δ 8.10 - 8.05, 7.72 - 7.69, 7.59 - 7.54 and 7.13 - 6.69. In the ¹³C NMR spectrum (benzene-*d*₆), the Cp peak was recorded at δ 92.38, the CH₃- peak was recorded at δ 26.15 and the aromatic carbons of -C₆H₄ were recorded at δ 138.22, 132.43, 130.56, 129.67, 128.90 and 126.03. In the ³¹P NMR spectrum, the phosphorus peak was recorded at δ 114.88 (refer to Appendix II) which is shifted to a lower field when compared to that of [Cp₂Mo₂(CO){(μ-C₆H₄S)₂(C₆H₄SMe-*o*)P}] (**41**) (δ 127.67).

2.15.5.3 Mass spectra

[Cp₂Mo₂(CO){(μ-C₆H₄S)₂(C₆H₄SMe-*o*)P}] (41)

The mass spectrum of **41** shows the parent ion $m/z = 719.8936$ [Cp₂Mo₂(CO){(μ-C₆H₄S)₂(C₆H₄SMe-*o*)P}] and its fragmentation ions as listed in Table 62.

Table 62. Electrospray ionization mass spectrum of [Cp₂Mo₂(CO){(μ-C₆H₄S)₂(C₆H₄SMe-*o*)P}] (**41**)

m/z	Assignments
720	[Cp ₂ Mo ₂ (CO){(μ-C ₆ H ₄ S) ₂ (C ₆ H ₄ SMe- <i>o</i>)P}]
677	Cp ₂ Mo ₂ {(C ₆ H ₄ SMe- <i>o</i>) ₃ P}
662	CpMo ₂ {(C ₆ H ₄ S) ₂ P(C ₆ H ₄ SMe- <i>o</i>)}
547	Mo ₂ {(C ₆ H ₄ S) ₃ P}
517	CpMo{(C ₆ H ₄ S) ₃ P}

Mo(CO)₃{P(C₆H₄SMe-*o*)₃} (42)

The mass spectrum of **42** shows the parent ion $m/z = 582.0000$ Mo(CO)₃{P(C₆H₄SMe-*o*)₃} and its fragmentation ions as listed in Table 63.

Table 63. Electrospray ionization mass spectrum of Mo(CO)₃{P(C₆H₄SMe-*o*)₃} (**42**)

m/z	Assignments
582	Mo(CO) ₃ {P(C ₆ H ₄ SMe- <i>o</i>) ₃ }
567	Mo(CO) ₃ {P(C ₆ H ₄ SMe- <i>o</i>) ₂ (μ-C ₆ H ₄ S)}

2.15.6 Molecular structures

[Cp₂Mo₂(CO){(μ-C₆H₄S)₂(C₆H₄SCH₂)P}] (**40**)

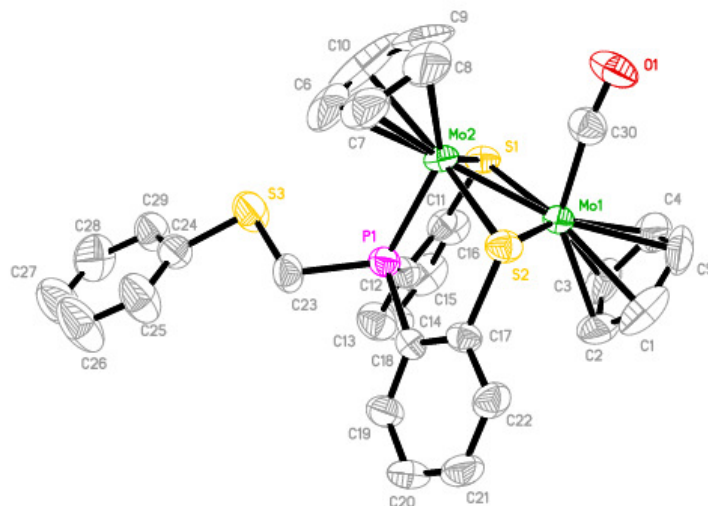


Figure 46. Molecular structure of [Cp₂Mo₂(CO){(μ-C₆H₄S)₂(C₆H₄SCH₂)P}] (**40**)

The molecular structure of **40** is shown in Figure 46. The selected bond lengths (Å) and bond angles (°) for **40** are shown in Table 64. [Cp₂Mo₂(CO){(μ-C₆H₄S)₂(C₆H₄SCH₂)P}] (**40**) crystallizes in triclinic, space group P-1. It is isostructural with [Cp₂Cr₂(CO){(μ-SPh)₂(*o*-MeSPh)P}] (**35**) where the Mo2-S2 fragment is non-planar. The dihedral angle between Mo(1)-S(1)-Mo(2) and Mo(1)-S(2)-Mo(2) is 166.07° which is similar to the dihedral angle [Mo(1)-S(1)-Mo(2)-S(2), 167.4°] found in [Cp₂Mo₂(CO){(μ-SPh)₂PPh}] (**38**). The bond distance of Mo(1)-Mo(2), 2.586(7) Å indicates a double bond which is comparable to [CpMo(SBz)S]₂ (**10a & b**) (average 2.58(6) Å) and [Cp₂Mo₂(CO){(μ-C₆H₄S)₂PPh}] (**38**) (2.598(4) Å). Both Mo1 and Mo2 atoms are in a tetragonal pyramidal coordination environment, with the Cp groups occupying the axial position but Mo2 maintains a distortion due to steric repulsion of the thiolaryl group leading to the axial displacement of the Cp group.

Table 64. Bond lengths [\AA] and angles [$^\circ$] for $[\text{Cp}_2\text{Mo}_2(\text{CO})\{\mu\text{-C}_6\text{H}_4\text{S}\}_2(\text{C}_6\text{H}_4\text{SCH}_2)\text{P}]$ (**40**)

Bond lengths

Mo(1)-C(30)	1.927(7)	O(1)-C(30)	1.171(7)
Mo(1)-S(1)	2.407(15)	S(1)-C(11)	1.789(6)
Mo(1)-S(2)	2.412(15)	S(2)-C(17)	1.804(6)
Mo(1)-Mo(2)	2.586(7)	S(3)-C(24)	1.770(6)
Mo(2)-P(1)	2.359(16)	S(3)-C(23)	1.790(6)
Mo(2)-S(2)	2.399(15)	P(1)-C(12)	1.834(6)
Mo(2)-S(1)	2.402(15)	P(1)-C(18)	1.835(6)
		P(1)-C(23)	1.851(5)

Bond angles

S(1)-Mo(1)-S(2)	113.08(5)	C(17)-S(2)-Mo(2)	109.80(19)
C(30)-Mo(1)-Mo(2)	73.88(18)	C(17)-S(2)-Mo(1)	103.14(18)
S(1)-Mo(1)-Mo(2)	57.38(4)	Mo(2)-S(2)-Mo(1)	65.04(4)
S(2)-Mo(1)-Mo(2)	57.25(4)	C(24)-S(3)-C(23)	102.3(3)
P(1)-Mo(2)-S(2)	81.92(5)	C(12)-P(1)-C(18)	108.8(3)
P(1)-Mo(2)-S(1)	81.84(5)	C(12)-P(1)-C(23)	101.7(3)
S(2)-Mo(2)-S(1)	113.70(5)	C(18)-P(1)-C(23)	99.5(3)
P(1)-Mo(2)-Mo(1)	86.77(4)	C(12)-P(1)-Mo(2)	111.17(19)
S(2)-Mo(2)-Mo(1)	57.71(4)	C(18)-P(1)-Mo(2)	111.77(18)
S(1)-Mo(2)-Mo(1)	57.55(4)	C(23)-P(1)-Mo(2)	122.6(2)
C(11)-S(1)-Mo(2)	109.10(19)	S(3)-C(23)-P(1)	111.1(3)
C(11)-S(1)-Mo(1)	104.24(18)	O(1)-C(30)-Mo(1)	172.0(5)
Mo(2)-S(1)-Mo(1)	65.07(4)		

$[\text{Cp}_2\text{Mo}_2(\text{CO})\{\mu\text{-C}_6\text{H}_4\text{S}\}_2(\text{C}_6\text{H}_4\text{SMe-}o)\text{P}]$ (**41**)

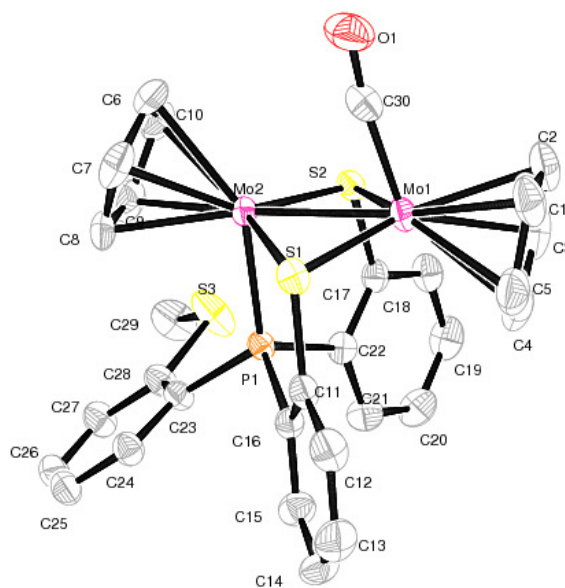


Figure 47. Molecular structure of $[\text{Cp}_2\text{Mo}_2(\text{CO})\{\mu\text{-C}_6\text{H}_4\text{S}\}_2(\text{C}_6\text{H}_4\text{SMe-}o)\text{P}]$ (**41**)

The molecular structure of **41** is shown in Figure 47. The selected bond lengths (Å) and bond angles (°) for **35** are shown in Table 65. **41** crystallizes in monoclinic, space group $P2_1/c$ and is isostructural with its Cr analogue of $[\text{Cp}_2\text{Cr}_2(\text{CO})\{(\mu\text{-C}_6\text{H}_4\text{S})_2(o\text{-PhSMe})\text{P}\}]$ (**35**). The Mo(1)-Mo(2) bond distance, 2.606(3) Å is comparable to the Mo=Mo bond found in $[\text{Cp}_2\text{Mo}_2(\text{CO})\{(\mu\text{-C}_6\text{H}_4\text{S})_2(o\text{-C}_6\text{H}_4\text{SCH}_2)\text{P}\}]$ (**40**) (2.586(7) Å). The bonding mode of **41** is very close to that found in **35**.

Table 65. Bond lengths [Å] and angles [°] for $[\text{Cp}_2\text{Mo}_2(\text{CO})\{(\mu\text{-C}_6\text{H}_4\text{S})_2(\text{C}_6\text{H}_4\text{SMe-}o)\text{P}\}](\mathbf{41})$

Bond lengths

Mo(1)-C(30)	1.921(3)	P(1)-C(22)	1.831(2)
Mo(1)-S(1)	2.408(6)	P(1)-C(16)	1.838(2)
Mo(1)-S(2)	2.410(6)	P(1)-C(23)	1.840(2)
Mo(1)-Mo(2)	2.606(3)	S(1)-C(11)	1.796(3)
Mo(2)-P(1)	2.354(6)	S(2)-C(17)	1.799(3)
Mo(2)-S(2)	2.398(6)	S(3)-C(28)	1.767(3)
Mo(2)-S(1)	2.401(6)	S(3)-C(29)	1.779(3)
		O(1)-C(30)	1.167(3)

Bond angles

C(30)-Mo(1)-S(1)	86.65(8)	P(1)-Mo(2)-Mo(1)	87.75(16)
C(30)-Mo(1)-S(2)	89.63(8)	S(2)-Mo(2)-Mo(1)	57.41(15)
S(1)-Mo(1)-S(2)	112.39(2)	S(1)-Mo(2)-Mo(1)	57.33(15)
C(30)-Mo(1)-Mo(2)	74.95(8)	Mo(2)-S(1)-Mo(1)	65.64(16)
S(1)-Mo(1)-Mo(2)	57.04(15)	Mo(2)-S(2)-Mo(1)	65.65(17)
S(2)-Mo(1)-Mo(2)	56.94(15)	C(27)-C(28)-S(3)	120.81(19)
P(1)-Mo(2)-S(2)	82.22(2)	C(23)-C(28)-S(3)	120.09(18)
P(1)-Mo(2)-S(1)	82.32(2)	O(1)-C(30)-Mo(1)	171.7(2)
S(2)-Mo(2)-S(1)	113.12(2)		

Mo(CO)₃{P(C₆H₄SMe-*o*)₃} (42)

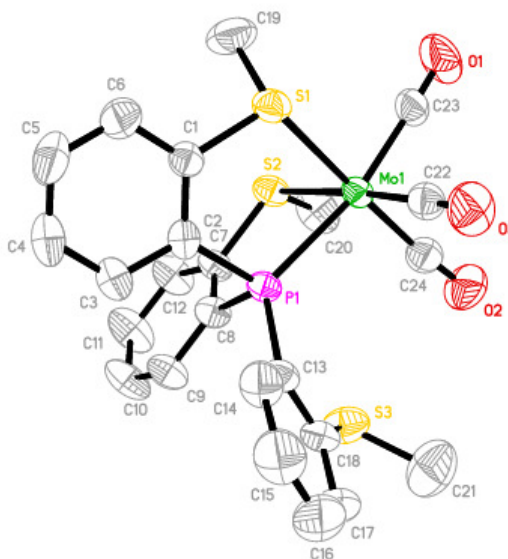


Figure 48. Molecular structure of Mo(CO)₃{P(C₆H₄SMe-*o*)₃} (**42**)

The molecular structure of **42** is shown in Figure 48. The selected bond lengths and bond angles of **42** are shown in Table 66. Mo(CO)₃{P(C₆H₄SMe-*o*)₃} (**42**) crystallizes in monoclinic, space group C2/c. **42** consists of a slightly distorted octahedral geometry where the S(2)-C(20) fragment is tilted towards the phosphine ligand which causes the P(1)-Mo(1)-S(2) (78.34(3)°) bond angle to be less than the ideal octahedral value of 90° which is most likely due to the constraint of the P-C-C-S chelate rings. A similar observation has also been reported for the molecular structure of the anion of [NMe₄][Mo{PPh(C₆H₄S)}(CO)₃] [121]. The phosphine ligand occupies one face of the octahedron and the three CO ligands are in a *cis* configuration. The Mo(1)-P(1) bond distance of 2.463(10) Å is longer than those observed in CpMo(CO){(μ-C₆H₄S)(μ-C₆H₄SMe-*o*)PPh} (**39**) (2.380(16) Å) and [Cp₂Mo₂(CO){(μ-C₆H₄S)₂(C₆H₄SMe-*o*)P}] (**41**) (2.354(6) Å) but is comparable to that in CpMo(CO)₂{*o*-(C₆H₄S)PPh₂} (**36**) (2.444(6) Å). These observations could be rationalized by the effect of π-back bonding in **42** (3 CO) and **36** (2 CO) which is stronger than that in **39** (1 CO) and **41** (1 CO), respectively. Therefore,

the reduced electron density at the Mo atom in **41** will result in a weaker Mo-P bond strength.

Table 66. Bond lengths [\AA] and angles [$^\circ$] for $\text{Mo}(\text{CO})_3\{\text{P}(\text{C}_6\text{H}_4\text{SMe-}o)_3\}$ (**42**)

Bond lengths			
Mo(1)-C(22)	1.947(5)	S(1)-C(1)	1.790(4)
Mo(1)-C(24)	1.958(5)	S(1)-C(19)	1.803(5)
Mo(1)-C(23)	1.982(4)	S(2)-C(7)	1.794(4)
Mo(1)-P(1)	2.463(10)	S(2)-C(20)	1.805(5)
Mo(1)-S(1)	2.506(11)	S(3)-C(18)	1.768(5)
Mo(1)-S(2)	2.542(11)	S(3)-C(21)	1.772(7)
P(1)-C(13)	1.819(4)	O(1)-C(23)	1.141(5)
P(1)-C(8)	1.831(4)	O(2)-C(24)	1.160(5)
P(1)-C(2)	1.844(4)	O(3)-C(22)	1.155(5)
Bond angles			
C(22)-Mo(1)-C(24)	87.73(18)	C(13)-P(1)-C(8)	106.44(18)
C(22)-Mo(1)-C(23)	92.11(17)	C(13)-P(1)-C(2)	103.67(18)
C(24)-Mo(1)-C(23)	88.80(19)	C(8)-P(1)-C(2)	97.29(18)
C(22)-Mo(1)-P(1)	96.57(12)	C(13)-P(1)-Mo(1)	126.33(13)
C(24)-Mo(1)-P(1)	99.50(13)	C(8)-P(1)-Mo(1)	110.59(13)
C(23)-Mo(1)-P(1)	168.19(13)	C(2)-P(1)-Mo(1)	108.52(13)
C(22)-Mo(1)-S(1)	88.70(13)	C(1)-S(1)-C(19)	101.1(2)
C(24)-Mo(1)-S(1)	176.42(14)	C(1)-S(1)-Mo(1)	108.60(13)
C(23)-Mo(1)-S(1)	90.99(14)	C(19)-S(1)-Mo(1)	112.50(19)
P(1)-Mo(1)-S(1)	81.24(3)	C(7)-S(2)-C(20)	99.8(2)
C(22)-Mo(1)-S(2)	174.89(12)	C(7)-S(2)-Mo(1)	109.01(14)
C(24)-Mo(1)-S(2)	92.61(14)	C(20)-S(2)-Mo(1)	109.59(19)
C(23)-Mo(1)-S(2)	93.00(13)	C(18)-S(3)-C(21)	101.5(3)
P(1)-Mo(1)-S(2)	78.34(3)	O(3)-C(22)-Mo(1)	178.2(4)
S(1)-Mo(1)-S(2)	90.98(4)	O(1)-C(23)-Mo(1)	178.2(4)
		O(2)-C(24)-Mo(1)	175.1(4)

CpMo₂(CO)₃(μ-S){(μ-C₆H₄S)₂(C₆H₄SMe-*o*)P} (43)

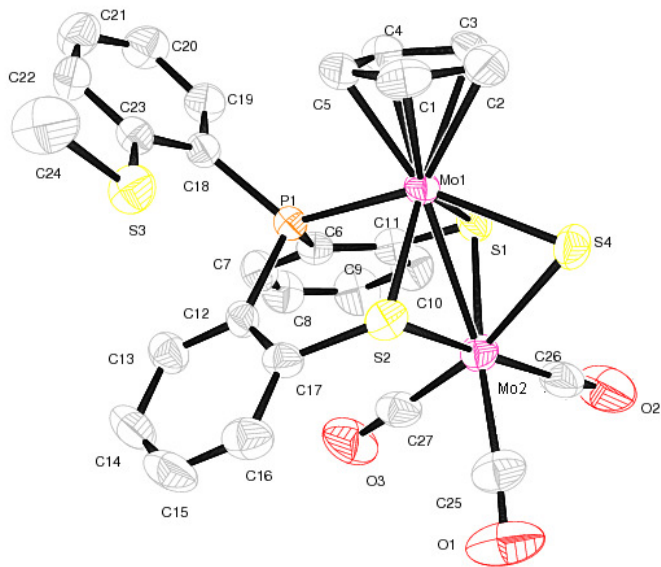


Figure 49. Molecular structure of CpMo₂(CO)₃(μ-S){(μ-C₆H₄S)₂(C₆H₄SMe-*o*)P} (**43**)

The molecular structure of **43** is shown in Figure 49. The selected bond lengths and bond angles of **43** are shown in Table 67. CpMo₂(CO)₃(μ-S){(μ-C₆H₄S)₂(C₆H₄SMe-*o*)P} (**43**) crystallizes in triclinic, space group P-1. Mo(1) possesses a distorted tetrahedral pyramidal coordination which consists of one sulfido, two thiolato and one phosphorus fragment with a Cp ring occupying the axial position. However, Mo(2) possesses a distorted octahedral coordination consisting of three CO, one sulfido and two thiolato ligands. Both the Mo atoms are linked by two thiolato bridges (S(1) and S(2)) and one sulfido bridge (S(4)). The bond distances of Mo(1)-S(1) (2.373(12) Å) and Mo(1)-S(2) (2.417(12) Å) are shorter than the Mo(2)-S(1) (2.503(13) Å) and Mo(2)-S(2) (2.526(13) Å) bond within the molecule because the electron donor effect from the Cp ring increases the electron density at Mo(1) thus strengthening the Mo-S bond. However, the electron density at Mo(2) is decreased as a result of the π-back donation towards the three CO ligands. Consequently, the electron density within the Mo-Mo bond (2.847(6) Å) will also be

decreased to give a single bond. The electron count at Mo(1) obeys the 18 e rule while Mo(2) has only 16e.

Table 67. Bond lengths [Å] and angles [°] for CpMo₂(CO)₃(μ-S){(μ-C₆H₄S)₂(C₆H₄SMe-*o*)P} (**43**)

Bond lengths			
Mo(1)-S(1)	2.373(12)	S(1)-C(11)	1.792(5)
Mo(1)-S(2)	2.417(12)	S(2)-C(17)	1.790(5)
Mo(1)-P(1)	2.424(12)	S(3)-C(23)	1.777(5)
Mo(1)-S(4)	2.536(12)	S(3)-C(24)	1.794(6)
Mo(1)-Mo(2)	2.847(6)	P(1)-C(12)	1.824(5)
Mo(2)-C(27)	1.919(6)	P(1)-C(18)	1.834(4)
Mo(2)-C(26)	1.996(6)	P(1)-C(6)	1.837(5)
Mo(2)-C(25)	2.007(6)	O(1)-C(25)	1.140(6)
Mo(2)-S(1)	2.503(13)	O(2)-C(26)	1.140(6)
Mo(2)-S(2)	2.526(13)	O(3)-C(27)	1.172(6)
Mo(2)-S(4)	2.561(13)		
Bond angles			
S(1)-Mo(1)-S(2)	111.33(4)	C(27)-Mo(2)-Mo(1)	112.88(15)
S(1)-Mo(1)-P(1)	82.37(4)	C(26)-Mo(2)-Mo(1)	128.86(15)
S(2)-Mo(1)-P(1)	81.47(4)	C(25)-Mo(2)-Mo(1)	137.91(15)
S(1)-Mo(1)-S(4)	79.36(4)	S(1)-Mo(2)-Mo(1)	52.18(3)
S(2)-Mo(1)-S(4)	76.90(4)	S(2)-Mo(2)-Mo(1)	53.04(3)
P(1)-Mo(1)-S(4)	144.13(4)	S(4)-Mo(2)-Mo(1)	55.63(3)
S(1)-Mo(1)-Mo(2)	56.42(3)	C(11)-S(1)-Mo(1)	109.64(16)
S(2)-Mo(1)-Mo(2)	56.65(3)	C(11)-S(1)-Mo(2)	100.71(16)
P(1)-Mo(1)-Mo(2)	87.74(3)	Mo(1)-S(1)-Mo(2)	71.40(4)
S(4)-Mo(1)-Mo(2)	56.46(3)	C(17)-S(2)-Mo(1)	109.54(15)
C(27)-Mo(2)-C(26)	89.0(2)	C(17)-S(2)-Mo(2)	100.72(15)
C(27)-Mo(2)-C(25)	82.7(2)	Mo(1)-S(2)-Mo(2)	70.30(3)
C(26)-Mo(2)-C(25)	88.3(2)	C(23)-S(3)-C(24)	103.8(3)
C(27)-Mo(2)-S(1)	96.01(15)	Mo(1)-S(4)-Mo(2)	67.92(3)
C(26)-Mo(2)-S(1)	81.16(16)	C(12)-P(1)-C(18)	104.4(2)
C(25)-Mo(2)-S(1)	169.37(15)	C(12)-P(1)-C(6)	106.1(2)
C(27)-Mo(2)-S(2)	99.16(15)	C(18)-P(1)-C(6)	103.4(2)
C(26)-Mo(2)-S(2)	169.94(17)	C(12)-P(1)-Mo(1)	110.09(15)
C(25)-Mo(2)-S(2)	86.91(15)	C(18)-P(1)-Mo(1)	122.70(15)
S(1)-Mo(2)-S(2)	103.70(4)	C(6)-P(1)-Mo(1)	108.95(16)
C(27)-Mo(2)-S(4)	168.49(15)	O(1)-C(25)-Mo(2)	173.4(6)
C(26)-Mo(2)-S(4)	98.41(16)	O(2)-C(26)-Mo(2)	175.6(5)
C(25)-Mo(2)-S(4)	106.21(17)	O(3)-C(27)-Mo(2)	178.4(5)
S(1)-Mo(2)-S(4)	76.54(4)		
S(2)-Mo(2)-S(4)	74.55(4)		

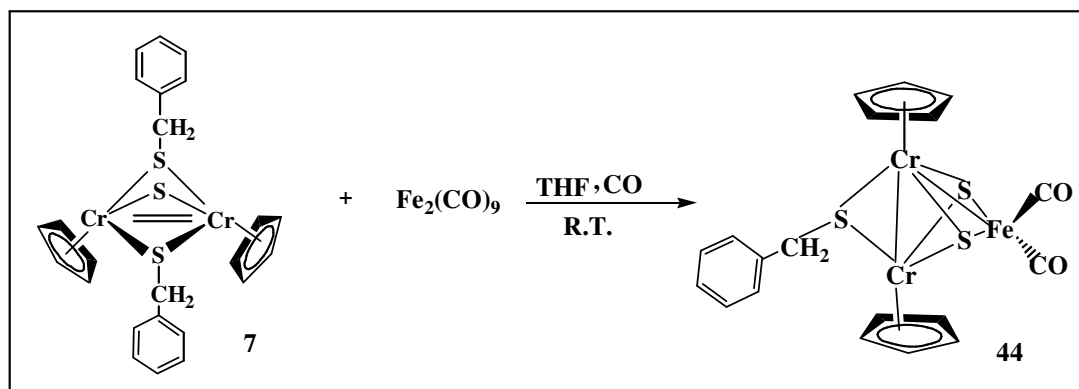
2.16 Coordination of the (μ -S) ligand to $\text{Fe}(\text{CO})_x$ ($x = 2$ or 3) fragments from $\text{Fe}(\text{CO})_9$

2.16.1 The reaction of $[\text{CpCr}(\text{SBz})]_2\text{S}$ with 2 mole equivalent of $\text{Fe}_2(\text{CO})_9$

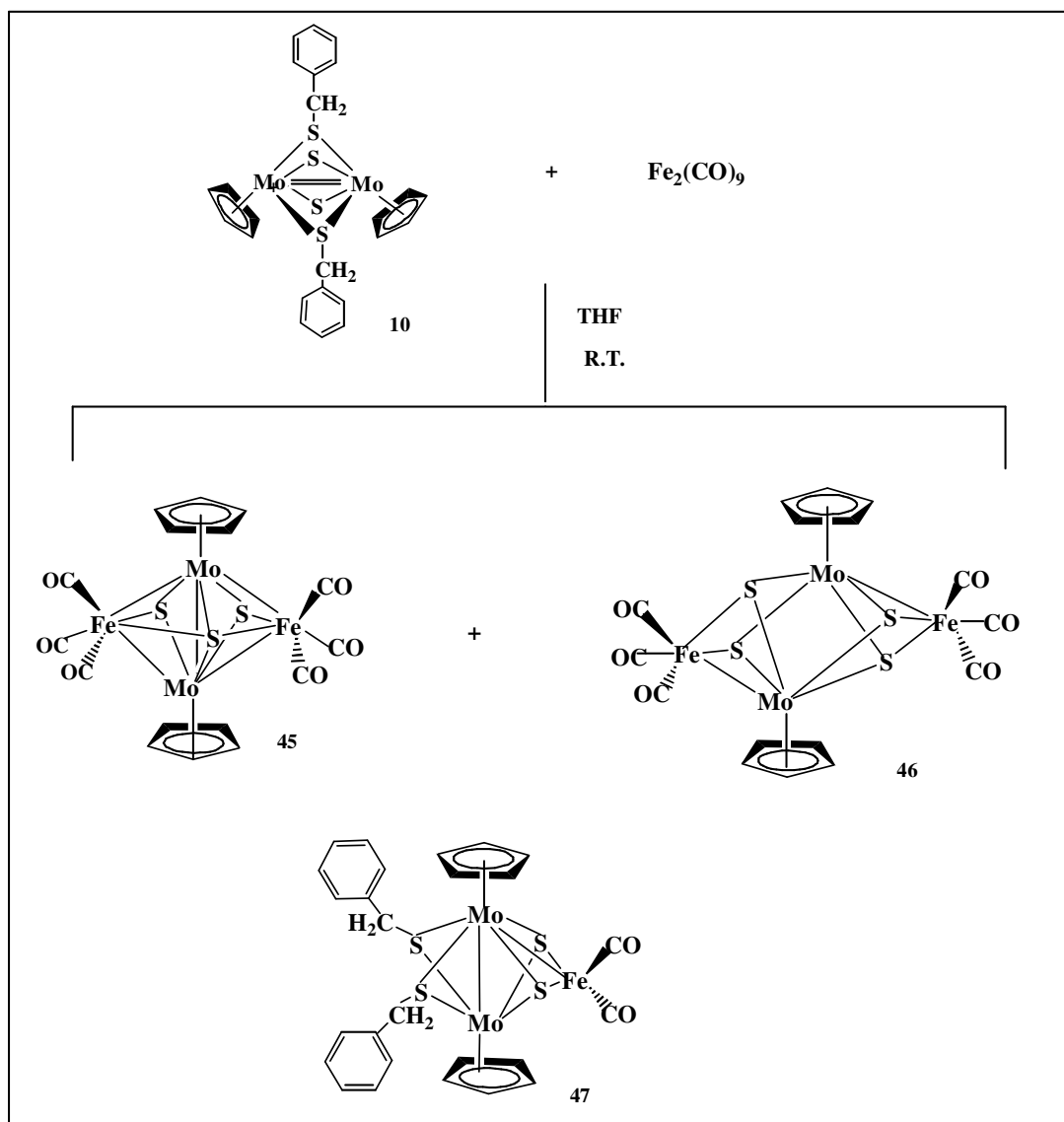
A heterogeneous 1:2 molar mixture of $[\text{CpCr}(\text{SBz})]_2\text{S}$ (**7**) and $\text{Fe}_2(\text{CO})_9$ undergoes a facile reaction in THF under an atmosphere of CO at ambient temperature for 3 h to give a brownish purple solution from which were isolated using column chromatography the following fractions of $[\text{Cp}_2\text{Cr}_2(\text{SBz})]_2\text{S}_2[\text{Fe}(\text{CO})_3]$ (**44**) as fine dark purplish brown crystals (33.2% yield) and an uncharacterized dark brown precipitate (7 mg) (Scheme 38).

2.16.2 The reaction of $[\text{CpMo}(\text{SBz})(\text{S})]_2$ with 2 mole equivalent of $\text{Fe}_2(\text{CO})_9$ at room temperature

A dark pink suspension of $[\text{CpMo}(\text{SBz})(\text{S})]_2$ with 2 equivolar of $\text{Fe}_2(\text{CO})_9$ in THF was stirred rigorously at ambient temperature under an inert atmosphere for 1.5 h to give a dark brownish pink reaction mixture from which were isolated dark green crystalline solids of $[\text{CpMo}]_2\text{S}_4[\text{Fe}(\text{CO})_3]_2$ (**45**) (19.8% yield), dark red crystalline solids of $[\text{CpMo}]_2\text{S}_3[\text{Fe}(\text{CO})_3]_2$ (**46**) (10.4% yield) and dark pink crystalline solids of $[\text{CpMo}(\text{SBz})]_2\text{S}_2[\text{Fe}(\text{CO})_2]$ (**47**) (18.3% yield) (Scheme 39).



Scheme 38. Formation of $[\text{Cp}_2\text{Cr}_2(\text{SBz})]_2\text{S}_2[\text{Fe}(\text{CO})_3]$ (**44**)



Scheme 39. Formation of $[\text{CpMo}]_2\text{S}_4[\text{Fe}(\text{CO})_3]_2$ (**45**), $[\text{CpMo}]_2\text{S}_3[\text{Fe}(\text{CO})_3]_2$ (**46**) and $[\text{CpMo}(\text{SBz})]_2\text{S}_2[\text{Fe}(\text{CO})_2]$ (**47**)

2.16.3 Physical properties

$[\text{Cp}_2\text{Cr}_2(\text{SBz})]_2\text{S}_2[\text{Fe}(\text{CO})_3]$ (**44**)

The complex **44** exists as a dark purplish brown crystalline solid. In the solid state, it is stable for a couple of days under an inert atmosphere. It is soluble in *n*-hexane/toluene mixture to give a brownish purple solution. In solution, it is stable at ambient temperature under an inert atmosphere for a few hours.

[CpMo]₂S₄[Fe(CO)₃]₂ (45)

The complex **45** exists as a green crystalline solid. In the solid state, it is stable at room temperature under an inert atmosphere. It is soluble in *n*-hexane to give a dark green solution. In solution, it is stable at ambient temperature under an inert atmosphere for a couple of days.

[CpMo]₂S₃[Fe(CO)₃]₂ (46)

The complex **46** exists as a dark red crystalline solid. In the solid state, it is stable at room temperature under an inert atmosphere. It is soluble in *n*-hexane to give a red solution. In solution, it is stable at ambient temperature under an inert atmosphere for a couple of days.

[CpMo(SBz)]₂S₂[Fe(CO)₂] (47)

The complex **47** exists as a pink crystalline solid. In the solid state, it is stable at room temperature under an inert atmosphere. It is soluble in *n*-hexane/toluene mixture to give a pink solution. In solution, it is stable at ambient temperature under an inert atmosphere for a couple of days.

2.16.4 Spectral characteristics

2.16.4.1 IR spectra

[CpMo]₂S₄[Fe(CO)₃]₂ (45)

[CpMo]₂S₄[Fe(CO)₃]₂ showed the ν_{CO} stretching frequencies at 2070vw, 2043m, 2034s, 1996s, 1970vs, 1949s cm⁻¹ in nujol (refer to Appendix I).

[CpMo(SBz)]₂S₂[Fe(CO)₂] (47)

[CpMo(SBz)]₂S₂[Fe(CO)₂] showed the ν_{CO} stretching frequencies at 2032vs, 1964s, 1935vs, 1927vs, 1860vs cm⁻¹ in nujol (refer to Appendix I).

2.16.4.2 NMR spectra

[Cp₂Cr₂(SBz)]S₂[Fe(CO)₃] (44)

The complex **44** is a heteronuclear complex with a Fe(CO)₃ fragment acting as an adduct. In the ¹H NMR spectrum (benzene-*d*₆), one Cp peak was recorded at δ 4.91, a CH₂- peak was recorded as a singlet at δ 3.30 and the aromatic protons for C₆H₅- were recorded as multiplets at δ 7.72 - 7.01. In the ¹³C NMR spectrum (benzene-*d*₆), one Cp peak was recorded at δ 90.34, the aromatic carbons for C₆H₅- were recorded at δ 138.63, 132.41, 130.56, 129.65 and 126.03 together with a CO peak at δ 196.02.

[CpMo]₂S₄[Fe(CO)₃]₂ (45)

The complex **45** is a heteronuclear complex with two Fe(CO)₃ fragments acting as adducts. In the ¹H NMR spectrum (benzene-*d*₆), two Cp peaks were recorded at δ 5.73 - 4.67. In the ¹³C NMR spectrum (benzene-*d*₆), two Cp peaks were recorded at δ 95.23 and 94.35.

[CpMo(SBz)]₂S₂[Fe(CO)₂] (47)

The complex **47** is a heteronuclear complex with a Fe(CO)₂ fragment acting as an adduct. In the ¹H NMR spectrum (benzene-*d*₆), one Cp peak was recorded at δ 4.58, two CH₂- peaks at δ 3.98 and 3.12, together with the aromatic protons for C₆H₅- as multiplets at δ 7.29-7.01. In the ¹³C NMR spectrum (benzene-*d*₆), one Cp peak was recorded at δ 92.76, the aromatic carbons for C₆H₅- were recorded at δ 141.12-127.42 and a CO peak at δ 221.35.

2.16.4.3 Mass spectra

[Cp₂Cr₂(SBz)]S₂[Fe(CO)₃] (44)

The mass spectrum of **44** shows the parent ion $m/z = 533.3639$ [Cp₂Cr₂(SBz)]S₂[Fe(CO)₃] and its fragmentation ions as listed in Table 68.

Table 68. Electrospray ionization mass spectrum of [Cp₂Cr₂(SBz)]S₂[Fe(CO)₃] (**44**)

m/z	Assignments
899	{[Cp ₂ Cr ₂ (SBz)]S ₂ [Fe]} ₂
533	[Cp ₂ Cr ₂ (SBz)]S ₂ [Fe(CO) ₃]

[CpMo]₂S₃[Fe(CO)₃]₂ (46)

The mass spectrum of **46** shows the parent ion $m/z = 700.5756$ [CpMo]₂S₃[Fe(CO)₃]₂.

[CpMo(SBz)]₂S₂[Fe(CO)₂] (47)

The mass spectrum of **47** shows the parent ion $m/z = 746.9559$ [CpMo(SBz)]₂S₂[Fe(CO)₂] and its fragmentation ions as listed in Table 69.

Table 69. Electrospray ionization mass spectrum of [CpMo(SBz)]₂S₂[Fe(CO)₂] (**47**)

m/z	Assignments
747	[CpMo(SBz)] ₂ S ₂ [Fe(CO) ₂]
721	[CpMo(SBz)] ₂ S ₂ [Fe(CO)]
692	[CpMo(SBz)] ₂ S ₂ [Fe]
657	Cp ₂ Mo ₂ (SBz) ₃ [Fe(CO) ₂]
566	Cp ₂ Mo ₂ S ₄ [Fe(CO) ₂]
538	Cp ₂ Mo ₂ S ₄ [Fe(CO)]

2.16.5 Molecular structures

[Cp₂Cr₂(SBz)]S₂[Fe(CO)₃] (**44**)

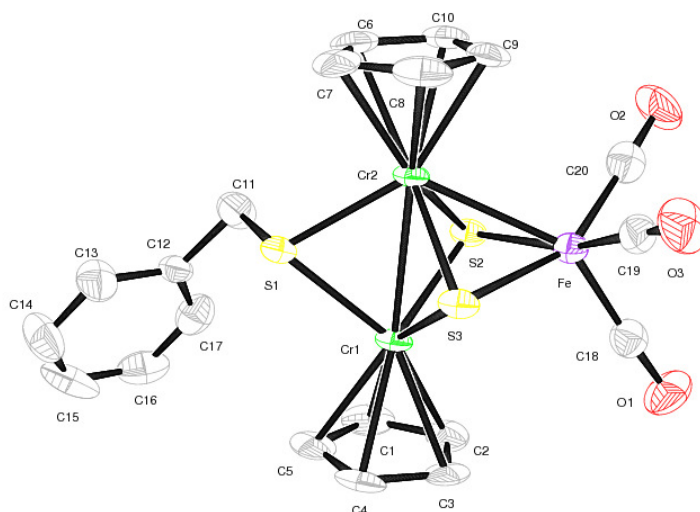


Figure 50. Molecular structure of [Cp₂Cr₂(SBz)]S₂[Fe(CO)₃] (**44**)

The molecular structure of **44** is shown in Figure 50. The selected bond lengths (Å) and bond angles (°) of **44** are shown in Table 70. [Cp₂Cr₂(SBz)]S₂[Fe(CO)₃] (**44**) crystallizes in monoclinic, space group P2₁/c. The structure of [Cp₂Cr₂(SBz)]S₂[Fe(CO)₃] (**44**) contains a distorted tetragonal-bipyramidal Cr₂FeS₃ core. Two Cp₂Cr₂ fragments are linked by a direct Cr-Cr bond (2.716 Å) and by a benzylthiolate and two sulfide bridges (Cr-S(thiolate) and the average Cr-S(sulfide) bond lengths are 2.333 and 2.307 Å, respectively. Both sulfide sulfur, S2 and S3, are linked with the Fe(CO)₃ fragment (average Fe-S bond length is 2.304 Å). The Fe atom is positioned asymmetrically with respect to the chromium atoms. Although Cr(1) is not bonded directly to Fe, the Cp ring coordinated at Cr(1) occupies a close axial position with the other Cp ring coordinated at Cr(2).

Table 70. Bond lengths [Å] and angles [°] for [Cp₂Cr₂(SBz)]S₂[Fe(CO)₃] (**44**)

Bond lengths

Cr(1)-S(3)	2.306(2)	S(2)-Fe	2.297(2)
Cr(1)-S(2)	2.308(2)	S(3)-Fe	2.311(2)
Cr(1)-S(1)	2.333(2)	Fe-C(19)	1.784(9)
Cr(1)-Cr(2)	2.716(16)	Fe-C(20)	1.789(9)
Cr(2)-S(3)	2.299(2)	Fe-C(18)	1.808(9)
Cr(2)-S(2)	2.299(2)	C(18)-O(1)	1.153(9)
Cr(2)-S(1)	2.351(2)	C(19)-O(3)	1.143(9)
Cr(2)-Fe	2.672(16)	O(2)-C(20)	1.136(9)
S(1)-C(11)	1.840(8)		

Bond angles

S(3)-Cr(1)-S(2)	87.74(8)	Cr(2)-S(2)-Cr(1)	72.26(7)
S(3)-Cr(1)-S(1)	86.47(8)	Cr(2)-S(3)-Cr(1)	72.29(7)
S(2)-Cr(1)-S(1)	92.92(8)	Cr(2)-S(3)-Fe	70.83(6)
S(3)-Cr(1)-Cr(2)	53.73(6)	Cr(1)-S(3)-Fe	85.86(7)
S(2)-Cr(1)-Cr(2)	53.71(6)	C(19)-Fe-C(20)	92.3(4)
S(1)-Cr(1)-Cr(2)	54.87(6)	C(19)-Fe-C(18)	97.7(4)
S(3)-Cr(2)-S(2)	88.13(7)	C(20)-Fe-C(18)	99.9(4)
S(3)-Cr(2)-S(1)	86.22(8)	C(19)-Fe-S(2)	161.7(3)
S(2)-Cr(2)-S(1)	92.68(8)	C(20)-Fe-S(2)	86.9(3)
S(3)-Cr(2)-Fe	54.80(6)	C(18)-Fe-S(2)	100.4(3)
S(2)-Cr(2)-Fe	54.43(6)	C(19)-Fe-S(3)	84.3(3)
S(1)-Cr(2)-Fe	125.43(7)	C(20)-Fe-S(3)	152.1(3)
S(3)-Cr(2)-Cr(1)	53.98(6)	C(18)-Fe-S(3)	108.0(3)
S(2)-Cr(2)-Cr(1)	54.02(6)	S(2)-Fe-S(3)	87.87(8)
S(1)-Cr(2)-Cr(1)	54.25(6)	C(19)-Fe-Cr(2)	108.0(3)
Fe-Cr(2)-Cr(1)	71.42(4)	C(20)-Fe-Cr(2)	101.3(3)
C(11)-S(1)-Cr(1)	109.3(3)	C(18)-Fe-Cr(2)	145.7(3)
C(11)-S(1)-Cr(2)	109.3(3)	S(2)-Fe-Cr(2)	54.48(6)
Cr(1)-S(1)-Cr(2)	70.88(7)	S(3)-Fe-Cr(2)	54.37(6)
Fe-S(2)-Cr(2)	71.09(7)	O(1)-C(18)-Fe	177.2(8)
Fe-S(2)-Cr(1)	86.15(7)	O(3)-C(19)-Fe	177.8(8)
		O(2)-C(20)-Fe	176.8(8)

[CpMo]₂S₄[Fe(CO)₃]₂ (45**)**

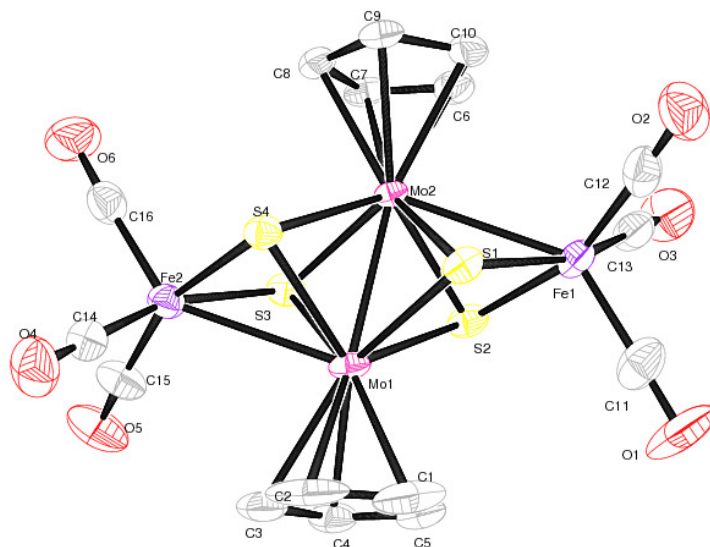


Figure 51. Molecular structure of [CpMo]₂S₄[Fe(CO)₃]₂ (**45**)

The molecular structure of **45** is shown in Figure 51. The selected bond lengths (Å) and bond angles (°) of **45** are shown in Table 71. [CpMo]₂S₄[Fe(CO)₃]₂ (**45**) crystallizes in monoclinic, space group P2₁/c. It contains a Fe₂Mo₂S₄ core. The distorted cubane-type structure is characterized for most other M₄S₄ system [122a-e]. The two Mo atoms are in a tetragonal-bipyramidal coordination environment, with both Cp rings occupying the axial position. The four metal atoms lie in a plane and are bridged by the four μ₃-sulfido ligands. The Mo-Mo distance of 2.625(5) Å indicates a double bond and is similar to those of [CH₃C₅H₄Mo₂S₂Fe(CO)₃]₂ (2.624(2) Å) [123]. The four μ₃-S atoms feature a square-planar arrangement perpendicular to the Mo-Mo bond which intersects the plane of the metal atoms plane. Most of the bonding features of **45** are similar to [CH₃C₅H₄Mo₂S₂Fe(CO)₃]₂ as reported by DuBois *et al.* and it has been proposed that the reason for the slight distortions of the Fe₂Mo₂S₄ core could be due to the change in the electronic environment of the core resulting from the sulfur coordination of the tricarbonyl iron fragments.

Table 71. Bond lengths [Å] and angles [°] for [CpMo]₂S₄[Fe(CO)₃]₂ (45)

Bond lengths

Mo(1)-S(3)	2.399(11)	Fe(1)-C(13)	1.808(6)
Mo(1)-S(4)	2.400(10)	Fe(1)-S(2)	2.235(13)
Mo(1)-S(1)	2.453(11)	Fe(1)-S(1)	2.238(13)
Mo(1)-S(2)	2.456(12)	Fe(2)-C(16)	1.783(5)
Mo(1)-Mo(2)	2.625(5)	Fe(2)-C(15)	1.801(5)
Mo(1)-Fe(2)	2.838(7)	Fe(2)-C(14)	1.803(5)
Mo(2)-S(2)	2.390(10)	Fe(2)-S(3)	2.226(13)
Mo(2)-S(1)	2.392(11)	Fe(2)-S(4)	2.229(12)
Mo(2)-S(3)	2.446(11)	O(1)-C(11)	1.128(6)
Mo(2)-S(4)	2.460(12)	O(2)-C(12)	1.135(6)
Mo(2)-Fe(1)	2.854(7)	O(3)-C(13)	1.142(6)
Fe(1)-C(12)	1.793(5)	O(4)-C(14)	1.139(6)
Fe(1)-C(11)	1.796(5)	O(5)-C(15)	1.142(6)
		O(6)-C(16)	1.147(5)

Bond angles

S(3)-Mo(1)-S(4)	76.00(4)	C(12)-Fe(1)-S(2)	160.70(15)
S(3)-Mo(1)-S(1)	114.14(4)	C(11)-Fe(1)-S(2)	99.31(19)
S(4)-Mo(1)-S(1)	70.54(3)	C(13)-Fe(1)-S(2)	88.71(17)
S(3)-Mo(1)-S(2)	70.28(4)	C(12)-Fe(1)-S(1)	88.85(16)
S(4)-Mo(1)-S(2)	114.39(4)	C(11)-Fe(1)-S(1)	97.37(17)
S(1)-Mo(1)-S(2)	74.60(4)	C(13)-Fe(1)-S(1)	162.30(15)
S(3)-Mo(1)-Mo(2)	58.06(3)	S(2)-Fe(1)-S(1)	83.37(4)
S(4)-Mo(1)-Mo(2)	58.41(3)	C(12)-Fe(1)-Mo(2)	106.99(15)
S(1)-Mo(1)-Mo(2)	56.08(3)	C(11)-Fe(1)-Mo(2)	139.96(18)
S(2)-Mo(1)-Mo(2)	55.99(3)	C(13)-Fe(1)-Mo(2)	108.30(15)
S(3)-Mo(1)-Fe(2)	49.43(3)	S(2)-Fe(1)-Mo(2)	54.37(3)
S(4)-Mo(1)-Fe(2)	49.51(3)	S(1)-Fe(1)-Mo(2)	54.42(3)
S(1)-Mo(1)-Fe(2)	119.39(3)	C(16)-Fe(2)-S(3)	98.84(17)
S(2)-Mo(1)-Fe(2)	119.13(3)	C(15)-Fe(2)-S(3)	88.75(17)
Mo(2)-Mo(1)-Fe(2)	82.533(18)	C(14)-Fe(2)-S(3)	160.17(15)
S(2)-Mo(2)-S(1)	76.94(4)	C(16)-Fe(2)-S(4)	99.09(15)
S(2)-Mo(2)-S(3)	70.60(4)	C(15)-Fe(2)-S(4)	161.61(17)
S(1)-Mo(2)-S(3)	114.65(4)	C(14)-Fe(2)-S(4)	88.74(15)
S(2)-Mo(2)-S(4)	114.61(4)	S(3)-Fe(2)-S(4)	83.10(4)
S(1)-Mo(2)-S(4)	70.56(4)	C(16)-Fe(2)-Mo(1)	141.94(16)
S(3)-Mo(2)-S(4)	74.06(4)	C(15)-Fe(2)-Mo(1)	107.01(17)
S(2)-Mo(2)-Mo(1)	58.41(3)	C(14)-Fe(2)-Mo(1)	105.74(15)
S(1)-Mo(2)-Mo(1)	58.32(3)	S(3)-Fe(2)-Mo(1)	54.98(3)
S(3)-Mo(2)-Mo(1)	56.33(3)	S(4)-Fe(2)-Mo(1)	54.97(3)
S(4)-Mo(2)-Mo(1)	56.21(2)	Fe(1)-S(1)-Mo(2)	76.03(4)
S(2)-Mo(2)-Fe(1)	49.48(3)	Fe(1)-S(1)-Mo(1)	99.98(4)
S(1)-Mo(2)-Fe(1)	49.55(3)	Mo(2)-S(1)-Mo(1)	65.60(3)
S(3)-Mo(2)-Fe(1)	119.32(3)	Fe(1)-S(2)-Mo(2)	76.15(4)
S(4)-Mo(2)-Fe(1)	119.33(3)	Fe(1)-S(2)-Mo(1)	100.01(4)
Mo(1)-Mo(2)-Fe(1)	81.916(19)	Mo(2)-S(2)-Mo(1)	65.61(3)

Fe(2)-S(3)-Mo(1)	75.59(4)	O(1)-C(11)-Fe(1)	178.4(5)
Fe(2)-S(3)-Mo(2)	100.96(4)	O(2)-C(12)-Fe(1)	177.9(4)
Mo(1)-S(3)-Mo(2)	65.61(3)	O(3)-C(13)-Fe(1)	179.2(5)
Fe(2)-S(4)-Mo(1)	75.51(3)	O(4)-C(14)-Fe(2)	178.1(4)
Fe(2)-S(4)-Mo(2)	100.45(4)	O(5)-C(15)-Fe(2)	177.1(5)
Mo(1)-S(4)-Mo(2)	65.39(3)	O(6)-C(16)-Fe(2)	177.2(5)

[CpMo]₂S₃[Fe(CO)₃]₂ (46)

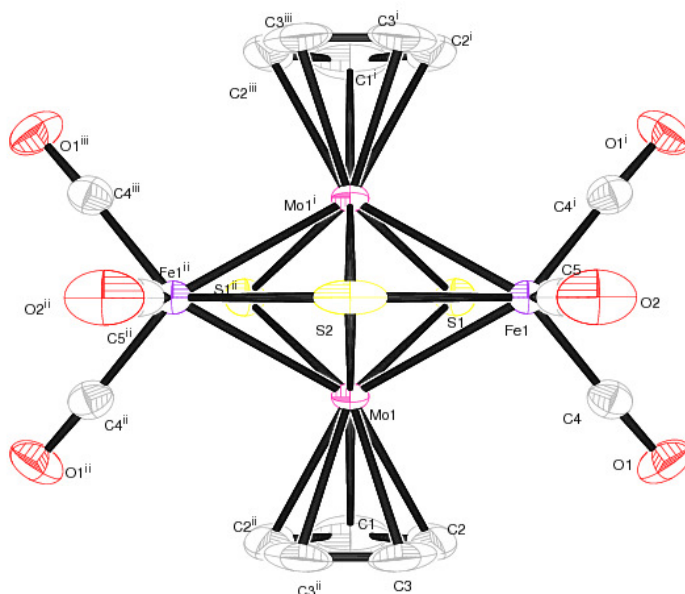


Figure 52. Molecular structure of [CpMo]₂S₃[Fe(CO)₃]₂ (**46**)

The molecular structure **46** is shown in Figure 52. The selected bond lengths (Å) and bond angles (°) of **46** are shown in Table 72. [CpMo]₂S₃[Fe(CO)₃]₂ (**46**) crystallizes in orthorhombic, space group Cmc₂m. **46** contains a highly symmetrical Fe₂Mo₂S₃ core whereby the Fe₂S₃ atoms form a pentagonal plane which is parallel to the two (η⁵-C₅H₅) planes. Each Fe(CO)₃ adduct is bonded to the Mo atom through one Mo-Fe bond, two μ₃-sulfido [S(1) and S(1ⁱⁱ)] and one μ₄-sulfido [S(2)] ligands. The two Mo atoms are in a tetragonal-bipyramidal coordination with both Cp rings occupying the axial position. The Mo-Mo bond distance of 2.675(6) Å indicates the presence of a double bond which agrees

with the 18 e rule. The Mo- μ_3 -S [2.380 (9) Å] bond distance in **46** is close in comparison with (CH₃C₅H₄)₂Mo₂S₃Fe₂(CO)₆ (2.370 Å) [123] while the Mo- μ_4 -S [2.284(13) Å] bond distance is slightly shorter than those in (CH₃C₅H₄)₂Mo₂S₃Fe₂(CO)₆ (2.308 Å).

Table 72. Bond lengths [Å] and angles [°] for [CpMo]₂S₃[Fe(CO)₃]₂ (**46**)

Bond lengths			
Mo(1)-S(2)	2.284(13)	Fe(1)-S(1)	2.214(12)
Mo(1)-S(1)	2.380(9)	Fe(1)-S(2)	2.579(9)
Mo(1)-S(1)#1	2.380(9)	Fe(1)-Mo(1)#2	2.794(5)
Mo(1)-Mo(1)#2	2.675(6)	S(1)-Mo(1)#2	2.380(9)
Mo(1)-Fe(1)#1	2.794(5)	S(2)-Mo(1)#2	2.284(13)
Mo(1)-Fe(1)	2.794(5)	S(2)-Fe(1)#1	2.579(9)
Fe(1)-C(4)#2	1.787(3)	O(1)-C(4)	1.140(4)
Fe(1)-C(4)	1.787(3)	O(2)-C(5)	1.142(6)
Fe(1)-C(5)	1.789(5)		
Bond angles			
S(2)-Mo(1)-S(1)	96.35(3)	C(4)#2-Fe(1)-Mo(1)#2	96.66(10)
S(2)-Mo(1)-S(1)#1	96.35(3)	C(4)-Fe(1)-Mo(1)#2	147.52(10)
S(1)-Mo(1)-S(1)#1	77.29(5)	C(5)-Fe(1)-Mo(1)#2	114.03(14)
S(2)-Mo(1)-Mo(1)#2	54.15(2)	S(1)-Fe(1)-Mo(1)#2	55.31(3)
S(1)-Mo(1)-Mo(1)#2	55.81(15)	S(2)-Fe(1)-Mo(1)#2	50.12(3)
S(1)#1-Mo(1)-Mo(1)#2	55.81(15)	C(4)#2-Fe(1)-Mo(1)	147.52(10)
S(2)-Mo(1)-Fe(1)#1	60.05(14)	C(4)-Fe(1)-Mo(1)	96.66(10)
S(1)-Mo(1)-Fe(1)#1	113.52(2)	C(5)-Fe(1)-Mo(1)	114.03(14)
S(1)#1-Mo(1)-Fe(1)#1	49.89(3)	S(1)-Fe(1)-Mo(1)	55.31(3)
Mo(1)#2-Mo(1)-Fe(1)#1	61.39(8)	S(2)-Fe(1)-Mo(1)	50.12(3)
S(2)-Mo(1)-Fe(1)	60.05(14)	Mo(1)#2-Fe(1)-Mo(1)	57.21(16)
S(1)-Mo(1)-Fe(1)	49.89(3)	Fe(1)-S(1)-Mo(1)	74.80(3)
S(1)#1-Mo(1)-Fe(1)	113.52(2)	Fe(1)-S(1)-Mo(1)#2	74.80(3)
Mo(1)#2-Mo(1)-Fe(1)	61.39(8)	Mo(1)-S(1)-Mo(1)#2	68.38(3)
Fe(1)#1-Mo(1)-Fe(1)	113.32(2)	Mo(1)#2-S(2)-Mo(1)	71.70(5)
C(4)#2-Fe(1)-S(1)	94.94(10)	Mo(1)#2-S(2)-Fe(1)#1	69.83(3)
C(4)-Fe(1)-S(1)	94.94(10)	Mo(1)-S(2)-Fe(1)#1	69.83(3)
C(5)-Fe(1)-S(1)	167.22(17)	Mo(1)#2-S(2)-Fe(1)	69.83(3)
C(4)#2-Fe(1)-S(2)	129.77(10)	Mo(1)-S(2)-Fe(1)	69.83(3)
C(4)-Fe(1)-S(2)	129.77(10)	Fe(1)#1-S(2)-Fe(1)	129.65(7)
C(5)-Fe(1)-S(2)	74.55(16)	O(1)-C(4)-Fe(1)	177.9(3)
S(1)-Fe(1)-S(2)	92.67(4)	O(2)-C(5)-Fe(1)	175.1(5)
Dihedral angle			
Fe(1)-Mo(1)-Mo(2)-Fe(2)	144.18		

[CpMo(SBz)]₂S₂[Fe(CO)₂] (47)

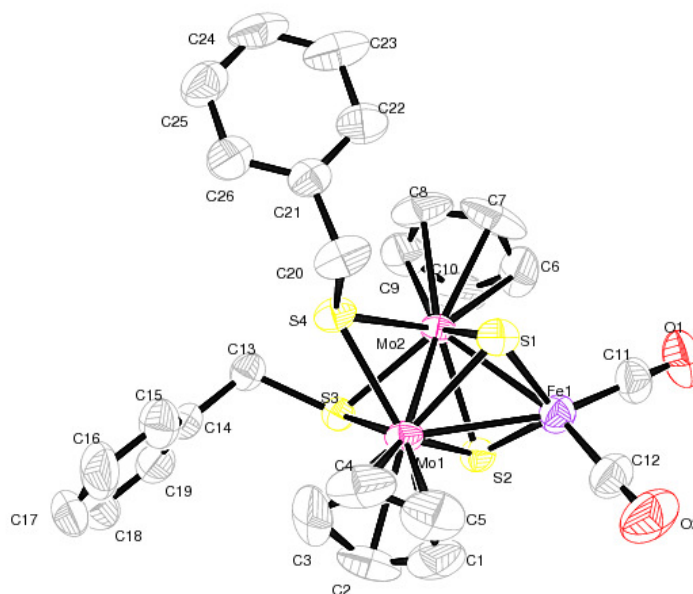


Figure 53. Molecular structure of [CpMo(SBz)]₂S₂[Fe(CO)₂] (**47**)

The molecular structure **47** is shown in Figure 53. The selected bond lengths (Å) and bond angles (°) of **47** are shown in Table 73. [CpMo(SBz)]₂S₂[Fe(CO)₂] (**47**) crystallizes in triclinic, space group P-1. The structure of **47** is similar with Cp*₂Mo₂Fe₂(CO)₂(μ₃-S)₄ [122e] which contains a trigonal-bipyramidal Mo₂FeS₂ core. The Mo₂Fe(CO)₂ moiety is perpendicular to the plane of the sulfur ligands. The Mo-Mo bond distance of 2.566 Å, Mo-Fe bond distances of 2.801 Å and 2.789 Å respectively are consistent with the observed M-M single bonds in Cp*₂Mo₂Fe₂(CO)₂(μ₃-S)₄ (Mo-Mo, 2.592(0) Å; Mo-Fe, 2.778(1) Å) and Cp*₂Mo₂Fe₂(CO)₂(μ₃-S)₂(μ₂-S₂CO) (Mo-Mo, 2.574(0) Å, Mo-Fe, 2.830(1) Å). These known analogues have been described on possessing a “bracketing effect” of the bridged ligands and the Fe(CO)₂ fragment acts as an adduct in complex **47**.

Table 73. Bond lengths [Å] and angles [°] for [CpMo(SBz)]₂S₂[Fe(CO)₂] (47)

Bond lengths			
Mo(1)-S(2)	2.420(7)	Mo(2)-Fe(1)	2.789(5)
Mo(1)-S(1)	2.445(8)	Fe(1)-C(12)	1.734(4)
Mo(1)-S(4)	2.460(8)	Fe(1)-C(11)	1.737(4)
Mo(1)-S(3)	2.517(8)	Fe(1)-S(1)	2.107(10)
Mo(1)-Mo(2)	2.565(3)	Fe(1)-S(2)	2.109(9)
Mo(1)-Fe(1)	2.801(5)	S(3)-C(13)	1.854(3)
Mo(2)-S(1)	2.422(8)	S(4)-C(20)	1.890(3)
Mo(2)-S(2)	2.456(8)	O(1)-C(11)	1.161(5)
Mo(2)-S(4)	2.478(8)	O(2)-C(12)	1.146(5)
Mo(2)-S(3)	2.486(7)		
Bond angles			
S(2)-Mo(1)-S(1)	87.37(3)	Mo(1)-Mo(2)-Fe(1)	62.91(13)
S(2)-Mo(1)-S(4)	116.06(3)	C(12)-Fe(1)-S(1)	107.44(13)
S(1)-Mo(1)-S(4)	72.56(3)	C(11)-Fe(1)-S(1)	117.80(14)
S(2)-Mo(1)-S(3)	65.95(2)	C(12)-Fe(1)-S(2)	120.69(13)
S(1)-Mo(1)-S(3)	115.91(3)	C(11)-Fe(1)-S(2)	111.57(12)
S(4)-Mo(1)-S(3)	70.20(2)	S(1)-Fe(1)-S(2)	105.71(4)
S(2)-Mo(1)-Mo(2)	58.93(19)	C(12)-Fe(1)-Mo(2)	158.95(14)
S(1)-Mo(1)-Mo(2)	57.76(2)	C(11)-Fe(1)-Mo(2)	105.86(13)
S(4)-Mo(1)-Mo(2)	59.06(2)	S(1)-Fe(1)-Mo(2)	57.29(2)
S(3)-Mo(1)-Mo(2)	58.55(18)	S(2)-Fe(1)-Mo(2)	58.22(2)
S(2)-Mo(1)-Fe(1)	46.95(2)	C(12)-Fe(1)-Mo(1)	105.78(14)
S(1)-Mo(1)-Fe(1)	46.76(2)	C(11)-Fe(1)-Mo(1)	160.11(13)
S(4)-Mo(1)-Fe(1)	111.30(2)	S(1)-Fe(1)-Mo(1)	57.71(3)
S(3)-Mo(1)-Fe(1)	106.11(19)	S(2)-Fe(1)-Mo(1)	57.00(2)
Mo(2)-Mo(1)-Fe(1)	62.45(12)	Mo(2)-Fe(1)-Mo(1)	54.64(11)
S(1)-Mo(2)-S(2)	87.08(3)	Fe(1)-S(1)-Mo(2)	75.66(3)
S(1)-Mo(2)-S(4)	72.62(3)	Fe(1)-S(1)-Mo(1)	75.53(3)
S(2)-Mo(2)-S(4)	114.06(3)	Mo(2)-S(1)-Mo(1)	63.62(2)
S(1)-Mo(2)-S(3)	117.95(3)	Fe(1)-S(2)-Mo(1)	76.05(3)
S(2)-Mo(2)-S(3)	65.91(2)	Fe(1)-S(2)-Mo(2)	74.90(3)
S(4)-Mo(2)-S(3)	70.40(2)	Mo(1)-S(2)-Mo(2)	63.49(19)
S(1)-Mo(2)-Mo(1)	58.62(2)	C(13)-S(3)-Mo(2)	114.38(11)
S(2)-Mo(2)-Mo(1)	57.58(18)	C(13)-S(3)-Mo(1)	121.55(10)
S(4)-Mo(2)-Mo(1)	58.34(19)	Mo(2)-S(3)-Mo(1)	61.71(18)
S(3)-Mo(2)-Mo(1)	59.74(18)	C(20)-S(4)-Mo(1)	114.00(9)
S(1)-Mo(2)-Fe(1)	47.05(2)	C(20)-S(4)-Mo(2)	123.70(8)
S(2)-Mo(2)-Fe(1)	46.88(2)	Mo(1)-S(4)-Mo(2)	62.60(19)
S(4)-Mo(2)-Fe(1)	111.09(2)	O(1)-C(11)-Fe(1)	178.00(3)
S(3)-Mo(2)-Fe(1)	107.34(2)	O(2)-C(12)-Fe(1)	176.90(4)

2.17 Reaction of [CpMo(CO)₂(S₂P(SC₆H₄Me)₂)] (**14**) with [CpCr(CO)₃]₂ (**1**)

2.17.1 The Reaction of [CpMo(CO)₂(S₂P(SC₆H₄Me)₂)] (**14**) with one mole equivalent of [CpCr(CO)₃]₂ (**1**) at 110 °C

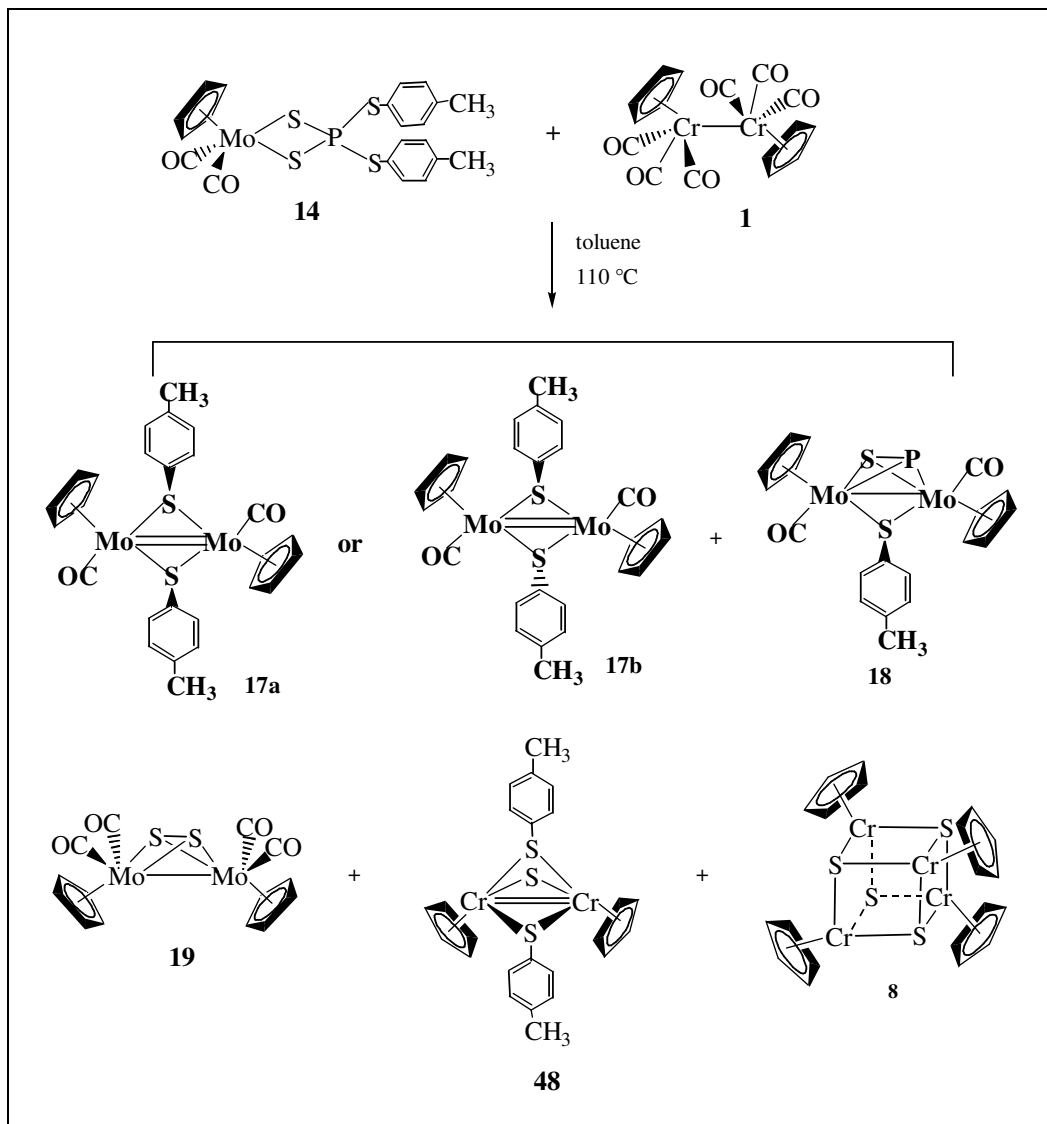
The reaction of [CpMo(CO)₂(S₂P(SC₆H₄Me)₂)] (**14**) with one mole equivalent of [CpCr(CO)₃]₂ (**1**) in toluene at 110 °C for 1.5 h led to the isolation of the unreacted [CpMo(CO)₂(S₂P(SC₆H₄Me)₂)] (14.4% recovery), Cp₂Mo₂(CO)₂(μ-PS)(μ-SC₆H₄Me) (**18**) (% yield), [CpMo(CO)₂(μ-S)]₂ (**19**) (10.8% yield), *trans-syn/trans-anti* isomer of [CpMo(CO)(SC₆H₄Me)]₂ (**17a & b**) (7.1% yield), purple crystalline solids of [CpCr(μ-SC₆H₄Me)]₂S (**48**) (7.9% yield), traces of Cp₄Cr₄S₄ (**8**) and an uncharacterized compounds (Scheme 40).

It is proposed that the formation of products **8**, **17**, **18**, **19** and **48** were initiated by the attack of 17e⁻ radical species, CpCr(CO)₃· (**1A**) towards the P-S bonds of the *p*-tolylthio fragment in **14** (cleavage at point a and b), yielding two radical species of **14A** and **14B** (Scheme 41). **14A** probably undergoes a sequence of molecular rearrangement steps with subsequent intermolecular association to form complex **17**, **18** and **19**. On the other hand, it is postulated that **14B** involves the loss of CO ligands with concomitant dimerization to generate a proposed intermediate of [CpCr(CO)₂(SC₆H₄Me)]₂. The thermal degradation of [CpCr(CO)₂(SC₆H₄Me)]₂ at 110 °C allowed it to transform to the more stable state of **48** and eventually to the final thermolyzed complex of Cp₄Cr₄S₄ (**8**). The above postulation agrees with the observations in the previous reactivity studies of **1** with Bz₂S₃ [87], and Ph₂E₂ (E = S [47], Se [48] and Te[49]).

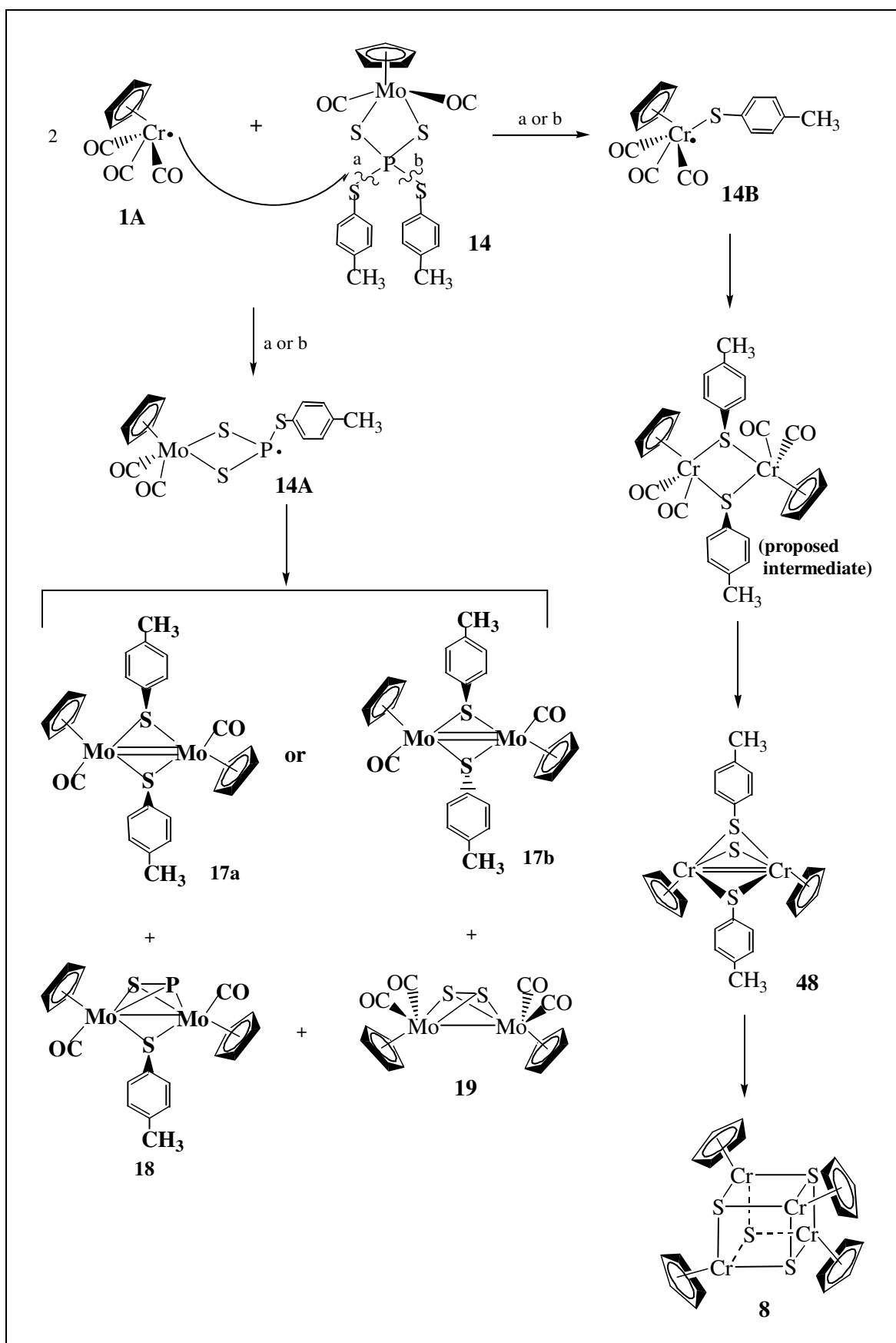
The complex **19** possesses a Cp resonance at δ 4.54 in the ¹H NMR and δ 86.65 in ¹³C NMR in C₆D₆. Only one CO resonance was observed in the ¹³C NMR at δ 227.25 which indicates that its molecular structure is highly symmetrical.

Complex **48** is a 17e⁻ paramagnetic species. Its Cp resonance was recorded as a broad peak at a low field δ 13.05 (ν_{1/2} = 47.8 Hz). Its CH₃ proton chemical shift falls

between on δ 2.20 and δ 2.46 which is due to the both $-\text{SC}_6\text{H}_4\text{Me}$ fragments at the *cis*-gauche/anti position in the molecule.



Scheme 40. Synthetic pathways for the formation of $[\text{CpCr}(\mu\text{-SC}_6\text{H}_4\text{Me})]_2\text{S}$ (**48**)



Scheme 41. Proposed fragmentation and synthetic pathways

2.17.2 Physical properties

[CpCr(μ -SC₆H₄Me)]₂S (**48**)

[CpCr(μ -SC₆H₄Me)]₂S exists as a fine purple crystalline solid. In the solid state, it is stable at ambient temperature under an inert atmosphere for a couple of weeks. It is soluble in ether to give a purple solution which is stable at room temperature for a couple of hours under an inert atmosphere.

2.17.3 Spectral characteristics

2.17.3.1 IR spectrum

[CpCr(μ -SC₆H₄Me)]₂S (**48**)

[CpCr(μ -SC₆H₄Me)]₂S showed the stretching frequencies at 1302vw, 1261vw, 1155w, 1103m, 1081m, 1060m, 1017m, 1011m, 839w, 802m, 496w, 490w, 399w cm⁻¹ in nujol (refer to Appendix I).

2.17.3.2 NMR spectrum

[CpCr(μ -SC₆H₄Me)]₂S (**48**)

Complex **48** is a dinuclear complex. In the ¹H NMR spectrum (benzene-*d*₆), a broad Cp peak was recorded at δ 13.05 (br, Cp, $\nu_{1/2}$ = 47.8 Hz) which possibly indicates that **48** is a paramagnetic species. Two CH₃- peaks were recorded at δ 2.46 and 2.20 also indicate that molecular structure of **48** is not fully symmetrical.

2.17.3.4 Mass spectrum

[CpCr(μ -SC₆H₄Me)]₂S (**48**)

The mass spectrum of **48** shows the parent ion m/z = 513.1781 [CpCr(μ -SC₆H₄Me)]₂S.

2.17.4 Molecular structures

[CpMo(CO)₂(μ-S)]₂ (**19**)

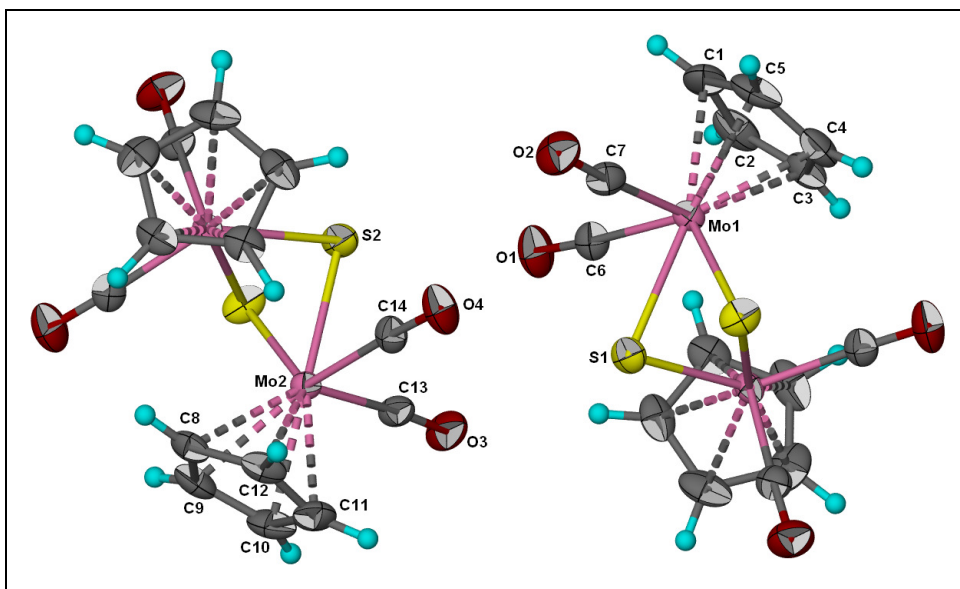


Figure 54. Molecular structure of [CpMo(CO)₂(μ-S)]₂ (**19**)

The molecular structure of **19** is shown in Figure 54. The selected bond lengths (Å) and bond angles (°) of **19** are shown in Table 74. Complex **19** crystallizes from a *n*-hexane/toluene mixture in P2₁/n space group which is isostructural with Cp₂Cr₂(CO)₄S₂ [46b] and Cp₂Cr₂(CO)₄Se₂ [46c]. They share similar properties in terms of the space group and unit cell dimensions (refer to Table 95). The structure of **19** shows a μ-η²-S₂ ligand bridging two metal atoms, the first of its kind reported for a Mo cyclopentadienylcarbonyl complex. The two Cp rings of **19** are tilted to the pseudo-trans position of S₂. The short S-S bond distance in **19** (2.085(16) Å) showed the presence of a single bond between the two sulfido ligands. Similarly, this bond shortening could be attributed to a partial charge transfer from the S₂ moiety to the metal fragment ‘electron sink’ thereby decreasing the electron-pair repulsion between the S atoms as suggested by Dahl *et al.* [124]. Thus, the four CO ligands will repel away from the Cp rings to reduce the steric tension between each other. The Mo-Mo distance of 3.0045(4) Å is similar with those μ-η²-E₂ (E = P and As)

compounds and defined as a single metal bond based on the assumption that the $\mu\text{-}\eta^2\text{-S}_2$ ligand serves as a 4 *e* donor. Hence, the noble gas configuration at each Mo atom is achieved.

Table 74. Bond lengths [\AA] and angles [$^\circ$] for $[\text{CpMo}(\text{CO})_2(\mu\text{-S})]_2$ (**19**)

Bond lengths			
Mo(1)-C(6)	1.970(3)	S(1)-S(1)#1	2.082(16)
Mo(1)-C(7)	1.986(3)	S(1)-Mo(1)#1	2.560(7)
Mo(1)-S(1)	2.459(7)	S(2)-S(2)#2	2.085(16)
Mo(1)-S(1)#1	2.560(7)	S(2)-Mo(2)#2	2.552(7)
Mo(1)-Mo(1)#1	3.002(4)	O(1)-C(6)	1.146(4)
Mo(2)-C(14)	1.979(3)	O(2)-C(7)	1.134(3)
Mo(2)-C(13)	1.983(3)	O(3)-C(13)	1.135(3)
Mo(2)-S(2)	2.461(7)	O(4)-C(14)	1.143(4)
Mo(2)-S(2)#2	2.552(7)		
Mo(2)-Mo(2)#2	2.992(4)		
Bond angles			
C(6)-Mo(1)-C(7)	85.64(12)	C(14)-Mo(2)-Mo(2)#2	87.37(8)
C(6)-Mo(1)-S(1)	120.83(9)	C(13)-Mo(2)-Mo(2)#2	129.50(7)
C(7)-Mo(1)-S(1)	88.08(8)	S(2)-Mo(2)-S(2)#2	49.12(4)
C(6)-Mo(1)-S(1)#1	72.19(8)	S(2)-Mo(2)-Mo(2)#2	54.76(16)
C(7)-Mo(1)-S(1)#1	78.66(8)	S(2)#2-Mo(2)-Mo(2)#2	51.96(16)
S(1)-Mo(1)-S(1)#1	48.95(4)	S(1)#1-S(1)-Mo(1)	68.06(3)
C(6)-Mo(1)-Mo(1)#1	86.70(9)	S(1)#1-S(1)-Mo(1)#1	62.99(3)
C(7)-Mo(1)-Mo(1)#1	129.66(8)	Mo(1)-S(1)-Mo(1)#1	73.43(2)
S(1)-Mo(1)-Mo(1)#1	54.83(17)	S(2)#2-S(2)-Mo(2)	67.72(3)
S(1)#1-Mo(1)-Mo(1)#1	51.74(16)	S(2)#2-S(2)-Mo(2)#2	63.16(3)
C(14)-Mo(2)-C(13)	87.46(12)	Mo(2)-S(2)-Mo(2)#2	73.28(2)
C(14)-Mo(2)-S(2)	120.16(8)	O(1)-C(6)-Mo(1)	176.2(3)
C(13)-Mo(2)-S(2)	85.89(8)	O(2)-C(7)-Mo(1)	175.9(3)
C(14)-Mo(2)-S(2)#2	71.23(8)	O(3)-C(13)-Mo(2)	175.7(2)
C(13)-Mo(2)-S(2)#2	79.00(7)	O(4)-C(14)-Mo(2)	175.8(3)

Symmetry transformations used to generate equivalent atoms: #1 $-x+1/2, y, -z+3/2$;
#2 $-x+3/2, y, -z+3/2$

[CpCr(μ -SC₆H₄Me)]₂S (48**)**

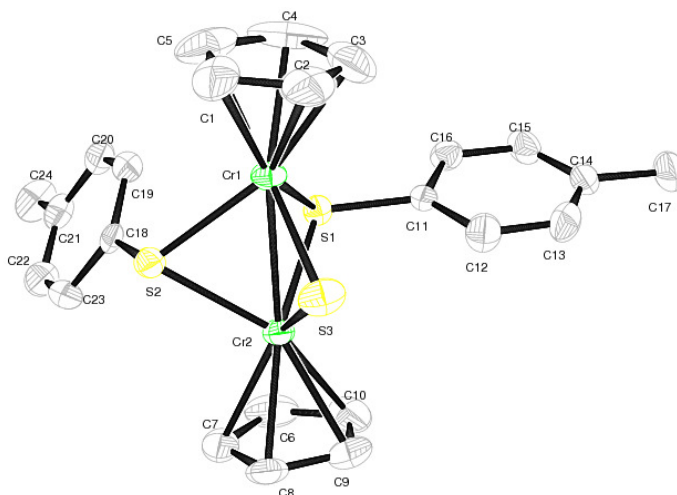


Figure 55. Molecular structure of [CpCr(μ -SC₆H₄Me)]₂S (**48**)

The molecular structure **48** is shown in Figure 55. The selected bond lengths (\AA) and bond angles ($^\circ$) of **48** are shown in Table 75. [CpCr(μ -SC₆H₄Me)]₂S (**48**) crystallizes in monoclinic, space group C2/c. **48** is isostructural with [CpCr(SBz)]₂S (**7**) and [CpCr(EPh)]₂E (E = S [47], Se [48], Te [49]). It consists of two thiolate bridges formed by two *p*-tolylthiolate groups and one thiolato-bridge with a free sulfur moiety in between the two CpCr fragments. The two *p*-tolylthiolate groups are *trans* orientated and each Cr atom is in a trigonal-pyramidal coordination environment, with the Cp ring occupying the axial position. The Cr=Cr double bond (2.680(9) \AA) formed in **48** is similar with those in known analogues as described earlier.

Table 75. Bond lengths [\AA] and angles [$^\circ$] for [CpCr(μ -SC₆H₄Me)]₂S (**48**)

Bond lengths

Cr(1)-S(3)	2.254(13)	Cr(2)-S(3)	2.242(14)
Cr(1)-S(1)	2.349(12)	Cr(2)-S(1)	2.357(12)
Cr(1)-S(2)	2.383(13)	Cr(2)-S(2)	2.374(12)
Cr(1)-Cr(2)	2.680(9)	S(2)-C(18)	1.786(4)
		S(1)-C(11)	1.786(4)

Bond angles

S(3)-Cr(1)-S(1)	96.88(5)	S(3)-Cr(2)-Cr(1)	53.63(4)
S(3)-Cr(1)-S(2)	85.55(5)	S(1)-Cr(2)-Cr(1)	55.13(3)
S(1)-Cr(1)-S(2)	86.52(4)	S(2)-Cr(2)-Cr(1)	55.88(4)
S(3)-Cr(1)-Cr(2)	53.20(4)	Cr(2)-S(3)-Cr(1)	73.17(4)
S(1)-Cr(1)-Cr(2)	55.44(3)	C(18)-S(2)-Cr(2)	106.35(15)
S(2)-Cr(1)-Cr(2)	55.56(3)	C(18)-S(2)-Cr(1)	114.31(14)
S(3)-Cr(2)-S(1)	96.98(5)	Cr(2)-S(2)-Cr(1)	68.56(4)
S(3)-Cr(2)-S(2)	86.05(5)	C(11)-S(1)-Cr(1)	110.91(14)
S(1)-Cr(2)-S(2)	86.53(4)	C(11)-S(1)-Cr(2)	113.15(14)
		Cr(1)-S(1)-Cr(2)	69.42(4)

Symmetry transformations used to generate equivalent atoms: 0.5-X, -Y, 0.5+Z; -X, 0.5+Y, 0.5-Z; 0.5+X, 0.5-Y, -Z

2.18 CONCLUSION

The study of $[\text{CpM}(\text{CO})_3]_2$ [$\text{M} = \text{Cr}$ (**1**) or Mo (**3**)] dimers and their $\text{M}\equiv\text{M}$ bonded congeners $[\text{CpM}(\text{CO})_2]_2$ [$\text{M} = \text{Cr}$ (**2**) or Mo (**4**)] have shown high reactivity toward organic ligands incorporating phosphorus, sulfur and selenium. Evidence from the present study indicates that the reaction proceeds via the radicals **1A** or **3A** or via the $[\text{CpM}(\text{CO})_2]_2$ ($\text{M}\equiv\text{M}$) triply bonded complexes **2** or **4**. Under mild condition, the facile nature of the reaction with **1** must have originated from the presence of the 15 or 17 electron $[\text{CpCr}(\text{CO})_n]\cdot$ ($n = 2, 3$) radical species as one-electron or as three-electron donors, respectively; in solution. The susceptibility of the S-S and P-E ($\text{E} = \text{S}, \text{Se}$) bonds in organic substrate to this radical-induced cleavage leads to radical-coupled intermediates containing cyclopentadienyl chromium or molybdenum was demonstrated by the reaction with Bz_2S_n ($n = 2, 3$), Davy's and Woolins' reagents. Primary products are formed via an initial homolytic S-S or P-E bond cleavage of these intermediates accompanied by incumbent coupling reactions. In cases under thermolytic conditions, **1** and **3** undergoes degradation via loss of CO ligands without undergoing bond homolysis to give the triply bonded **2** and **4**, which readily adds soft nucleophiles such as phosphines, S atoms or fragments from organic ligands with concomitant or subsequent intermolecular association to form secondary products. Prolonged thermolytic reaction subsequently leads to ultimate thermolytic derivatives such as $\text{Cp}_4\text{Cr}_4\text{S}_4$. The role of sulfur as a good π -acceptor increases the heterodonor ability in thioarylphosphine to stabilize complexes with electron-rich transition metals. Finding concludes that sulfur is an ideal substituent in tertiary phosphines especially for metal complex synthesis and indeed presents a new approach to coordination chemistry.